# QUANTIFICATION OF UNCERTAINTIES DUE TO OPACITIES IN A LASER-DRIVEN RADIATIVE-SHOCK PROBLEM

A Dissertation

by

ADAM CHRISTOPHER HETZLER

Submitted to the Office of Graduate Studies of
Texas A&M University
in partial fulfillment of the requirements for the degree of

DOCTOR OF PHILOSOPHY

Approved by:

| | |
|---|---|
| Chair of Committee, | Marvin L. Adams |
| Committee Members, | Bani K. Mallick |
| | Ryan G. McClarren |
| | Jim E. Morel |
| Head of Department, | Yassin A. Hassan |

May 2013

Major Subject: Nuclear Engineering

ABSTRACT

This research presents new physics-based methods to estimate predictive uncertainty stemming from uncertainty in the material opacities in radiative transfer computations of key quantities of interest (QOIs). New methods are needed because it is infeasible to apply standard uncertainty-propagation techniques to the $O(10^5)$ uncertain opacities in a realistic simulation. The new approach toward uncertainty quantification applies the uncertainty analysis to the physical parameters in the underlying model used to calculate the opacities. This set of uncertain parameters is much smaller ($O(10^2)$) than the number of opacities. To further reduce the dimension of the set of parameters to be rigorously explored, we use additional screening applied at two different levels of the calculational hierarchy: first, physics-based screening eliminates the physical parameters that are unimportant from underlying physics models a priori; then, sensitivity analysis in simplified versions of the complex problem of interest screens out parameters that are not important to the QOIs. We employ a Bayesian Multivariate Adaptive Regression Spline (BMARS) emulator for this sensitivity analysis. The high dimension of the input space and large number of samples test the efficacy of these methods on larger problems. Ultimately, we want to perform uncertainty quantification on the large, complex problem with the reduced set of parameters. Results of this research demonstrate that the QOIs for target problems agree at for different parameter screening criteria and varying sample sizes. Since the QOIs agree, we have gained confidence in our results using the multiple screening criteria and sample sizes.

DEDICATION

To Ashley

ACKNOWLEDGEMENTS

Writing this dissertation has been an exciting challenge for me. I would like to acknowledge the support of my committee, colleagues, friends, and family. These people have supported me both personally and academically. At many points, I doubted whether I would ever finish this dissertation, and I am thankful for their support in this pursuit and encouragement to finish my dissertation.

My faculty advisor, Dr. Adams, and my committee members, Drs. Mallick, McClarren, and Morel, have provided me with a solid foundation to become a successful researcher. They taught me where the current state of research in my field is and how to contribute to it. I am grateful for their time and knowledge.

I would like to thank a few friends and colleagues for their support and genuine care. These include Dr. Cable Kurwitz, Dr. Paul Nelson, Dr. John Poston, Lana Wilson, Jay Haines, John Creasy, and Adam Shephard. They have helped me in many ways, such as telling me about job opportunities, reviewing my presentations, and providing comments on this dissertation. One thing that I will not miss is being asked by them, "when are you going to finally leave?" Finally, I would like to thank my wife and parents for their patience and understanding.

## NOMENCLATURE

| | |
|---|---|
| ARD | Absorption Rate Density |
| BATSRUS | Block-Adaptive Tree, Solar-wind Roe-type Upwind Scheme |
| BMARS | Bayesian Multivariate Adaptive Regression Spline |
| CRASH | Center for Radiative Shock Hydrodynamics |
| HEDP | High-Energy High-Density Physics |
| LANL | Los Alamos National Laboratory |
| LHD | Latin Hypercube Design |
| LHS | Latin Hypercube Sample |
| LTE | Local Thermodynamic Equilibrium |
| MARS | Multivariate Adaptive Regression Spline |
| PCA | Principal Component Analysis |
| PSAAP | Predictive Science Alliance Academic Program |
| PDF | Probability Density Function |
| PDT | Parallel Deterministic Transport |
| QOI | Quantity of Interest |
| RT | Radiative Transfer |
| UQ | Uncertainty Quantification |

TABLE OF CONTENTS

Page

LIST OF FIGURES

Page

LIST OF TABLES

Page

# 1. INTRODUCTION

We aim to perform uncertainty quantification for a two-dimensional laser-driven radiative shock problem, called the CRASH-like test problem, modeled with radiative transfer (RT) computations. We use physics-based and statistical dimension reduction techniques to overcome the high dimensionality of the tabulated opacities to study how the uncertainty in tabulated opacities used in the RT computations affects Quantities of interest (QOIs) for the CRASH-like test problem. We achieve dimension reduction first by focusing on uncertain parameters that are inputs to the opacity-generation model and then by utilizing simplified one-dimensional RT problems and statistical screening to cull unimportant parameters. In this dissertation we provide an overview of relevant physics and statistics, a description of our methodology its importance, descriptions of computed problems, and discussion of results and conclusions.

## 1.1 Predictive Science

Predictive science uses computations and previous experiments to predict the outcome of new experiments with quantified uncertainty. Outcome uncertainty stems from both the experiments and the computation, and predictively quantifying this outcome uncertainty is a central concept in predictive science. A survey of predictive science is given in *Assessing the Reliability of Complex Models* (Ref. 1).

Physics models, mathematical models of physical phenomena, used in computations are unable to precisely model reality for many reasons. The model itself may be a simplified model for many reasons, such as inherent lack of knowledge or necessity for computational tractability, physical data in the model not being known with

certainty, or the computational implementation of the physics model having simplifications. These simplifications, as well as others not described here, mean that the physical model may not be able to predict exactly the outcomes that it is intended to predict; however, "[r]emember that all models are wrong; the practical question is how wrong do they have to be to not be useful," as Box and Draper (Ref. 2) state.

A verification, validation, and uncertainty quantification study is performed to quantitatively assess the usefulness of a model to compute QOIs. There are two parts to verification. Code verification is verifying that the computational implementation is correct. Solution verification is verifying how much numerical error is made by the current computational settings for a given problem of the computational implementation. Validation determines how well the computer implementation and a physical observation agree for a QOI in a given problem.

Verification and validation studies are necessary steps to perform a quantitative assessment of how well the physics model matches reality. Uncertainty quantification is the process of quantifying uncertainties and errors that affect uncertainties in the QOIs. The uncertainties and errors arise in the physics model, numerical and code errors, and model input and parameters uncertainties. Uncertainty quantification studies are performed for model parameter uncertainties to determine their effect on QOIs. The uncertainties arise from the lack of knowledge about the model parameters' precise values; instead, there is knowledge about the range and possible distribution of values.

## 1.2 Description of Physical Models of Interest

Radiative transfer, one physics model useful for making predictions in high-energy, high-density physics, describes the interactions of a photon field with the surrounding material. Opacities, denoted by the symbol $\sigma$, describe the probability that a photon interacts with the matter per unit path length. The RT equations are

$$\frac{1}{c}\frac{\partial I}{\partial t} + \vec{\nabla}\bullet\vec{\Omega} I + \sigma I = \frac{\sigma_s}{4\pi}\phi + \sigma_a B \tag{1.1}$$

$$C_v \frac{dT}{dt} = \int_0^\infty (\phi - B) d\nu + Q_{fixed} \,. \tag{1.2}$$

Here $I$ is the radiation intensity, $\phi$ is the angular-integrated radiation intensity, $B$ is the Planck distribution, $T$ is the material temperature, $C_v$ is the material heat capacity, and $Q_{fixed}$ is an energy source. The purpose of this research is to quantify the uncertainty in quantities of interest relevant for RT problems, such as material temperature at a specific point and time, that arise from uncertainties in physical data underlying the opacities.

Opacities are calculated using statistical and atomic physics. Since the primary interaction between the photon and the atom is through the electric field of the photon, we must determine the distribution of ionization and excitation states for the atoms and the density of free electrons. The ionization state distribution is the distribution of the atoms among the ionization states. The excitation state distribution is the distribution of the electrons among the many energy levels of the atoms. These distributions of states depend on the temperature and density of the surrounding material. If one assumes Local Thermodynamic Equilibrium (LTE), one is able to use statistical mechanics to determine these distributions. Under the assumption of LTE, one is able to either treat

the gas as a Boltzmann gas or a Fermi gas. The opacity-generation code developed by the Center for Radiative Shock Hydrodynamics (CRASH), the center that sponsored the research described here, uses the assumption of LTE and treats the gas as a Fermi gas for the calculation of ionization state and energy level populations. After the populations are calculated, opacities can be calculated for the different materials using atomic physics, which account for the different interactions photons have with materials.

## 1.3 CRASH Project Description

This research is in support of the uncertainty quantification goals of the CRASH project. The CRASH project is a five-year collaborative research effort between three universities, which is part of the Predictive Science Alliance Academic Program (PSAAP) of the Department of Energy's National Nuclear Security Administration. The purpose of the center is to develop methods to assess the predictive capability for complex laboratory experiments using computations and previous experiments. The laboratory experiment is a laser-driven radiative shock tube experiment, which is a high-energy-density physics (HEDP) experiment like those in Drake (Ref. 3). Specifically, four years of relevant experiments and computations are used to predict a different experiment in the fifth year.

### 1.3.1 CRASH Experiments

The basic laboratory experiment for the first four years is shown in Figure 1 and described subsequently.

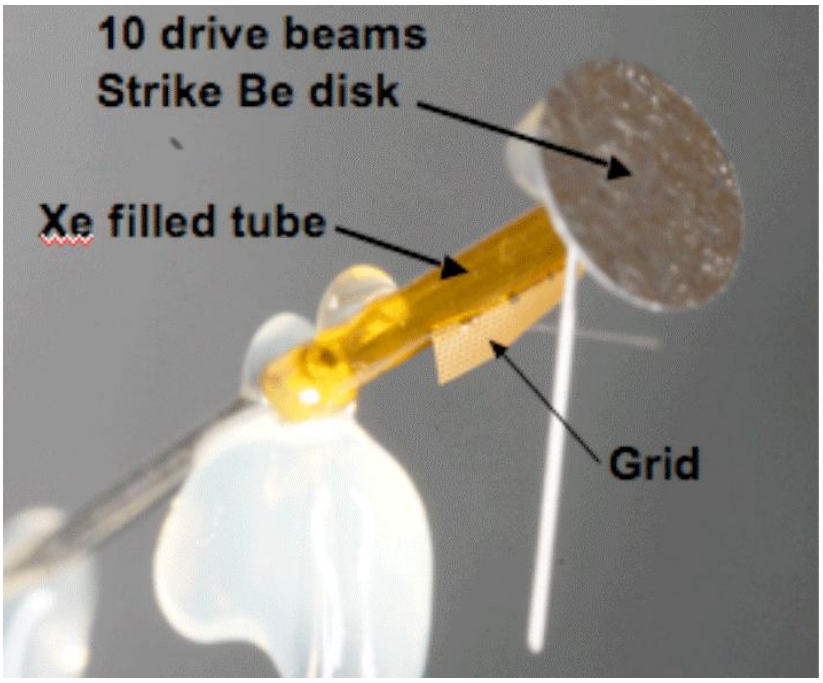


**Figure 1. CRASH Experiment.**

The experiment involves striking the beryllium surface for 1 nanosecond with 10 laser beams, whose wavelength is 0.35 micrometers, depositing about 4,000 Joules. This impulse creates a beryllium plug that travels into the xenon-filled tube, and this creates a shock wave in the xenon. For the fifth-year experiment, an oval tube is used instead of a circular tube.

### 1.3.2 CRASH Computations

Two different massively parallel computer codes are used to perform computations for this project: Block-Adaptive Tree, Solar-wind Roe-type Upwind Scheme (BATSRUS) and Parallel Deterministic Transport (PDT). BATSRUS is a coupled radiation-hydrodynamics code, which can be used to solve the Eulerian hydrodynamics equations and the radiation diffusion equation, which is described by van

der Holst (Ref. 4). PDT is a transport code that is discretized in spatial with finite elements, in angle with discrete ordinates, in energy with multigroups, and it is able to solve the RT equation using massively parallel computer architectures. For futher reading see Hawkins, et al. (Ref. 5). The results from the first four years of the project are used to tune parameters used in the computations to more accurately predict the fifth year experiment.

### 1.4 Sources of Uncertainty in the CRASH Project

The CRASH project is a complex undertaking having both experimental and simulation uncertainties. The experimental uncertainties include:

1. differences in predicted laser energy deposition versus actual laser energy deposition;
2. uncertainty in as built dimensions versus design dimensions; and
3. measurement uncertainty.

The simulation uncertainties include:

1. model form error in the hydrodynamics and RT models;
2. approximations made in the treatment of the initial and boundary conditions;
3. approximations in numerical methods; and
4. model parameter uncertainties.

This is not an exhaustive list of sources of uncertainty; rather, it demonstrates the complexity associated with the entire project. This research focuses on model parameter uncertainty for the opacities used in the RT equation. This may seem like an overly simplified study of uncertainty, but we note that opacities are generally tabulated

for hundreds of temperatures, hundreds of densities, tens of energy groups, and tens of materials, which results in around a million uncertain opacities that feed into the RT calculations. Assessing the impacts of uncertainties in such a large set of parameters is among the more difficult challenges in predictive science. This challenge is often described as the "curse of dimensionality."

### 1.5 Our Research Focus

Our focus is on uncertainties in opacities, which appear as "model parameters" in the RT equations. These opacities are calculated using an opacity-generation code developed by the CRASH project. We choose to model the uncertainties in the model parameters in these opacity calculations provided by the CRASH code rather than the opacities themselves because there are fewer uncertain parameters that feed into the opacity calculations. The opacities produced by CRASH are accurate for low atomic number elements (low Z) but become inaccurate for high atomic number elements. Since the xenon opacities produced by CRASH are inaccurate, we develop a hybrid method, which combines the mean value of the xenon opacities generated by Los Alamos National Laboratory (LANL) with the uncertainty generated by the CRASH package. The opacity tables produced from the opacity calculations with the uncertain parameters are used the first step in the uncertainty quantification framework that is developed in this research.

Our research has produced a physics-based methodology for addressing the uncertainties that arise from the high-dimensional set of opacities, as we describe in detail in later sections. We have also developed a "CRASH-like" RT problem and

associated QOIs on which to apply and test our methodology. This problem is realistic in many ways, including that it is a computationally expensive calculation, and it is designed to provide information about absorption rate densities at specific points downstream from the shock, which in turn provide information about the effects of radiation transport on key experimental observables (such as wall shock). This is described in later sections.

### 1.6 Overview of Uncertainty Quantification Framework

We devise a novel approach to analyze the uncertainties in quantities of interest (QOIs) for problems relevant to the Center for Radiative Shock Hydrodynamics (CRASH) project, and presumably other high-energy-density applications, by using physics-based dimension reduction. First, we construct a Latin Hypercube Design for our uncertain parameters in the opacity calculation to generate many independent sets of opacities. Then, we use these opacities as input into PDT to generate sets of solutions for two simple 1-D RT problems. QOIs are extracted from the solutions to the problems. Then, a low-order emulator is built to relate the LHD parameter and QOI data sets. We perform statistical analysis on this emulator to determine if the QOI is sensitive to the uncertain parameters. We reduce the set of uncertain parameters by leaving out those parameters that the QOIs are not sensitive to. With this reduced subset of uncertain parameters, we calculate QOIs using a different size reduced sets and different size LHDs for the computationally expensive problem. Finally, uncertainty quantification is performed to determine how these underlying uncertainties affect the QOIs of the RT solution calculated with Parallel Deterministic Transport (PDT) code.

This research is presented as follows in this document. Section 2 discusses the background and theory of this research as it pertains to RT, opacities, and the uncertain parameters. Section 3 describes the methodology used to determine the uncertainty in important QOIs for the CRASH project. A method is discussed for generating of a set of parameters, using these parameters to calculate opacities, using the opacities in radiation transport calculations, and parsing the radiation transport calculations for the QOIs. In Section 4 and 5, the test cases and the results are presented, respectively, to demonstrate the effectiveness of the UQ methodology. Results, conclusions, and areas for additional work are discussed in Section 6.

# 2 BACKGROUND AND THEORY

In the following sections, we describe the radiative transfer and opacity calculations employed in this research. Radiative transfer describes the propagation of photons within a material. Our RT solutions are obtained numerically with the PDT code. The opacity calculations involve statistical and atomic physical models, which are solved numerically using software developed as part of the CRASH project.

## 2.1 Introduction to Radiative Transfer

Eq. (1.1) and (1.2), the RT equations, describe the way in which a photon field interacts with material. These equations, as well as many of the terms, are developed in detail in this section. The amount of energy, *dE*, is the specific intensity $I\left(\vec{r},\vec{\Omega},\nu,t\right)$ at position $\vec{r}$, direction $\vec{\Omega}$, photon frequency $\nu$, and time $t$ multiplied by the phase-space volume is defined as the amount of energy given as

$$dE = I\left(\vec{r},\vec{\Omega},\nu,t\right)d\vec{r}\,d\vec{\Omega}\,d\nu\,dt \tag{2.1}$$

The spatial component $\vec{r}$ depends on three spatial variables, which, in Cartesian coordinates, are given as $(x,y,z)$. The angular variable $\vec{\Omega}$ depends on three angular variables $(\mu,\eta,\xi)$, but only two of these variable are independent since $\vec{\Omega}$ is unit length. Both frequency $\nu$ and time $t$ are scalar values. Specific intensity is dependent on seven independent variables.

The amount of energy that is absorbed, emitted, and scattered from the beam of photons described above is defined using standard terminology and nomenclature (Ref. 6, 7, 8). The amount of energy absorbed from the beam of photons entering normal to

the cross sectional area $dA$ of a differential volume of material with and length $ds$ is given as

$$dE = \rho \kappa_a I d\vec{r} d\vec{\Omega} d\nu dt , \tag{2.2}$$

where $\kappa_a$ is defined as the mass absorption coefficient (area per unit mass of material) (Ref. 9). The amount of energy that is scattered from the beam of photons is given as

$$dE = \rho \kappa_s I d\vec{r} d\vec{\Omega} d\nu , \tag{2.3}$$

where $\kappa_s$ is defined as the scattering coefficient (area per unit mass of material). In addition, a total removal term, known as the extinction coefficient, is defined as $k = \kappa_a + \kappa_s$. The amount of energy that is emitted back into the beam of photons in direction $\vec{\Omega}$ in $d\vec{\Omega}$ is given as

$$dE = j \rho d\vec{r} d\vec{\Omega} d\nu dt , \tag{2.4}$$

where $j$ is the emission source rate density (per unit mass).

When a material is at a temperature $T$, under the assumption of local thermodynamic equilibrium (LTE) we can approximate the emission source rate density as

$$j^t = \kappa B(\nu, T) , \tag{2.5}$$

where the superscript $t$ represents thermal emission and $B(\nu, T)$ is the Planck function:

$$B(\nu, T) = \frac{2h\nu^3}{c^2}\left(e^{h\nu/kT} - 1\right)^{-1} . \tag{2.6}$$

Eq. (2.5) is known as the Kirchhoff-Planck law. The condition of LTE is not strictly met in most settings but is commonly assumed and is often a very good approximation.

Another way photons can enter the beam is through scattering (sometimes referred to as "in-scattering"). Photons are scattered, absorbed, and emitted by matter in a variety of ways that are discussed subsequently.

**2.2 The Radiative Transfer Equation**

The RT equation is derived following the typical approach (Ref. 6, 7), but more detail is given for the mathematics that is typically glossed over. The goal is to write an equation that models the transfer of energy between the photon field and the material. First, the specific intensity, given by (2.1), describes the energy of radiation travelling in a beam. The photon beam can be enhanced with sources (via the emission sources) or attenuated with sinks (via the extinction coefficient). So, to calculate the change in specific intensity $dI$, we write a balance equation by adding the sources and subtracting the sinks,

$$\frac{dI}{ds}\left(\vec{r},\vec{\Omega},\nu,t\right) = \rho\, j\left(\vec{r},\vec{\Omega},\nu,t\right) - \rho k\left(\vec{r},\nu,t\right) I\left(\vec{r},\vec{\Omega},\nu,t\right). \tag{2.7}$$

This equation equates the change in specific intensity per unit path length of photon travel to the sources and sinks. The macroscopic total cross-section is defined as

$$\sigma_T\left(\vec{r},\nu,t\right) = \rho k\left(\vec{r},\nu,t\right). \tag{2.8}$$

We insert (2.8) into (2.7) and arrive at

$$\frac{dI\left(\vec{r},\vec{\Omega},\nu,t\right)}{ds} = \rho\, j\left(\vec{r},\vec{\Omega},\nu,t\right) - \sigma_T I\left(\vec{r},\vec{\Omega},\nu,t\right). \tag{2.9}$$

Using the chain rule on (2.9), we have

$$\frac{1}{c}\frac{\partial I\left(\vec{r},\vec{\Omega},\nu,t\right)}{\partial t} + \vec{\Omega}\bullet\nabla I\left(\vec{r},\vec{\Omega},\nu,t\right) = \rho\, j\left(\vec{r},\vec{\Omega},\nu,t\right) - \sigma_T I\left(\vec{r},\vec{\Omega},\nu,t\right). \tag{2.10}$$

With the assumption of the condition of LTE, the application of the Kirchhoff-Planck law from Eq. (2.5) produces

$$\frac{1}{c}\frac{\partial I\left(\vec{r},\vec{\Omega},\nu,t\right)}{\partial t}+\vec{\Omega}\bullet\vec{\nabla}I\left(\vec{r},\vec{\Omega},\nu,t\right)=\rho\kappa B\left(\nu,T\right)-\sigma_T I\left(\vec{r},\vec{\Omega},\nu,t\right). \tag{2.11}$$

We negelect scattering and apply Eq. (2.8), which produces

$$\frac{1}{c}\frac{\partial I\left(\vec{r},\vec{\Omega},\nu,t\right)}{\partial t}+\vec{\Omega}\bullet\vec{\nabla}I\left(\vec{r},\vec{\Omega},\nu,t\right)=\sigma_T\left(B\left(\nu,T\right)-I\left(\vec{r},\vec{\Omega},\nu,t\right)\right). \tag{2.12}$$

**2.3 Interactions of Photons with Matter**

Photons interact with free and atomic electrons. These interactions are divided into three different kinds of interactions based on the initial and final state of the electron. These are bound-bound interactions, bound-free interactions, and free-free interactions. The change in energy for the electron is shown in Figure 2. Each of these is discussed in detail in the following sections, and the detailed methods to compute the interaction coefficients are presented later.

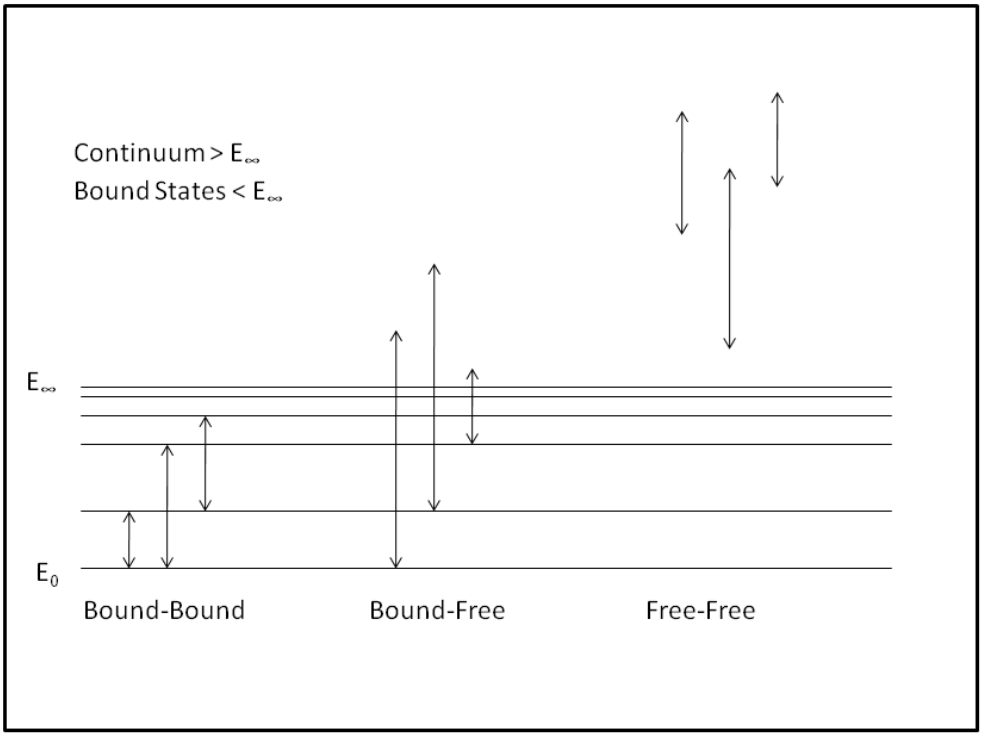


**Figure 2. Possible Electron Transitions within Atomic Levels and Ccontinuum.**

### 2.3.1 Bound-bound Interactions

A bound-bound interaction occurs when an atomic electron undergoes a transition in energy state. An example of an absorption process follows from (Ref. 7). If a photon is absorbed by the atom, an electron is excited from a lower energy level to a higher energy level, which leaves the atom in an excited state. If the excited atom de-excites by an inelastic collision with another particle, the energy of the photon is converted into kinetic energy of the two interacting particles. The energy of this photon,

not accounting for line broadening (which is described in detail in section 2.5.2), is given by the Bohr relation as

$$h\nu_{nm} = E_n - E_m, \tag{2.13}$$

where $E_n$ and $E_m$ are the upper and lower energy level energies, $\nu_{nm}$ is the frequency of the photon, and $h$ is Planck's constant. The absorption process at these energies creates lines or resonances in the absorption coefficient. This effect also creates emission and absorption lines in the radiation spectrum. The calculations for these interactions are presented in more detail in the Opacity Calculations section.

### 2.3.2 Bound-free Interactions

Bound-free interactions involve the creation or destruction of a photon. Photoionization occurs when a photon whose energy is greater than the ionization energy of the outermost bound electron is absorbed by an atom, whereupon an electron is excited into the continuum becoming free. Photoionization is a threshold reaction, which causes edges in the absorption coefficient as a function of energy. The calculational details of this interaction are presented in the Opacity Calculations section.

### 2.3.3 Free-free Interactions

Free-free interactions involve free electrons, which can absorb or create photons. Bremmstrahlung occurs when an electron slows down giving up its energy as photons. There is an inverse of this process, whereby an electron absorbs a photon and accelerates. From these processes, photons are either created or destroyed and a transfer of energy between radiant energy and electron kinetic energy occurs. Technically, a single free electron cannot directly absorb a photon; rather, a complex underlying

process occurs to facilitate a reaction that appears to be a free-free absorption. As with the other interactions, we discuss later the calculation of this contribution to the absorption coefficient.

### 2.3.4 CRASH Opacity Code Parameter and Calculation Flow

Figure 3 shows the flow of parameters used in the calculation of opacities in the CRASH code and the order of the calculations performed. The parameter data includes the excitation energies, ionization energies, and oscillator strengths. The user-specified input to this problem includes density, temperature, and concentration of species present. First, the excitation energies and ionization energies are used to calculate the energy-level populations and ionization-state populations, and the average number of free electrons per atom.

Next, the oscillator strength, energy-level populations and ionization-state populations are used to calculate the bound-bound absorption coefficient as a function of photon frequency. Then, the energy-level populations, ionization-state populations, excitation energies, and ionization energies are used to calculate the bound-free absorption coefficient as a function of photon frequency. Note that the energy level populations and associated excitation energies reduce the amount of energy a photon must have to ionize the given electron since it is in an excited state. The average density of free electrons is used to calculate the free-free absorption coefficient. Finally, the absorption coefficients are used to calculate the opacities, which are weighted averages of coefficients over given frequency intervals.

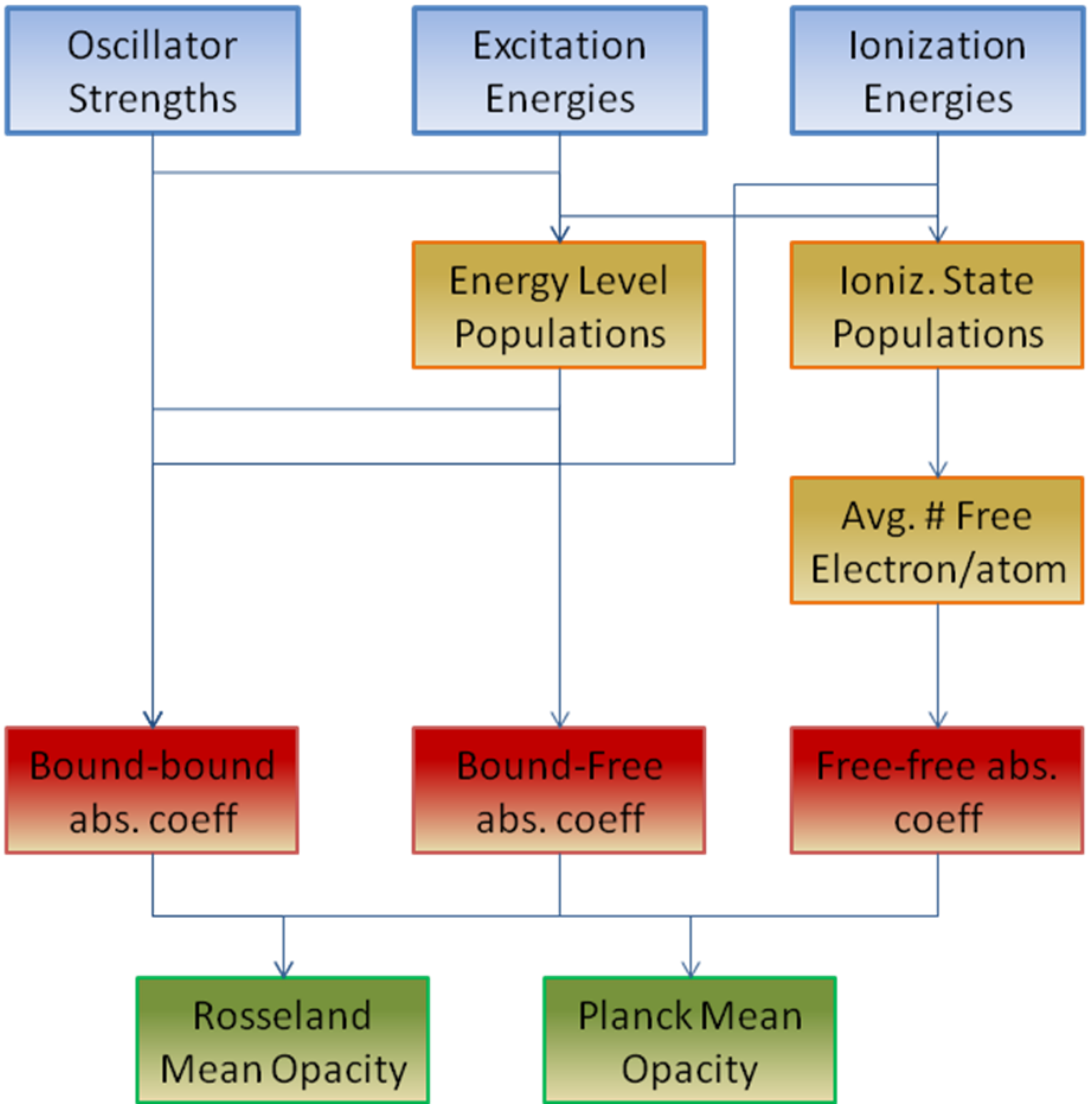


**Figure 3. Parameter and Calculation Flow in the CRASH Opacity Code.**

This expressed as a three-step process:

1. Calculate Electron Populations;
2. Calculate Absorption Coefficients; and
3. Calculate Opacities.

A description of these calculations follows, and an algorithm describing the order that these calculations are performed is discussed.

Oscillator strengths, excitation energies, and ionization potentials can be measured and/or calculated using atomic structure codes utilizing methods from Cowan (Ref. 10). An interesting avenue for future work on opacity uncertainties would be to focus on such atomic-structure codes and the uncertain parameters that form their inputs. These parameters are a layer deeper into the underlying physics, and there are probably fewer of them. We mention this as an interesting path for future exploration, but we did not attempt such exploration in our effort.

## 2.4 Introduction to Atomic Energy Levels and Ion Population

Since photons interact with free electrons, neutral atoms, and ions, one must characterize the population of electrons if one is to quantify interaction probabilities. This is similar to characterizing the number density and temperature of materials for macroscopic neutron cross sections. Characterizing the population of electrons requires application of thermodynamics and statistical mechanics. In our work the assumption of LTE is imposed. This assumption allows the use of thermodynamics and equilibrium statistical mechanics to calculate the desired quantities.

### 2.4.1 Introduction to Thermodynamics

If one were to try to characterize even a simple system of neutral non-interacting particles for any realistic system, one would immediately realize that the number of unknowns is too large for even the most sophisticated computers. Take for example one liter of a monatomic gas. To characterize this gas we would need 3 spatial terms and 3 momentum terms for each atom, and we would need this for approximately $10^{20}$ particles in the liter. Then, the equations of motion for all of these particles would have

to be solved which would also require correct initial conditions for each particle. The same number of partial differential equations would need to be solved independently. Also, if the particles were interacting these differential equations would now contain interaction terms and would have to be solved simultaneously.

However, such a characterization of a gas is not useful or insightful for typical applications. Instead, the macroscopic properties are useful and necessary. This problem can be solved statistically. A simple way to think of this is that one particle does not change a macroscopic property like specific heat, but rather it is the ensemble of particles acting in an average sense that affects these properties.

To use statistical mechanics for the problem at hand, a few important concepts are introduced. First, an extensive parameter changes proportionally as the system size changes, and an intensive parameter is constant no matter the system size. For example, volume, energy, entropy, and number of particles are extensive parameters, and temperature and pressure are examples of intensive parameters. Also, the first postulate of thermodynamics states that, "there exist particular states (equilibrium states) of simple systems that, macroscopically, are characterized completely by internal energy, volume, and mole number" (Ref. 11). So, a thermodynamic system can fully characterized with only three properties. The equation used to characterize this system is known as a fundamental equation and can be expressed with either entropy or energy (we have chosen energy):

$$U = U\left(S, V, \vec{N}\right), \tag{2.14}$$

where $S$ is entropy, $U$ is internal energy, $V$ is volume, and $\vec{N}$ are the mole numbers for the various constituents of the system. From this equation, if one knows the entropy, volume, and mole number of a system, then one could immediately calculate the internal energy.

The derivatives of the fundamental equation are equations of state and have significant meaning. If one takes the total derivative of the fundamental equation, one obtains:

$$dU = \left(\frac{\partial U}{\partial S}\right) dS + \left(\frac{\partial U}{\partial V}\right) dV + \sum_i \left(\frac{\partial U}{\partial N_i}\right) dN_i \tag{2.15}$$

We define the derivative terms as:

$$\begin{aligned} \frac{\partial U}{\partial S} &= T \\ -\frac{\partial U}{\partial V} &= P \\ \frac{\partial U}{\partial N} &= \mu \end{aligned} , \tag{2.16}$$

where $T$ is temperature, $P$ is pressure, and $\mu$ is electrochemical potential. Most people have a more intuitive understanding of temperature and pressure than of energy and entropy, and temperature and pressure can be directly measured unlike energy and entropy. These definitions, where one takes the derivative of the fundamental equation, are known as equations of state. Assuming that the number of moles is held constant and inserting these definitions from (2.16) into (2.15), we obtain:

$$dU = TdS - PdV \tag{2.17}$$

which states that the change in energy is equal to the influx of heat minus the work done by the system.

An equation of state is an equation that expresses an intensive parameter, such as temperature or pressure, in terms of extensive parameters, such as energy, volume, and mole numbers. One common misunderstanding is that an equation of state fully characterizes a system; however, this is untrue, because the fundamental equation that characterizes the thermodynamic system under consideration. In fact it takes knowledge of all three equations of state to fully characterize a system at thermal equilibrium (Ref. 11).

Also, derivatives of these intensive parameters have physical meaning in thermodynamics. One parameter of interest in radiation hydrodynamics calculations is heat capacity, which can be defined with either pressure or volume held constant. The two definitions of heat capacity can be related by using fundamental thermodynamic relationships as well; however, the relationships are just stated as

$$C_p = \left( \frac{\partial H}{\partial T} \right)_p = \left( \frac{\partial Q}{\partial T} \right)_p \tag{2.18}$$

and

$$C_v = \left( \frac{\partial U}{\partial T} \right)_V = \left( \frac{\partial Q}{\partial T} \right)_V , \tag{2.19}$$

where $H$ is enthalpy and $Q$ is heat. The subscript next to the term in parentheses is a common notation, which denotes the quantity in parentheses varies while the subscript term is held constant. These two definitions can be related as

$$C_p - C_V = T\left(\frac{\partial P}{\partial T}\right)_{V,N}\left(\frac{\partial V}{\partial T}\right)_{P,N} = VT\frac{\alpha^2}{\beta_T}, \tag{2.20}$$

where $\alpha$ is thermal coefficient of expansion, and $\beta_T$ is isothermal compressibility. These can be expressed in terms of derivatives as

$$\alpha = \frac{1}{V}\left(\frac{\partial V}{\partial T}\right)_P \tag{2.21}$$

and

$$\beta_T = -\frac{1}{V}\left(\frac{\partial V}{\partial P}\right)_T. \tag{2.22}$$

It is very difficult to hold volume constant while one performs a heat capacity measurement. However, it is straightforward to hold pressure constant when the same measurement is performed. Thus, one can perform the measurement on $C_p$ and then relate it to $C_v$ with Eq. (2.20). This relationship is important because $c_v$ is necessary in energy equation, and, although specific heat at constant volume cannot be easily determined experimentally, it can be from the relationship.

### 2.4.2 Legendre Transforms and Thermodynamic Potentials

Other forms of fundamental equations use the temperature, pressure, or chemical potential variables in place of entropy, volume, or number of particles. For example, enthalpy was used in Eq. (2.18). It is much easier to measure these intensive parameters than the extensive parameters. In this section, a methodology for transforming between the different thermodynamic potentials is presented.

One particular way of formulating these fundamental equations is to use Legendre transforms (Ref. 11). Legendre transforms for general equations are now introduced. First, given the equation

$$f = f(x_o, x_1, \ldots, x_n), \tag{2.23}$$

one wishes to formulate this equation in terms of the derivative of one of its variables like

$$y_m = \frac{\partial f}{\partial x_m}, \tag{2.24}$$

such that no information is lost, which would typically result from taking a derivative of a function because terms that are constant in the given differentiation variable are lost. So, the goal is to create a new equation that contains the same amount of information as the old equation as

$$g = g(x_0, x_1, \ldots, y_m, \ldots, x_n), \tag{2.25}$$

There is a duality between conventional point geometry and Pluecker line geometry (Ref. 11). The reader is directed to this reference for a more comprehensive description of this. A one-dimensional case is provided below to understand the essence of this transformation. First, one can describe a point in a plane with two values (its x and y coordinates). Similarly, one can describe a line with two values (slope and y-intercept). For one dimension one could have

$$f = f(x), \tag{2.26}$$

where both $f$ and $x$ are point values, and we could have

$$g = g(y), \tag{2.27}$$

where $g$ is the $y$-intercept and $y$ is the slope. We see that $f$ selects a subset of points in a plane, whereas $g$ selects a subset of lines, and this can be done in such a manner that these lines are tangential to the points in $f$. We note here that $f$ is a subset of zeroth order values where as $g$ is a subset of first order values in the plane, which means that $g$ contains more information. So, if we want to equate a set of points with a set of lines where each line contains one point, we can calculate where this intercept would occur as (Ref. 11)

$$y = \frac{f - g}{x - 0}, \tag{2.28}$$

where we could simplify this to be

$$g = f - yx, \tag{2.29}$$

where $y = \frac{df}{dx}$. There is a transform that can map one equation into another equation containing the derivative, but we must be able to perform the inverse transform to get back the original equation. These inverse transforms are given as

$$x = -\frac{dg}{dy} \tag{2.30}$$

and

$$f = g + xy. \tag{2.31}$$

Similarly, this can be performed for multivariate equations as well. As mentioned before, not only can one take the Legendre transform on a single variable, but this can be

extended further by taking the Legendre transform on more than one variable, which can include all the variables.

Three different transformations, called thermodynamic potentials, are given with the energetic fundamental equation (Ref. 11). First, the Helmholtz free energy, $F\left(T, V, \vec{N}\right)$, where entropy has been transformed into temperature using the derivative $\frac{\partial U}{\partial S} = T$, is given as

$$F = U - TS \,, \tag{2.32}$$

and its inverse transform, using the derivative $\frac{\partial F}{\partial T} = -S$, is given as

$$U = F + TS \,. \tag{2.33}$$

Similarly, replacing the volume, $V$, with its derivative, $\frac{\partial U}{\partial V} = -P$, as $H\left(S, P, \vec{N}\right)$, gives the following transform

$$H = U + PV \,, \tag{2.34}$$

and the inverse transform as

$$U = H - PV \,. \tag{2.35}$$

This thermodynamic potential is known as the Enthalpy. The last potential mentioned, and the only one that includes two transforms, is the Gibbs free energy and is given as $G\left(T, P, \vec{N}\right)$ using both of the previous two derivatives the transform is given as

$$G = U - TS + PV \,, \tag{2.36}$$

and its inverse is given as

$$U = G + TS - PV \ . \tag{2.37}$$

In the following section, the relationship between these potentials and statistical mechanics and to the calculation of ionization state and energy level populations is described.

### 2.4.3 Introduction to the Canonical Ensemble

In the canonical ensemble, volume, temperature, and number of particles are taken as the independent variables. Thus, the description of the canonical ensemble corresponds to the Helmholtz Free Energy $F(T, V, N)$. This framework is used to calculate the population of the different ionization states in the CRASH opacity code. There are transforms that can be performed on the Helmholtz free energy to compute internal energy of the system. Also, the derivatives of the free energy can provide the equations of state. This has been implemented in the CRASH code.

### 2.4.4 Calculation of Ionization-state Populations

From (Ref. 12) the free energy is formulated as

$$F = -T \sum_{i=0}^{Z} N_i \ln \left[ g_i \frac{eV}{N_i} \left( \frac{MT}{2\pi\hbar^2} \right)^{3/2} \exp\left( -\frac{E_i}{T} \right) \right] + F_e \ , \tag{2.38}$$

where $g_i$ is the statistical weight of the $i^{\text{th}}$ charge state, $N_i$ is the number of ions in the $i^{\text{th}}$ ionization state, $F_e$ is the free energy of the electrons, $E_i$ is the ionization energy, and $T$ is the temperature of the system multiplied by Boltzmann's constant. This equation states that the energy of the system is the sum of the energy over all ionization states plus the energy in free electrons. Now, if one requires ionization equilibrium meaning that when an atom is ionized from the $i^{\text{th}}$ charge state to the $(i+1)^{\text{th}}$ charge state one can

equate this as $i \rightleftarrows (i+1) + e$. Also, when this equilibrium is reached the Helmholtz Free Energy will be at a minimum, and we can take the derivative of the free energy with respect to the number of electrons and apply the chain rule as (Ref. 12)

$$\frac{\partial F}{\partial N_e} + \frac{dN_i}{dN_e}\frac{\partial F}{\partial N_i} + \frac{dN_{i+1}}{dN_e}\frac{\partial F}{\partial N_{i+1}} = 0 \,, \tag{2.39}$$

and, from the reaction statement, it is known that

$$\begin{matrix} \frac{dN_i}{dN_e} = -1 \\ \frac{dN_{i+1}}{dN_e} = 1 \end{matrix} \,, \tag{2.40}$$

and the derivative $\frac{\partial F}{\partial N_e}$ is defined as the chemical potential of the electrons as $\mu_e$. Now, solving these derivatives as

$$\frac{\partial F}{\partial N_i} = -T \ln\left(\frac{g_i}{N_i}\exp\left(\frac{-E_i}{T}\right)\right) \tag{2.41}$$

and substituting

$$\mu_e + T \ln\left(\frac{g_i}{N_i}\exp\left(\frac{-E_i}{T}\right)\right) - T \ln\left(\frac{g_{i+1}}{N_{i+1}}\exp\left(\frac{-E_{i+1}}{T}\right)\right) = 0 \,, \tag{2.42}$$

as shown in (Ref. 12). Dividing through by the temperature, taking the exponential, and rearranging one obtains

$$\frac{N_{i+1}}{g_{i+1}} = \frac{N_i}{g_i}\exp\left(\frac{-\mu_e - I_i}{T}\right), \tag{2.43}$$

where $I_i$ is the ionization potential of the $i^{\text{th}}$ electron. This can be written for the ionization equilibrium $(i-1) \rightleftarrows i + e$ as

$$\frac{N_i}{g_i} = \frac{N_{i-1}}{g_{i-1}} \exp\left( \frac{-\mu_e - I_{i-1}}{T} \right), \tag{2.44}$$

and this scheme could be applied recursively to the zeroth ionization state to yield

$$N_i = g_i (g_e)^i \frac{N_0}{g_0} \exp\left( -\frac{E_i}{T} \right), \tag{2.45}$$

where $g_e = \exp\left( -\frac{\mu_e}{T} \right)$. Now, the partition function is defined as $p_i = N_i / N_a$ and applying to the previous equation as

$$p_i = \frac{g_i (g_e)^i \exp\left( -\frac{E_i}{T} \right)}{\sum_{j=0}^{Z} g_j (g_e)^j \exp\left( -\frac{E_j}{T} \right)}, \tag{2.46}$$

where $S = \sum_{j=0}^{Z} g_j (g_e)^j \exp\left( -\frac{E_j}{T} \right)$. The partition function simply gives the fraction of atoms or ions in the $i^{\text{th}}$ charge state. In equation (2.46) all of the terms are known except for $g_e$. Thus, this equation is solved for this term. The average charge of the system is defined as

$$Z = \langle i \rangle = \frac{N_e}{N_a}. \tag{2.47}$$

Assuming the system is a Fermi gas (Ref. 12), one also obtains

$$Z = g_{e1} Fe_{1/2} (g_e), \tag{2.48}$$

where the Fermi function is defined as

$$Fe_\lambda (g_e) = \frac{1}{\Gamma(\lambda + 1)} \int \frac{x^\lambda}{g_e e^x + 1} dx, \tag{2.49}$$

and $\Gamma$ -function is defined recursively as

$$\begin{aligned} \Gamma(1/2) &= \pi^{1/2} \\ \Gamma(\lambda+1) &= \lambda\Gamma(\lambda) \end{aligned}. \tag{2.50}$$

Now, the density of states is defined as

$$g_{e1} = \frac{2V}{N_a}\left(\frac{m_e T}{2\pi\hbar^2}\right)^{3/2}. \tag{2.51}$$

$g_e$ can be solved by finding where the two definitions for average charge given by Eqs. (2.47) and (2.48) intersect, which is performed using Newton's method as

$$\begin{aligned} \langle i \rangle &= g_{e1} Fe_{1/2}(g_e) \\ f(g_e) &= 0 = \langle i \rangle - g_{e1} Fe_{1/2}(g_e) \end{aligned}. \tag{2.52}$$

Recalling Newton's method for a single variable, the following equations defines the iterative scheme used to obtain $g_e$

$$g_{e,new} = g_{e,old} - \frac{f(g_{e,old})}{f'(g_{e,old})}. \tag{2.53}$$

$f'(g_{e,old})$ can be obtained from Eq. (2.52) as,

$$f'(g_{e,old}) = \langle i^2 \rangle - \langle i \rangle^2 + \langle i \rangle \frac{Fe_{-1/2}(g_{e,old})}{Fe_{1/2}(g_{e,old})}, \tag{2.54}$$

and using Newton's method one obtains the following scheme

$$g_{e,new} = g_{e,old} - \frac{\langle i \rangle - g_{e1} Fe_{1/2}(g_e)}{\langle i^2 \rangle - \langle i \rangle^2 + \langle i \rangle \dfrac{Fe_{-1/2}(g_{e,old})}{Fe_{1/2}(g_{e,old})}}. \tag{2.55}$$

This has been incorporated in the CRASH code in the set_ionization_equilibrium in ModPartition.f90 by Igor Sokolov. After solving for $g_e$, $S$ and $p_i$ are obtained. To obtain the population of each ion charge state the partition function is multiplied by the total number of atoms $N_a$.

### 2.4.5 Calculation of Energy-level Populations

From statistical mechanics the statistical weights of the $i^{\text{th}}$ ionization state and $n^{\text{th}}$ principal quantum state is defined as

$$w_{i,n} = g_{i,n} g_e^i \exp\left(-\frac{E^*_{i,n}}{T}\right), \tag{2.56}$$

where $g_{i,n}$ is the degeneracy of the atomic level, $g_e$ has been previously defined, and $E^*_{i,n}$ is the modified excitation energy, and its form is given in (Ref. 12). This is just a Maxwell-Boltzmann distribution. To obtain the statistical weight of the $i^{\text{th}}$ charge state, $g_i$, one sums over all of the quantum states as

$$g_i = \sum_{n=n_{ground}}^{N} w_{i,n} \,. \tag{2.57}$$

Again, the atom has an infinite number of principal quantum states, but only the first $N$ states are used in this approximate calculation. It is necessary to calculate the partition function for the energy levels so that the bound-bound and bound-free absorption coefficients can be calculated. This is obtained by first taking the sum of all of the statistical weights as

$$S = \sum_{i=0}^{I} \sum_{n=n_{ground}}^{N} w_{i,n} \,, \tag{2.58}$$

and similarly the partition function is calculated as

$$p_{i,n} = \frac{w_{i,n}}{S}. \tag{2.59}$$

It is important to note that $n_{ground}$ is the highest ground state that is occupied and is not the first ground state.

### 2.4.6 Algorithm for Calculation of Average Ionization State and Populations

The algorithm for solving is straightforward. First, an initial guess of the electron statistical weight, $g_e$, is made. Then, the excitation level populations are calculated using Eqs. (2.56) and (2.57), $g_i$ is calculated. $g_i$ is used in Eq. (2.46) to calculate the ionization-state population. Then, the average ionization state, $\langle i \rangle$, the average square-ionization state, $\langle i^2 \rangle$, and the Fermi functions, $Fe_{\pm 1/2}(g_{e,old})$, are calculated. Finally, $g_e$ is updated using (2.55), and convergence is checked. If $g_e$ has not been converged the iteration is continued. This is implemented in the CRASH code in ModStatSum.f90, ModPartition.f90, ModExcitation.f90, and ModFermiGas.f90. It should be noted that some data is stored in other FORTRAN files, but these contain the actual computation. We have modified the CRASH code for this work to allow for varying ionization potentials and oscillator strengths for the UQ study.

## 2.5 Opacity Calculations

The purpose of the discussion of electron interactions and electron and ion populations was to be able to perform opacity calculations. In this section, we give the equations used by the CRASH code to calculate opacities which mainly come from

MacFarlane (Ref. 13). The opacity calculation is implemented in the CRASH code in the ModMultiGroup.f90 module; some other helper modules are separately located, but the majority of the calculation is done in this module.

### 2.5.1 Free-free Contribution to Opacity

First, the free-free coefficient, also known as inverse Bremsstrahlung coefficient, is given by (Ref. 13) :

$$\alpha_{ff}(\nu) = \sum_{k=1}^{kMax} c_k \, 2.41 \cdot 10^{-37} \cdot N_a \cdot 10^{-6} \cdot \left\langle i_k^2 \right\rangle \cdot g_{ff} \cdot N_a \cdot \left\langle i \right\rangle \cdot 10^{-6} \frac{1 - e^{-h\nu/kT}}{(kT)^{1/2} (h\nu)^3}, \quad (2.60)$$

where

$$g_{ff} = \text{Gaunt Factor} = 1 + 0.44 \exp\left\{ -0.25 \left[ \log_{10} \left( \frac{13.6 \left\langle i^2 \right\rangle}{kT} \right) + 0.25 \right]^2 \right\}, \quad (2.61)$$

$$\left\langle i \right\rangle = \text{average \# of free electrons per atom} = \sum_k c_k \sum_{j=1}^{z_k} j f_{jk}, \quad (2.62)$$

and

$$\left\langle i_k^2 \right\rangle = \text{average number of squared free electrons per atom} = \sum_{j=1}^{z_k} j^2 f_{jk}. \quad (2.63)$$

where $c_k$ is the concentration of the $k^{\text{th}}$ species given as input, $i_k$ is the atomic number of the $k^{\text{th}}$ species, and $f_{jk}$ is the ion partition function for the $j^{\text{th}}$ ionization state of the $k^{\text{th}}$ species. $f_{jk}$ is defined as:

$$f_{jk} = \frac{g_j \left(g_e\right)^j e^{-\sum_{l=1}^{j-1} I_l / kT}}{\sum_{i=1}^{Z_k} g_i \left(g_e\right)^i e^{-\sum_{l=1}^{i-1} I_l / kT}}. \tag{2.64}$$

The absorption coefficient equation is identical to eq. (4.3) given in MacFarlane (Ref. 13), and (2.64) is just the partition function. However, MacFarlane uses the Saha equation to calculate his partition function, and the CRASH code uses Fermi statistics to calculate the partition function since it is a more accurate model.

### 2.5.2 Bound-bound Contribution to Opacity

A bound-bound, or photoexcitation, coefficient is obtained from MacFarlane (Ref. 13). The photoexcitation coefficient for the absorption of a photon, which causes a transition from the $n^{\text{th}}$ energy level to the $m^{\text{th}}$ energy level for the $j^{\text{th}}$ ionization state of the $k^{\text{th}}$ atomic species, is calculated as

$$\alpha_{bb}^{n \to m, j, k} = \frac{2.65 \cdot 10^{-2} \cdot f_{n \to m} \cdot L\left(\Gamma, \Delta\nu\right)}{1 - e^{-h\nu / kT}}, \tag{2.65}$$

where $f_{n \to m}$ is the oscillator strength, $L\left(\Gamma, \Delta\nu\right)$ is the line shape, $\Gamma$ is the damping or broadening factor, and $\Delta\nu$ is the photon frequency shift. The $\left(1 - e^{-h\nu / kT}\right)^{-1}$ factor is the effective decrease in line absorption due to stimulated emission (Ref. 9). The line is broadened from three main contributions: natural, Doppler, and collisional broadening. The sum of these broadening factors gives the total broadening factor. These terms are given by:

$$\begin{aligned}
\Gamma_{nat} &= 2.29 \cdot 10^{6} \cdot E_{n \to m}{}^{2} \\
\Gamma_{dop} &= 1.41 \cdot 10^{11} \cdot E_{n \to m} \cdot \langle v \rangle \\
\Gamma_{col} &= 4.58 \cdot 10^{6} \cdot N_a{}^{1/3} \cdot \langle v \rangle \\
\Gamma &= \Gamma_{nat} + \Gamma_{dop} + \Gamma_{col}
\end{aligned} , \tag{2.66}$$

where

$$\langle v \rangle = \left( kT / A \right)^{1/2} \tag{2.67}$$

and

$$E_{n \to m} = E_m - E_n . \tag{2.68}$$

where $A$ is in atomic mass units (amu), $kT$ is in electron-Volts (eV), $E_n$ is the excitation energy (eV) of the $n^{\text{th}}$ level, and $\langle v \rangle$ is the average thermal velocity. There is no Doppler broadening when the thermal velocity is zero. This holds for photons as well. From Zel'dovich and Raizer (Eq. 5-78) (Ref. 8), the oscillator strength can be calculated as

$$f_{n \to m} = \frac{32}{3\pi\sqrt{3}} \frac{1}{n^5} \frac{1}{m^3} \frac{1}{\left( 1/n^2 - 1/m^2 \right)^3} . \tag{2.69}$$

This oscillator strength formula is found using Balmer's series formula, which is strictly appropriate only for hydrogen, and a table of values for some of these transitions is used in CRASH. Also, the CRASH code assumes that the oscillator strengths are the same for all elements. This assumption may be a source of error.

The line shape must be calculated. CRASH can use either the Voight or Lorentzian profile. The Voight profile is the default and is given as (Ref. 13)

$$L\left(\Gamma,\Delta\nu,\Delta\nu_D\right)=\frac{H\left(\Gamma,\Delta\nu,\Delta\nu_D\right)}{\pi^{1/2}\Delta\nu_D}, \tag{2.70}$$

where

$$\begin{aligned}\Delta\nu &= \left(\Delta E_{n\to m}-h\nu_{photon}\right)/h\\ \Delta\nu_D &= \frac{\Gamma_{Dop}}{12.566}\end{aligned}. \tag{2.71}$$

To calculate the total bound-bound contribution, the contributions of mixtures of ionization states for transitions from initial quantum states ($n$) to final quantum states ($m$) are summed as

$$\alpha_{bb}(\nu)=N_a\sum_k c_k\sum_{j=0}^{jMax-1}p_{j,k}\sum_{n=1}^{Ms-1}p_{n,j,k}\sum_{m=n+1}^{Ms}\alpha_{bb}^{n\to m,j,k}. \tag{2.72}$$

The ionization state, $p_{j,k}$, and excitation level $p_{n,j,k}$ populations are calculated as previously described, and the species concentration, $c_k$, is known.

### 2.5.3 Bound-free Contribution to Opacity

The calculation of the bound-free contribution is as follows (Ref. 13)

$$\alpha_{bf}(\nu)=\frac{64\pi\alpha a_0^2}{3\sqrt{3}}\cdot N_a\sum_k c_k\sum_{j=j'}^{jMax}p_{j,k}\sum_{n=1}^{Ms}p_{n,j,k}\alpha_{n,j,k}^{bf}, \tag{2.73}$$

where $\alpha$ represents the fine structure constant and $a_0$ is the Bohr radius. $j'$ represents lowest ionization state whose potential is less than the energy of the photon denoted by $I_{j'}<h\nu$. This definition is important since a photon cannot ionize an electron whose ionization potential energy is greater than the photon's energy. $\alpha_{n,j,k}^{bf}$ is the opacity of

the $n^{th}$ quantum state, of the $j^{th}$ ionization state, for the $k^{th}$ atomic species. The bound-free opacity for each quantum state is obtained as (Ref. 13)

$$\alpha^{bf}_{n,j,k} = \frac{n_e}{(j+1)^2} g_{bf} \frac{\left(1 - e^{h\nu/kT}\right)\left(k\left(I_j - E_n\right)\right)^3}{\left(1 + e^{h\nu/kT}\right) e^{\left(I_j - E_n\right) - \mu}}, \tag{2.74}$$

where the transition energy is $I_j - E_n$, which is the ionization potential minus the energy level of the electron, and $n_e$ is the number of electrons in the level.

## 2.6 Absorption Coefficient Versus Opacity

There is some ambiguity in terminology between absorption coefficient and opacity. Historically, all opacities were known as mean absorption coefficients, as is seen from one of Rosseland's famous papers (Ref. 14). Here we note that the terms opacity and absorption coefficient are somewhat interchangeably used. For the purpose of this paper, absorption coefficient refers to the opacity that has not been averaged in energy, and opacity refers to a cross section that has been averaged. In nuclear engineering parlance, the absorption coefficient would be similar to a point wise cross section, and the opacity would be similar to multigroup cross sections.

## 2.7 Mean-averaged Opacities

Two different opacities have been used in this research. The Planck-weighted Opacity is given as

$$\kappa_P = \frac{\int_0^\infty \kappa(\nu) B(\nu, T)\, d\nu}{\int_0^\infty B(\nu, T)\, d\nu}, \tag{2.75}$$

which is weighted with the thermal spectrum $B(\nu, T)$. This can be simply referred to as the Planck Opacity. A different weight-averaged opacity, known as the Rosseland Mean Opacity, which is important in the diffusion limit, is defined as:

$$\frac{1}{\kappa_R} = \frac{\int_0^\infty \frac{1}{\kappa(\nu)} \frac{\partial B}{\partial T} d\nu}{\int_0^\infty \frac{\partial B}{\partial T} d\nu}. \tag{2.76}$$

For a more detailed description see (Ref. 14) or (Ref. 7). We integrate over "group" intervals, instead of zero to infinity, to calculate group opacities when using the multigroup approximation.

**2.8 Assumptions of CRASH Opacity code**

The CRASH opacity code makes many assumptions in order for the computation of the opacity to be a tractable problem. Many scholars have gone about this problem with many different sets of assumptions (Ref. 12, 15, 16). The code used in this research is developed from the assumptions made by (Ref. 12); however, this reference does not include all of the assumptions that are made. A partial description of the known approximations and assumptions not explicitly included in the aforementioned reference are described here. It is assumed that the oscillator strengths for every atom and every ionization state are the same. It is assumed that electrons not in the outer shell, referred to as core electrons, do not contribute to the opacity.

**2.9 Choice of Uncertain Parameters**

For this research a subset of uncertain parameters has been considered. Since there are three interaction types, bound-bound, bound-free, and free-free, uncertain

parameters should be chosen that could affect each interaction. However, it is known that the free-free interaction contains little uncertainty, so it is neglected in the study of uncertain parameters. Oscillator strength given in (2.69) is taken as an uncertain parameter, and this affects the bound-bound interaction. A description of the evaluation of the oscillator strengths is provided in Section 3.3.1.

Ionization potentials have been taken as uncertain parameters as well. The ionization potentials affect both the bound-bound and bound-free interactions. A discussion of the evaluation of ionization potentials is presented in section 3.3.2. Oscillator strengths affect only the opacities whereas the ionization potentials affect both the statistical physics (which affects the equations of state) and the opacities. As previously mentioned, ionization potentials and oscillator strengths can be computed from atomic physics models, which have their own uncertain parameters, but this research has taken distributions of the ionization potentials and oscillator strengths as given.

# 3 UNCERTAINTY QUANTIFICATION METHODOLOGY

This research develops new methods for performing uncertainty quantification for large parameter sets and large response sets. To perform the uncertainty quantification (UQ), an UQ framework is developed. First, various complete opacity tables are computed using various values of the uncertain parameters in the underlying physics model. Each opacity table is used in a transport simulation of one or more CRASH-like test problems, and then the outputs of these simulations are parsed to obtain a probability density for each QOI in each problem. This procedure is performed for the two 1-D CRASH-like test problems. An emulator is constructed using Bayesian Multivariate Adaptive Regression Splines (BMARS). Sensitivity analysis is performed using this emulator to determine which of the uncertain parameters should be kept for study in the more computationally expensive 2-D CRASH-like test problem. Finally, the reduced set of uncertain parameters is sampled to create more opacity tables, and these tables are used in transport simulations of the 2-D CRASH-like test problem. The outputs of these simulations are then parsed for relevant QOIs. In the following sections, this process is discussed in detail.

## 3.1 Development of a Model Surrogate

To develop a model surrogate, or emulator, many simulations of the high-order model must be performed. The model simulation that is being emulated in our case is a RT simulation using PDT, which is computationally expensive to use. Emulators are used explore the response to the chosen input parameters to understand the sensitivity to uncertain parameters in a computationally inexpensive manner. To create an emulator,

the uncertain input parameters are first sampled using a Latin Hypercube Design (LHD). Each sample point is a set of inputs for the opacity-generation code, which is run to generate an opacity table for each point. Each table is used as input for the simulator (PDT) to produce QOIs, which are then used to build emulators. The specific emulator type employed in this research is Bayesian Multivariate Adaptive Regression Splines (BMARS) (Ref. 17). In the following sections, the theory and background of LHDs and BMARS emulators are introduced. Also, a brief discussion of the sensitivity analysis tools used in this work is presented.

### 3.1.1 Latin Hypercube Designs

The first step in creating a LHD is to subdivide each dimension (i.e., the range for each parameter) in a domain into *k* subdivisions of equal probability, where *k* is the number of samples desired. A random point in each subdivision in each dimension is selected to create *k* values of each input parameter. These values are combined to form *k* sets of parameters such that each value of each parameter is used only once. More formally, assume one desires $k$ samples in a $d$ dimensional domain. First, one divides each dimension $d_j$ where $j \in d$ into $k$ subdivisions, as $d_{jk}$. Next, one chooses samples such that only one point is placed in each subdivision, $d_{jk}$ for all $k$ samples. The design matrix is constructed with shape $d \times k$ where the $k$ columns represent a LH sample of every dimension. This is a rather naïve way to build a Latin Hypercube because it may not fill the space well, and the points may be highly correlated. However, much work has been pursued to choose criteria to improve the space filling and/or reduce

correlations of the LHD. Two criteria commonly in use are distance-based and correlation-based.

The purpose of the distance-based criterion is to maximize the minimum distance between the points. A description of the distance-based method described by Morris and Mitchell (Ref. 18) is provided subsequently. A distance metric using the L-norm is defined as

$$d_{L_p}(\vec{x}_s, \vec{x}_t) = \left( \sum_{l=1}^{k} \left| x_s^{(l)} - x_t^{(l)} \right|^p \right)^{1/p} \tag{3.1}$$

A vector $(d_1, \cdots, d_m)$ is defined as a set of distances, which can range in length from 1 to $\binom{n}{2}$, where $\binom{n}{2}$ is the binomial coefficient for *n* choose 2. If all the distances were distinct, one would have $\binom{n}{2}$ distances, and if the distances were all equal, there would be only one distance. This vector is the set of the distances between all of the points. Then, a list $(J_1, \cdots, J_m)$, where each $J_i$ corresponds to the number of pairs whose distance is $d_i$ is created. Now, the sum of this vector should be equal to the binomial coefficient. A maxi-min condition of the minimum index can be described by which $d_1$ is maximized and $J_1$ is minimized. Morris and Mitchell extend this for all of the distances and pairs and describe a metric to evaluate the optimality of the LHD. Then, they go on to describe an algorithm for accomplishing this.

Tang suggests using a correlation criteria for selecting LHDs (Ref. 19). The idea is to set up a LHD in such a manner as to minimize the correlation between any two

samples of the LHD. Given two samples $U = (U_1, \cdots, U_d)$ and $V = (V_1, \cdots, V_d)$, let us define a correlation coefficient as:

$$\rho(U, V) = \frac{\sigma_{uv}^2}{\sigma_u \sigma_v}. \tag{3.2}$$

This can be calculated by finding the largest eigenvalue, sometimes referred to as the spectral radius, of the following matrix:

$$\Sigma_{uu}^{-1} \Sigma_{uv} \Sigma_{vv}^{-1} \Sigma_{vu}. \tag{3.3}$$

as noted by Tang, where $\Sigma_{uv} = \Sigma_{vu}$ is the covariance matrix of $U$ and $V$. The specific implementation and algorithm to reduce the correlation between the all of the LHSs is beyond the scope of this work, but Tang and Owen (Ref. 20) is an excellent source for more information. MATLAB provides methods to generate LHDs using either of the criteria.

### 3.1.2 Bayesian Multivariate Adaptive Regression Splines

Multivariate adaptive regression splines (MARS) were originally developed by Friedman (Ref. 21). The purpose of MARS is to create a low-order emulator $\hat{y} = \hat{f}(\vec{x})$ that is a close approximation to the high-order function (or simulation) $y = f(\vec{x})$, in such a manner that $y$ and $\hat{y}$ are almost identical. The advantage of this low-order emulator is that it can be sampled much faster to approximate the original high-order model. The MARS emulator has the following functional form

$$\hat{f}(\vec{x}) = \sum_{i=1}^{k} a_i B_i(\vec{x}), \tag{3.4}$$

where $\vec{x}$ is the parameter space, $B_i$ are basis functions, and $a_i$ are fitting coefficients. The basis functions are given as

$$B_i(\vec{x}) = \begin{cases} 1, & i = 1 \\ \prod_{j=1}^{J_i} \left[ s_{ji} \left( x_{v(ji)} - t_{ji} \right) \right]_+^o, & i = 2, 3, \cdots \end{cases} \tag{3.5}$$

where $J_i$ is the degree of interaction, $[\cdot]_+ = \max(0, \cdot)$, $s_{ji} = \pm 1$, $t_{ji}$ is the knot point, and $v(j,i)$ is the index of the predictor variable meaning it corresponds to $x_j$ for the $i^{\text{th}}$ spline. These splines are nonnegative. To construct the splines a Bayesian approach is used (Ref. 17).

The Bayesian approach allows one to construct an ensemble of MARS model samples. To build a new model, a spline can be added, changed or removed from the current model. This new model is either accepted or rejected using Gibbs sampling. After enough models have been accepted or rejected to reach the stationary point, a process called burn-in, new accepted models can be saved as sample models. It is typical to save a model only after many samples have been taken since the previous saved model, because each new model differs from the previous model by only one spline. This process builds up an ensemble of models. Each low-order model can be thought of as a sample from the distribution all possible models that could represent this response.

The emulator allows for the estimation of the response to a new set of input-parameter values. Three purposes for emulators are stated. First, they allow for the computation of sensitivity to the uncertain parameters. Also, they allow for the

prediction of a new, untried experiment, which may be useful when trying to optimize choice of experimental parameters. Last, they allow for the creation of a PDF of responses given different distributions of uncertain parameters. In the following section, the use of the emulator for sensitivity analysis is explored.

### 3.1.3 Sensitivity Analysis Tools

Sensitivity analysis is performed on the BMARS model to determine which of the parameters account for the most uncertainty. The parameters that account for very little uncertainty can be screened, and more computationally expensive simulations can be performed with a smaller subset of parameters. Two of the tools used for this screening process are main effects and marginal effects. To calculate the main effects, the variance of the response is calculated for the mean value of all of the models where only the parameter of interest is allowed to vary, as in

$$\text{Main Effect}\left(x_i\right) = \text{var}\left[\frac{1}{n_{\text{models}}}\sum_{k=1}^{n_{\text{models}}} \hat{y}_k\left(\vec{x}_{(1,p)\neq i} = \vec{x}_{(1,p)\neq i,median}, x_i\right)\right]. \tag{3.6}$$

To calculate the marginal effects, the variance of the response is calculated for the mean value of all of the MARS model samples where all of the parameters are allowed to vary except for the parameter of interest, which is held fixed at a certain value, as in

$$\text{Marginal Effect}\left(x_i\right) = \text{var}\left[\frac{1}{n_{\text{models}}}\sum_{\text{models}} \hat{y}\left(\vec{x}_{(1,p)\neq i}, x_i = x_{i,fixed}\right)\right]. \tag{3.7}$$

In the following sections, marginal effects plots are shown with error bars. These error bars denote the minimum and maximum values for this quantity for various fixed values of the parameter.

A parameter with a large main effect and a small marginal effect is an important parameter.

## 3.2 Introduction to Uncertain Parameters in Opacity Calculations

The ionization potentials and oscillator strengths compose the uncertain parameter data that has been studied in this research. In the materials used in problems of interest, there are 53 ionization potentials and 36 oscillator strength per level-to-level transition. This work focuses on the uncertainty in ionization potentials, which affect the photoionization and photoexcitation absorption coefficients, and oscillator strengths, which affect only the photoexcitation absorption coefficients.

## 3.3 Analysis of Relevant Uncertain Data Used in the CRASH Code

The physical data used in the calculation of opacities is analyzed to understand the appropriate bounds and distributions. There is not a definitive resource where this data has been collected and evaluated; thus, part of this research has been to create reasonable values for this data. The data analyzed includes the oscillator strengths and ionization potentials.

### 3.3.1 Evaluation of Oscillator Strengths

The oscillator strength describes the strength of the transition from one bound state to another. In the CRASH code, the transitions from the first through fourth to the second through fifth are given by Table 1 as data:

**Table 1. Oscillator Strength for Transitions from $n_i \rightarrow n_f$.**

| | | $n_i$ | | | |
|---|---|---|---|---|---|
| | | 1 | 2 | 3 | 4 |
| | 2 | 0.4246 | 0 | 0 | 0 |
| | 3 | 0.0808 | 0.65 | 0 | 0 |
| | 4 | 0.0296 | 0.1214 | 0.858 | 0 |
| $n_f$ | 5 | 0.0142 | 0.0452 | 0.153 | 1.058 |

For transitions from values higher than the 5th energy level to values higher than the 6th energy level, the following formula is used:

$$f_{n_i \rightarrow n_f} = 1.96 \cdot n_i \cdot \frac{n_f - n_f^2}{\left(n_f^2 - n_i^2\right)^3} . \tag{3.8}$$

Table 1 and Eq. (3.8) have been compiled in Table 2 as:

**Table 2. Compiled Oscillator Strength for Transitions $n_i \rightarrow n_f$.**

| | | **$n_i$** | | | | | | | |
|---|---|---|---|---|---|---|---|---|---|
| | | 1 | 2 | 3 | 4 | 5 | 6 | 7 | 8 |
| | 2 | 0.4246 | 0 | 0 | 0 | 0 | 0 | 0 | 0 |
| | 3 | 0.0808 | 0.65 | 0 | 0 | 0 | 0 | 0 | 0 |
| | 4 | 0.0296 | 0.1214 | 0.858 | 0 | 0 | 0 | 0 | 0 |
| | 5 | 0.0142 | 0.0452 | 0.153 | 1.058 | 0 | 0 | 0 | 0 |
| | 6 | 0.009876 | 0.025844 | 0.064536 | 0.21171 | 1.590611 | 0 | 0 | 0 |
| | 7 | 0.00608 | 0.014757 | 0.031518 | 0.074839 | 0.243192 | 1.836257 | 0 | 0 |
| | 8 | 0.004014 | 0.009293 | 0.018098 | 0.036301 | 0.084599 | 0.274325 | 2.081673 | 0 |
| **$n_f$** | 9 | 0.002791 | 0.00626 | 0.011486 | 0.020814 | 0.040687 | 0.094093 | 0.305277 | 2.32696 |

In better models, oscillator strength data would be different for the transitions of different ions. The omission of this difference introduces some error into the CRASH opacity calculations. This error has not studied in our work.

### 3.3.2 Evaluation of Ionization Potentials

Approximate bounds for ionization potentials for xenon and beryllium are presented below. These values have been developed using data from the SPECTR-w3 database (Ref. 22) . There may be values that are more accurate available for the ionization potentials; however, these values are obtained from an extensive survey of open literature used to develop the database, and they are what CRASH opacity code uses. In the following table, upper and lower bounds have been listed for the first 28 ionization potentials for xenon. Higher ionization potentials are not relevant because the temperatures reached by the 1-D CRASH-like problem do not ionize these electrons. If the upper bound of a lower ionization potential overlaps with the lower bound of a higher ionization potential, then the bounds in the CRASH code are modified so that there is no overlap. Bounds for xenon ionization potentials are presented in Table 3. Table 4 is a table of the upper and lower bounds of beryllium used in the LH samples. Again, the values in the table may not reflect the best-known data, but only the range given by the database used by CRASH opacity code. This is more than adequate for the purposes of our UQ work.

**Table 3. Bounds for Relevant Xenon Ionization Potentials.**

| Ionization Potential | Lower Bound | Upper Bound |
|---|---|---|
| 1 | 12.1298 | 12.1299 |
| 2 | 21.20979 | 21.20979 |
| 3 | 32.123 | 32.123 |
| 4 | 45.515 | 47.845 |
| 5 | 58.2 | 61.18 |
| 6 | 70.035 | 73.625 |
| 7 | 95.6 | 100.5 |
| 8 | 109.5 | 115.1 |
| 9 | 166.55 | 175.05 |
| 10 | 196.65 | 206.75 |
| 11 | 226.8 | 238.4 |
| 12 | 256.9 | 270.1 |
| 13 | 287.05 | 301.75 |
| 14 | 317.15 | 333.45 |
| 15 | 349.35 | 367.25 |
| 16 | 379.85 | 399.35 |
| 17 | 410.35 | 431.45 |
| 18 | 440.9 | 463.5 |
| 19 | 558.2 | 586.8 |
| 20 | 592.5 | 622.9 |
| 21 | 626.8 | 659 |
| 22 | 661.15 | 695.05 |
| 23 | 706 | 742 |
| 24 | 737.568 | 781.45 |
| 25 | 831.4 | 855 |
| 26 | 855.847 | 912.85 |
| 27 | 1359 | 1453 |
| 28 | 1453.4 | 1528.5 |

**Table 4. Bounds for Beryllium Ionization Potentials.**

| Ionization Potential | Lower Bound | Upper Bound |
|---|---|---|
| 1 | 8.045 | 9.323 |
| 2 | 18.026 | 18.69 |
| 3 | 149.3 | 153.9 |
| 4 | 214.9 | 217.72 |

For plastic, the ionization potentials of each element are considered uncertain. The bounds are listed in Table 5, Table 6, and Table 7 for carbon, nitrogen, and oxygen, respectively.

**Table 5. Bounds for Carbon Ionization Potentials.**

| Ionization Potential | Lower Bound | Upper Bound |
|---|---|---|
| 1 | 10.772 | 11.26 |
| 2 | 24.047 | 24.383 |
| 3 | 45.786 | 47.888 |
| 4 | 64.374 | 64.4967 |
| 5 | 374.2 | 392.098 |
| 6 | 475.6 | 489.9933 |

**Table 6. Bounds for Nitrogen Ionization Potentials.**

| Ionization Potential | Lower Bound | Upper Bound |
|---|---|---|
| 1 | 13.8 | 14.5341 |
| 2 | 29.157 | 32.02 |
| 3 | 47.177 | 51.55 |
| 4 | 75.018 | 82.57 |
| 5 | 97.76 | 103.1 |
| 6 | 524 | 552.076 |
| 7 | 643.3 | 667.052 |

**Table 7. Bounds for Oxygen Ionization Potentials.**

| | Lower Bound | Upper Bound |
|---|---|---|
| 1 | 13.618 | 13.6181 |
| 2 | 34.552 | 35.121 |
| 3 | 54.548 | 60.73 |
| 4 | 77.224 | 77.4159 |
| 5 | 113.896 | 113.997 |
| 6 | 138.116 | 138.2 |
| 7 | 739.316 | 739.34 |
| 8 | 871.39 | 871.417 |

### 3.4 Use of LANL Opacities to Fix Up CRASH Opacities for Xenon

Los Alamos National Laboratory (LANL) and CRASH opacities have both been calculated for temperatures less than $kT = 50$ eV. LANL provided opacity tables at various densities between $10^{-7}$ and $10^{3}$ $\mathrm{g/cm^3}$ for temperatures of 10, 12.5, 15, 20, 25, 30, 40, and 50 eV. The capability of calculating opacities for each of the three types of interaction has been added to the CRASH code, and a method to adjust the variance in the CRASH opacities to be centered on the LANL opacity values has been developed.

The LANL opacity tables for xenon span only the temperature range of 10 eV to 50 eV; however, the CRASH-like Test Problems encounter temperatures above and below the LANL range. There are three cases for the temperature values, which are:

$$\begin{aligned} &T_C < T_{L,\min} \\ &T_{L,lower} < T_C < T_{L,upper} \\ &T_{L,\max} < T_C \end{aligned} \tag{3.9}$$

where $T_C$ is a CRASH opacity table temperature point, and $T_L$ is a LANL opacity table temperature point. We describe the case where the CRASH opacity temperature point for a given set of uncertain parameters, $\sigma_{C,r}(\tilde{T}_i)$, lies between two LANL opacity temperature points, $\sigma_{L,r}(T_i)$ and $\sigma_{L,r}(T_{i+1})$. The subscript, $r$, indicates a specific interaction type such as bound-bound, bound-free, or free-free. The linearly interpolated value of the LANL opacity temperature point is defined as:

$$\sigma_{L,r}(\tilde{T}_i) = \sigma_{L,r}(T_i) + \left[\sigma_{L,r}(T_{i+1}) - \sigma_{L,r}(T_i)\right]\frac{(\tilde{T}_i - T_i)}{(T_{i+1} - T_i)} \tag{3.10}$$

We define an uncertainty factor that accounts for the difference between the mean value of the CRASH opacity point $\bar{\sigma}_{C,r}(\tilde{T}_i)$ and the CRASH opacity point for a given set of uncertain parameters $\sigma_{C,r}(\tilde{T}_i)$, as:

$$\Sigma_{C,r}(\tilde{T}_i) = \frac{\sigma_{C,r}(\tilde{T}_i)}{\bar{\sigma}_{C,r}(\tilde{T}_i)} \tag{3.11}$$

To correct our CRASH opacities using the CRASH uncertainty factor and the LANL interpolation factor, the following equation is used:

$$\hat{\sigma}_{C,r}(\tilde{T}_i) = \sigma_{L,r}(\tilde{T}_i)\cdot\Sigma_{C,r}(\tilde{T}_i). \tag{3.12}$$

The uncertainty factor is not affected by the values of the LANL table, so extrapolation formulas on either side are needed. To do the extrapolation for higher temperatures the following formula is used

$$\hat{\sigma}_{C,r}(\tilde{T}_i) = \frac{\sigma_{L,r}(T_{\max})}{\sigma_{C,r}(T_{\max})}\sigma_{C,r}(\tilde{T}_i), \tag{3.13}$$

where $T_i > T_{\max}$ and for this case $T_{\max} = 50$ eV. For lower temperatures, the following formula is used

$$\hat{\sigma}_{C,r}(T_i) = \frac{\sigma_{L,r}(T_{\min})}{\sigma_{C,r}(T_{\min})}\sigma_{C,r}(T_i), \tag{3.14}$$

where $T_i < T_{\min}$ and for this case $T_{\min} = 10$ eV.

Some of the advantages of, and the motivations behind, this method are now discussed. First, it is known that the CRASH opacity model has shortcomings. These can be partly overcome by centering the uncertainty of the CRASH opacities on the LANL values. Our goal is not to obtain perfect opacities, but to obtain reasonable values around which to study the effects of uncertainties. We assess that the CRASH model does produce reasonable quantifications of uncertainty for each of the contributing interactions used to calculate the opacity as functions of the uncertainties in inputs. For the extrapolation regions, we assume that the LANL opacities and CRASH opacities vary proportionally, which is demonstrated by using a proportionality constant in Eq. (3.14).

In the following section, we describe the test problems and QOIs used to test this methodology. This includes two 1-D CRASH-like test problems, which are employed to screen uncertain parameters for use in a 2-D CRASH-like problem.

# 4 TEST PROBLEMS FOR UNCERTAINTY QUANTIFICATION METHODOLOGY

We are interested in computing QOIs for a two-dimensional RT problem referred to as the CRASH-like test problem. The CRASH-like test problem is designed to provide distributions of ARDs downstream from the shock in the tube. This problem is a computationally expensive problem to solve; so, we devised two simpler one-dimensional RT problems used to screen parameters. After the screening, the smaller set of parameters can be used in the more computationally expensive model. The one-dimensional problems, radial and axial slices of the two-dimensional problems, are described in the following sections.

## 4.1 Description of 2-D CRASH-like Problem

The 2-D CRASH-like problem is the most relevant test problem to the CRASH problem. This problem is a much more computationally demanding problem; however, from the screening we perform on the first two test problems, we are able to reduce the input space. It is shown in Figure 4.

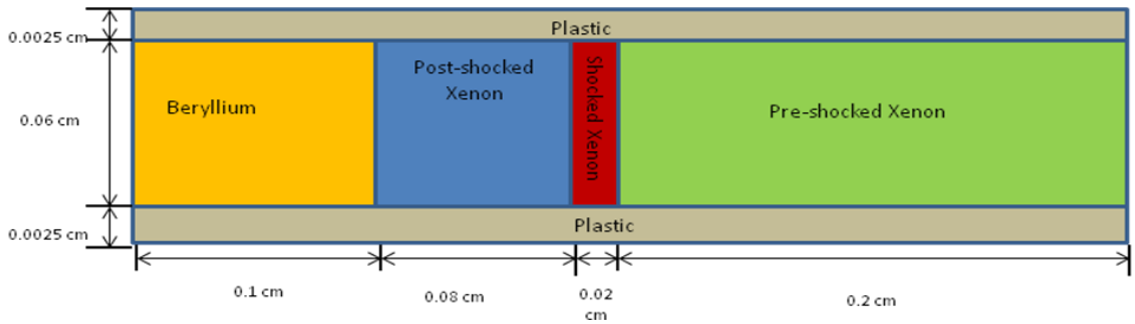


**Figure 4. 2-D Cartesian CRASH-like Test Problem.**

The initial conditions for the test problem are described in

Table 8, and the zoning is described in Table 9.

**Table 8. Initial Conditions of the 2-D CRASH-like Test Problem.**

| | Temperature (eV) | Density ($g/cm^3$) | Source ($eV/cm^3$-s) |
|---|---|---|---|
| **Beryllium** | 10 | 0.008 | 0 |
| **Post-Shocked Xe** | 10 | 0.018 | 0 |
| **Shocked Xe** | 10 | 0.1 | $4.25*10^{33}$ |
| **Pre-Shocked Xe** | 10 | 0.00589 | 0 |
| **Plastic** | 10 | 1.43 | 0 |

**Table 9. Axial and Radial Zoning**

| | Dimension (cm) | # of Cells | Log Factor |
|---|---|---|---|
| Axial | (0,0.1) | 25 | N/A |
| | (0.1, 0.18) | 20 | N/A |
| | (0.18, 0.2) | 5 | N/A |
| | (0.2, 0.4) | 50 | N/A |
| Radial | (0,0.0025) | 2 | N/A |
| | (0.0025,0.045626) | 6 | N/A |
| | (0.045625, 0.6) | 16 | N/A |
| | (0.06,0.0625) | 16 | 1.1065 |

We found from scoping studies that the beryllium and post-shocked xenon did not affect the QOIs; so, these parts we not included in the actual model. The coordinate point (0,0) corresponds to the lower left hand corner of the shocked xenon. Also, we have defined a region using logarithmic spacing with a log factor. To compute a cell width with this factor and the previous cell width, which is the original zone width for the first cell, as

$$\Delta x_{i+1} = \Delta x_i \sum_{n=0}^{n-1} f^n , \tag{4.1}$$

where $\Delta x_i$ is the original or previous zone width, $\Delta x_{i+1}$ is the width of the new cell, *f* is the log factor, and *n* is the number of cells remaining. So, for successive cell calculation *n* will decrease by one. For the 2-D CRASH-like test problem a Level Symmetric 10 quadrature set and 10 energy groups were used.

In the next section results of the screening and uncertainty quantification for the test problems is presented. We present results of both the ionization potentials and oscillator strengths. We now describe the Latin Hypercube Sampling.

### 4.1.1 Description of Quantities of Interest

The complex experiments that motivate our work involve radiation and hydrodynamics. One of the interesting phenomena in the CRASH experiments is the wall shock in the plastic, which develops in front of the shocked xenon. This is driven purely by radiation absorption in the wall, which means that radiation-transport-only calculations can provide meaningful information about the effects of the radiation.

The QOIs chosen in the 1-D studies are meant to inform the 2-D problem about the variance in propagation of radiation in both the pre-shocked xenon and plastic. The radiation must propagate through in order to create a wall shock. Thus, if an uncertain parameter is important in the 1-D studies we expect that it may be important in the 2-D studies. Likewise, we expect that if a parameter is unimportant in the 1-D studies it should not be important in the 2-D studies, at least if the 1-D QOIs are chosen well.

The QOIs relevant for the wall shock in the 2-D problem are ARDs in the plastic:

- the ARD at 0.1 $\mu$ m in plastic 0.02 cm from preshocked xenon at 0.258 ns,
- the ARD at 0.25 $\mu$ m in plastic 0.02 cm from preshocked xenon at 0.59 ns,
- and the time when the temperature reaches 40 eV at 0.1 $\mu$ m in plastic 0.02 cm from preshocked xenon.

**4.2 1-D Axial CRASH-like Problem Uncertainty Quantification**

The 1-D Axial CRASH-like problem is one of the two 1-D test problems used for screening purposed for the 2-D CRASH-like test problem. The two cases we examine are allowing either the ionization potentials or the oscillator strengths to be uncertain.

For the ionization potential case, which includes xenon and beryllium (a total of 32 ionization potentials), we use 1,000 and 32,000 LHD to create samples of uncertain ionization potentials. These samples of ionization potentials are used in the CRASH opacity code to compute samples of uncertain opacity tables. The samples of opacity tables are used in PDT to solve the RT. QOIs are extracted from the PDT solutions, and sensitivity analysis is used to perform parameter screening.

For the oscillator strength case, which includes 36 transitions, we use 1,000 and 32,000 LHD to create realizations of oscillator strengths. These realizations of oscillator strengths are used in the CRASH opacity code to compute samples of uncertain opacity tables. The samples of opacity tables are used in PDT to solve the RT. QOIs are extracted from the PDT solutions, and sensitivity analysis is used to perform parameter screening.

### 4.2.1 Description of 1-D Axial CRASH-like Problem

The densities of the materials in the 1-D Axial CRASH-like problem depicted in Figure 5 are given in Table 10.

**Table 10. Initial Conditions of the 1-D Axial CRASH-like Problem.**

| | Temperature (eV) | Density (g/cm$^3$) | Source (eV/cm$^3$-s) | # of cells |
|---|---|---|---|---|
| **Beryllium** | 10 | 0.008 | 0 | 25 |
| **Post-Shocked Xe** | 10 | 0.018 | 0 | 20 |
| **Shocked Xe** | 10 | 0.1 | $4.25*10^{33}$ | 5 |
| **Pre-Shocked Xe** | 10 | 0.00589 | 0 | 50 |

Initially, all of the material is at a temperature of 10 eV, and the shocked xenon contains a source of $4.25 \cdot 10^{33}$ eV/cm$^3$ – s. For this calculation, a Level Symmetric 8 quadrature set and 10 energy groups are used.

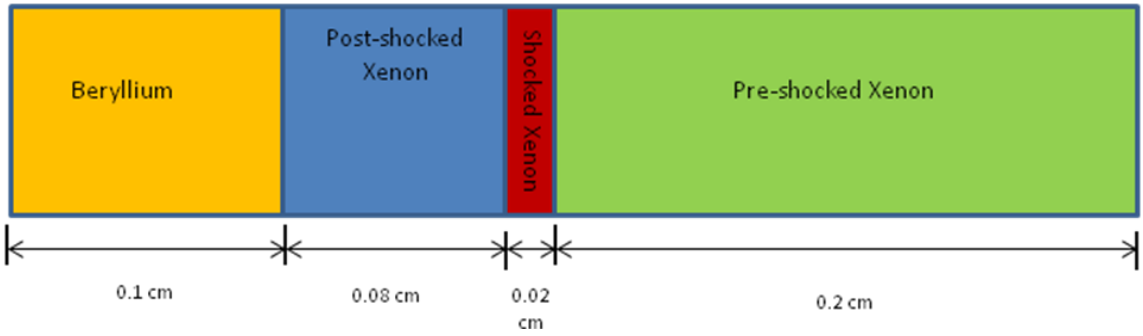


**Figure 5. Dimensions of 1-D Axial CRASH-like problem.**

The QOIs chosen for this problem are described in the following section.

### 4.2.2 Description of Quantities of Interest

We are interested in studying QOIs that are relevant to the 2-D case. For the 1-D problem, this is an area in the preshocked region. We have chosen the absorption rate densities at the following points:

- 0.1 cm to the right of the shocked xenon at 0.1 ns,
- 0.1 cm to the right of the shocked xenon at 1 ns.

Thus, we have two QOIs for this case.

## 4.3 1-D Radial CRASH-like Test Problem Uncertainty Quantification

The 1-D Radial CRASH-like problem is used to reduce the set of parameters for the 2-D CRASH-like test problem. The two cases we examine are allowing either the ionization potentials or the oscillator strengths to be uncertain.

For the ionization potential case, which includes the polyimide tube (constituted of oxygen, nitrogen, carbon, and hydrogen) and xenon (a total of 49 ionization potentials), we use 1,000 and 32,000 LHD to create samples of uncertain ionization potentials. These samples of ionization potentials are used in the CRASH opacity code to compute samples of uncertain opacity tables. The samples of opacity tables are used in PDT to solve the RT. QOIs are extracted from the PDT solutions, and sensitivity analysis is used to perform parameter screening.

For the oscillator strength case, which includes 36 transitions, we use 1,000 and 32,000 LHD to create realizations of oscillator strengths. These realizations of oscillator strengths are used in the CRASH opacity code to compute samples of uncertain opacity tables. The samples of opacity tables are used in PDT to solve the RT. QOIs are

extracted from the PDT solutions, and sensitivity analysis is used to perform parameter screening.

### 4.3.1 Description of 1-D Radial CRASH-like Problem

The dimensions, densities, and initial conditions of the materials in the 1-D Axial CRASH-like problem are depicted in Figure 6 and Table 11.

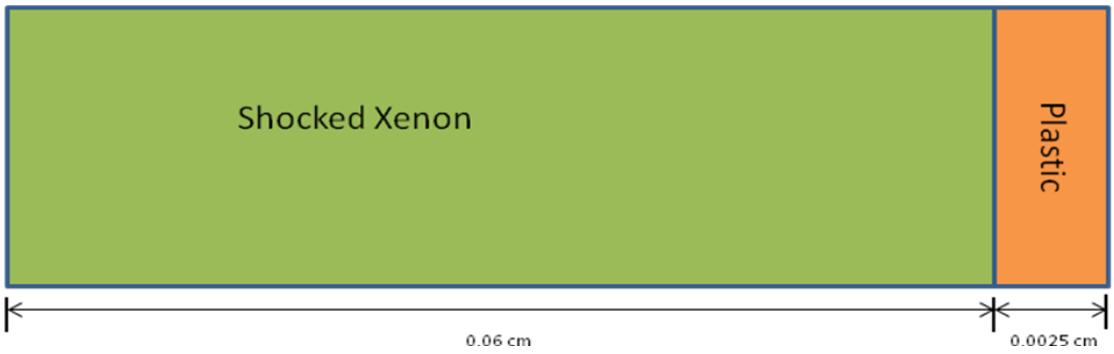


**Figure 6. Dimensions of Radial 1-D CRASH-like problem.**

**Table 11. Initial Conditions of the Radial 1-D CRASH-like Test Problem.**

| | Temperature (eV) | Density ($g/cm^3$) | Source ($eV/cm^3$-s) | # of Radial Cells | Log Factor |
|---|---|---|---|---|---|
| **Shocked Xe** | 10 | 0.1 | $4.25*10^{33}$ | 160 | 0.95 |
| **Plastic** | 10 | 1.43 | 0 | 160 | 1.02065 |

For the Radial 1-D CRASH-like test problem, a Level Symmetric 16 quadrature set and 10 energy groups were used.

### 4.3.2 Description of Quantities of Interest

For the 1-D Radial CRASH-like test problem, we describe the QOIs that are studied during the analysis. The 4 QOIs, which are all ARDs, are listed below:

- at 0.01 $\mu$ m at 0.01 ns,
- at 0.1 $\mu$ m at 0.01 ns,
- at 0.01 $\mu$ m at 0.1 ns,
- and at 0.1 $\mu$ m at 0.1 ns.

This gives us four QOIs to use to screen parameters.

**4.4 Method to Quantify Uncertainty and Analyze Sensitivity**

Since it is computationally costly to sample points using the radiation transport code for the 2-D CRASH-like problem, we need to build a simpler model that is easier to analyze but that adequately describes the output space. One method is to build a Bayesian multivariate adaptive regression spline (BMARS) model to approximate the relationship between the uncertain parameters and the output space. After this model is created, samples can be taken from the computationally simpler model (emulator) to perform sensitivity analysis on the uncertain parameters.

Two ways to analyze the sensitivity of our QOI to the input parameters are to examine the main and marginal effects. The main effect of a parameter describes how the variance changes if all inputs are held constant except for that parameter across the design space. The marginal effect of a parameter describes how the variance changes if each input is held constant across the design space. Thus, if the variance is small for the main effect for a parameter, it means that this parameter does not contribute much to the variance in the output response. On the contrary, if the variance is small for the marginal effect for a parameter, it means that the parameter contributed much to the variance in the output response.

In the following section, we apply the new UQ techniques that we have presented to the CRASH-relevant problems that we have described.

# 5 RESULTS

As a preliminary examination of how the uncertainties in a given set of input parameters affect a given QOI, we can look at the distribution of that QOI that is generated by sampling the input space. If there is not much spread in the distribution, we can determine that the uncertainties in the given set of input parameters do not have a significant effect on the particular QOI. If there is a reasonable spread in the QOI, then we can use sensitivity analysis to determine whether there is a particular subset of uncertain parameters that account for a large fraction of the uncertainty in the QOI. This work can be done with the BMARS low-order emulator. Both the main and marginal effects are used to study the sensitivity.

We can use the subsets of the 1-D test problems to create a reduced set of uncertain parameters for the 2-D test problem. In the following sections, we present the results for the two 1-D test problems and determine the subset of uncertain parameters for the 2-D CRASH-like problem.

## 5.1 Results for the 1-D Axial CRASH-like Test Problem

The most basic result that can be given is a distribution of the quantity of interest for a given 1-D CRASH-like problem, produced by sampling many points in the uncertain input space. In the following sections, we present the results of the uncertainty quantification for the 1-D Axial CRASH-like test problem for many cases. These cases include allowing the ionization potentials or the oscillator strengths to vary. Also, we compare these results to those created when we adjust the CRASH Xenon opacity using the LANL data.

### 5.1.1 Results Using Ionization Potentials

We have solved the 1-D Axial CRASH-like test problem allowing the ionization potentials of the xenon and beryllium to vary uniformly between the values in Table 3 and Table 4. The PDF, main effect, and marginal effect plots for the 1,000 sample LHD are presented in Figure 7 through Figure 12, and the results for the 32,000 sample LHD are presented in Figure 13 through Figure 18.

#### 5.1.1.1 Results with the 1,000 Sample Latin Hypercube Design

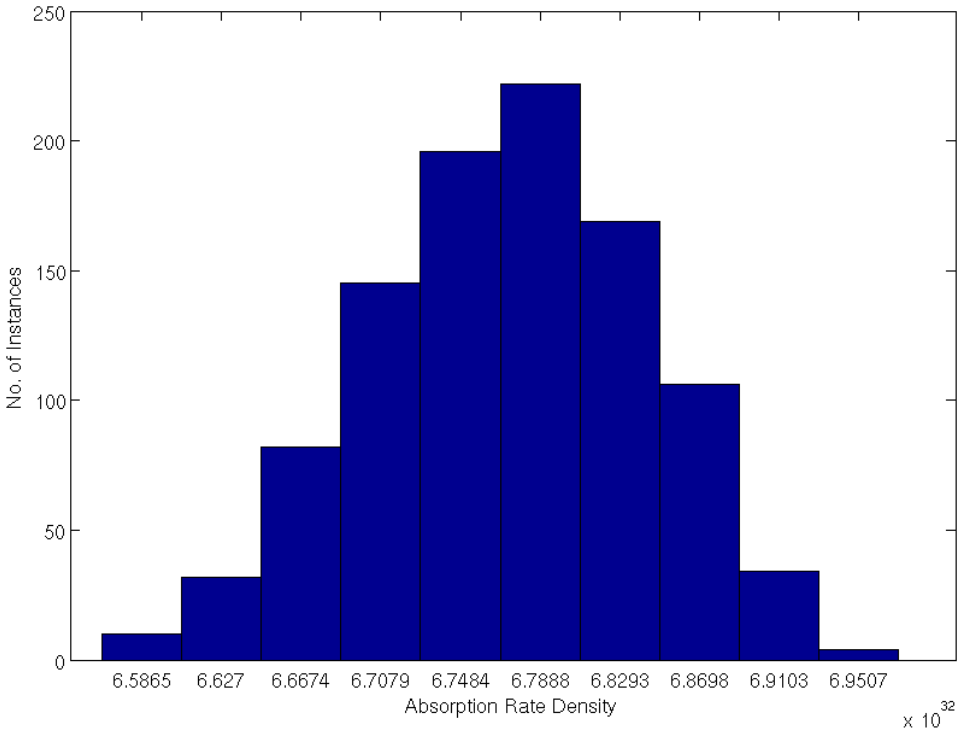


**Figure 7. QOI 1 for 1-D Axial Ionization Potential Problem with 1,000 Sample LHD.**

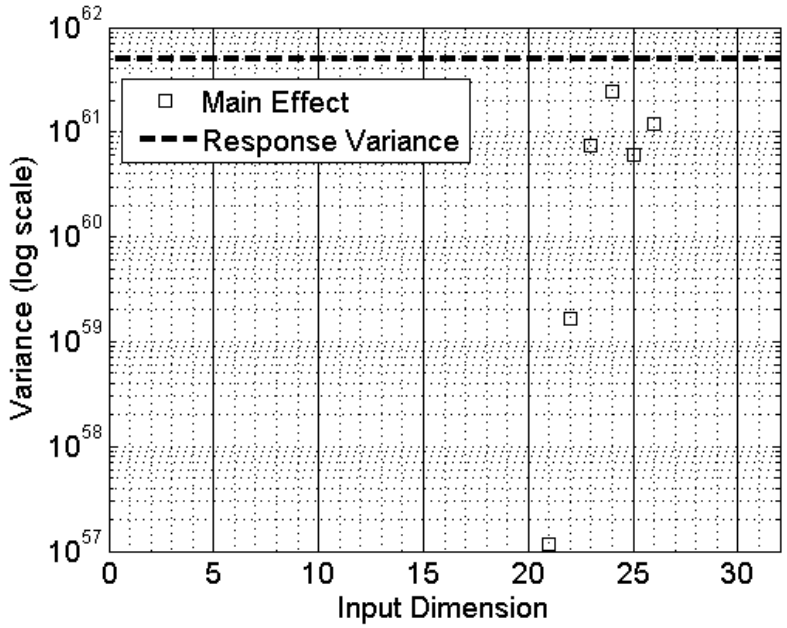


**Figure 8. QOI 1 Main Effects for 1-D Axial Ionization Potential Problem with 1,000 Sample LHD.**

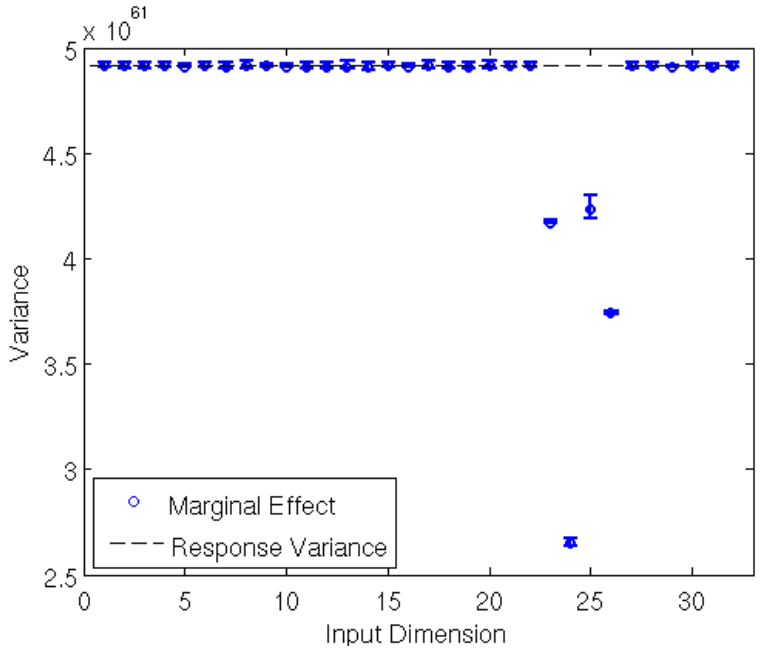


**Figure 9. QOI 1 Marginal Effects for 1-D Axial Ionization Potential Problem with 1,000 Sample LHD.**

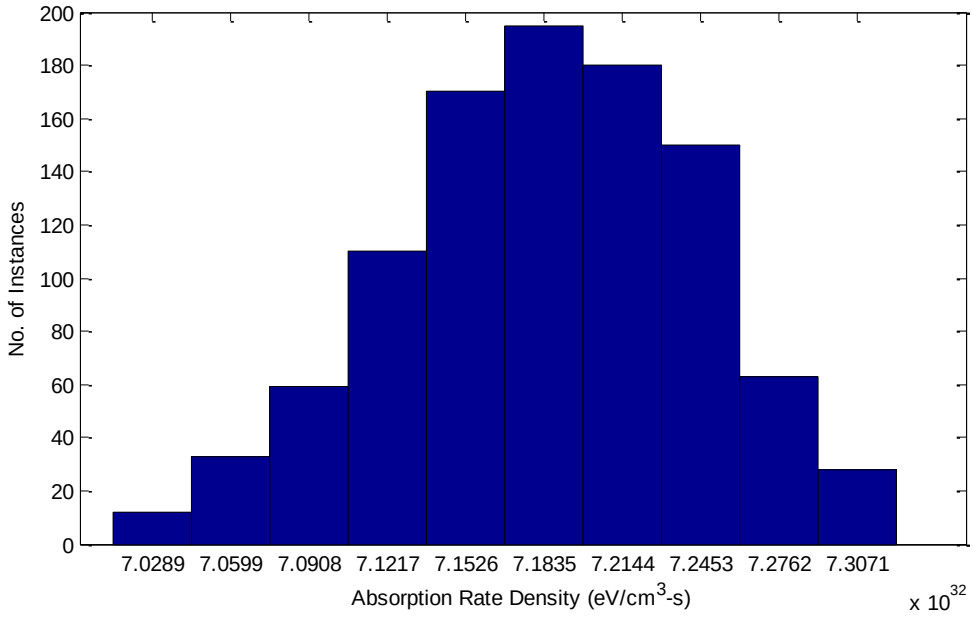


**Figure 10. QOI 2 for the 1-D Axial Ionization Potential Problem with 1,000 Sample LHD.**

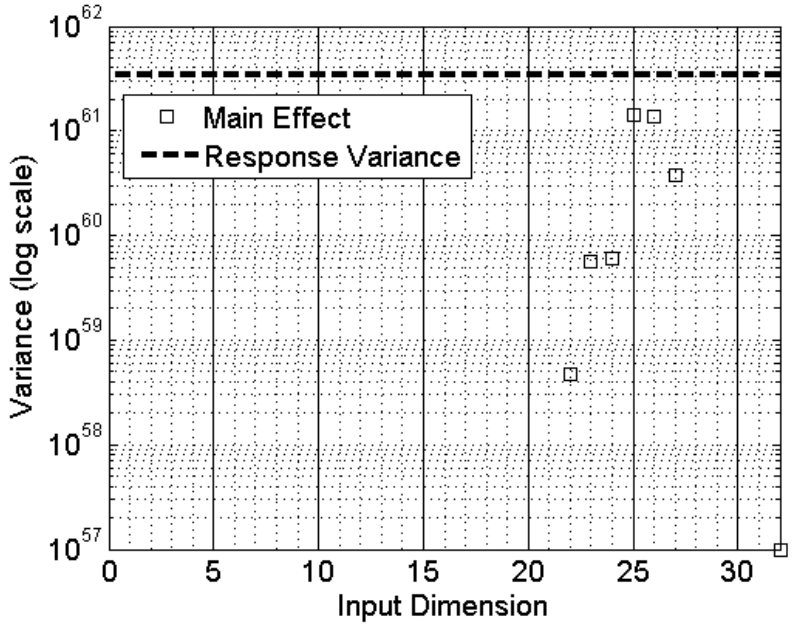


**Figure 11. QOI 2 Main Effects for 1-D Axial Ionization Potential Problem with 1,000 Sample LHD.**

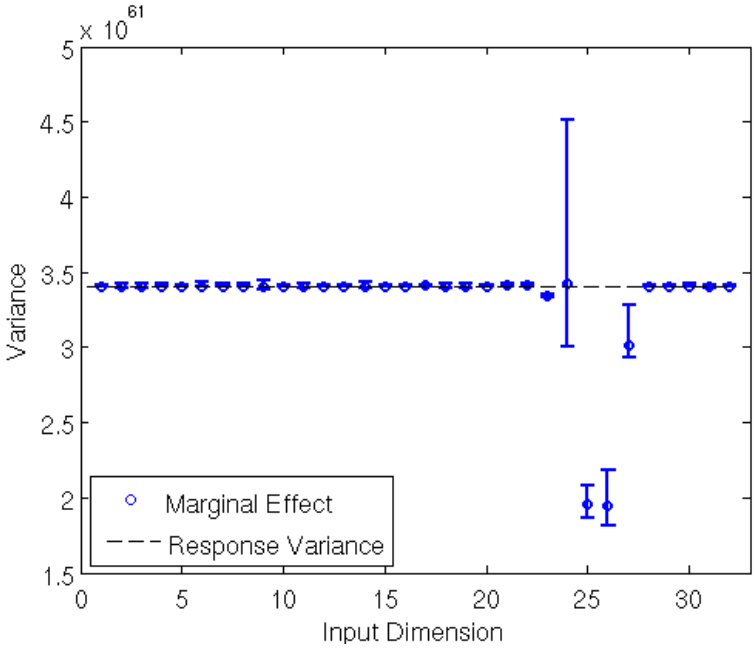


**Figure 12. QOI 2 Marginal Effects for 1-D Axial Ionization Potential Problem with 1,000 Sample LHD.**

### 5.1.1.2 Results with the 32,000 Sample Latin Hypercube Design

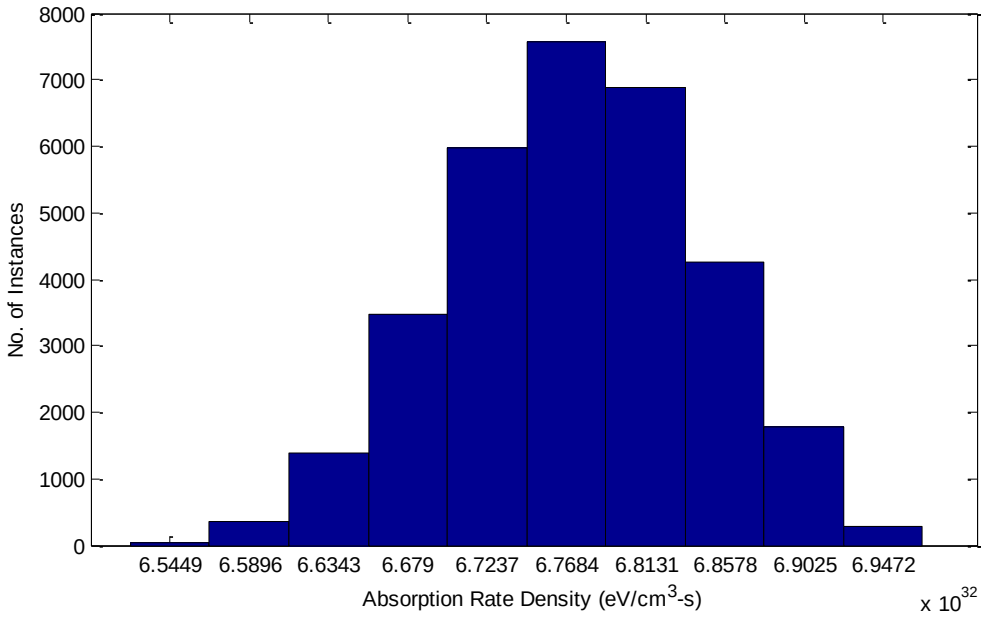


**Figure 13. QOI 1 for the 1-D Axial Ionization Potential Problem with 32,000 Sample LHD.**

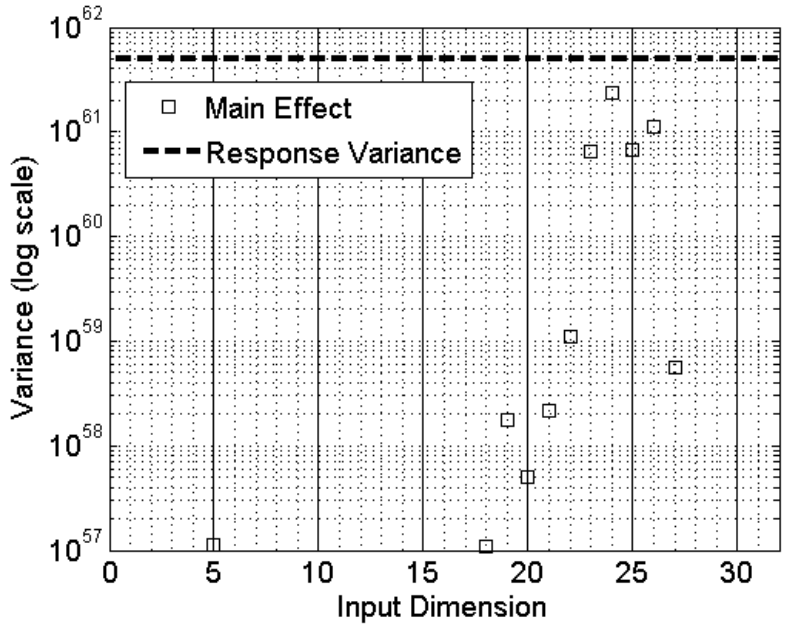


**Figure 14. QOI 1 Main Effects for 1-D Axial Ionization Potential Problem with 32,000 Sample LHD.**

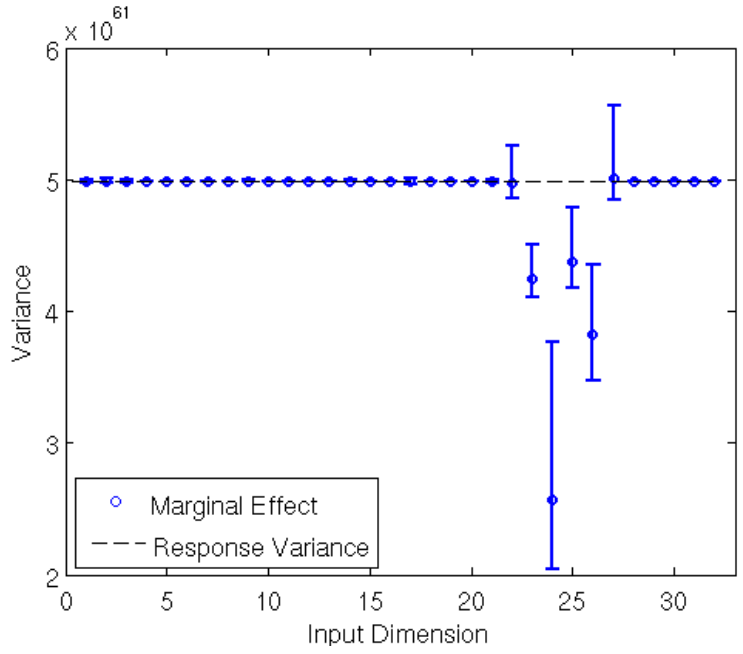


**Figure 15. QOI 1 Marginal Effects for 1-D Axial Ionization Potential Problem with 32,000 Sample LHD.**

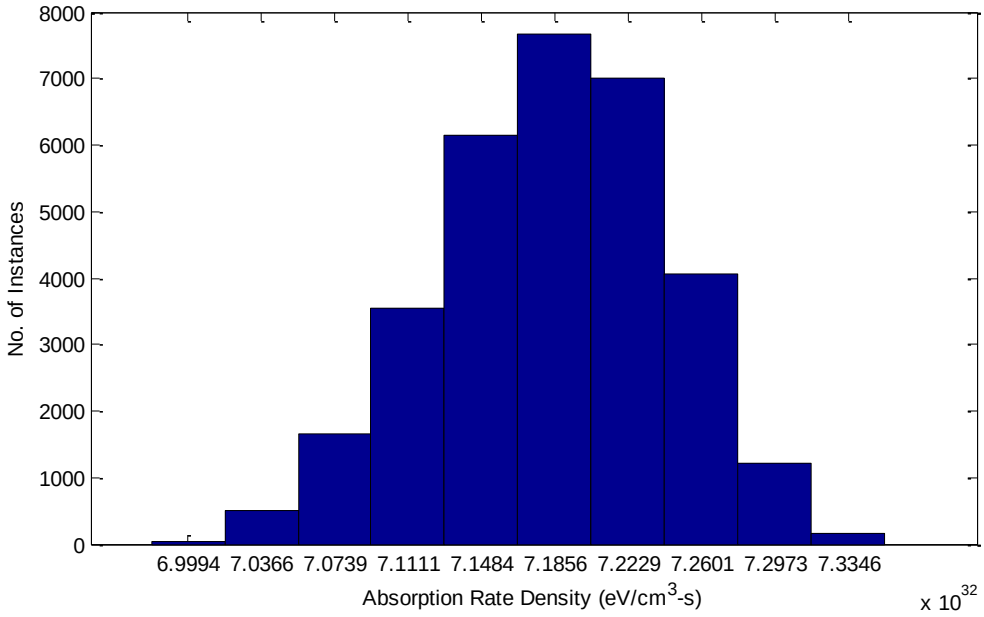


**Figure 16. QOI 2 for the 1-D Axial Ionization Potential Problem with 32,000 Sample LHD.**

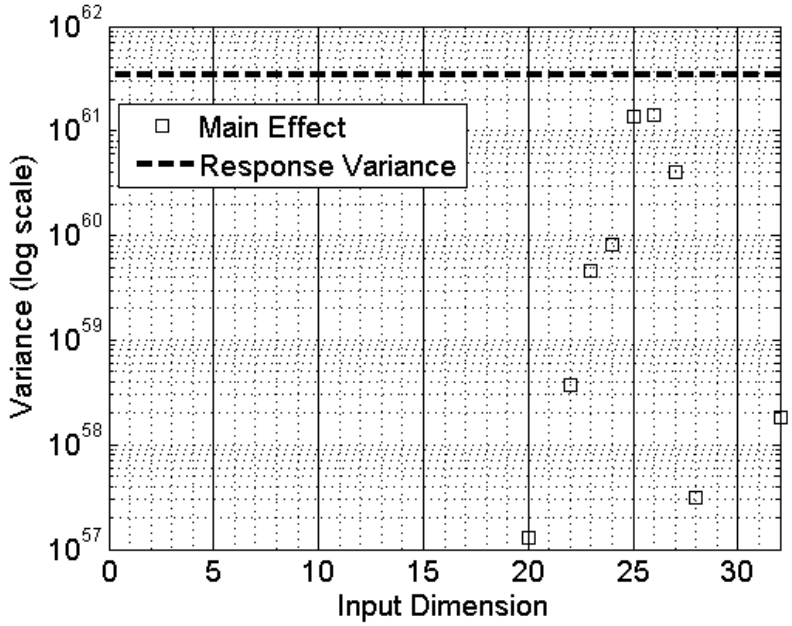


**Figure 17. QOI 2 Main Effects for 1-D Axial Ionization Potential Problem with 32,000 Sample LHD.**

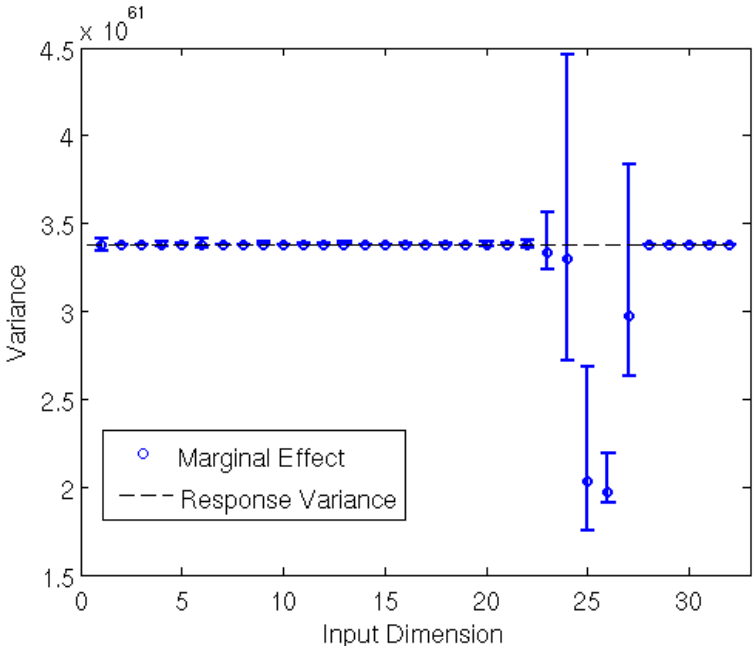


**Figure 18 QOI 2 Marginal Effects for 1-D Axial Ionization Potential Problem with 32,000 Sample LHD.**

#### 5.1.1.3 Important Parameters for the 1-D Axial Ionization Potential Case

The important parameters for the 1,000 and 32,000 LHDs are presented in Table 12 .

**Table 12. Important Parameters for the 1-D Axial Ionization Potential Case.**

| LHD | QOI | $10^{-4}$ Screening | $10^{-3}$ Screening |
|---|---|---|---|
| 1000 | 1 | 22, 23, 24, 25, 26 | 22,23,24,25,26 |
| | 2 | 22 - 27 | 22,23,24,25,26,27 |
| 32000 | 1 | 19-27 | 22,23,24,25,26,27 |
| | 2 | 21-28, 32 | 22,23,24,25,26,27 |

We observe that the 22nd through 27th ionization potentials of xenon are important for the 1-D Axial problem for both screening criteria. These parameters become important for high temperatures when xenon can be ionized to this level, which occurs for both QOIs. Also, we see that the results for the second QOI include a larger set of parameters, and that set of parameters completely subsumes the first QOI. Also, we see that the fourth ionization potential of beryllium (the 32nd parameter) is important in only one case, but it is still kept for the 2-D CRASH-like test problem.

### 5.1.2 Results Using Ionization Potentials with Adjusted Xenon Opacity

Recall from section 3.4 that we devised a method to adjust the mean of the CRASH xenon opacities using the LANL opacities while still keeping the useful uncertainty, which was created by varying uncertain parameters in the CRASH opacity calculations. In this section, we present PDF, main effect, and marginal effects plots for the uncertainty analysis using adjusted xenon opacities in the 1-D axial CRASH-like problem. Results for the 1,000 sample LHD are presented in Figure 19 through Figure 24, and results for the 32,000 sample LHD are presented in Figure 25 through Figure 30.

#### 5.1.2.1 Results with the 1,000 Sample Latin Hypercube Design

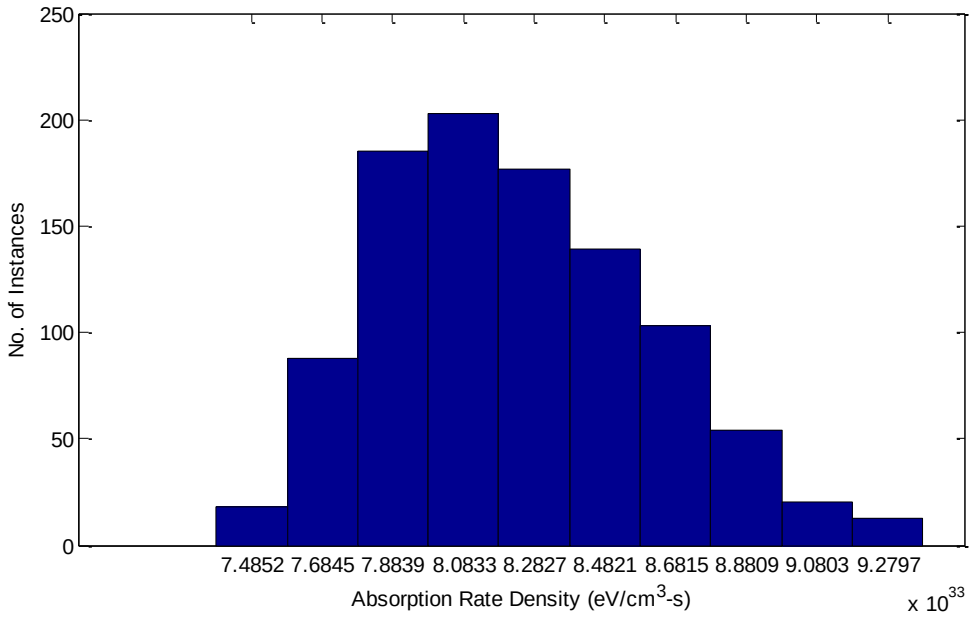


**Figure 19. QOI 1 for the Xenon Adjusted 1-D Axial Ionization Potential Problem with 1,000 Sample LHD.**

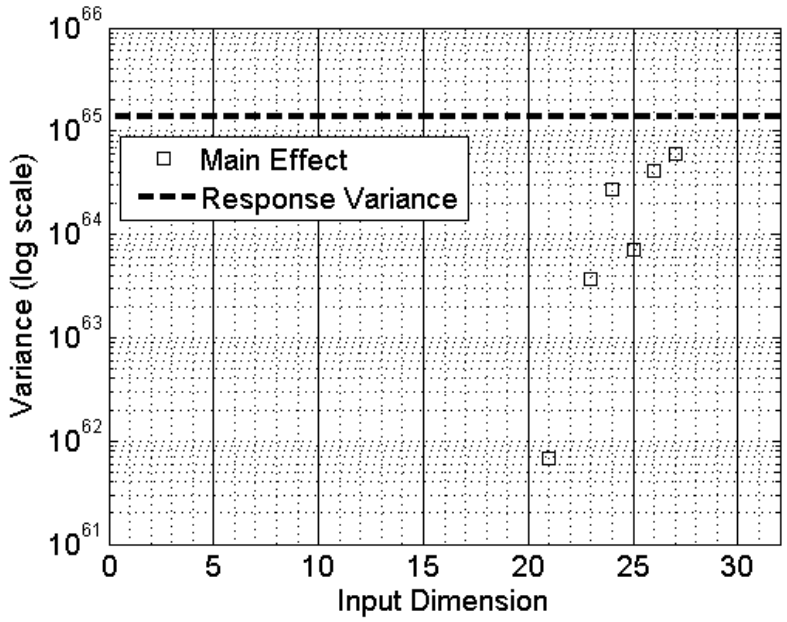


**Figure 20. QOI 1 Main Effects for Xenon Adjusted 1-D Axial Ionization Potential Problem with 1,000 Sample LHD.**

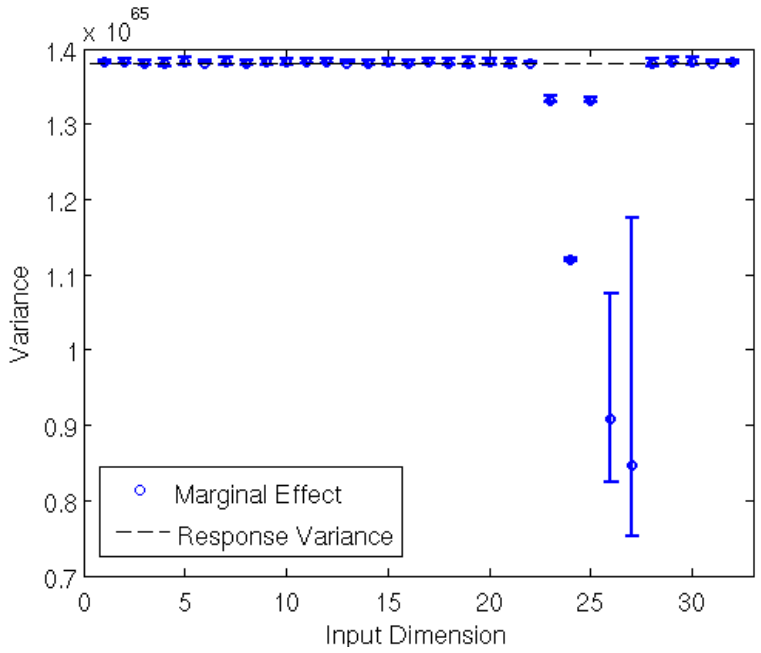


**Figure 21. QOI 1 Marginal Effects for Xenon Adjusted 1-D Axial Ionization Potential Problem with 1,000 Sample LHD.**

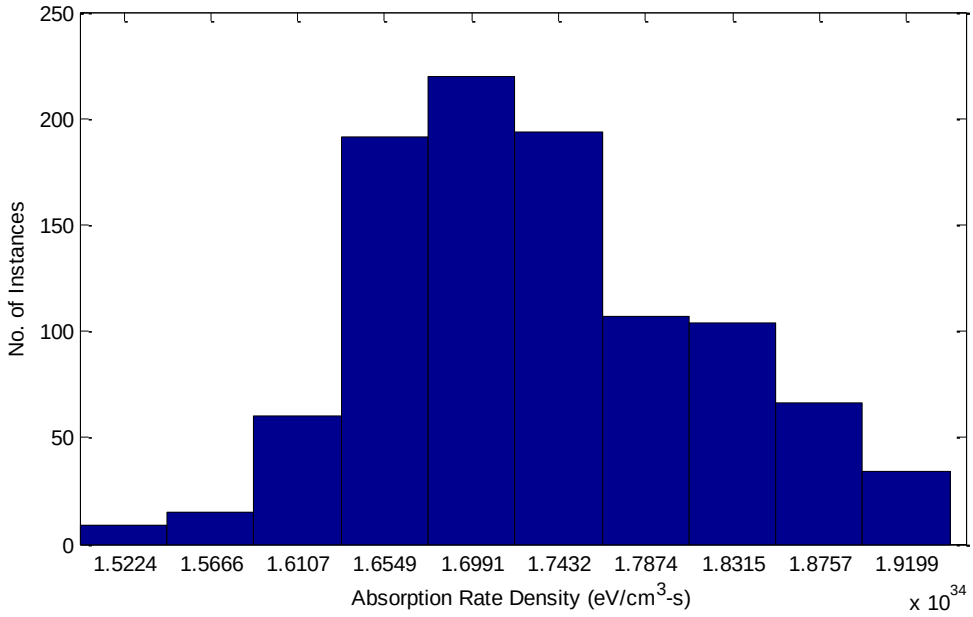


**Figure 22. QOI 2 for the Xenon Adjusted 1-D Axial Ionization Potential Problem with 1,000 Sample LHD.**

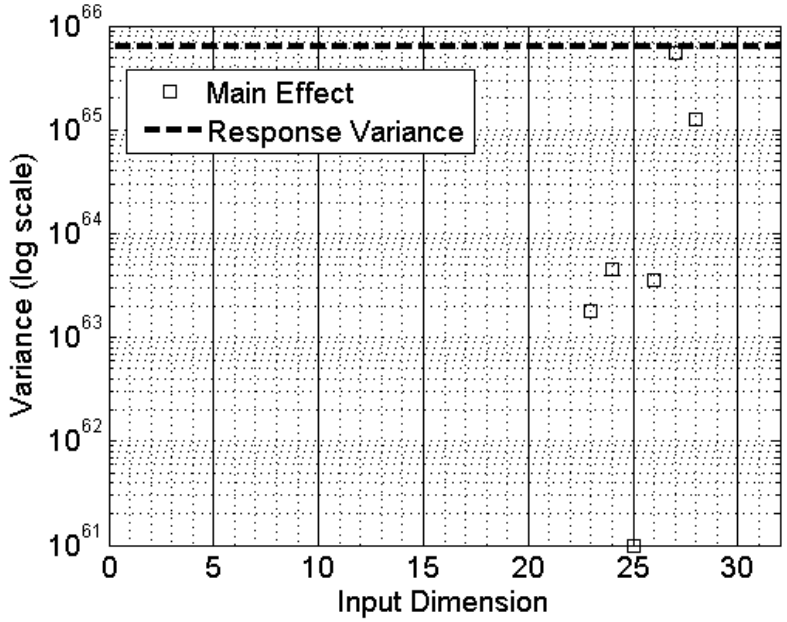


**Figure 23. QOI 2 Main Effects for Xenon Adjusted 1-D Axial Ionization Potential Problem with 32,000 Sample LHD.**

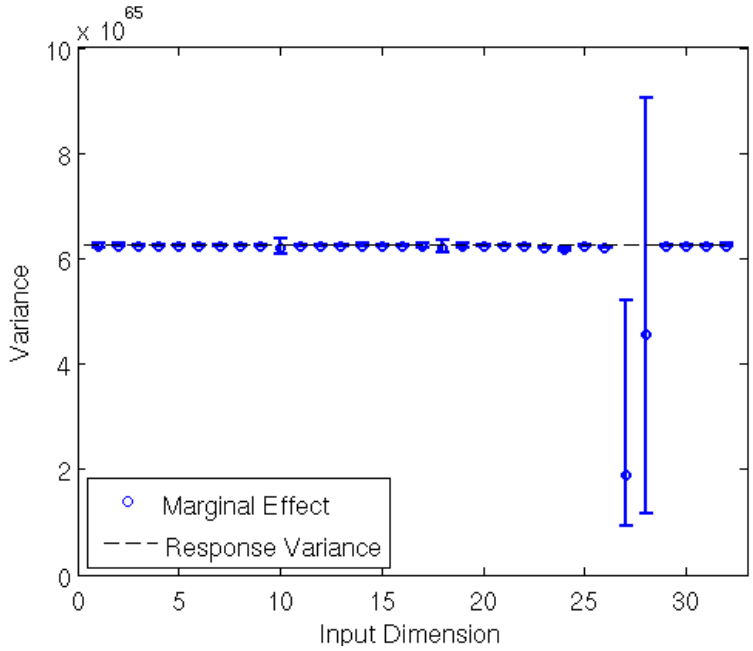


**Figure 24. QOI 2 Marginal Effects for Xenon Adjusted 1-D Axial Ionization Potential Problem with 32,000 Sample LHD.**

### 5.1.2.2 Results with the 32,000 Sample Latin Hypercube Design

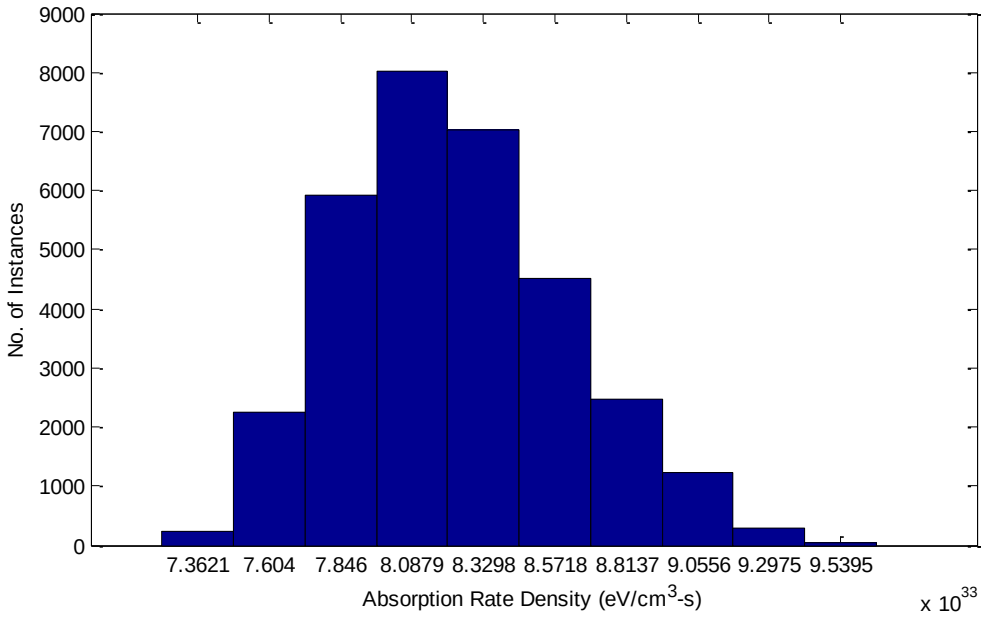


**Figure 25. QOI 1 for the Xenon Adjusted 1-D Axial Ionization Potential Problem with 32,000 Sample LHD.**

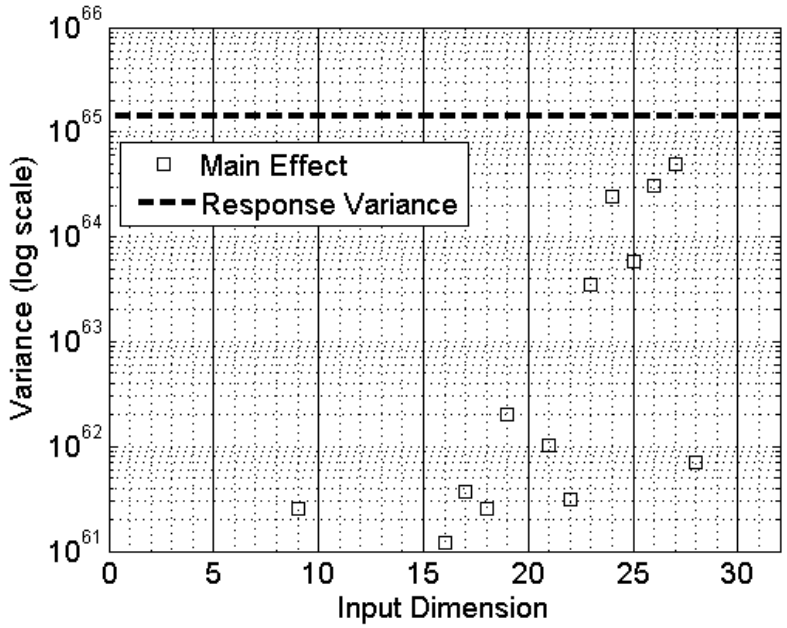


**Figure 26. QOI 1 Main Effects for Xenon Adjusted 1-D Axial Ionization Potential Problem with 32,000 Sample LHD.**

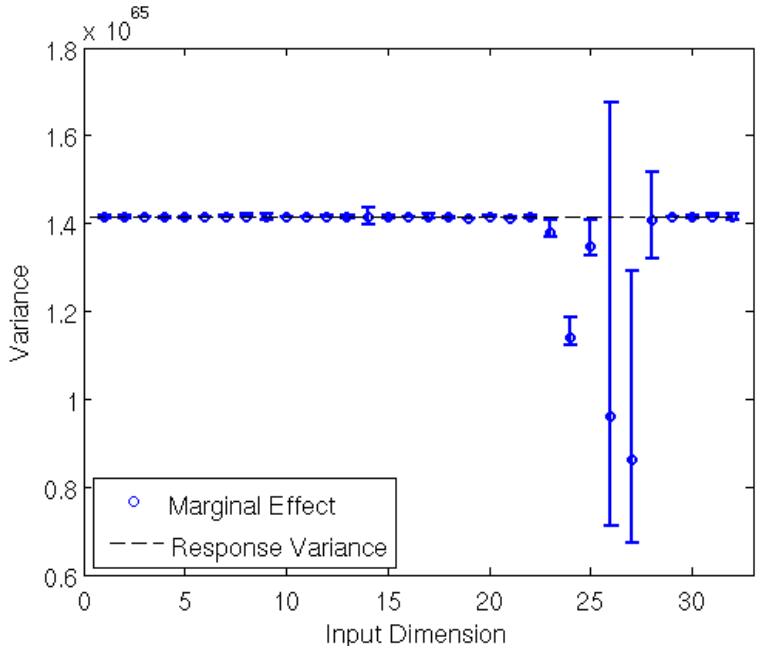


**Figure 27. QOI 1 Marginal Effects for Xenon Adjusted 1-D Axial Ionization Potential Problem with 32,000 Sample LHD.**

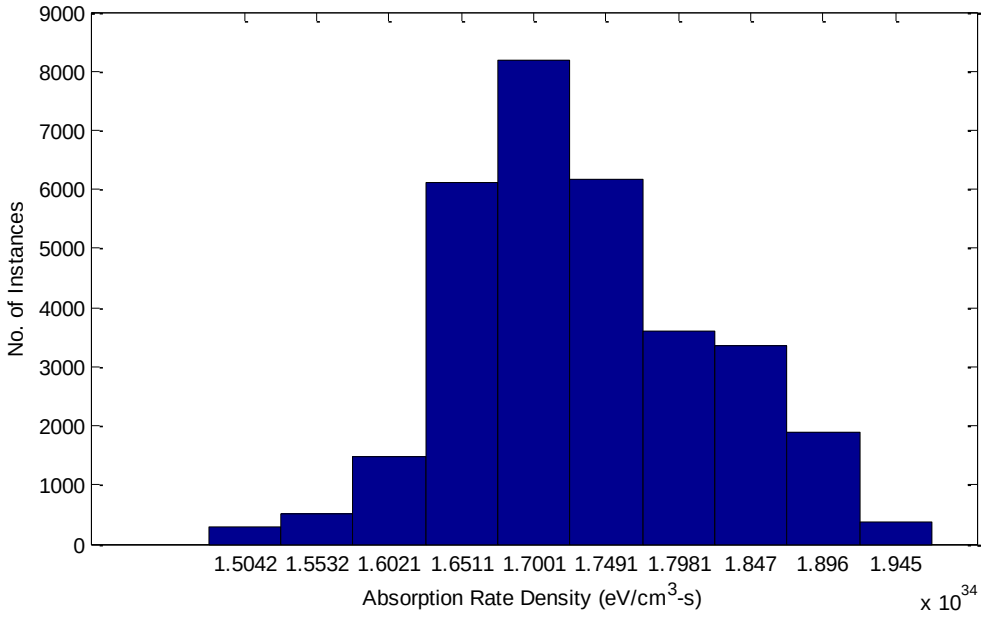


**Figure 28. QOI 2 for the Xenon 1-D Axial Ionization Potential Problem with 32,000 Sample LHD.**

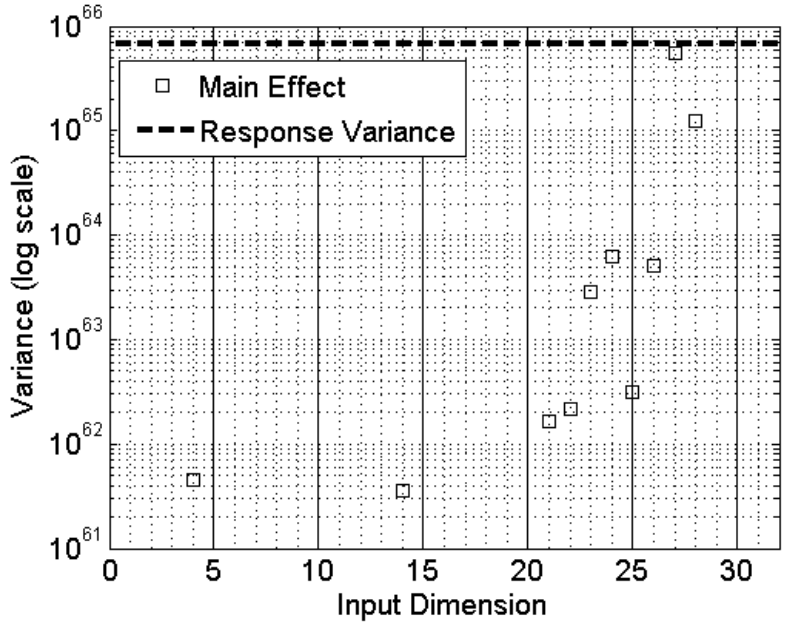


**Figure 29. QOI 2 Main Effects for Xenon Adjusted 1-D Axial Ionization Potential Problem with 32,000 Sample LHD.**

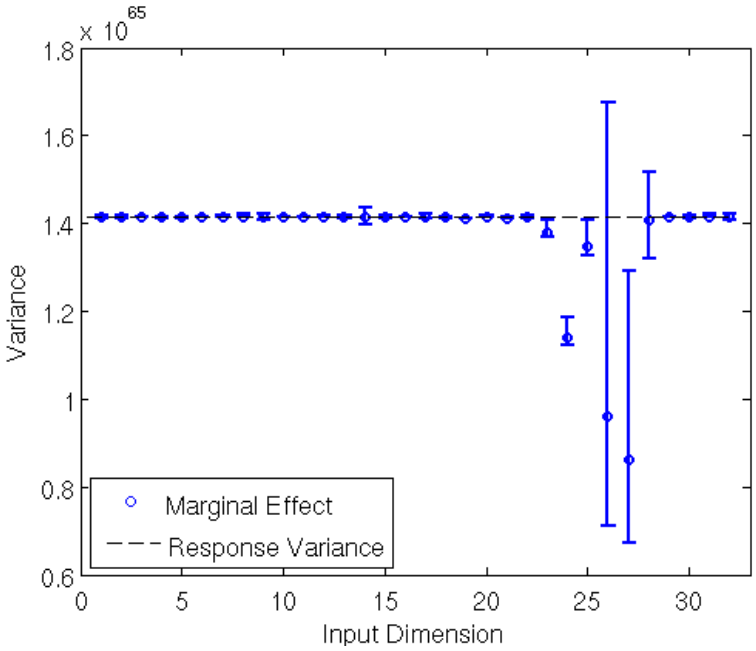


**Figure 30. QOI 2 Marginal Effects for Xenon Adjusted 1-D Axial Ionization Potential Problem with 32,000 Sample LHD.**

#### 5.1.2.3 Important Parameters for the 1-D Axial Ionization Potential Case with Adjusted Xenon Opacities

The results of the screening study are presented in Table 13.

**Table 13. Important Parameters for the 1-D Axial Ionization Potential Case with Adjusted Xenon Opacities.**

| LHD | QOI | $10^{-4}$ Screening | $10^{-3}$ Screening |
|---|---|---|---|
| 1000 | 1 | 21, 23-27 | 23,24,25,26,27 |
| | 2 | 23, 24, 26, 27, 28 | 23,24,26,27,28 |
| 32000 | 1 | 9, 16, 17, 18, 19, 21-28 | 19,21,23,24,25,26,27 |
| | 2 | 21 - 28 | 23,24,26,27,28 |

When we compare the important parameter set for the adjusted xenon opacities with the unadjusted xenon opacities, we see that there are many more xenon potentials that are important. The $9^{th}$, $16^{th}$, $17^{th}$, and $18^{th}$ xenon ionization potentials, not included in the parameter set using CRASH xenon opacities, are included in the final set of important parameters. The xenon opacity is higher when it is adjusted to the LANL xenon opacity, which causes the QOIs to be sensitive to the more xenon ionization potentials.

### 5.1.3 Results Using Oscillator Strengths

We have tabulated the oscillator strengths that are used in the CRASH code in Table 2. It is known that oscillator strengths have some associated uncertainty with them. We model the uncertainty in the oscillator strengths using a uniform distribution of 5% about their nominal values. In this section, we present results for the uncertainty analysis. PDF, main effect, and marginal effect plots are presented for the 1,000 sample LHD in Figure 31 through Figure 36 and for the 32,000 sample LHD in Figure 37 through Figure 42.

### 5.1.3.1 Results with the 1,000 Sample Latin Hypercube Design

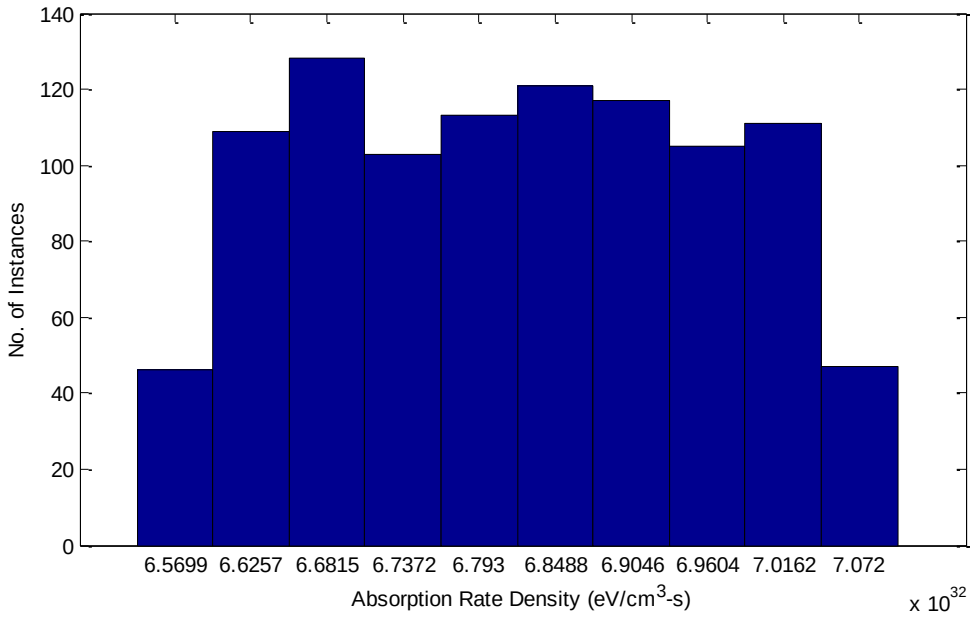


**Figure 31. QOI 1 for the 1-D Axial Oscillator Strength Problem with 1,000 Sample LHD.**

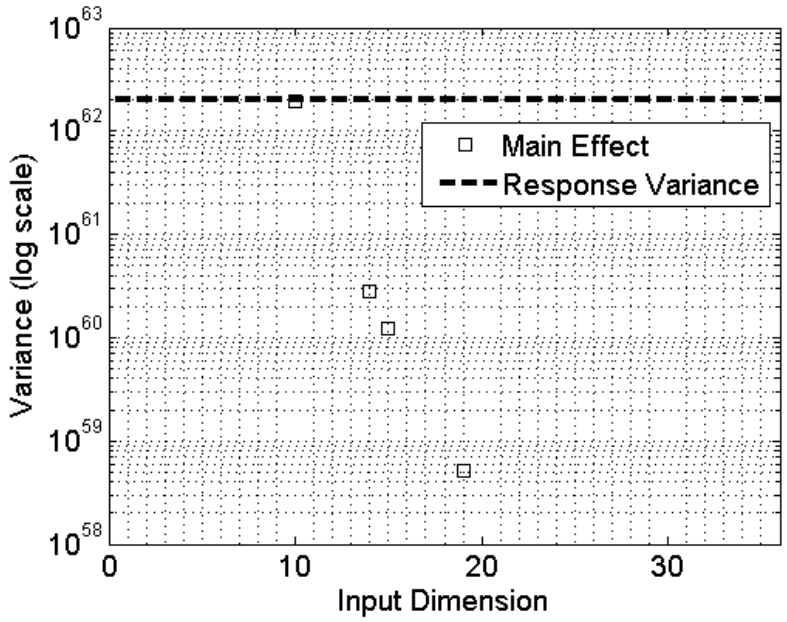


**Figure 32. QOI 1Main Effects for 1-D Axial Oscillator Strength Problem with 1,000 Sample LHD.**

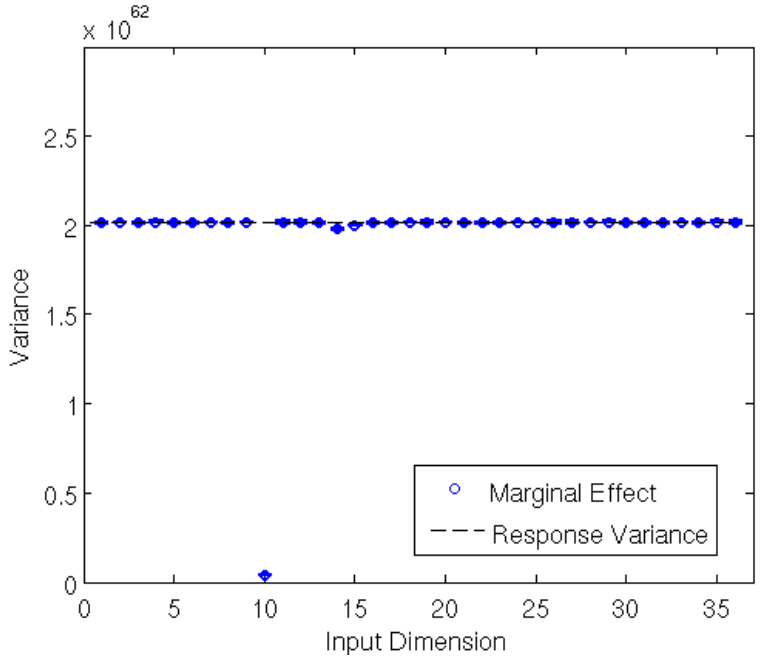


**Figure 33. QOI 1 Marginal Effects for 1-D Axial Oscillator Strength Problem with 1,000 Sample LHD.**

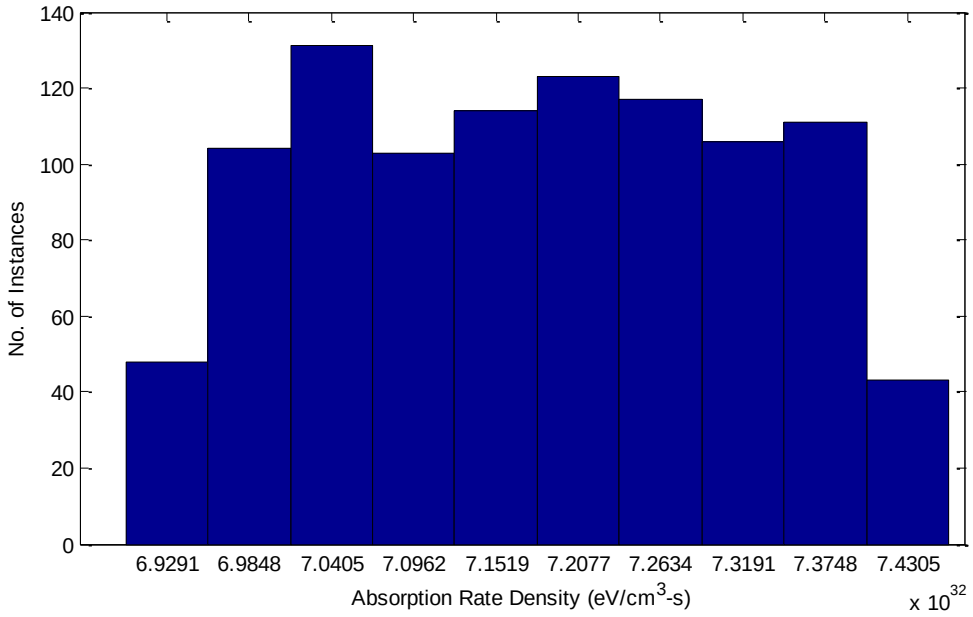


**Figure 34. QOI 2 for the 1-D Axial Oscillator Strength Problem with 1,000 Sample LHD.**

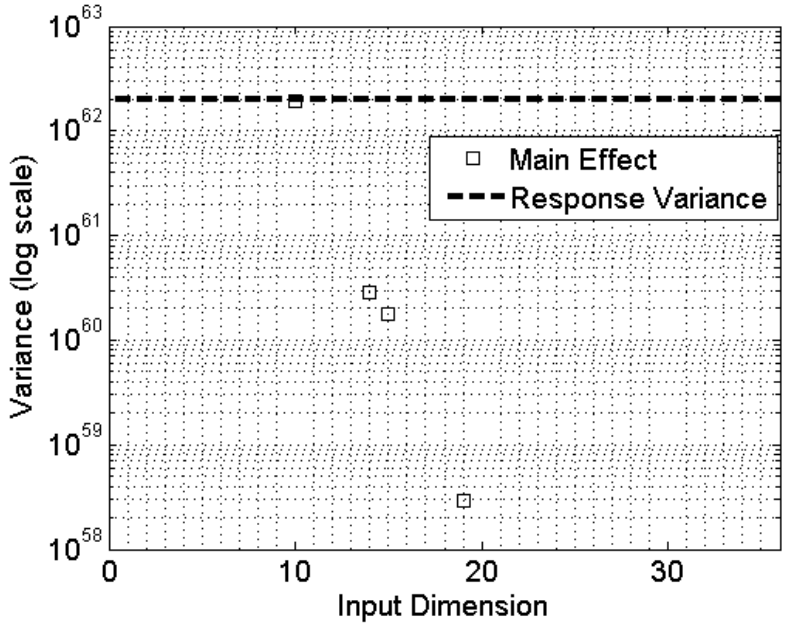


**Figure 35. QOI 2 Main Effects for 1-D Axial Oscillator Strength Problem with 1,000 Sample LHD.**

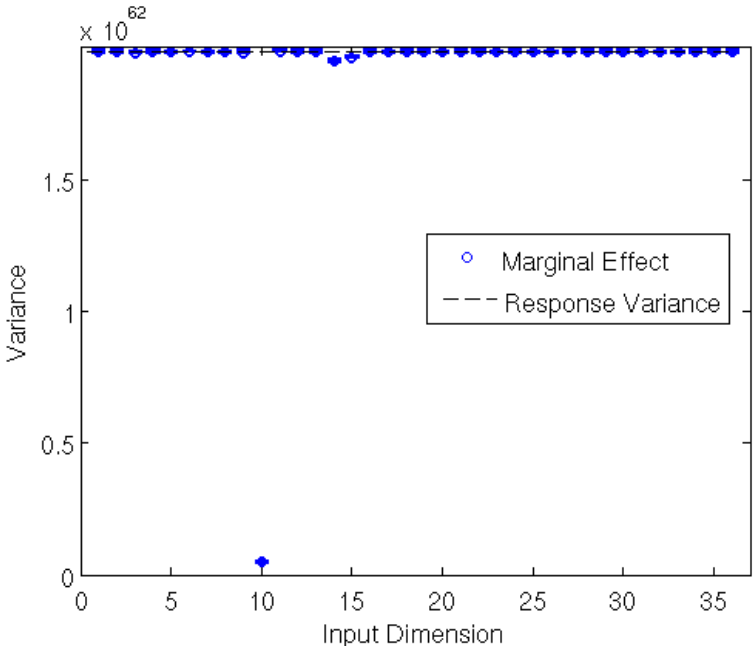


**Figure 36. Marginal Effects for the 1-D Axial Oscillator Strength Problem with 1,000 Sample LHD.**

### 5.1.3.2 Results for the 32,000 Sample Latin Hypercube Design

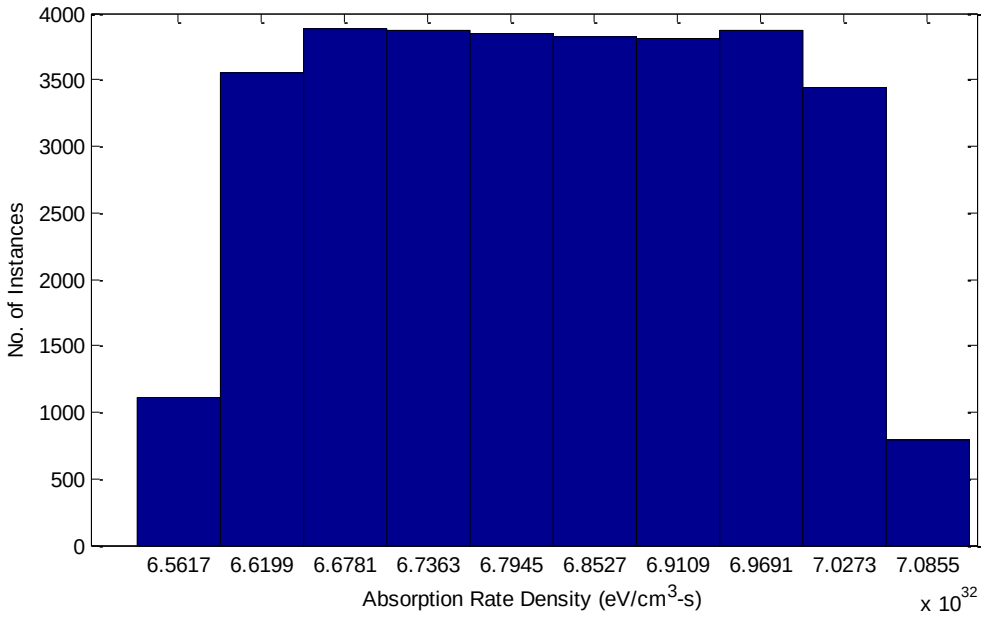


**Figure 37. QOI 1 for the 1-D Axial Oscillator Strength Problem with 32,000 Sample LHD.**

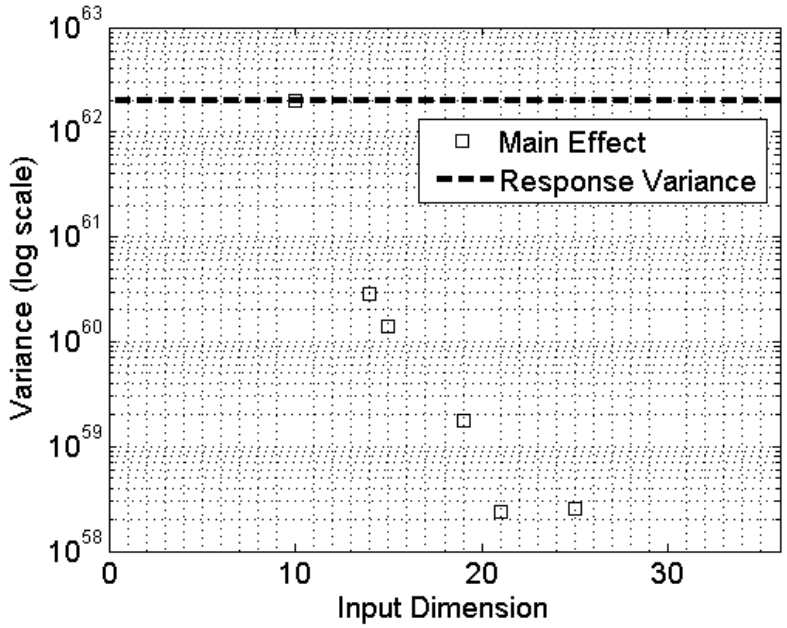


**Figure 38. QOI 1 Main Effects for 1-D Axial Oscillator Strength Problem with 32,000 Sample LHD.**

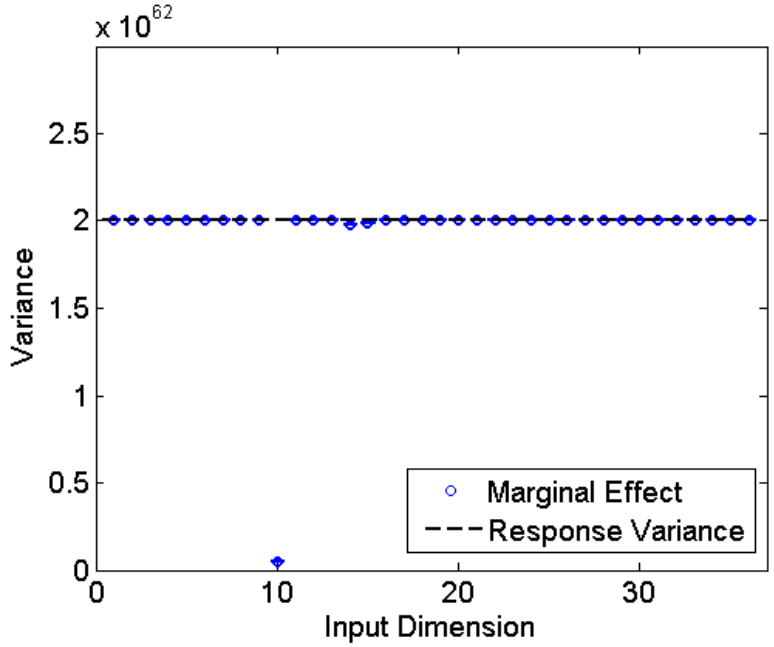


**Figure 39. QOI 1 Marginal Effects for the 1-D Axial Oscillator Strength Problem with 32,000 Sample LHD.**

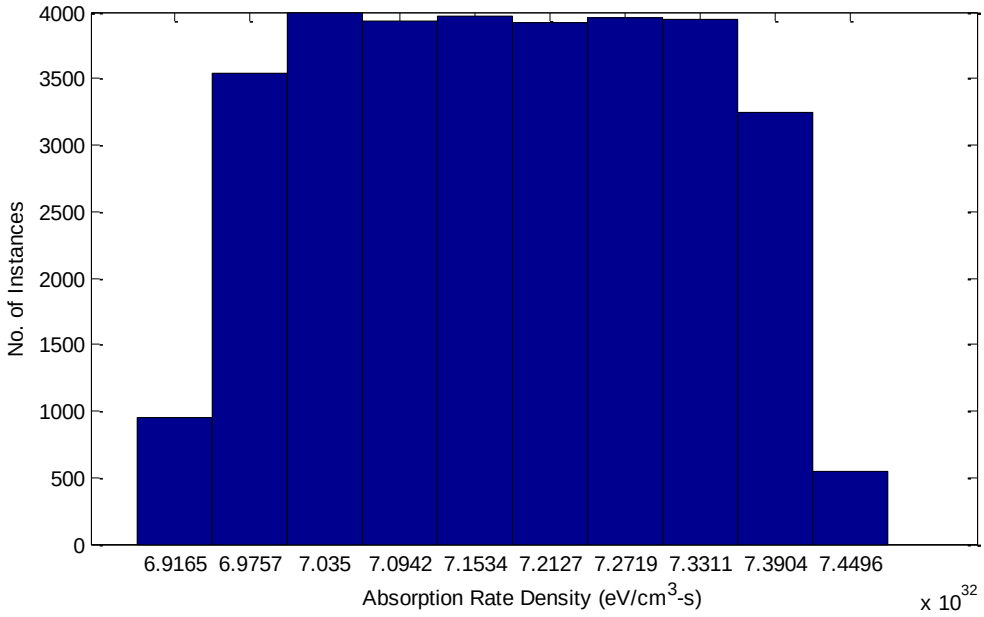


**Figure 40. QOI 2 for the 1-D Axial Oscillator Strength Problem with 32,000 Sample LHD.**

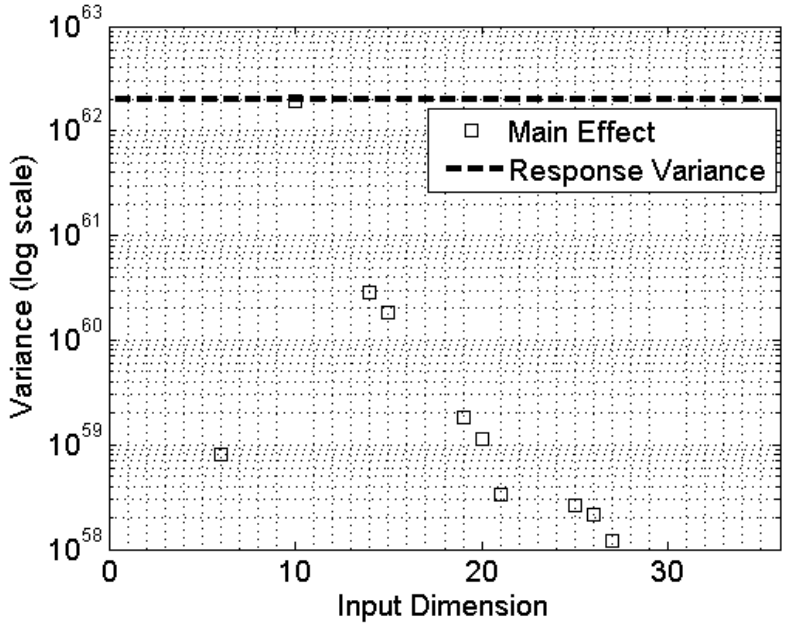


**Figure 41. QOI 2 Main Effects for 1-D Axial Oscillator Strength Problem with 32,000 Sample LHD.**

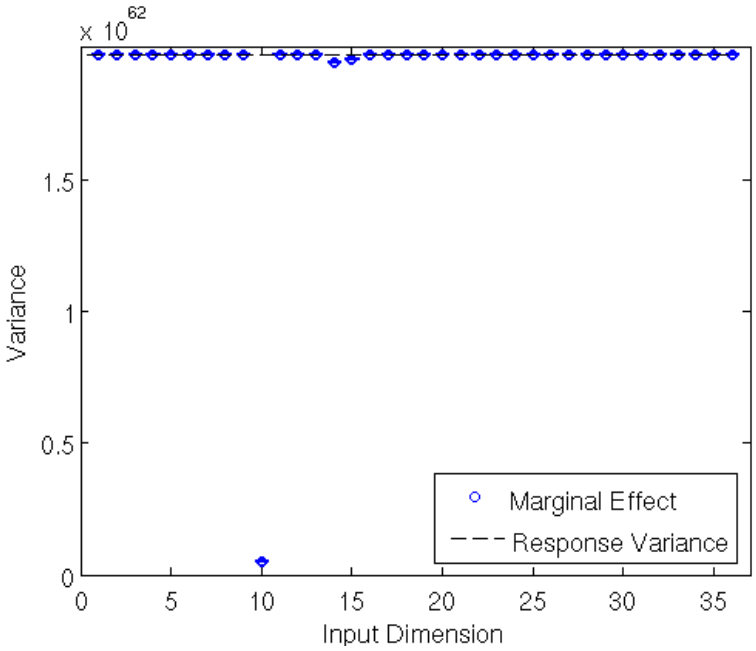


**Figure 42. QOI 2 Marginal Effects for the 1-D Axial Oscillator Strength Problem with 32,000 Sample LHD.**

### 5.1.3.3 Important Parameters for 1-D Axial Oscillator Strength Case.

Results for the screening analysis are presented in Table 14.

**Table 14. Important Parameters for the 1-D Axial Oscillator Strength Case.**

| LHD | QOI | $10^{-4}$ Screening | $10^{-3}$ Screening |
|---|---|---|---|
| 1000 | 1 | 10, 14, 15, 19 | 10,14,15 |
| | 2 | 10, 14, 15, 19 | 10,14,15 |
| 32000 | 1 | 10, 14, 15, 19, 21, 25 | 10,14,15,19 |
| | 2 | 6, 10, 14, 15, 19, 20, 21, 25, 26 | 10,14,15,19 |

In general, an oscillator strength is not important if there are no electrons occupying the orbital for its transition. The 10th, 15th, and 21st parameters correspond to

transitions 4 to 5, 5 to 6, and 6 to 7, which have very large values of oscillator strengths and have electrons populating the orbitals. The other important parameters in these lists correspond to orbitals that are occupied by electrons. The 32,000 LHD case for both QOIs includes more important parameters, and the more inclusive screening case includes more parameters. Recall that the only difference between the two QOIs is the observation time, which are 0.1 ns and 1 ns. The parameters set kept for the two QOIs only slightly differ, which means that the conditions affecting both QOIs are very similar. If these sets were very different, we would need to add more QOIs and perform more sensitivity analysis to understand how the conditions affecting the QOIs differed.

### 5.1.4 Results Using Oscillator Strengths with Adjusted Xenon Opacity

We perform the same uncertainty analysis as is done in the previous section; however, we use the LANL-adjusted xenon opacity. We present the PDF, main effect, and marginal effect plots for the 1,000 sample LHD in Figure 43 through Figure 48 and for the 32,000 sample LHD in Figure 49 through Figure 54.

#### 5.1.4.1 Results with the 1,000 Sample Latin Hypercube Design

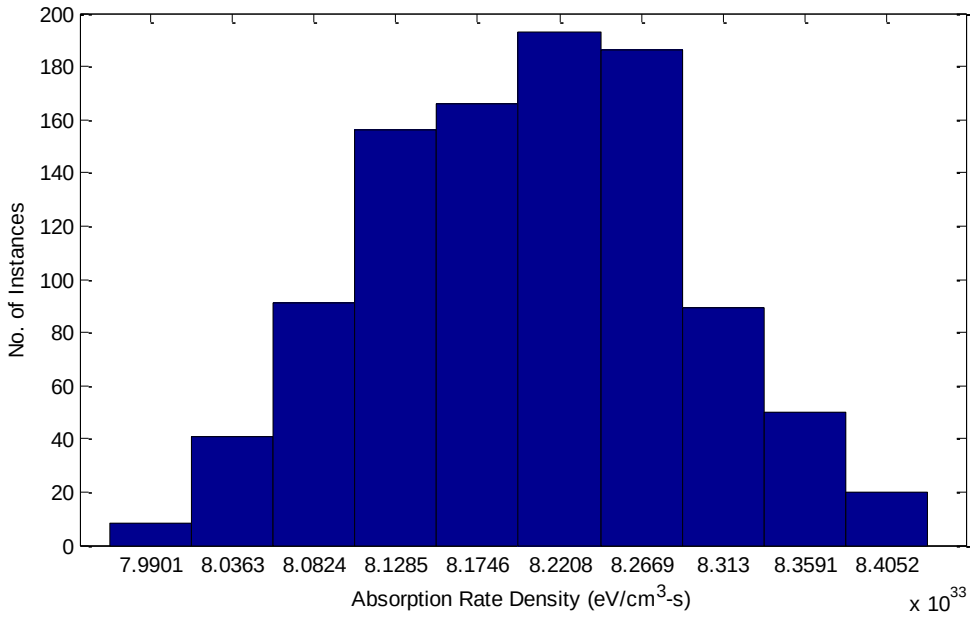


**Figure 43. QOI 1 for the Adjusted Xenon 1-D Axial Oscillator Strength Problem with 1,000 Sample LHD.**

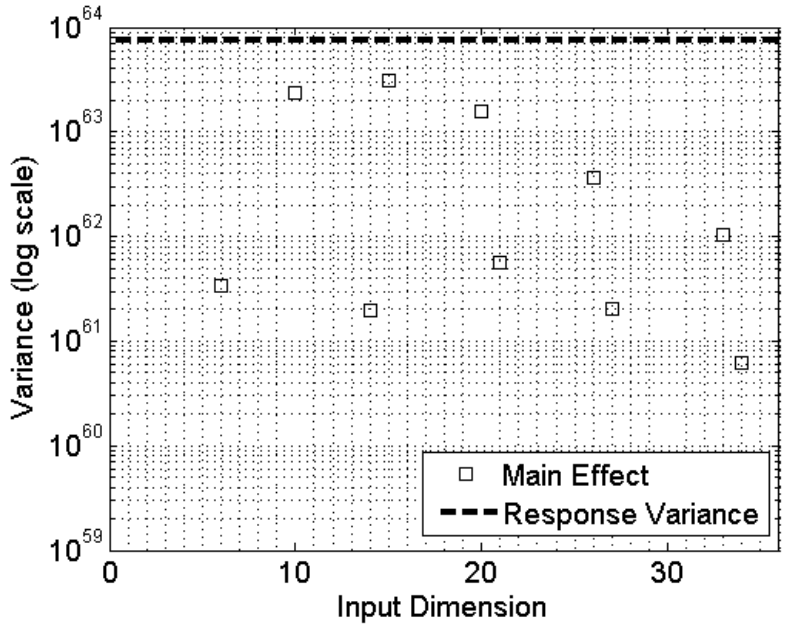


**Figure 44. QOI 1 Main Effects for Adjusted Xenon 1-D Axial Oscillator Strength Problem with 1,000 Sample LHD.**

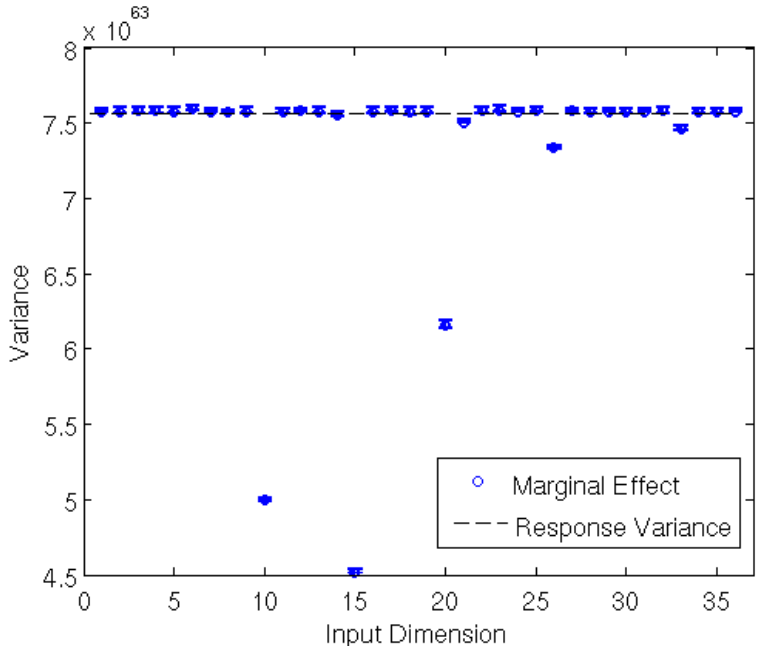


**Figure 45. QOI 1 Marginal Effects for 1-D Axial Oscillator Strength Problem with 1,000 Sample LHD.**

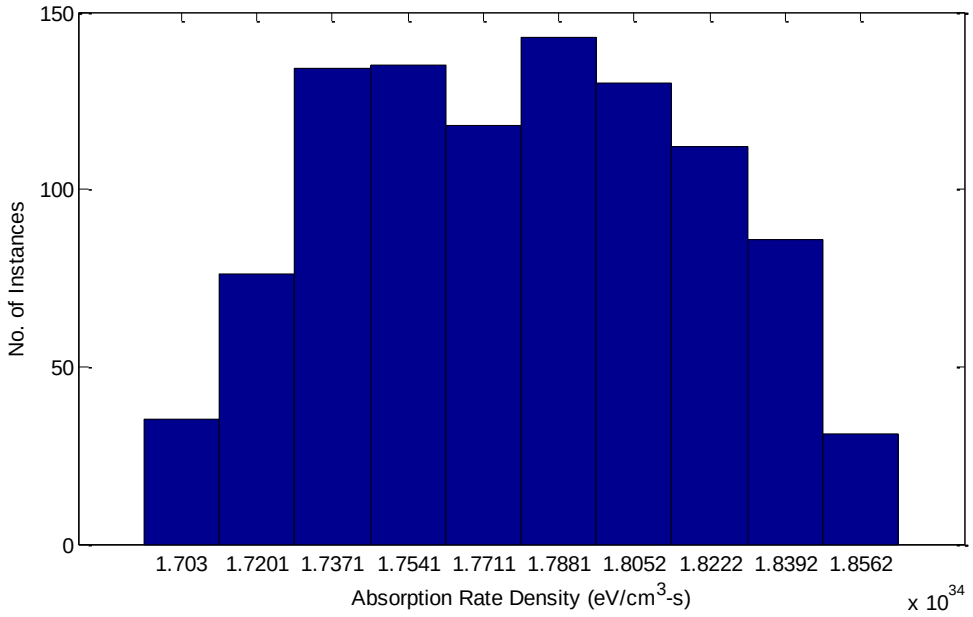


**Figure 46. QOI 2 for the Adjusted Xenon 1-D Axial Oscillator Strength Problem with 1,000 Sample LHD.**

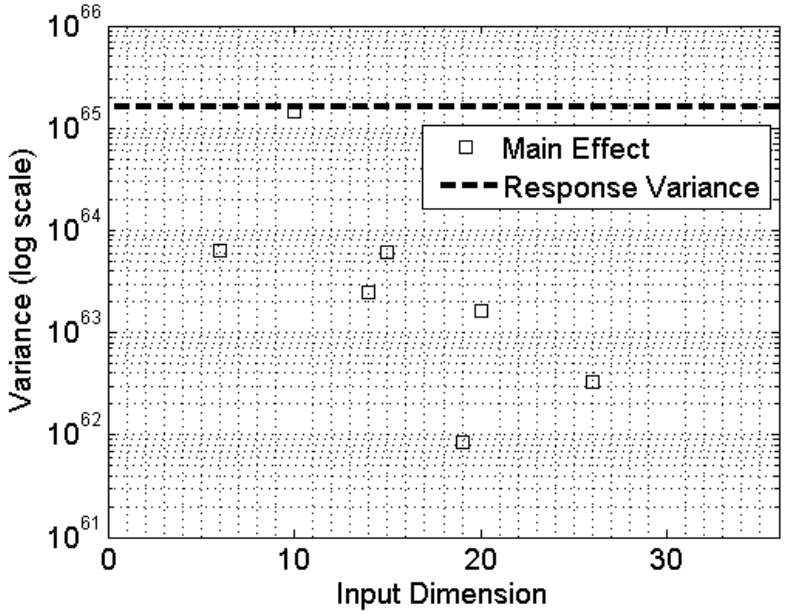


**Figure 47. QOI 2 Main Effects for Adjusted Xenon 1-D Axial Oscillator Strength Problem with 1,000 Sample LHD.**

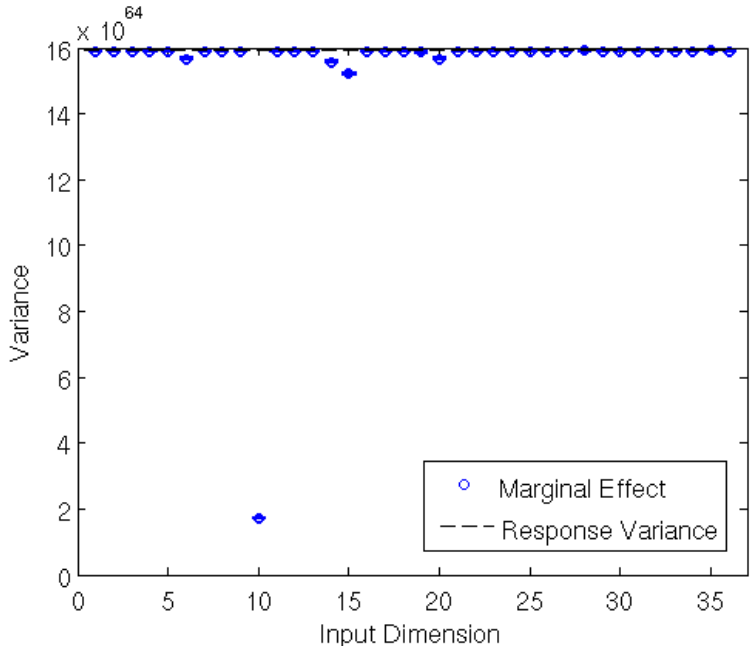


**Figure 48. QOI 2 Marginal Effects for Adjusted Xenon 1-D Axial Oscillator Strength Problem with 1,000 Sample LHD.**

### 5.1.4.2 Results with the 32,000 Sample Latin Hypercube Design

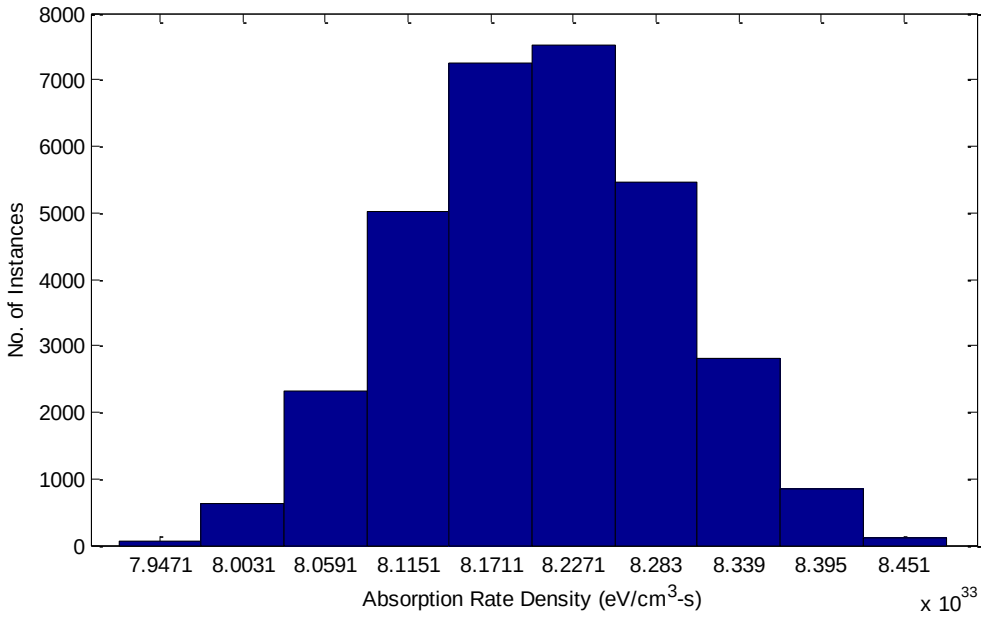


**Figure 49. QOI 1 for the Adjusted Xenon 1-D Axial Oscillator Strength Problem with 32,000 Sample LHD.**

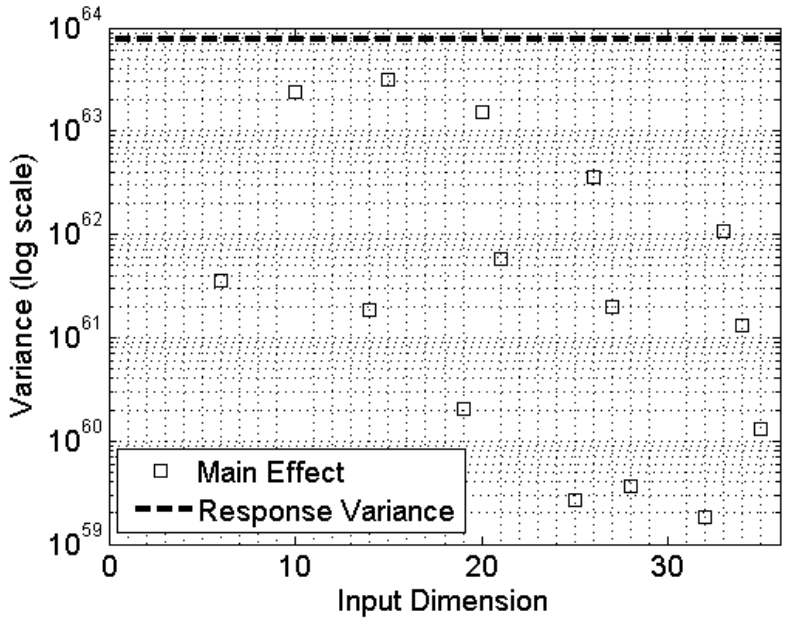


**Figure 50. QOI 1 Main Effects for Adjusted Xenon 1-D Axial Oscillator Strength Problem with 32,000 Sample LHD.**

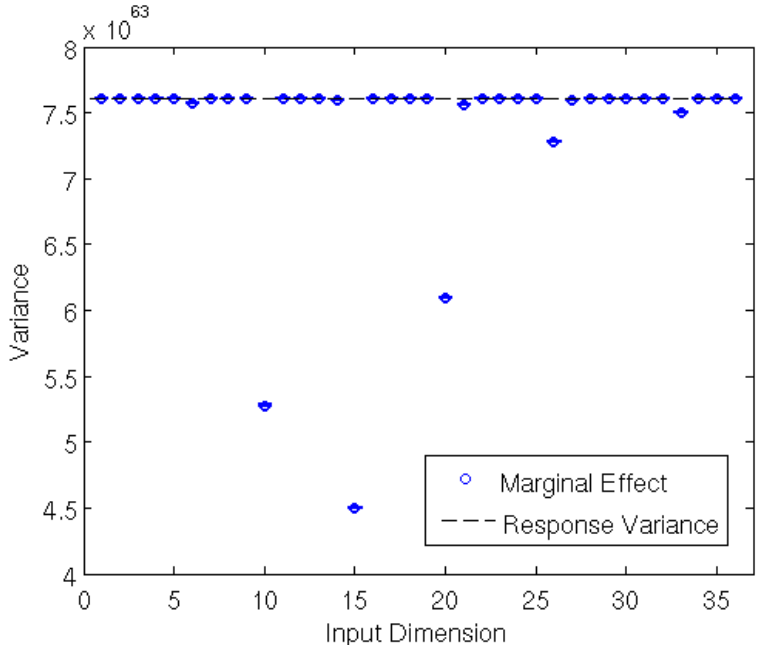


**Figure 51. QOI 1 Marginal Effects for Adjusted Xenon 1-D Axial Oscillator Strength Problem with 32,000 Sample LHD.**

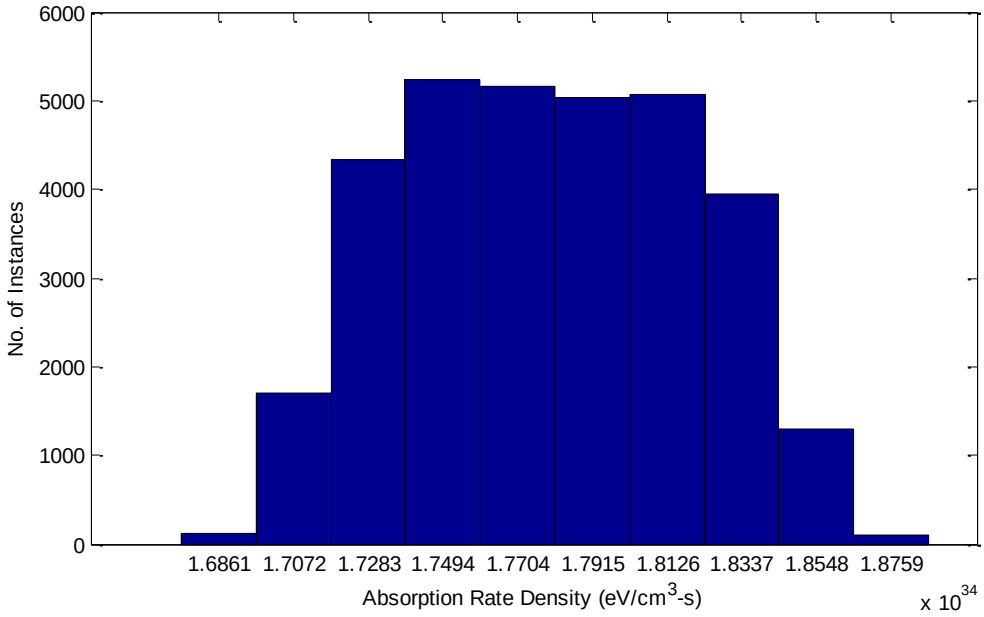


**Figure 52. QOI 2 for the Adjusted Xenon 1-D Axial Oscillator Strength Problem with 32,000 Sample LHD.**

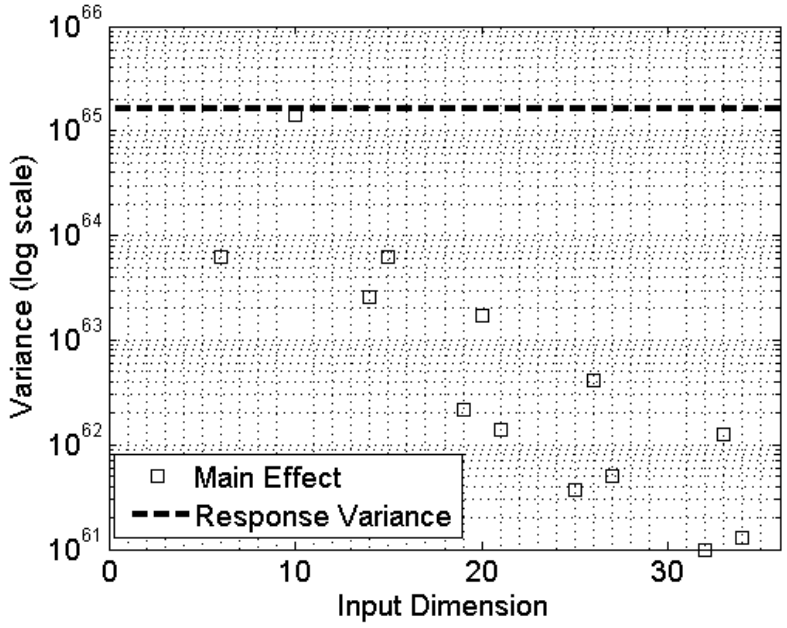


**Figure 53. QOI 2 Main Effects for Adjusted Xenon 1-D Axial Oscillator Strength Problem with 32,000 Sample LHD.**

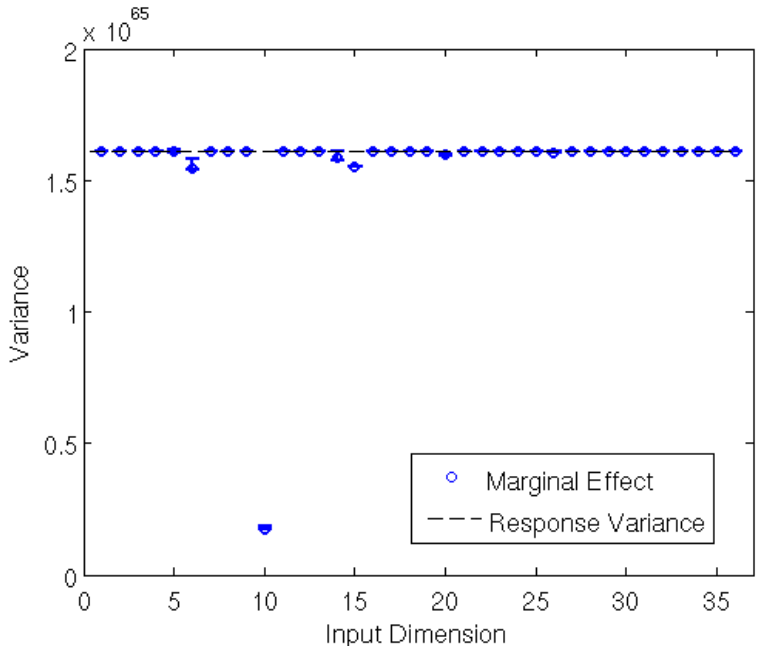


**Figure 54. QOI 2 Marginal Effects for Adjusted Xenon 1-D Axial Oscillator Strength Problem with 32,000 Sample LHD.**

### 5.1.4.3 Important Parameters for the 1-D Axial Oscillator Strength Case with Adjusted Xenon Opacities

We present the results of the screen study in Table 15.

**Table 15. Important Parameters for 1-D Axial Oscillator Strength Case with Adjusted Xenon Opacities.**

| LHD | QOI | $10^{-4}$ Screening | $10^{-3}$ Screening |
|---|---|---|---|
| 1000 | 1 | 6, 10, 14, 15, 20, 21, 26, 27, 33, 34 | 6, 10, 14, 15, 20, 21, 26, 27, 33 |
| | 2 | 6, 10, 14, 15, 19, 20, 26 | 6, 10, 14, 15, 20, 26 |
| 32000 | 1 | 6, 10, 14, 15, 19, 20, 21, 26, 27 , 33, 34, 35 | 6,10,14,15,20,21,26,27,33,34 |
| | 2 | 6, 10, 14, 15, 19, 20, 21, 25, 26, 27, 33 | 6,10,14,15,19,20,21,16,33 |

There are many more oscillator strengths kept for the adjusted xenon opacity case when compared to the case with no adjusted opacities. We adjusted the xenon opacities because the CRASH opacities did not account well for the bound-bound transitions. The adjustment increased the opacity contribution for the bound-bound transition significantly for a wide range of photon energies. This is what has caused the increased set of parameters.

## 5.2 Results for the 1-D Radial CRASH-like Test Problem

We present the results from the same procedures that were performed for the 1-D Axial CRASH-like test problem. We note that the quantities of interest are different for this case. These cases include allowing the ionization potentials or the oscillator strengths to vary, and now the ionization potentials include those in the plastic but not in the beryllium. Also, we compare these results to those created when we adjust the CRASH Xenon opacity using the LANL data.

### 5.2.1 Results Using Ionization Potentials

We have performed this computation where we allowed the ionization potentials of the beryllium and xenon vary. We present the PDF, main effect, and marginal effect for the 1,000 sample LHD in Figure 55 through Figure 66 and for the 32,000 sample LHD in Figure 67 through Figure 78.

#### 5.2.1.1 Results with the 1,000 Sample Latin Hypercube Design

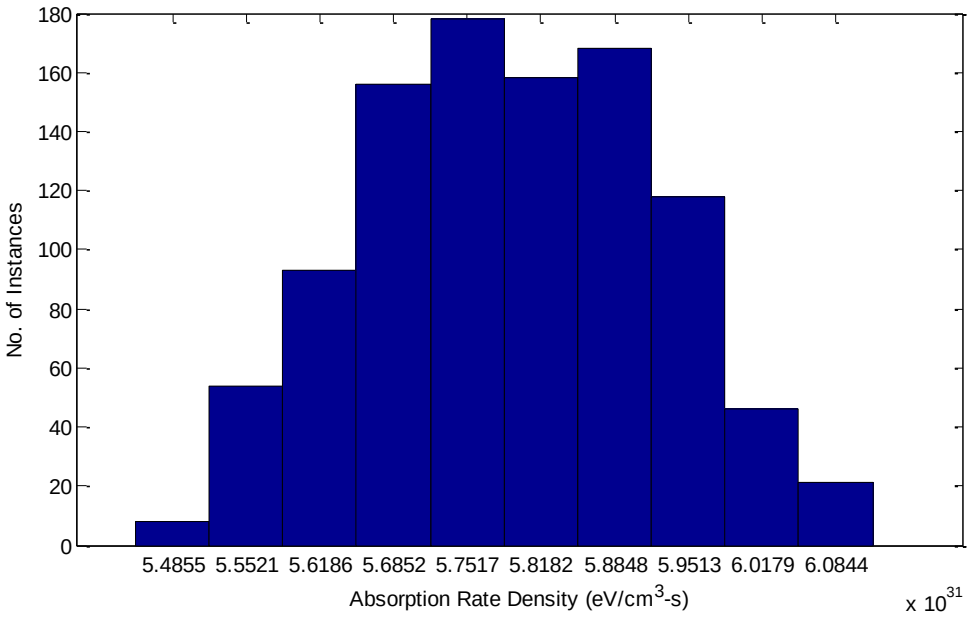


**Figure 55. QOI 1 for the 1-D Radial Ionization Potential Problem with 1,000 Sample LHD.**

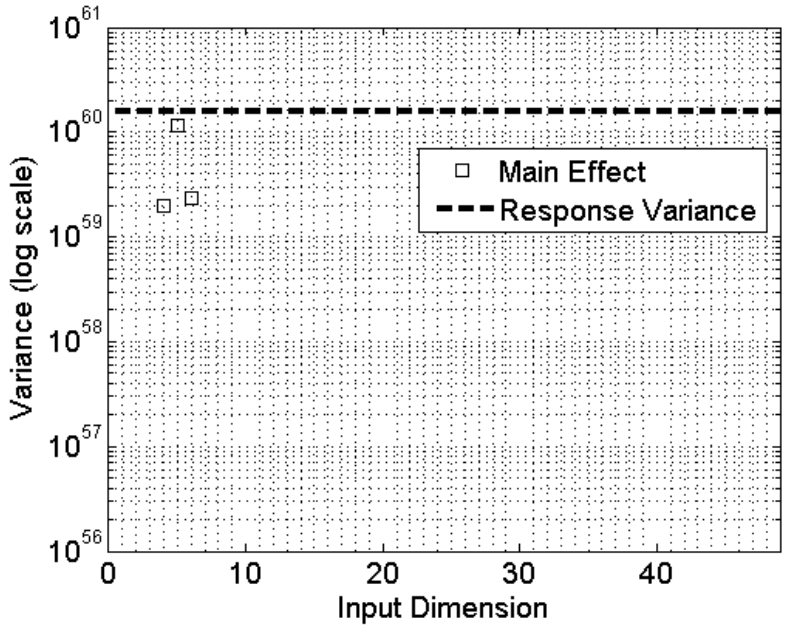


**Figure 56. QOI 1 Main Effects 1-D Radial Ionization Potential Problem with 1,000 Sample LHD.**

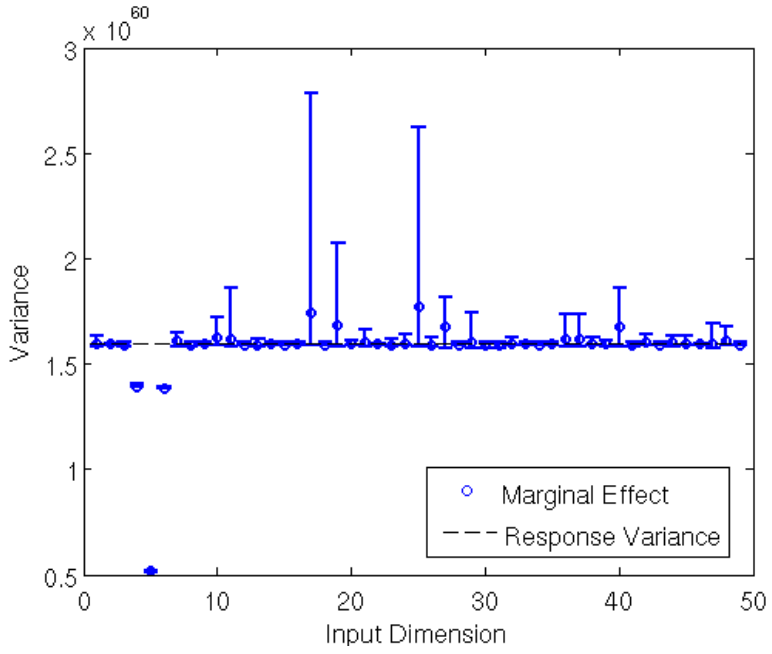


**Figure 57. QOI 1 Marginal Effects 1-D Radial Ionization Potential Problem with 1,000 Sample LHD.**

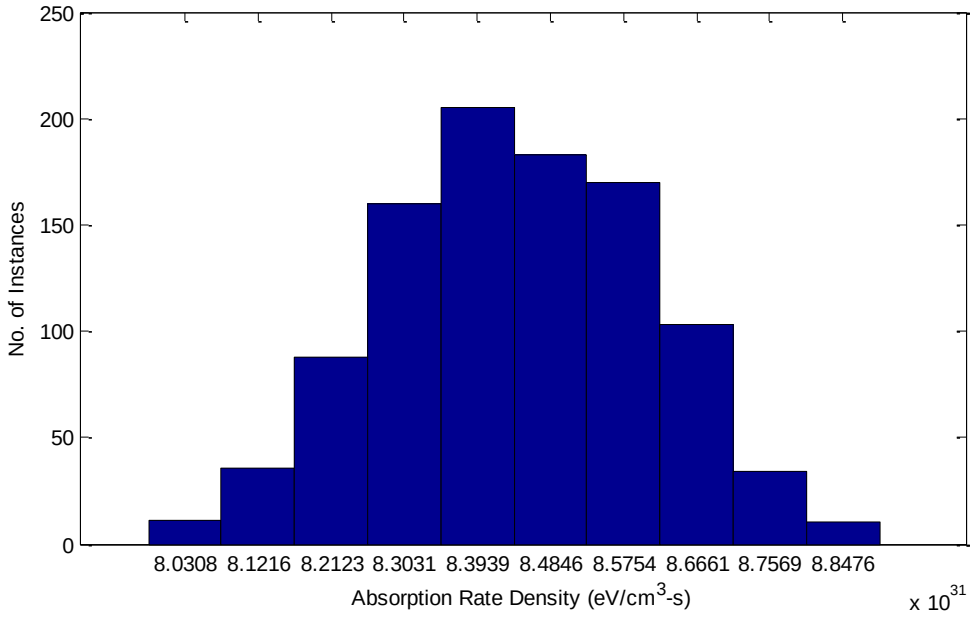


**Figure 58. QOI 2 for the 1-D Radial Ionization Potential Problem with 1,000 Sample LHD.**

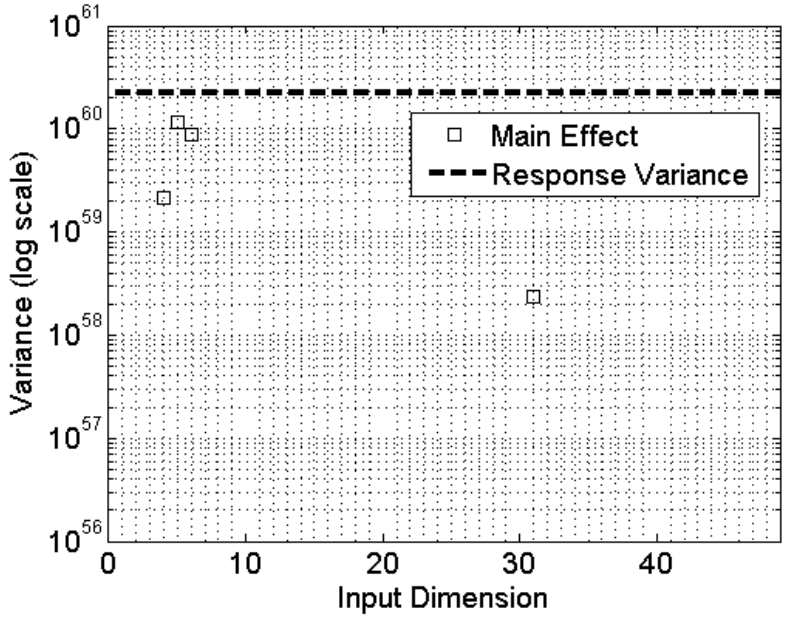


**Figure 59. QOI 2 Main Effects 1-D Radial Ionization Potential Problem with 1,000 Sample LHD.**

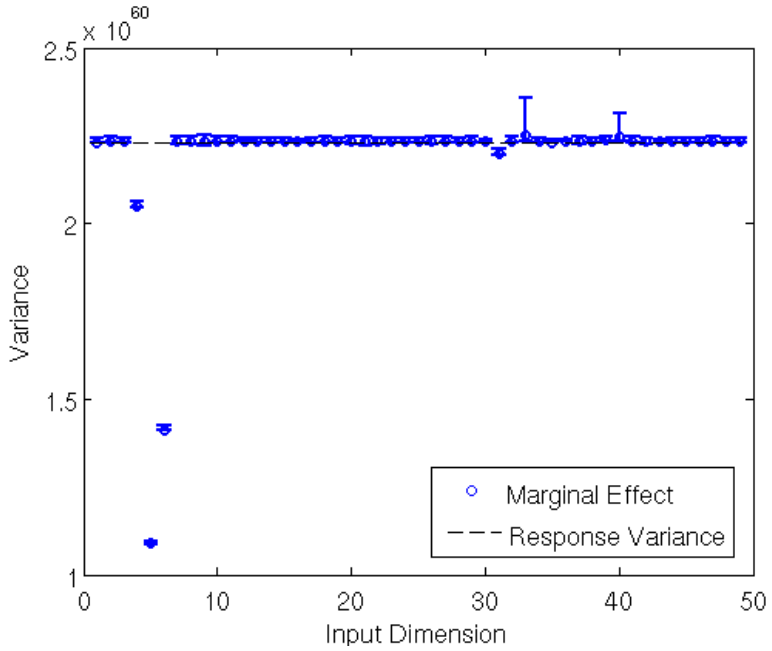


**Figure 60. QOI 2 Marginal Effects 1-D Radial Ionization Potential Problem with 1,000 Sample LHD.**

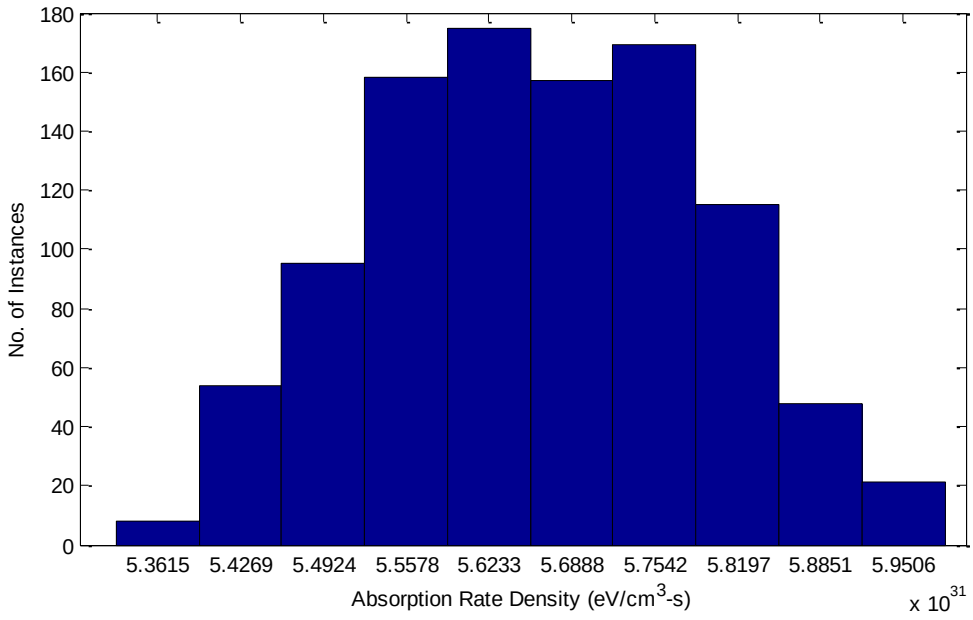


**Figure 61. QOI 3 for the 1-D Radial Ionization Potential Problem with 1,000 Sample LHD.**

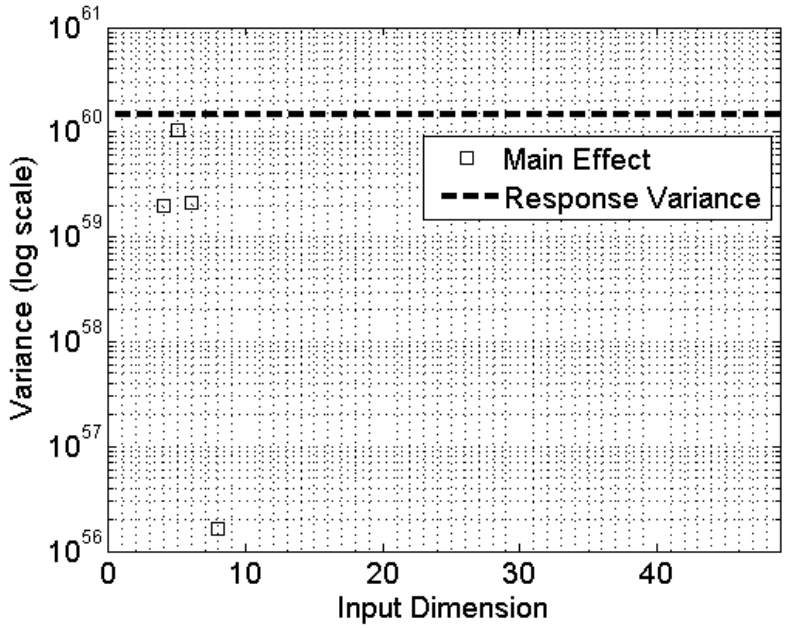


**Figure 62. QOI 3 Main Effects 1-D Radial Ionization Potential Problem with 1,000 Sample LHD.**

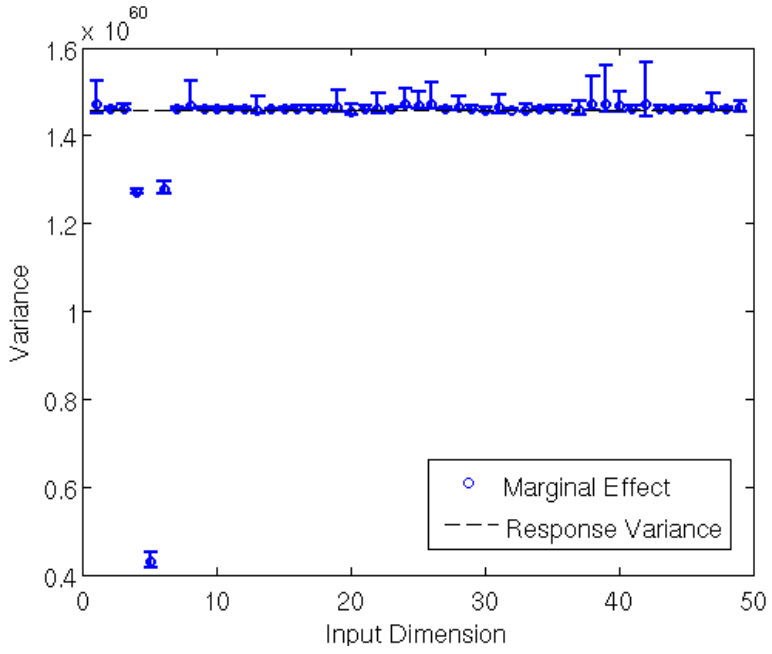


**Figure 63. QOI 3 Marginal Effects 1-D Radial Ionization Potential Problem with 1,000 Sample LHD.**

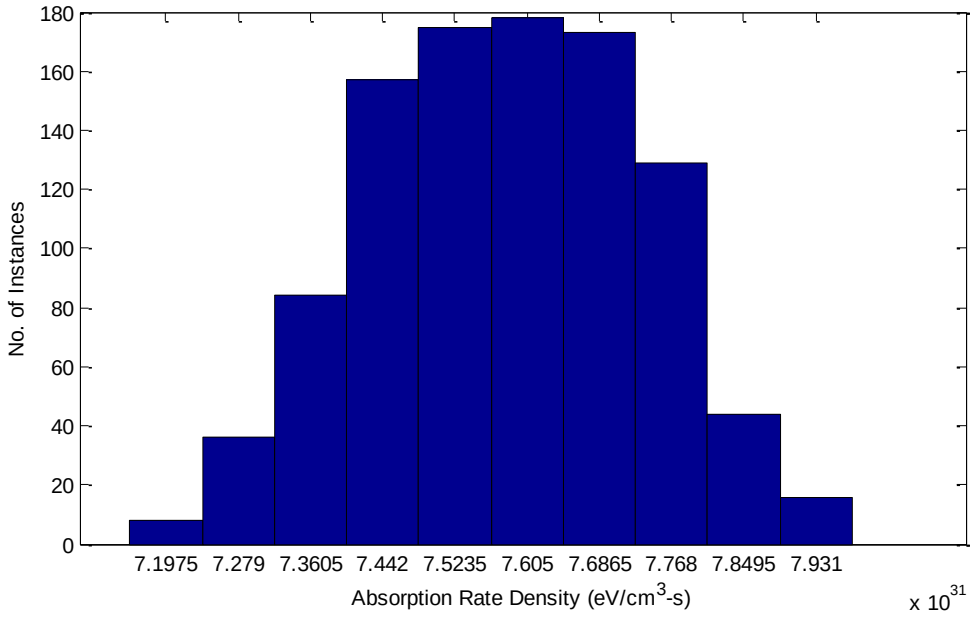


**Figure 64. QOI 4 for the 1-D Radial Ionization Potential Problem with 1,000 Sample LHD.**

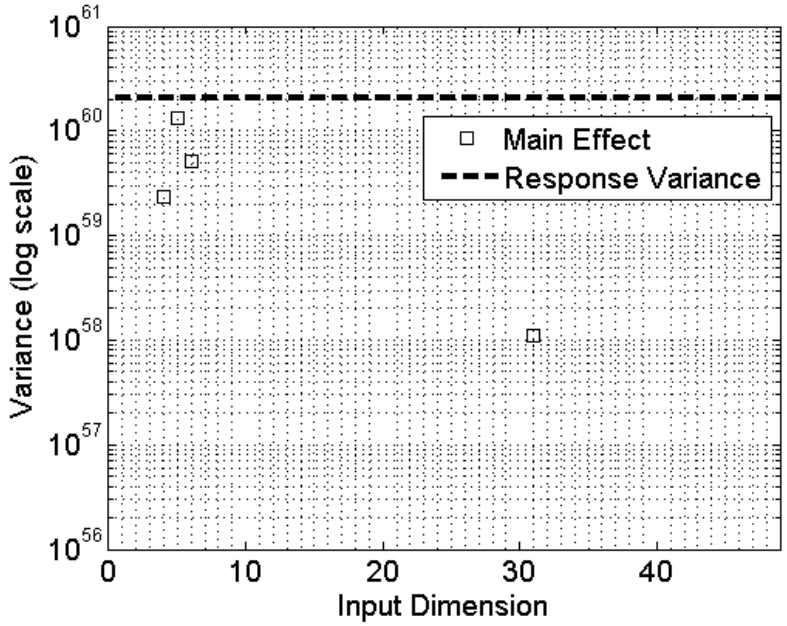


**Figure 65. QOI 4 Main Effects 1-D Radial Ionization Potential Problem with 1,000 Sample LHD.**

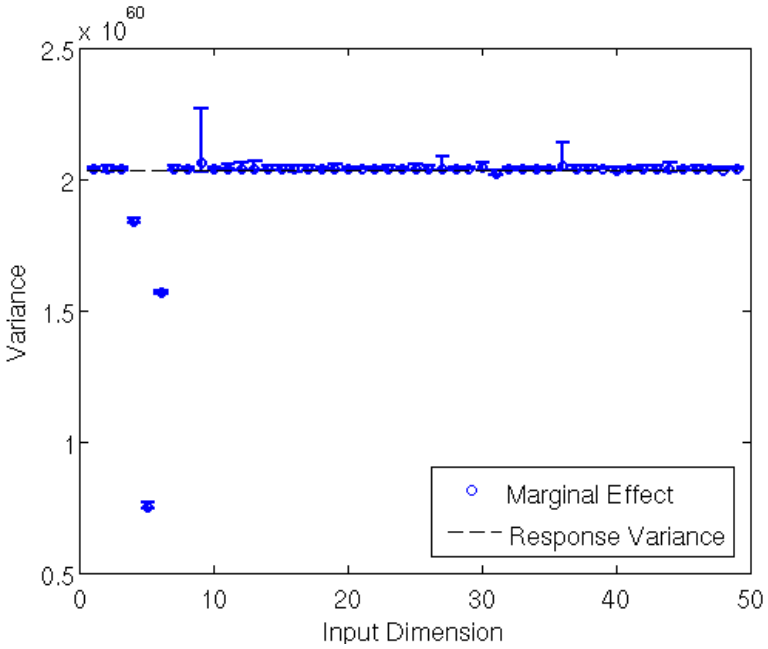


**Figure 66. QOI 4 Marginal Effects 1-D Radial Ionization Potential Problem with 1,000 Sample LHD.**

#### 5.2.1.2 Results with the 32,000 Sample Latin Hypercube Design

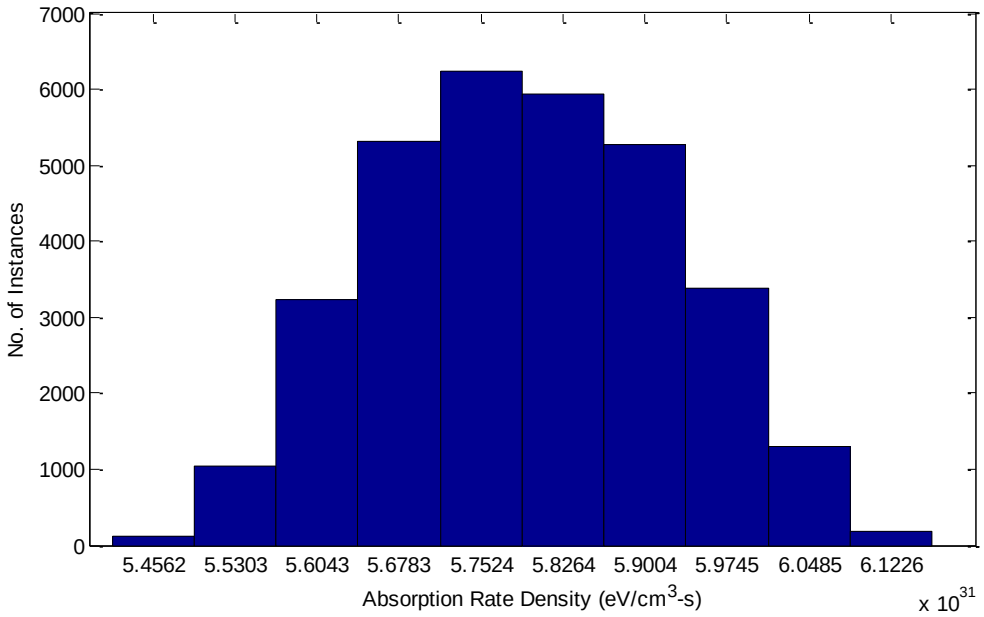


**Figure 67. QOI 1 for the 1-D Radial Ionization Potential Problem with 32,000 Sample LHD.**

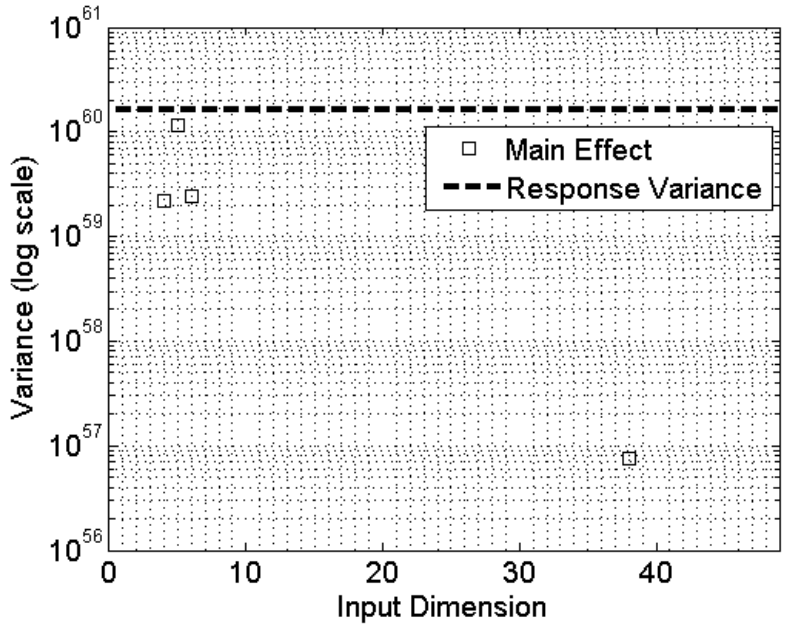


**Figure 68. QOI 1 Main Effects 1-D Radial Ionization Potential Problem with 32,000 Sample LHD.**

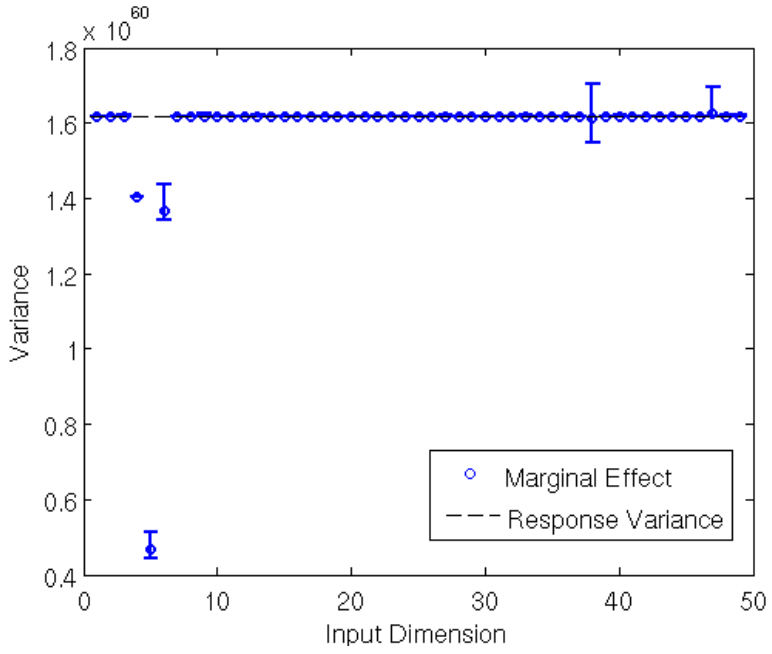


**Figure 69. QOI 1 Marginal Effects 1-D Radial Ionization Potential Problem with 32,000 Sample LHD.**

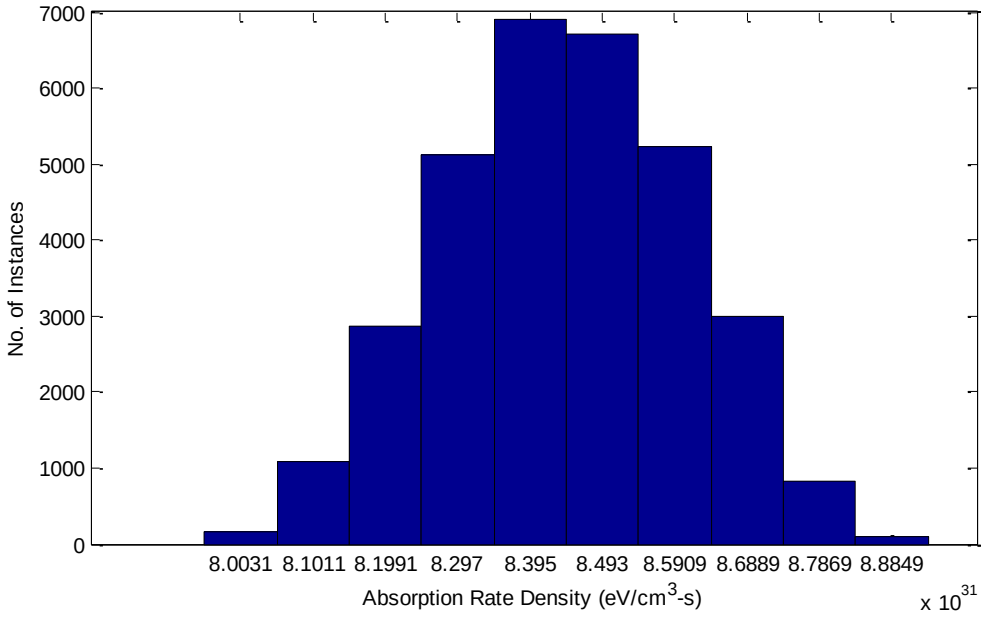


**Figure 70. QOI 2 for the 11-D Radial Ionization Potential Problem with 32,000 Sample LHD.**

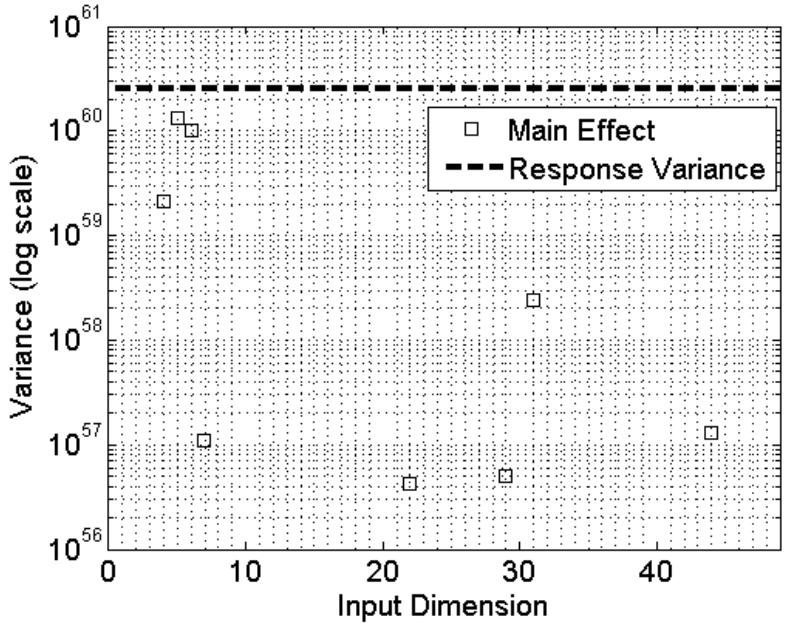


**Figure 71. QOI 2 Main Effects 1-D Radial Ionization Potential Problem with 32,000 Sample LHD.**

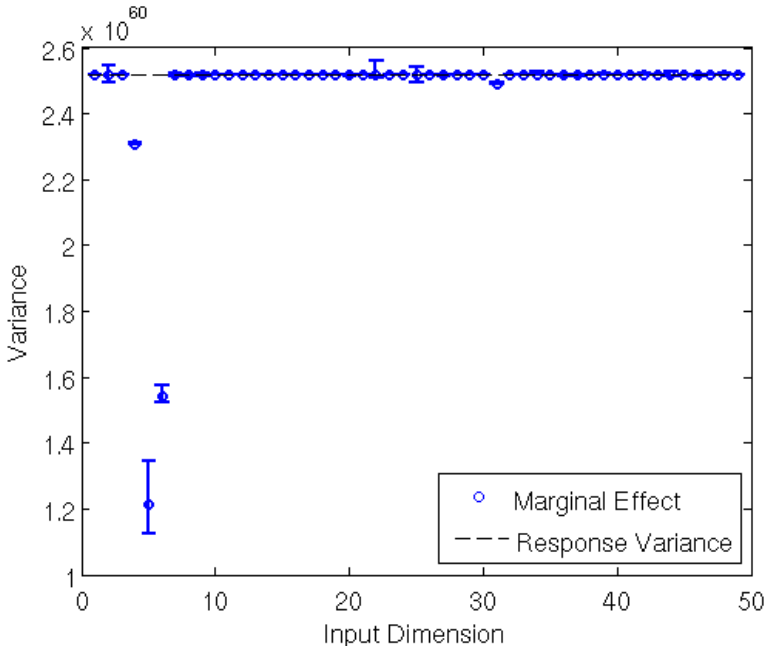


**Figure 72. QOI 2 Marginal Effects 1-D Radial Ionization Potential Problem with 32,000 Sample LHD.**

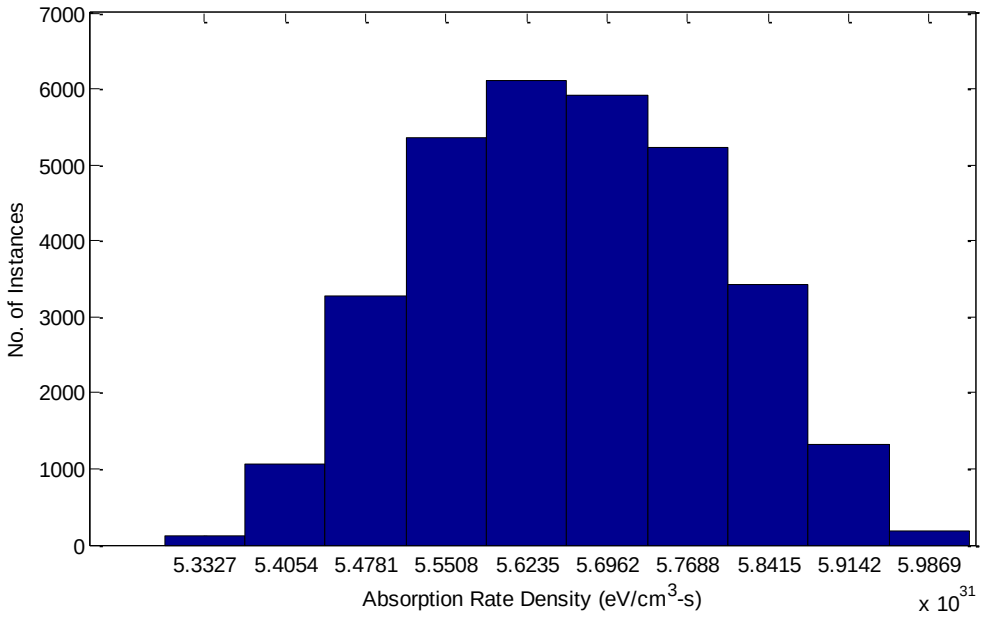


**Figure 73. QOI 3 for the 1-D Radial Ionization Potential Problem with 32,000 Sample LHD.**

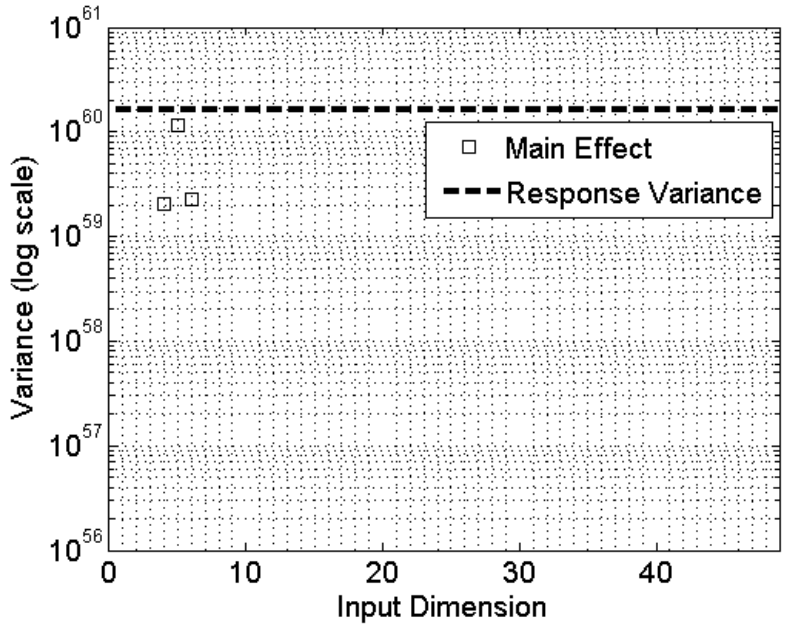


**Figure 74. QOI 3 Main Effects 1-D Radial Ionization Potential Problem with 32,000 Sample LHD.**

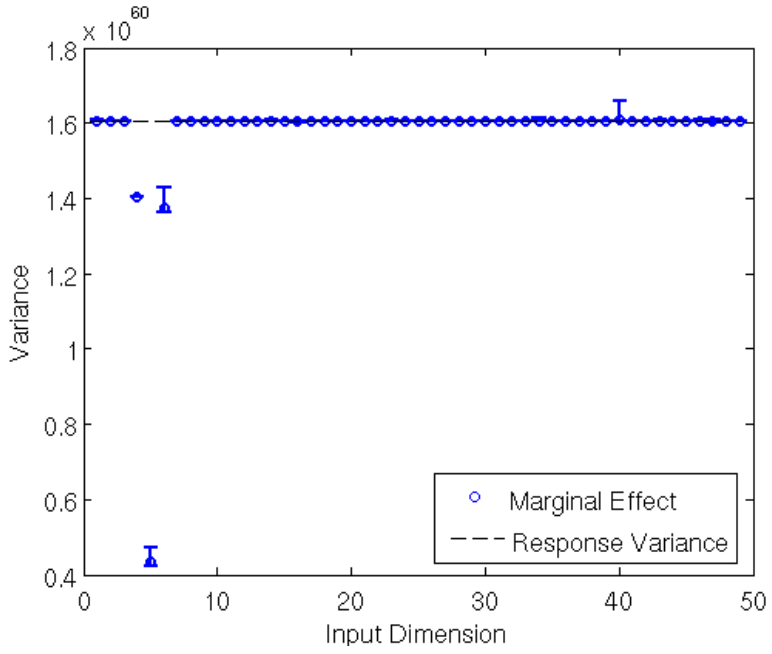


**Figure 75. QOI 3 Marginal Effects 1-D Radial Ionization Potential Problem with 32,000 Sample LHD.**

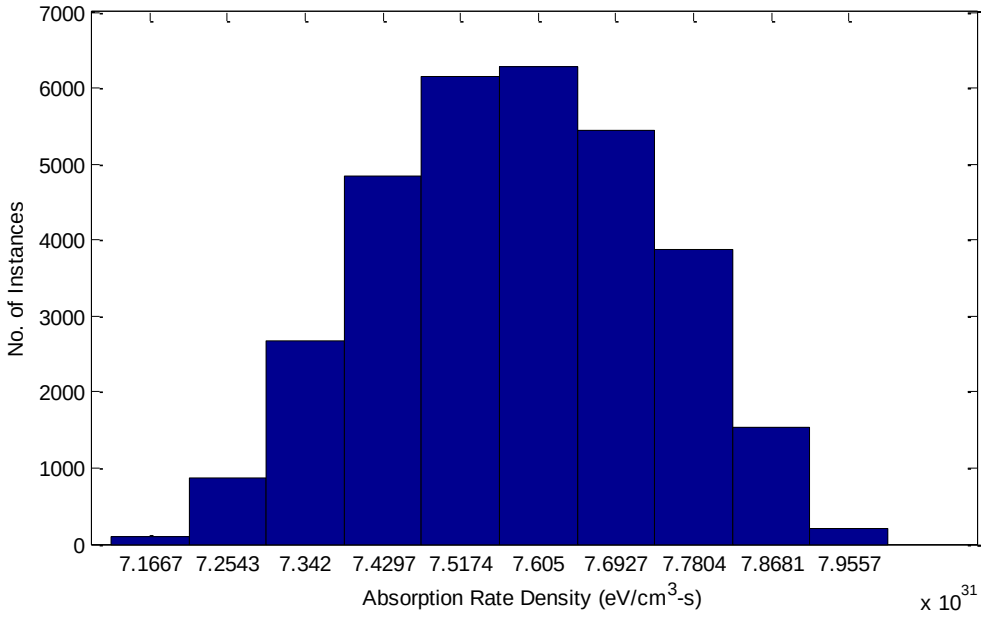


**Figure 76. QOI 4 for the 1-D Radial Ionization Potential Problem with 32,000 Sample LHD.**

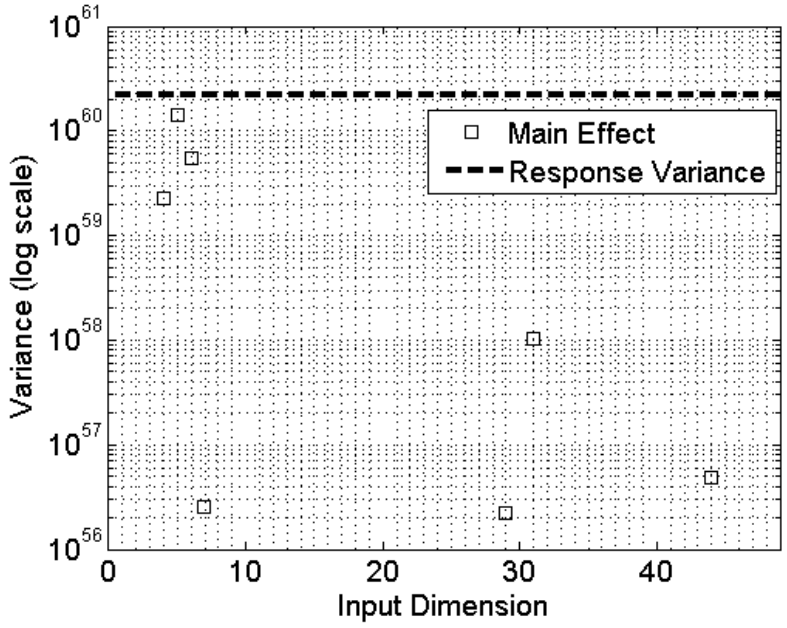


**Figure 77. QOI 4 Main Effects 1-D Radial Ionization Potential Problem with 32,000 Sample LHD.**

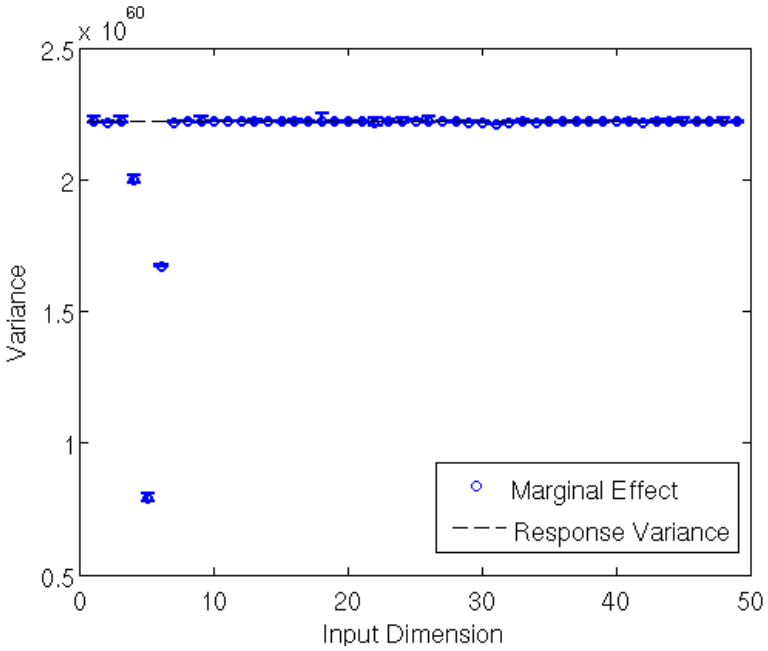


**Figure 78. QOI 4 Marginal Effects 1-D Radial Ionization Potential Problem with 32,000 Sample LHD.**

### 5.2.1.3 Important Parameters for the 1-D Radial Ionization Potential Case

We present the important parameters for the screening study in Table 16.

**Table 16. Important Parameters for 1-D Radial Ionization Potential Case.**

| LHD | QOI | $10^{-4}$ Screening | $10^{-3}$ Screening |
|---|---|---|---|
| 1000 | 1 | 4, 5, 6 | 4,5,6 |
| | 2 | 4, 5, 6, 31 | 4, 5, 6, 31 |
| | 3 | 4, 5, 6, 8 | 4,5,6 |
| | 4 | 4, 5, 6, 31 | 4, 5, 6, 31 |
| 32000 | 1 | 4, 5, 6, 38 | 4,5,6 |
| | 2 | 4 - 8, 22, 29, 31, 44 | 4,5,6,31 |
| | 3 | 4, 5, 6 | 4,5,6 |
| | 4 | 4 - 8, 29, 31, 44 | 4,5,6,31 |

The less inclusive set has three important xenon potentials and one important carbon potential. For the more inclusive set, we include a potential for oxygen and nitrogen. Since the 2nd and 4th QOI are deeper in the plastic, the plastic ionization potentials become more important.

### 5.2.2 Results Using Ionization Potentials with Adjusted Xenon Opacity

Recall from section 3.4 that we devised a method to adjust the mean of the CRASH xenon opacities using the LANL opacities while still keeping the useful uncertainty created by varying uncertain parameters in the CRASH opacity generation. In this section, we present the PDF, main effect, and marginal effect plots for the 1,000 sample LHD in Figure 79 through Figure 90 and for the 32,000 LHD in Figure 91 through Figure 102.

#### 5.2.2.1 Results with the 1,000 Sample Latin Hypercube Design

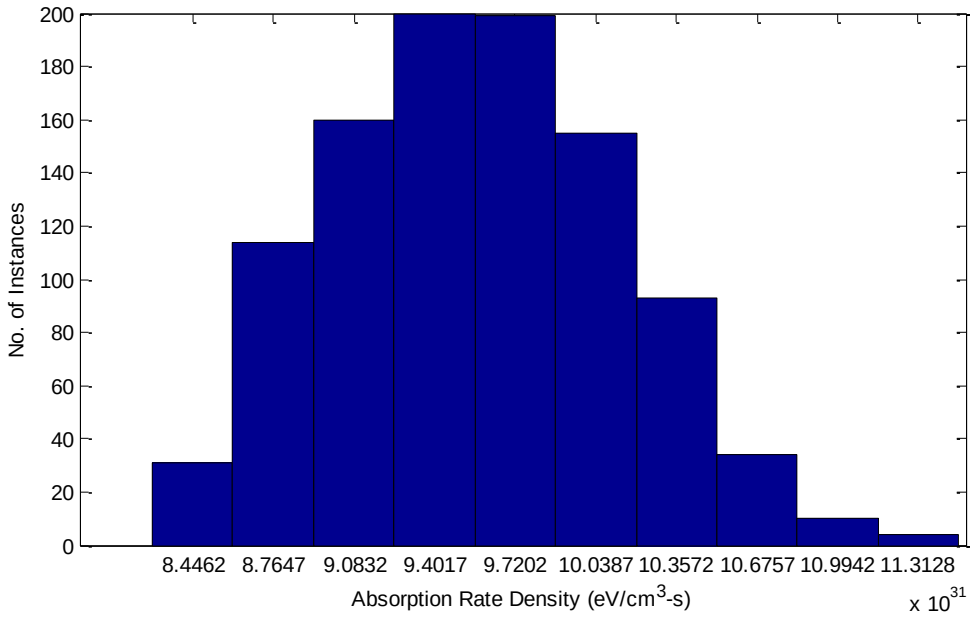


**Figure 79. QOI 1 for the Adjusted Xenon 1-D Radial Ionization Potential Problem with 1,000 Sample LHD.**

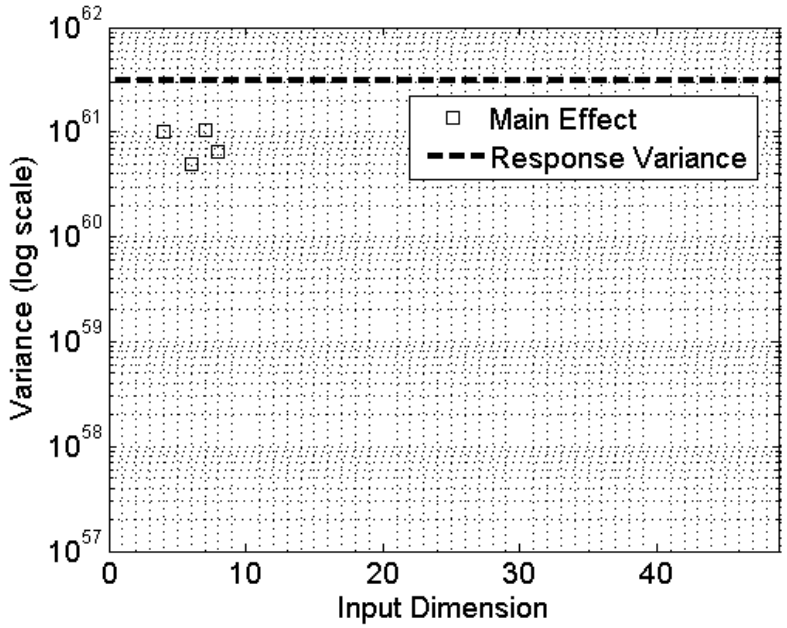


**Figure 80. QOI 1Main Effects Xenon Adjusted 1-D Radial Ionization Potential Problem with 1,000 Sample LHD.**

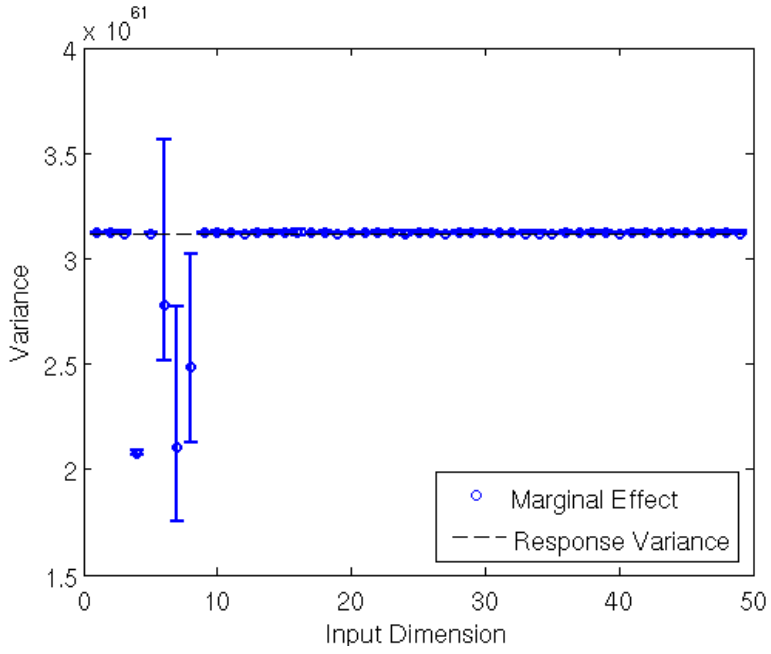


**Figure 81. QOI 1 Marginal Effects Xenon Adjusted 1-D Radial Ionization Potential Problem with 1,000 Sample LHD.**

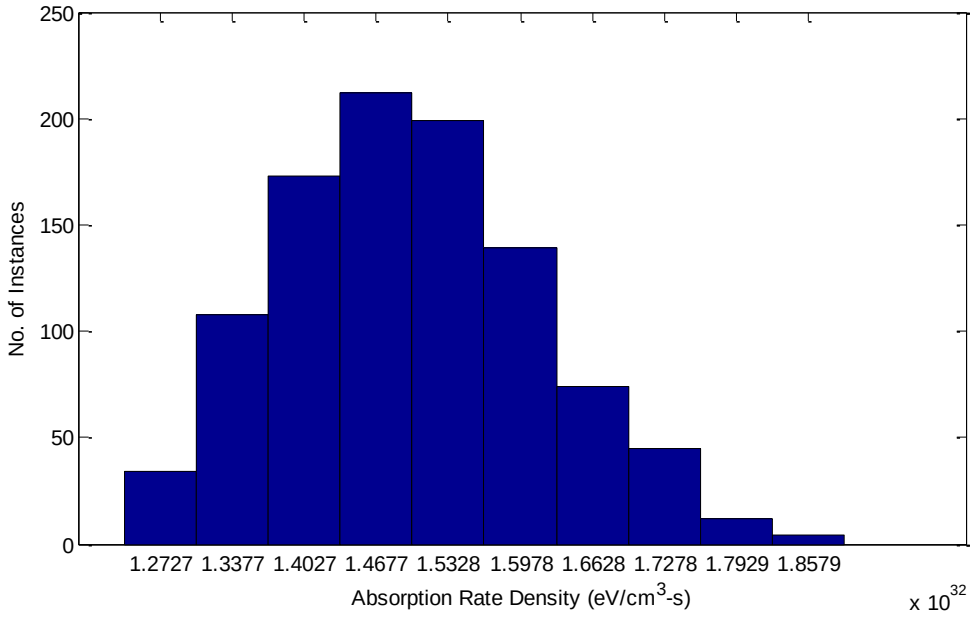


**Figure 82. QOI 2 for the Adjusted Xenon 1-D Radial Ionization Potential Problem with 1,000 Sample LHD.**

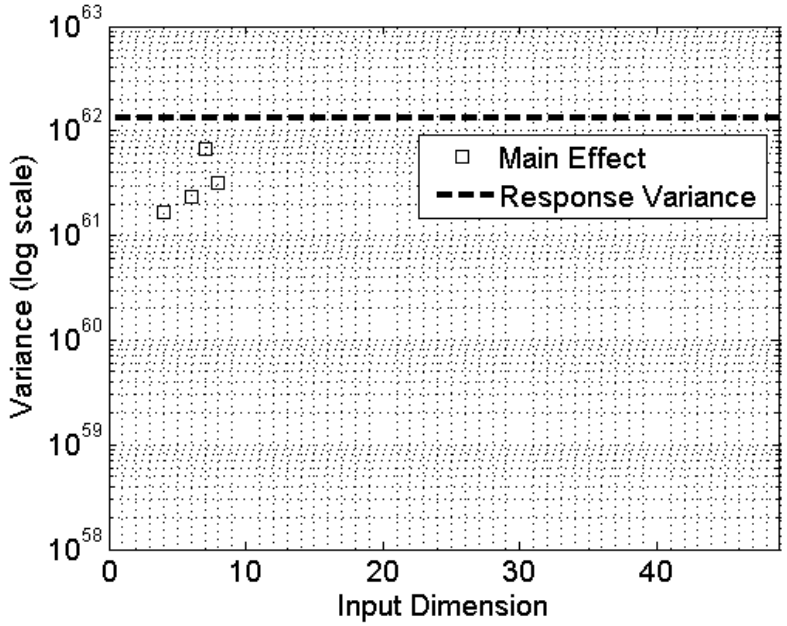


**Figure 83. QOI 2 Main Effects Xenon Adjusted 1-D Radial Ionization Potential Problem with 1,000 Sample LHD.**

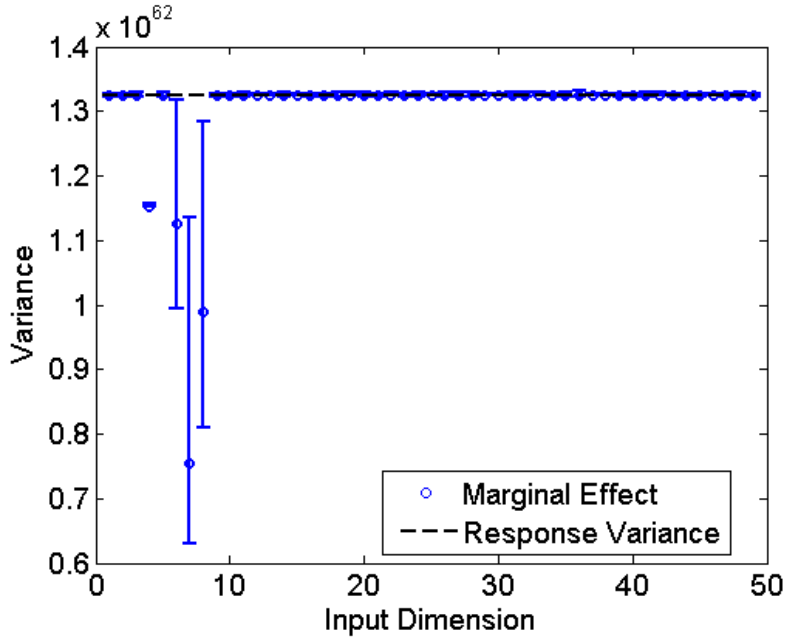


**Figure 84. QOI 2 Marginal Effects Xenon Adjusted 1-D Radial Ionization Potential Problem with 1,000 Sample LHD.**

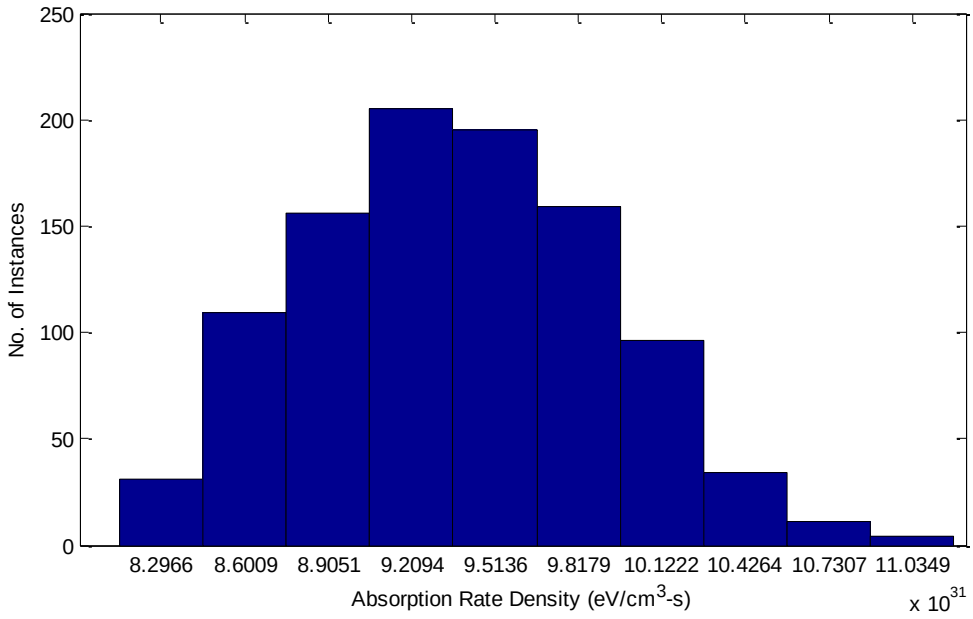


**Figure 85. QOI 3 for the Adjusted Xenon 1-D Radial Ionization Potential Problem with 1,000 Sample LHD.**

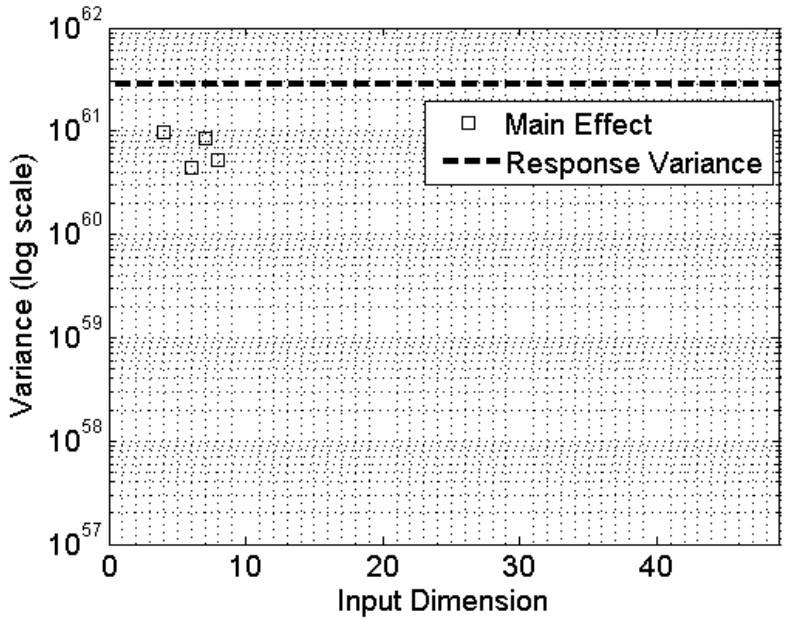


**Figure 86. QOI 3 Main Effects Xenon Adjusted 1-D Radial Ionization Potential Problem with 1,000 Sample LHD.**

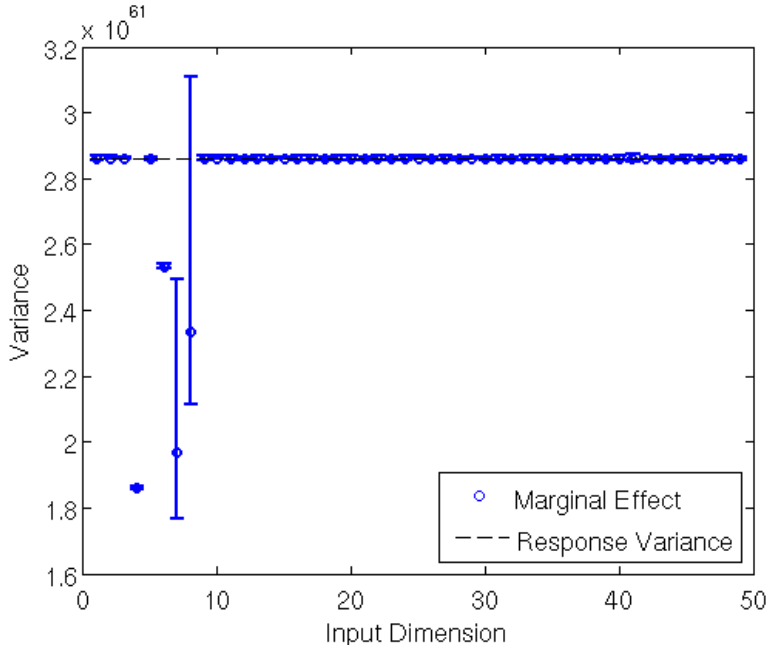


**Figure 87. QOI 3 Marginal Effects Xenon Adjusted 1-D Radial Ionization Potential Problem with 1,000 Sample LHD.**

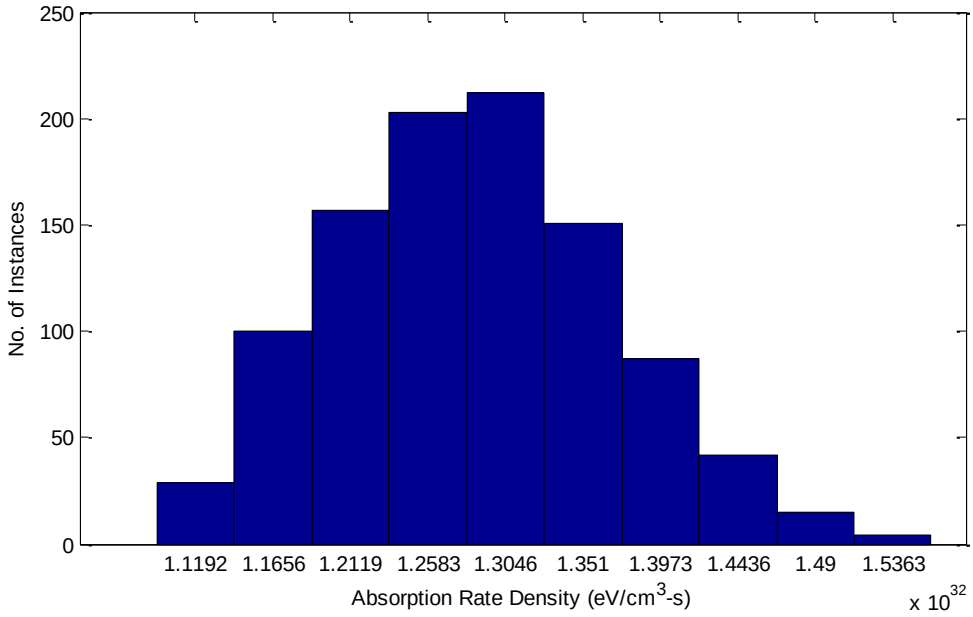


**Figure 88. QOI 4 for the Adjusted Xenon 1-D Radial Ionization Potential Problem with 1,000 Sample LHD.**

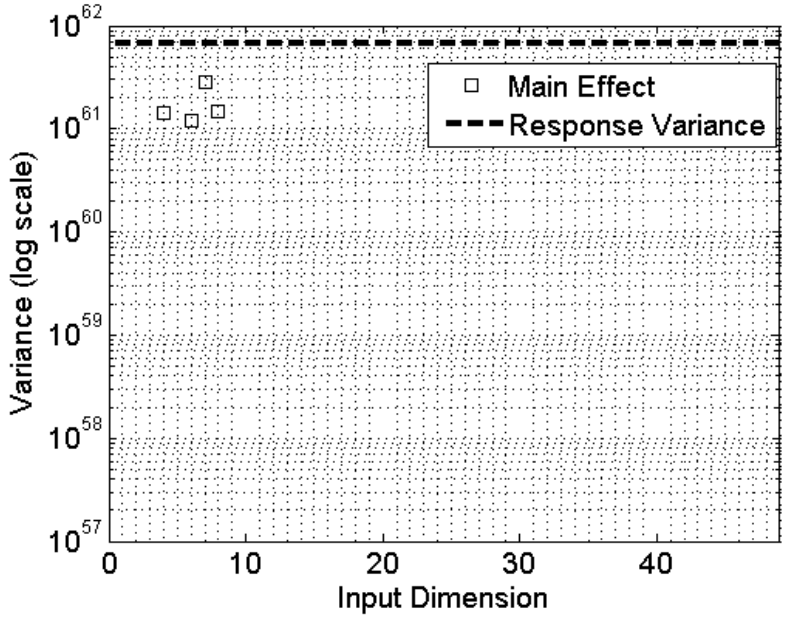


**Figure 89 QOI 4 Main Effects Xenon Adjusted 1-D Radial Ionization Potential Problem with 1,000 Sample LHD.**

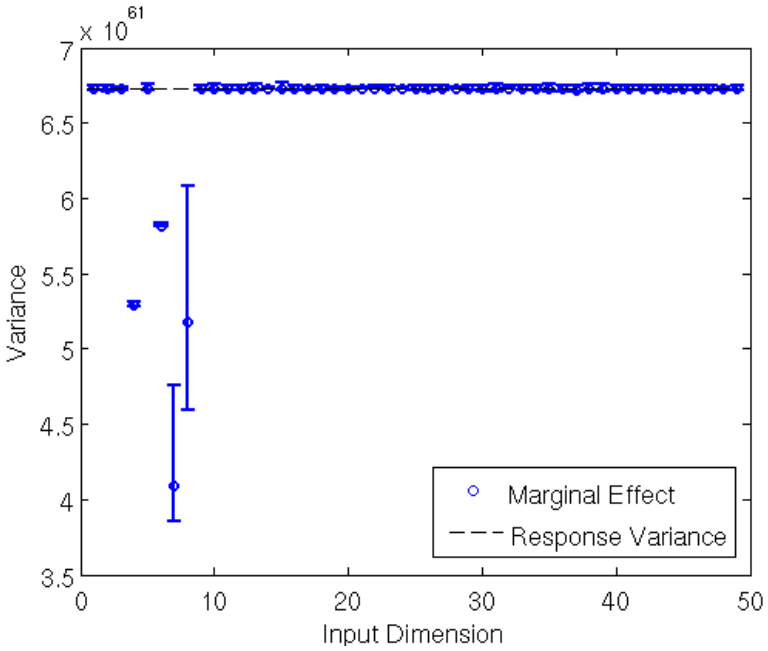


**Figure 90. QOI 4 Marginal Effects Xenon Adjusted 11-D Radial Ionization Potential Problem with 1,000 Sample LHD.**

### 5.2.2.2 Results with the 32,000 Sample Latin Hypercube Design

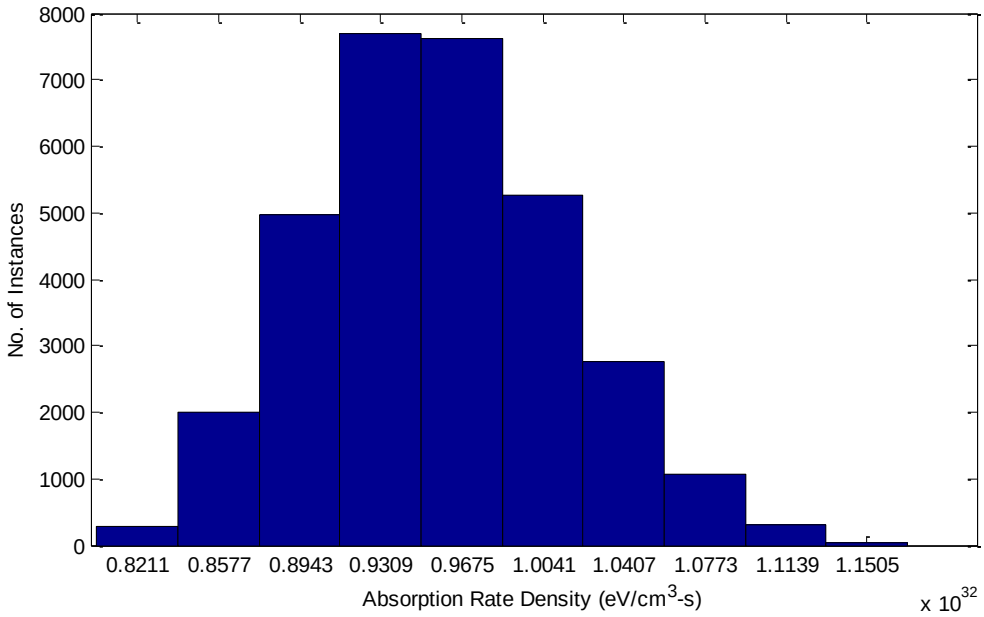


**Figure 91. QOI 1 for the Adjusted Xenon 1-D Radial Ionization Potential Problem with 32,000 Sample LHD.**

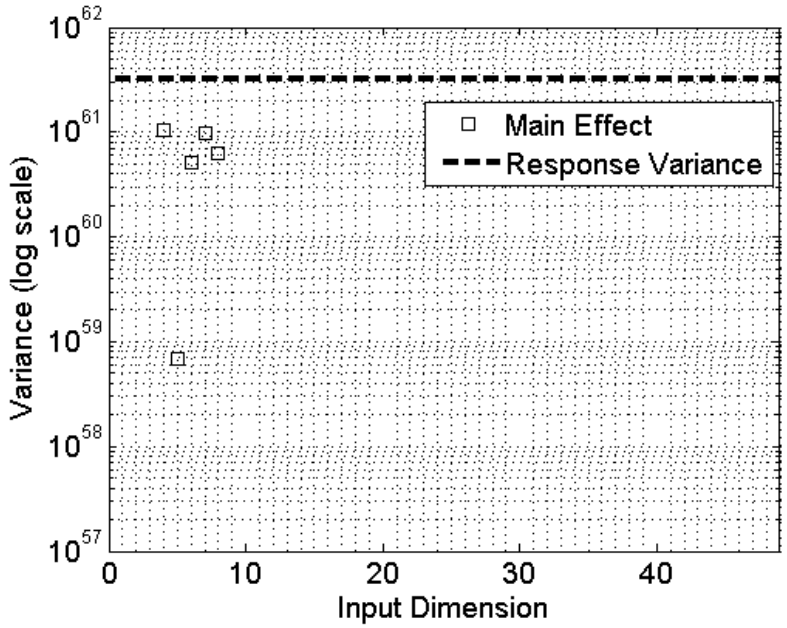


**Figure 92. QOI 1 Main Effects Xenon Adjusted 1-D Radial Ionization Potential Problem with 32,000 Sample LHD.**

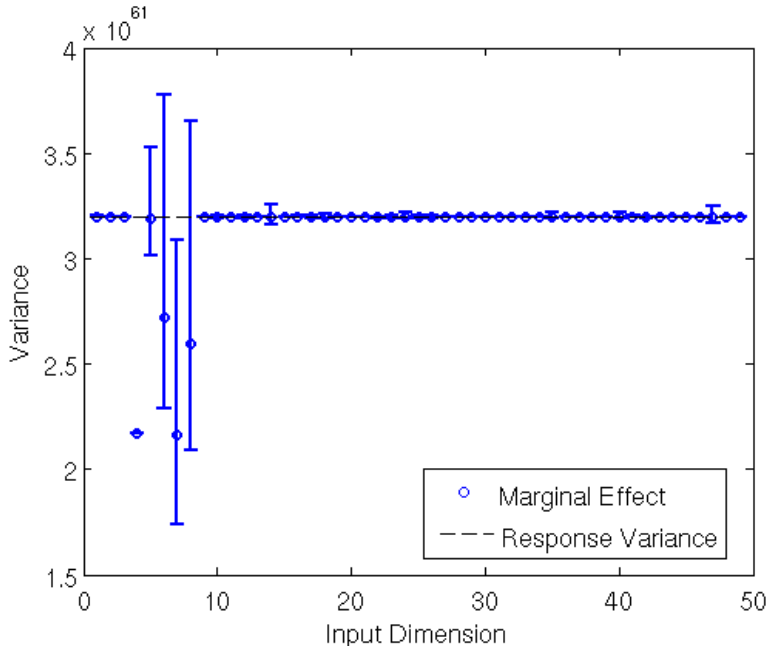


**Figure 93. QOI 1 Marginal Effects Xenon Adjusted 1-D Radial Ionization Potential Problem with 32,000 Sample LHD.**

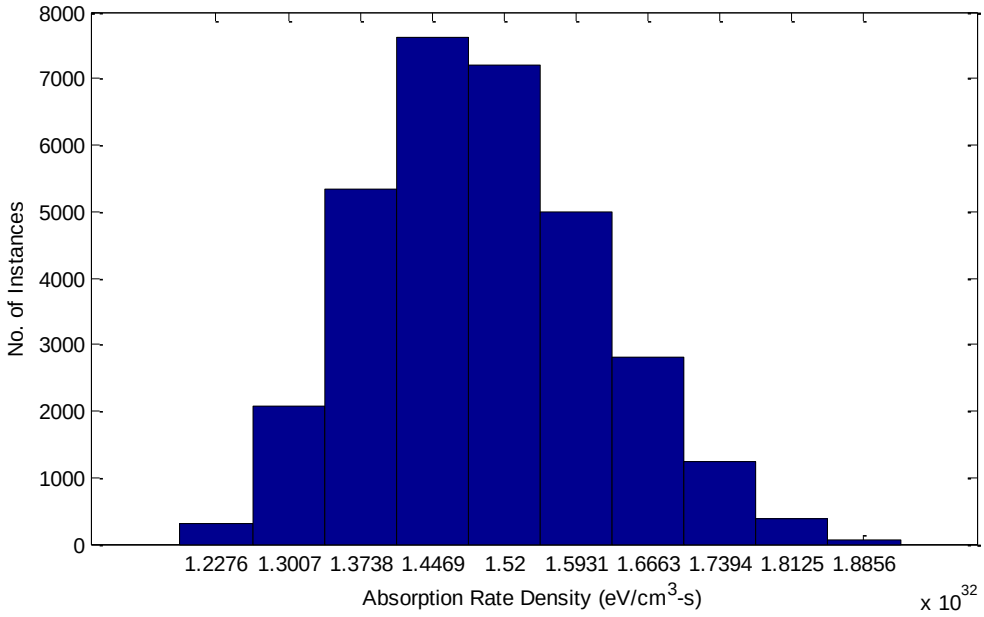


**Figure 94. QOI 2 for the Adjusted Xenon 1-D Radial Ionization Potential Problem with 32,000 Sample LHD.**

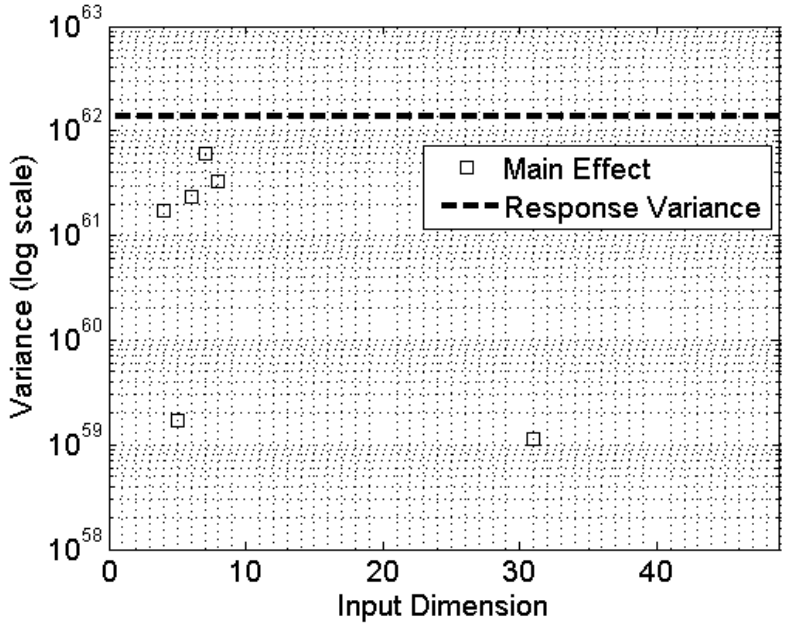


**Figure 95. QOI 2 Main Effects Adjusted Xenon 1-D Radial Ionization Potential Problem with 32,000 Sample LHD.**

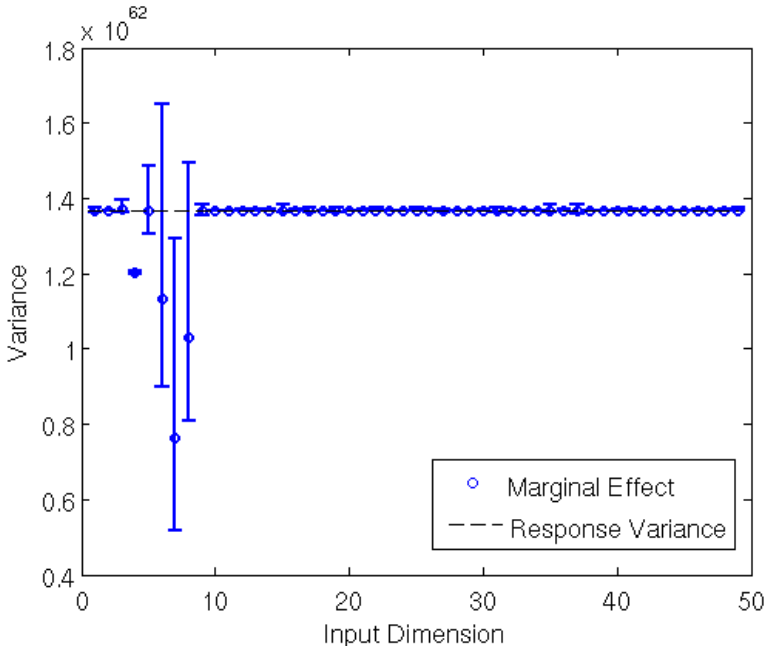


**Figure 96. QOI 2 Marginal Effects Adjusted Xenon 1-D Radial Ionization Potential Problem with 32,000 Sample LHD.**

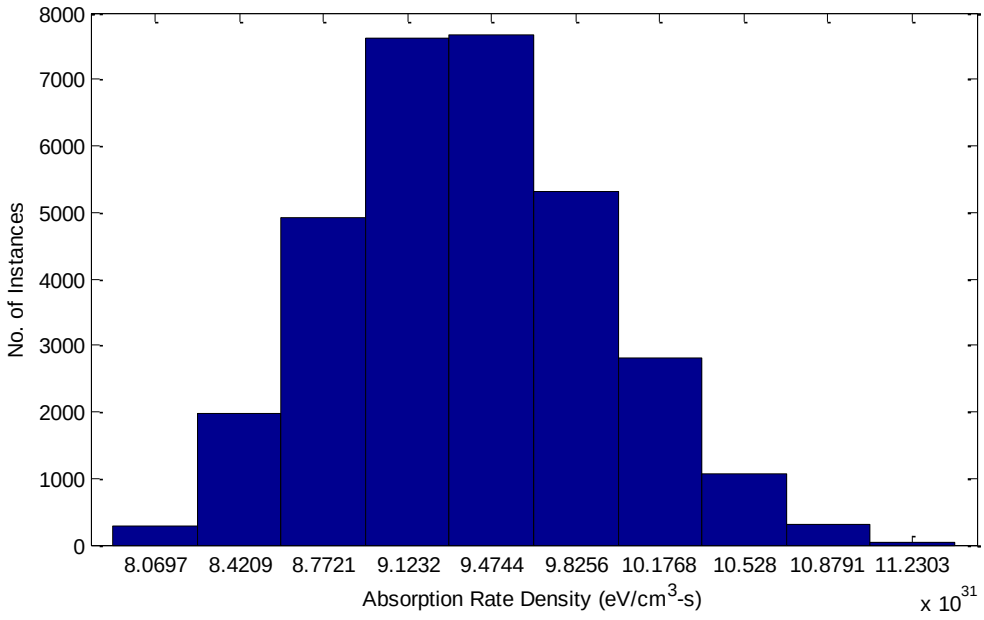


**Figure 97. QOI 3 for the Adjusted Xenon 1-D Radial Ionization Potential Problem with 32,000 Sample LHD.**

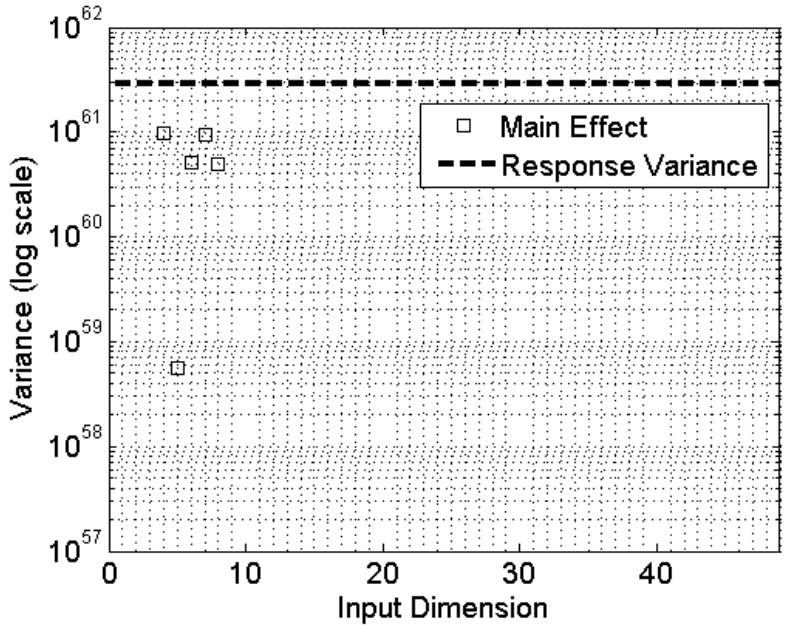


**Figure 98. QOI 3 Main Effects Adjusted Xenon 1-D Radial Ionization Potential Problem with 32,000 Sample LHD.**

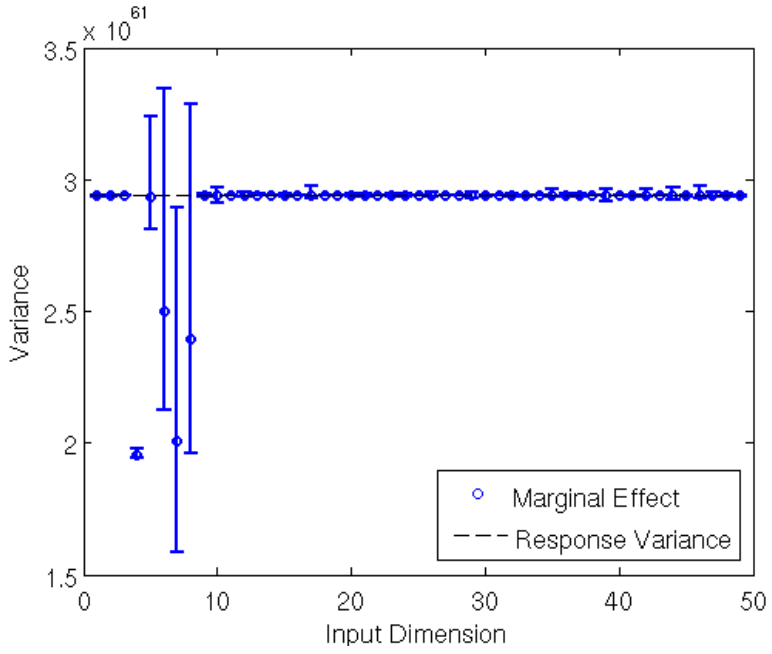


**Figure 99. QOI 3 Marginal Effects Adjusted Xenon 1-D Radial Ionization Potential Problem with 32,000 Sample LHD.**

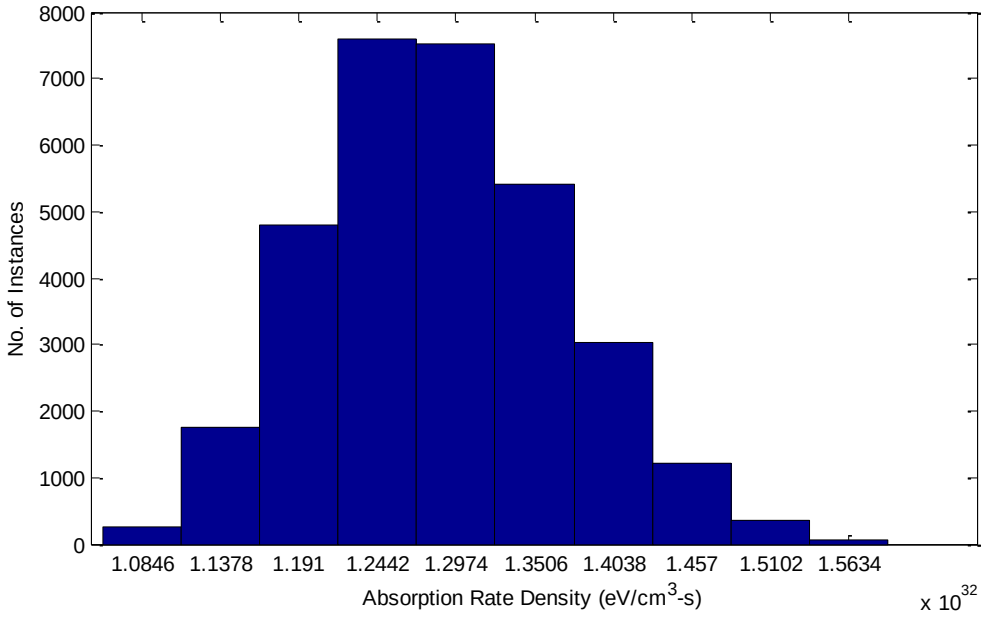


**Figure 100. QOI 4 for the Adjusted Xenon 1-D Radial Ionization Potential Problem with 32,000 Sample LHD.**

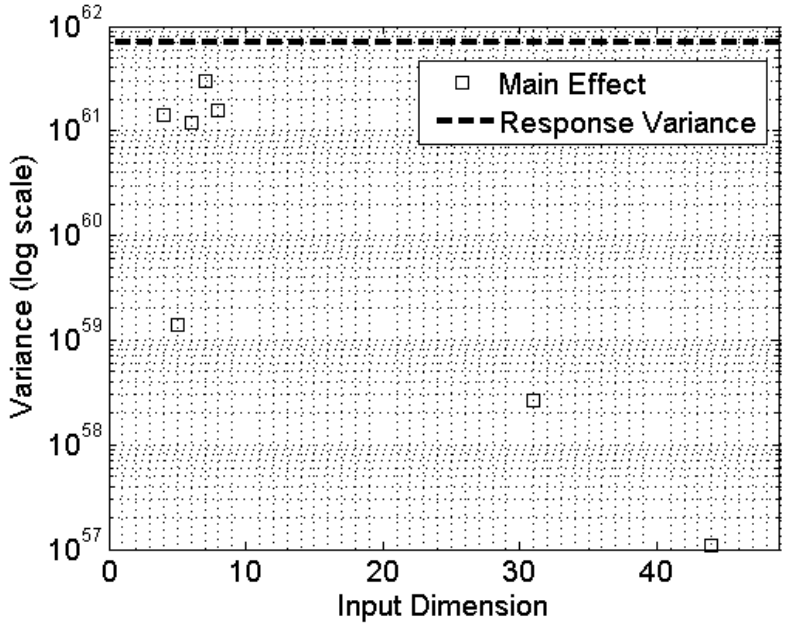


**Figure 101. QOI 4 Main Adjusted Xenon 1-D Radial Ionization Potential Problem with 32,000 Sample LHD.**

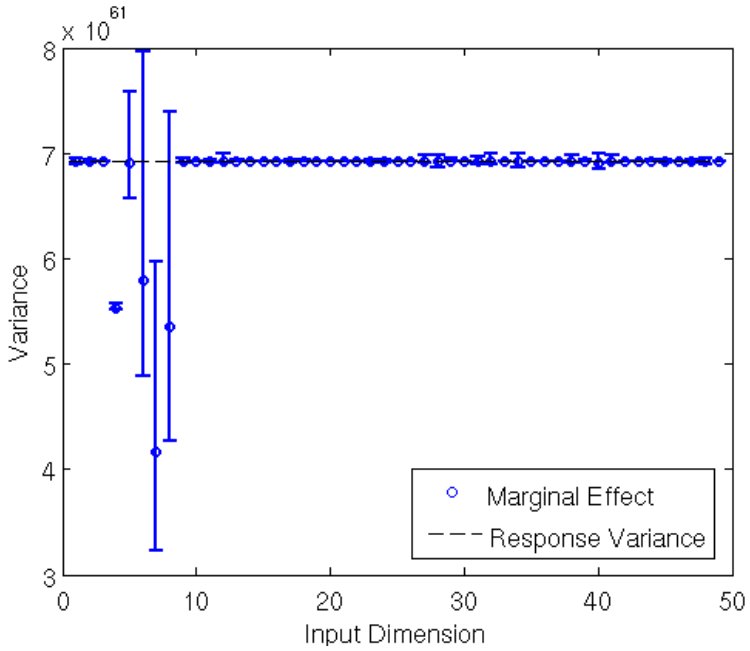


**Figure 102. QOI 4 Marginal Effects Adjusted Xenon 1-D Radial Ionization Potential Problem with 32,000 Sample LHD.**

#### 5.2.2.3 Important Parameters for the 1-D Radial Ionization Potential Case with Adjusted Xenon Opacities

We present a list of the parameters that are kept from the 1-D Radial problem for the ionization potential case with adjusted xenon opacities in Table 17.

**Table 17. Important Parameters for 1-D Radial Ionization Potential Case with Adjusted Xenon Opacities.**

| LHD | QOI | $10^{-4}$ Screening | $10^{-3}$ Screening |
|---|---|---|---|
| 1000 | 1 | 4, 6, 7, 8 | 4,6,7,8 |
| | 2 | 4, 6, 7, 8 | 4,6,7,8 |
| | 3 | 4, 6, 7, 8 | 4,6,7,8 |
| | 4 | 4, 6, 7, 8 | 4,6,7,8 |
| 32000 | 1 | 4-8 | 4,5,6,7,8 |
| | 2 | 4-8, 31 | 4,5,6,7,8,31 |
| | 3 | 4-8 | 4,5,6,7,8 |
| | 4 | 4-8, 31 | 4,5,6,7,8 |

When the xenon opacities are increased, they have a greater relative importance than when they were not adjusted. For the 2nd and 4th QOI, an ionization potential for carbon is now kept. This is because these QOIs are deeper in the plastic giving the opacity of the plastic a greater opportunity to affect the ARD.

### 5.2.3 Results Using Oscillator Strengths

We have tabulated the oscillator strengths that are used in the CRASH code in Table 2. It is known that oscillator strengths have some associated uncertainty with them. For this work, we take the uncertainty to be a uniform 5% about the value of the oscillator strength given in the table. In this section, we present results for the uncertainty analysis for the 1-D radial CRASH-like test problem. We present the PDF, main effect, and marginal effect plots for the 1,000 sample LHD in Figure 103 through Figure 114 and for the 32,000 sample LHD in Figure 115 through Figure 126.

#### 5.2.3.1 Results with the 1,000 Sample Latin Hypercube Design

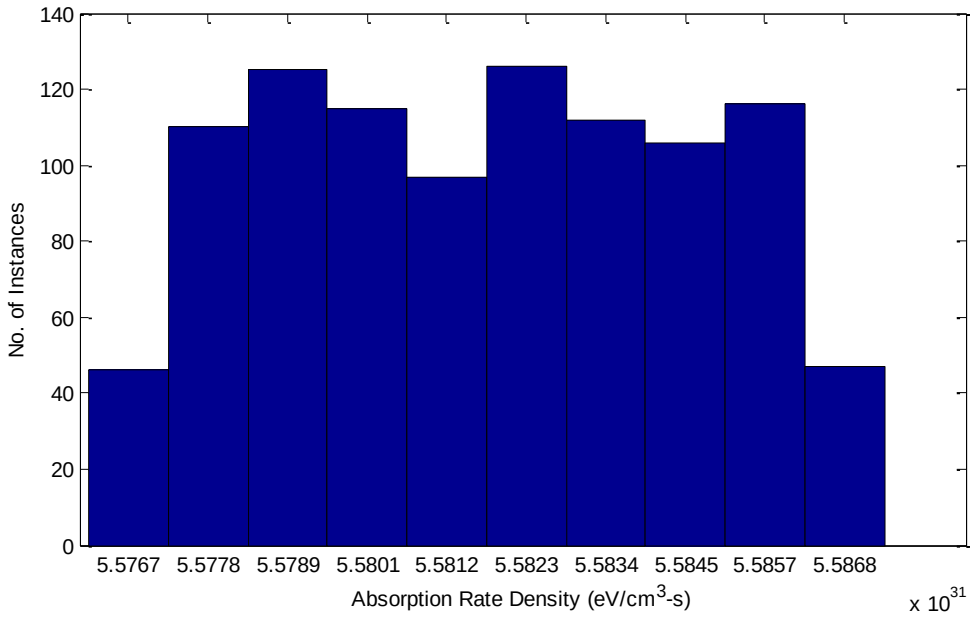


**Figure 103. QOI 1 for the 1-D Radial Oscillator Strength Problem with 1,000 Sample LHD.**

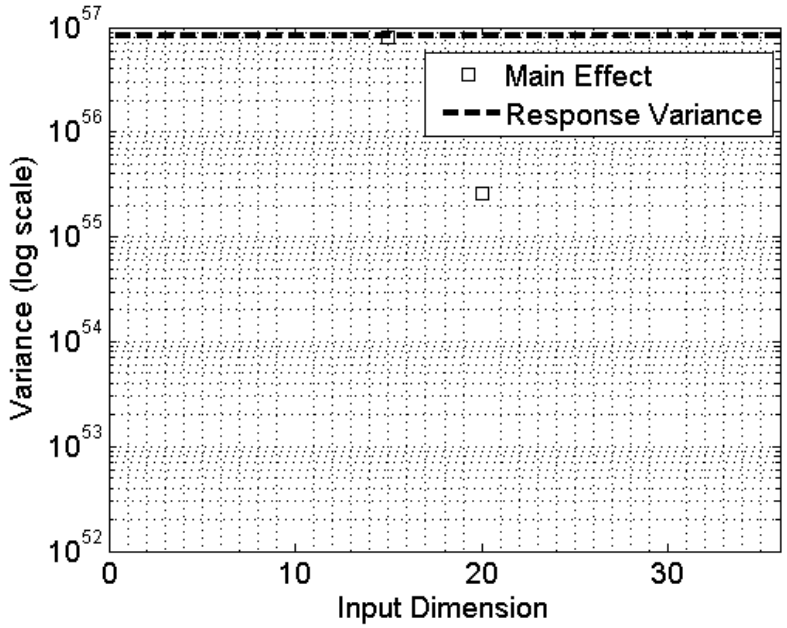


**Figure 104. QOI 1 Main Effects for 1-D Radial Oscillator Strength Problem with 1,000 Sample LHD.**

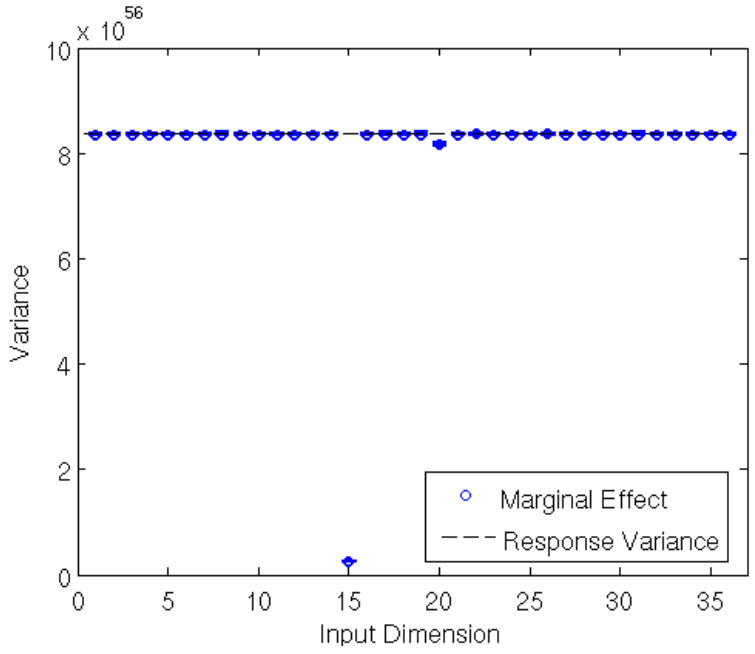


**Figure 105. QOI 1 Marginal Effects for 1-D Radial Oscillator Strength Problem with 1,000 Sample LHD.**

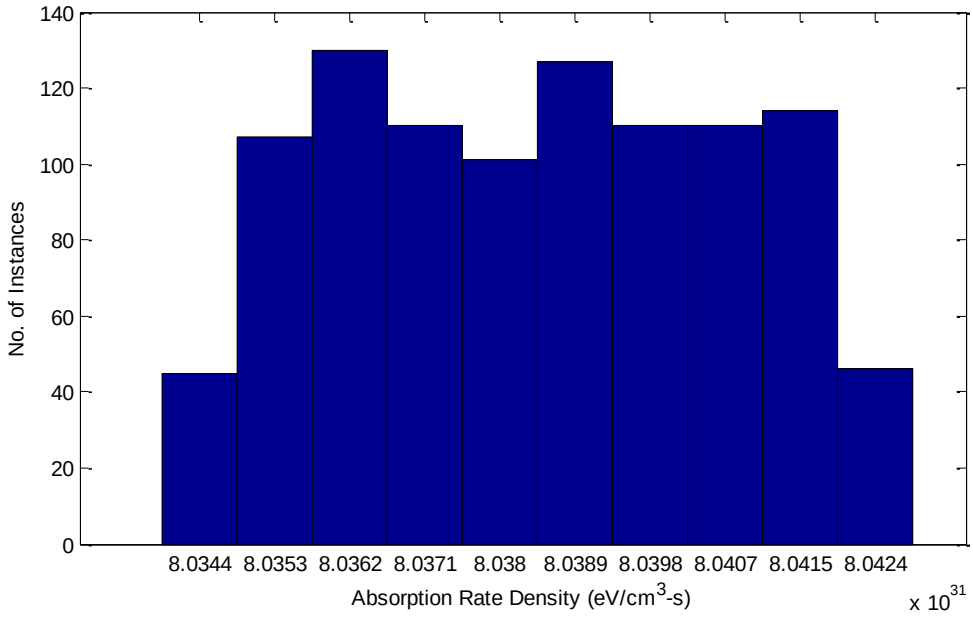


**Figure 106. QOI 2 for the 1-D Radial Oscillator Strength Problem with 1,000 Sample LHD.**

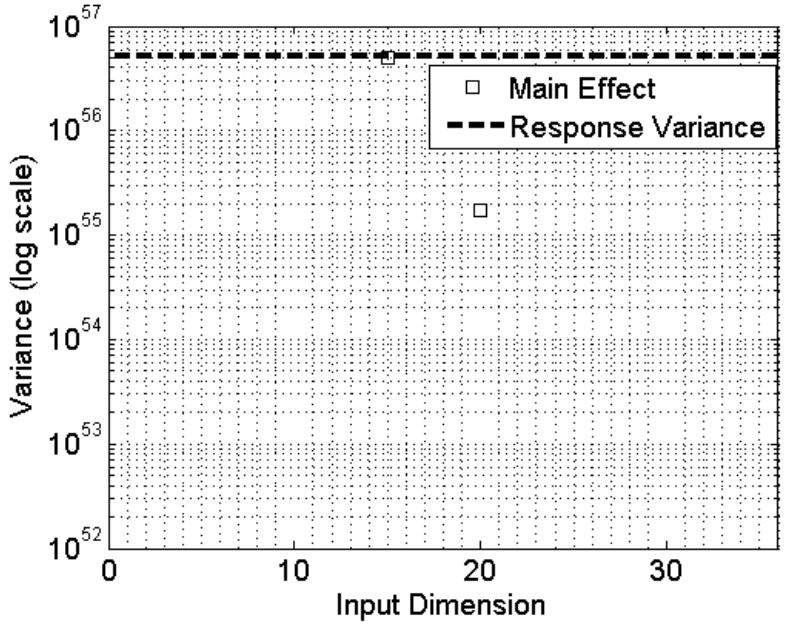


**Figure 107. QOI 2 Main Effects for 1-D Radial Oscillator Strength Problem with 1,000 Sample LHD.**

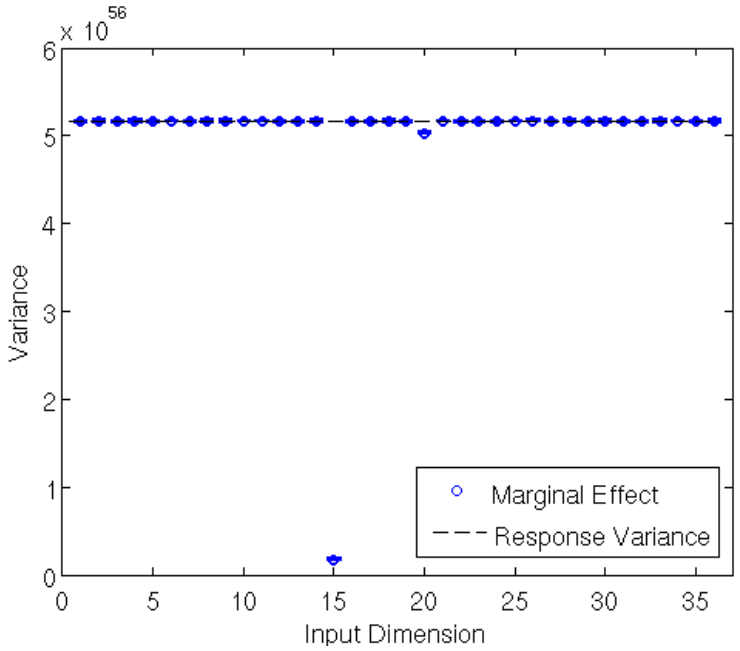


**Figure 108. QOI 2 Marginal Effects for 1-D Radial Oscillator Strength Problem with 1,000 Sample LHD.**

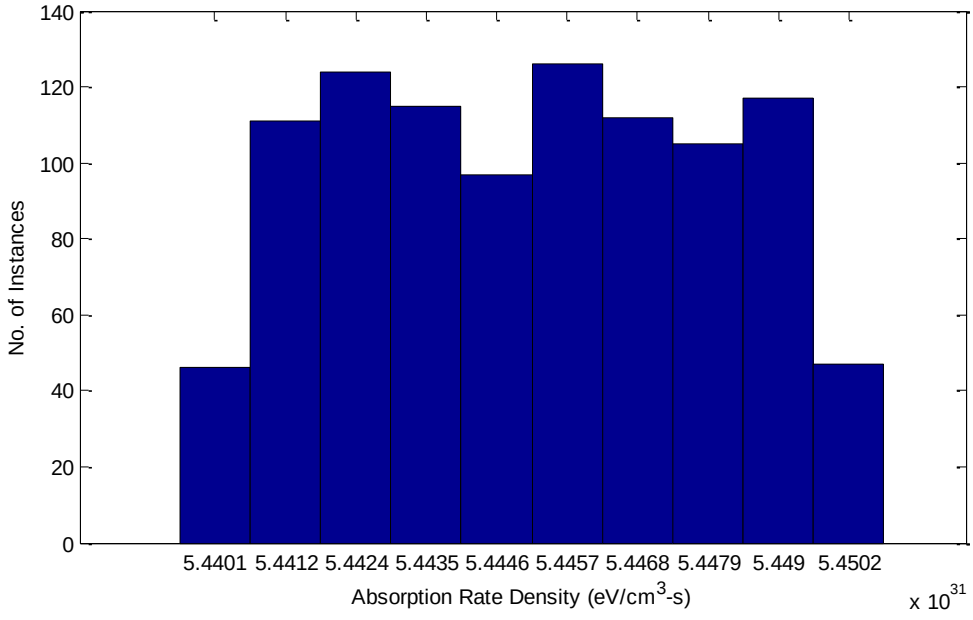


**Figure 109. QOI 3 for the 1-D Radial Oscillator Strength Problem with 1,000 Sample LHD.**

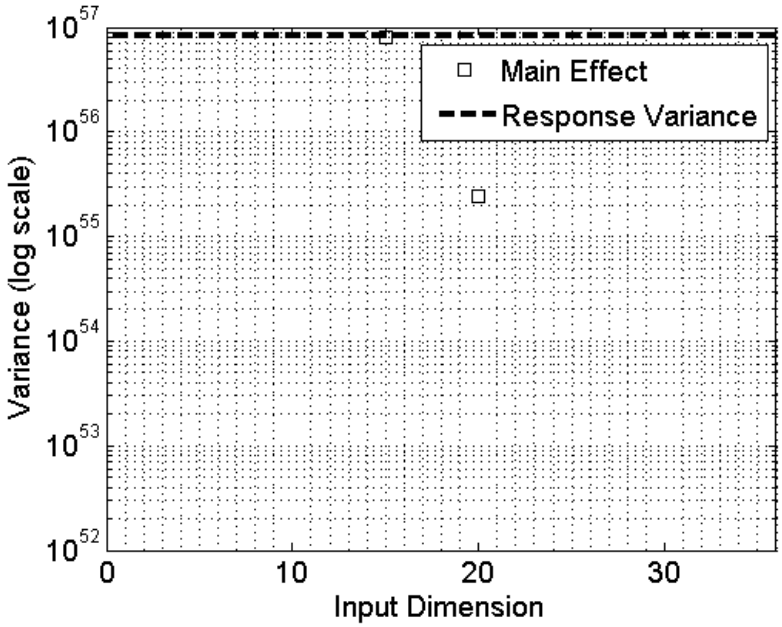


**Figure 110. QOI 3 Main Effects for 1-D Radial Oscillator Strength Problem with 1,000 Sample LHD.**

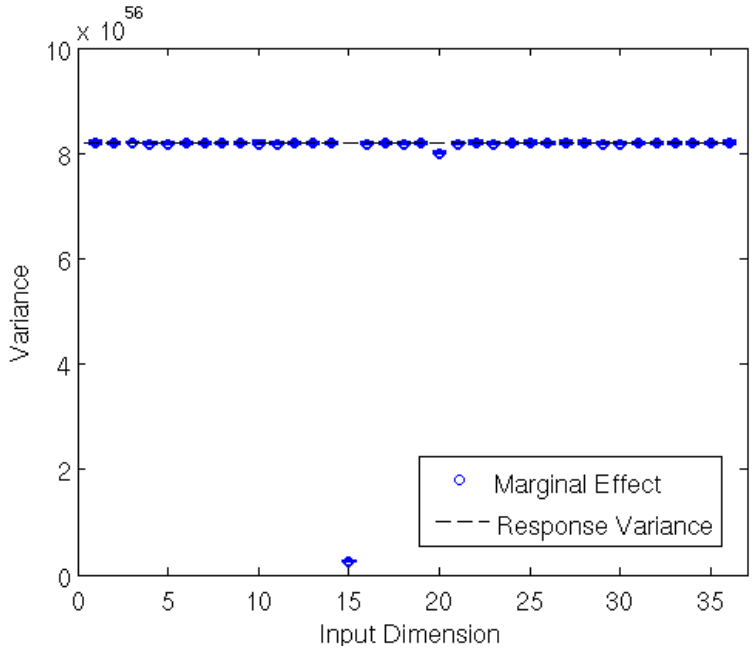


**Figure 111. QOI 3 Marginal Effects for 1-D Radial Oscillator Strength Problem with 1,000 Sample LHD.**

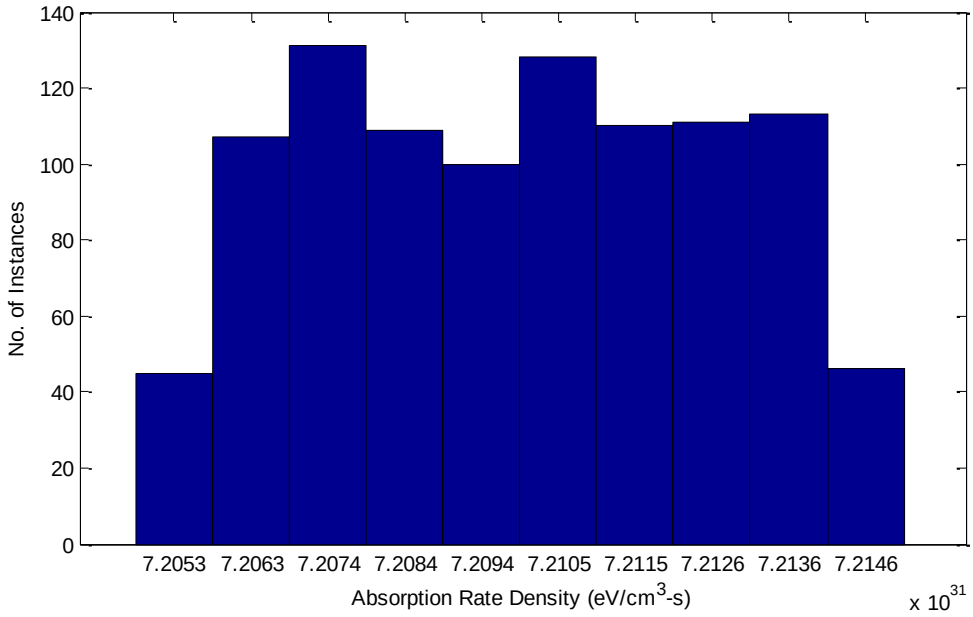


**Figure 112. QOI 4 for the 1-D Radial Oscillator Strength Problem with 1,000 Sample LHD.**

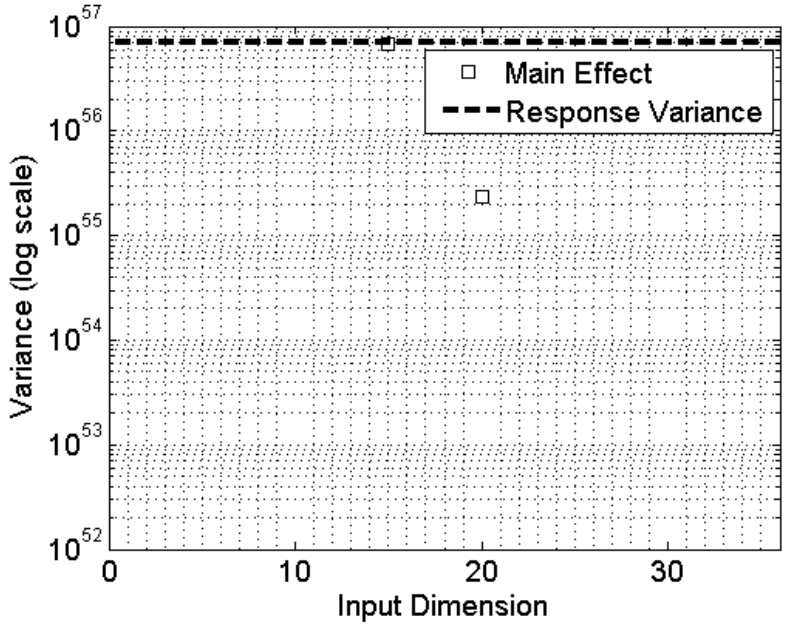


**Figure 113. QOI 4 Main Effects for 1-D Radial Oscillator Strength Problem with 1,000 Sample LHD.**

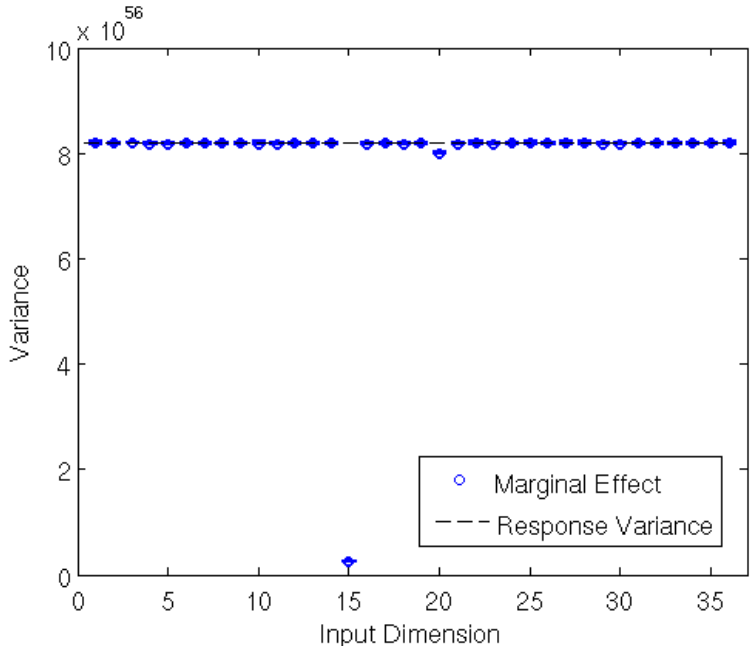


**Figure 114. QOI 4 Marginal Effects for 1-D Radial Oscillator Strength Problem with 1,000 Sample LHD.**

### 5.2.3.2 Results with the 32,000 Sample Latin Hypercube Design

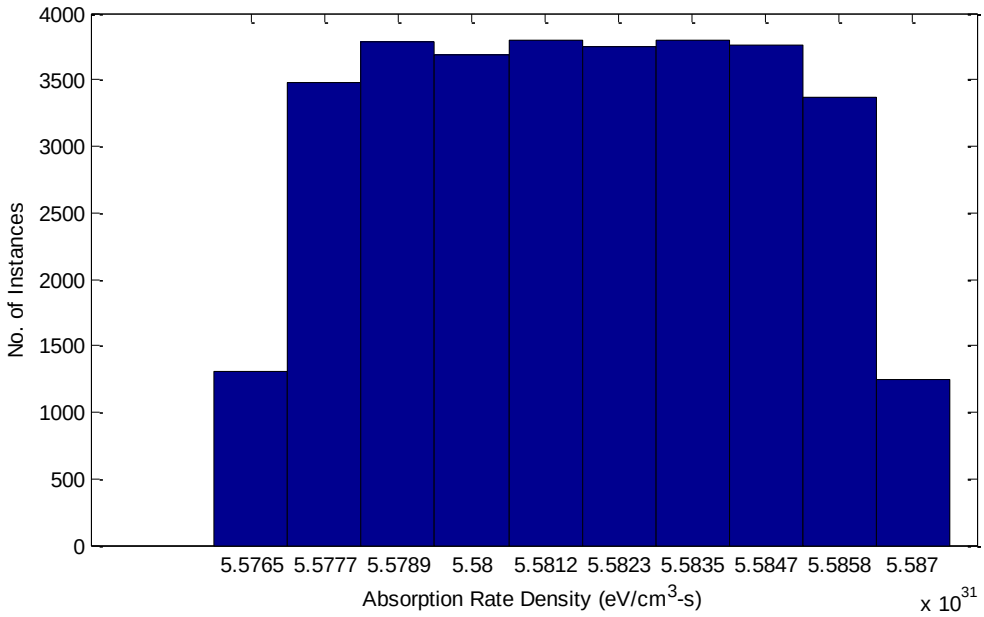


**Figure 115. QOI 1 for the 1-D Radial Oscillator Strength Problem with 32,000 Sample LHD.**

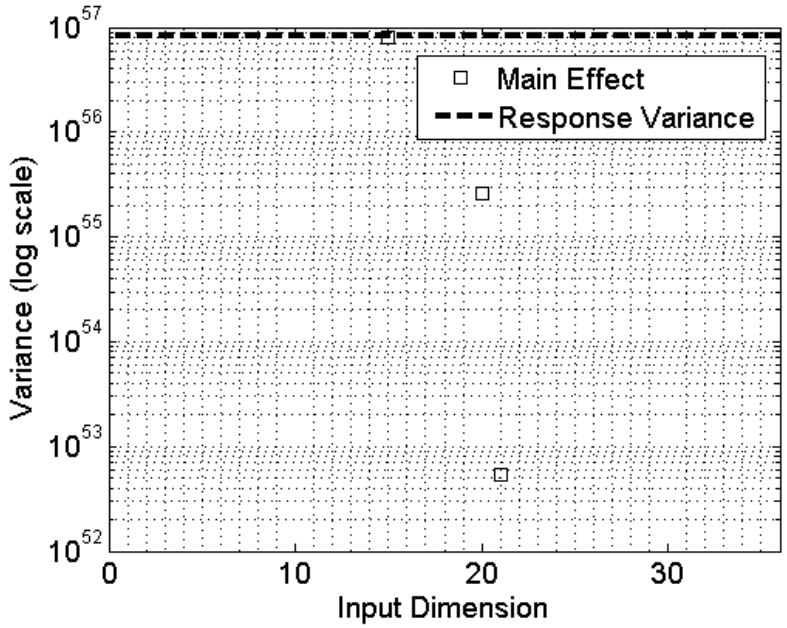


**Figure 116. QOI 1 Main Effects for 1-D Radial Oscillator Strength Problem with 32,000 Sample LHD.**

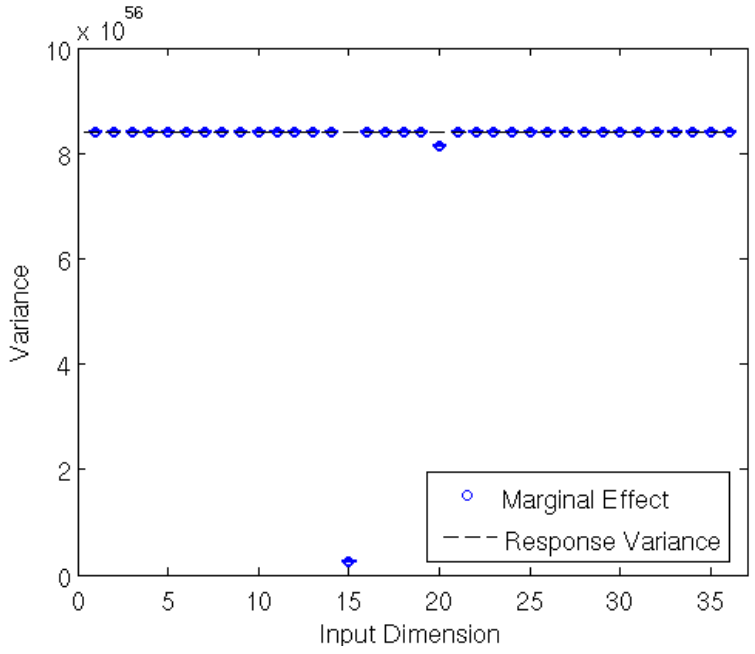


**Figure 117. QOI 1 Marginal Effects 1-D Radial Oscillator Strength Problem with 32,000 Sample LHD.**

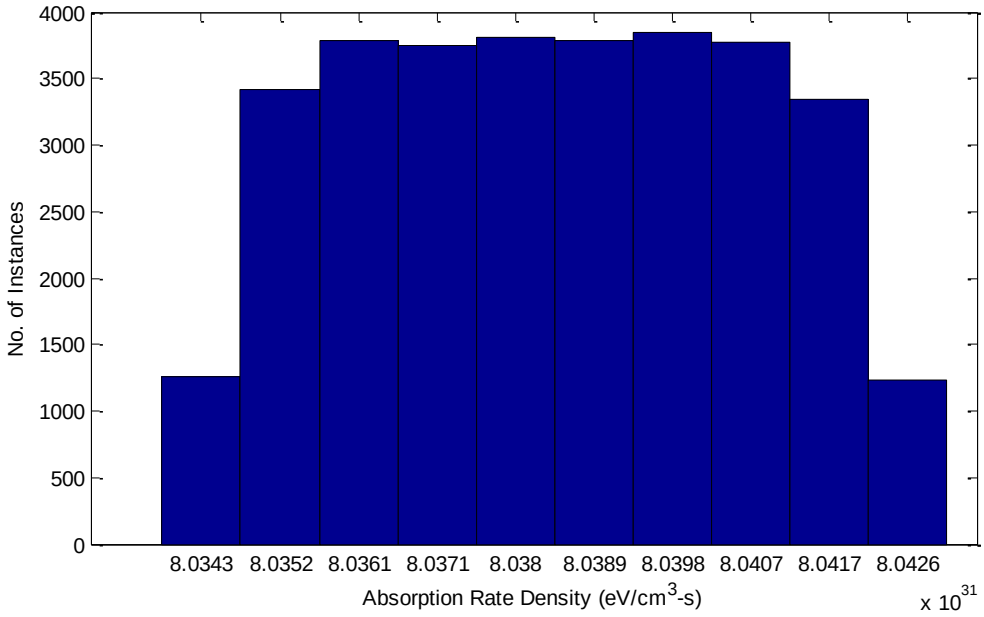


**Figure 118. QOI 2 for the 1-D Radial Oscillator Strength Problem with 32,000 Sample LHD.**

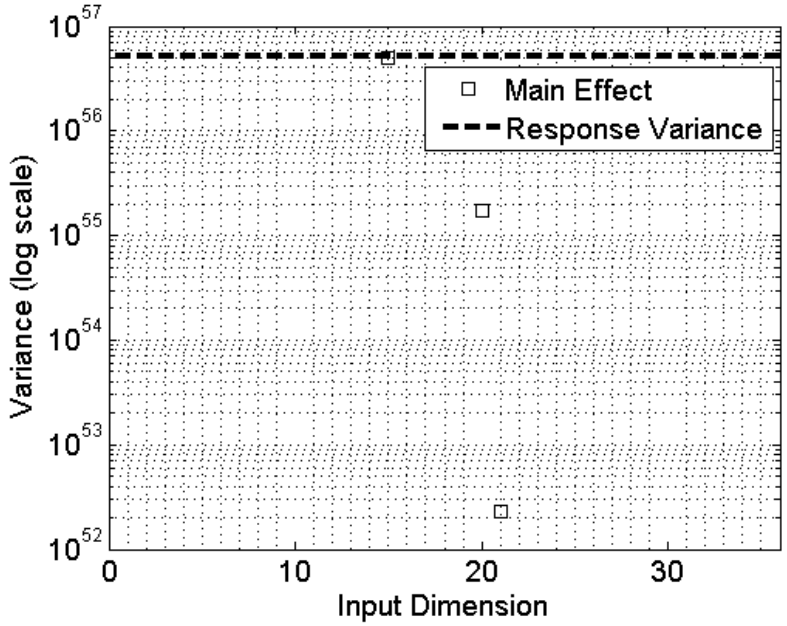


**Figure 119. QOI 2 Main Effects for 1-D Radial Oscillator Strength Problem with 32,000 Sample LHD.**

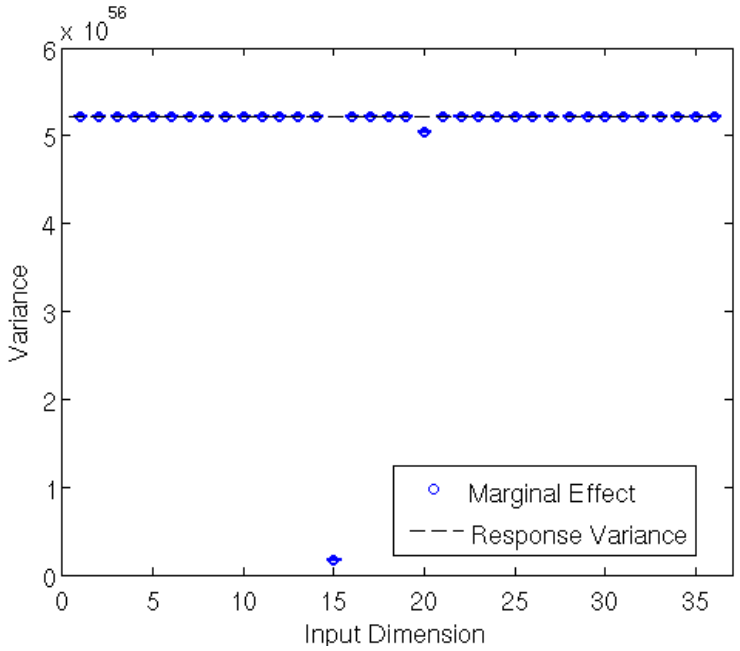


**Figure 120. QOI 2 Marginal Effects for 11-D Radial Oscillator Strength Problem with 32,000 Sample LHD.**

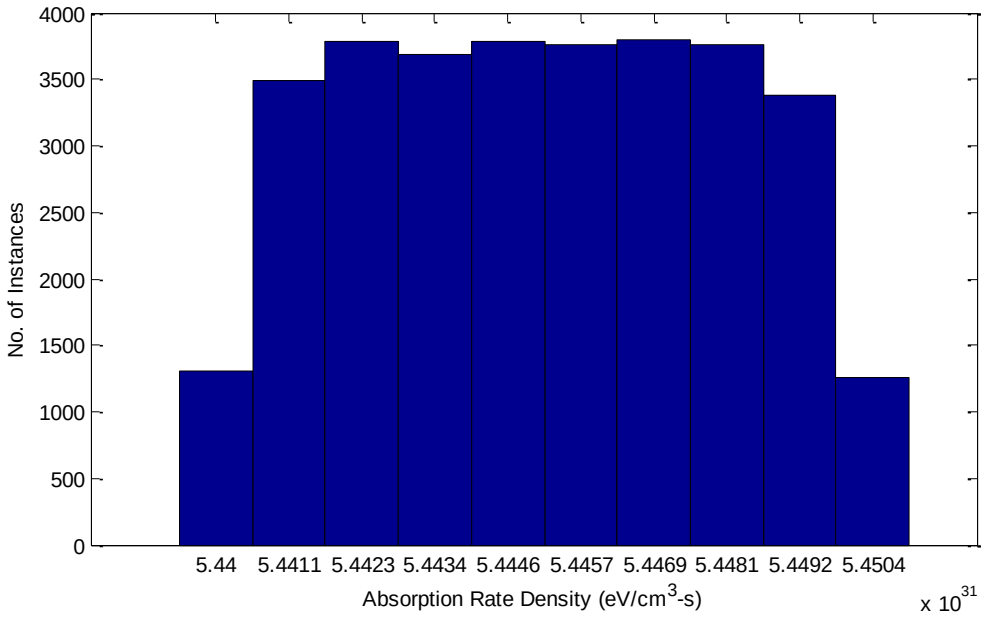


**Figure 121. QOI 3 for the 1-D Radial Oscillator Strength Problem with 32,000 Sample LHD.**

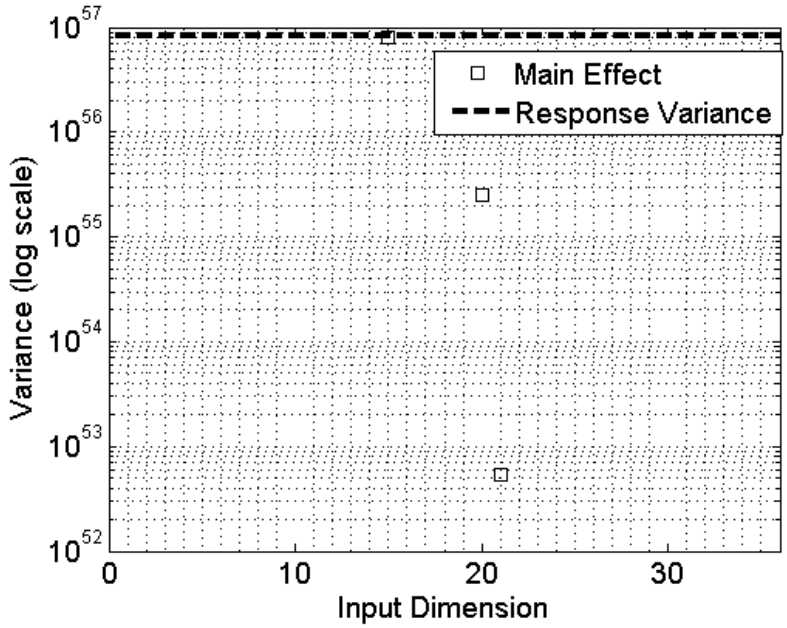


**Figure 122. QOI 3 Main Effects for 1-D Radial Oscillator Strength Problem with 32,000 Sample LHD.**

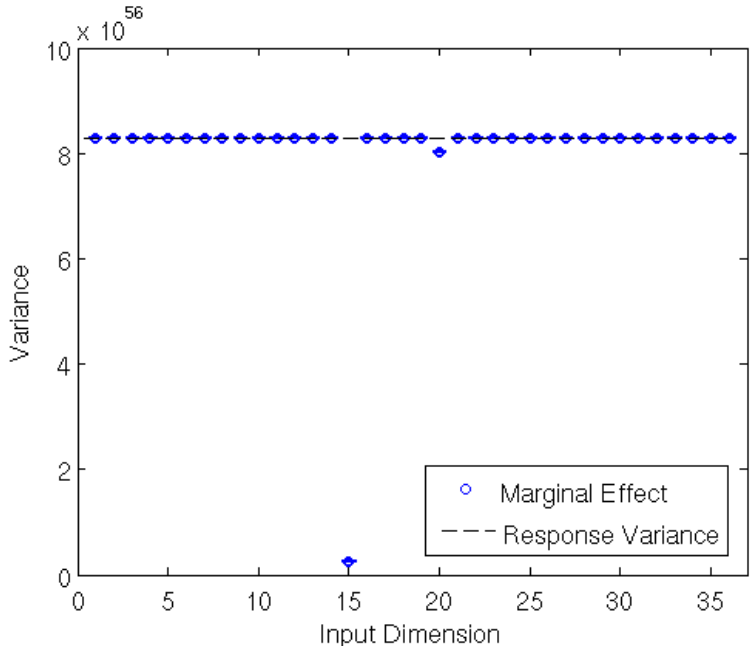


**Figure 123. QOI 3 Marginal Effects for 1-D Radial Oscillator Strength Problem with 32,000 Sample LHD.**

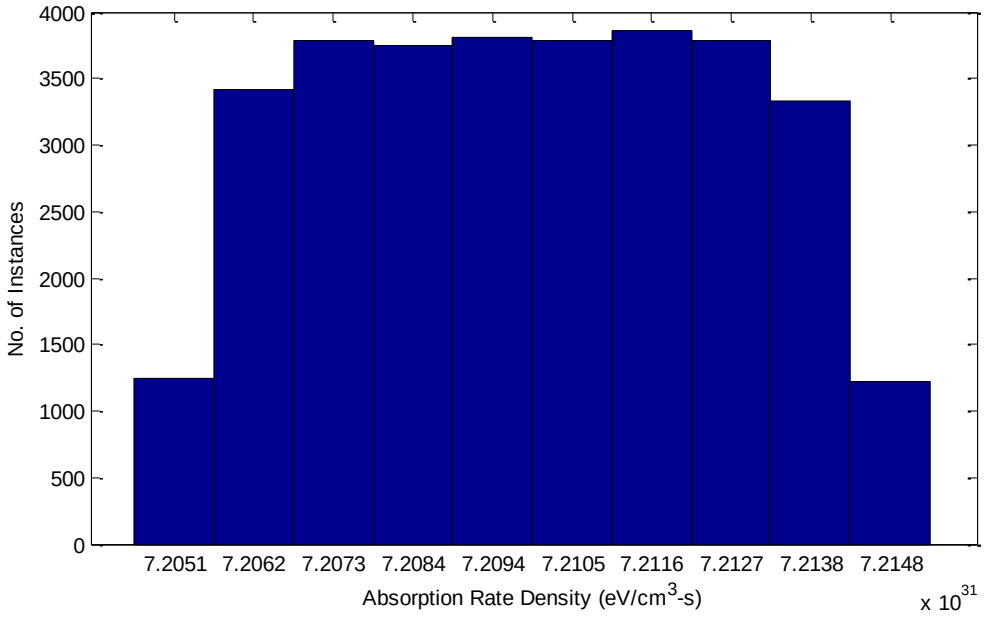


**Figure 124. QOI 4 for the 1-D Radial Oscillator Strength Problem with 32,000 Sample LHD.**

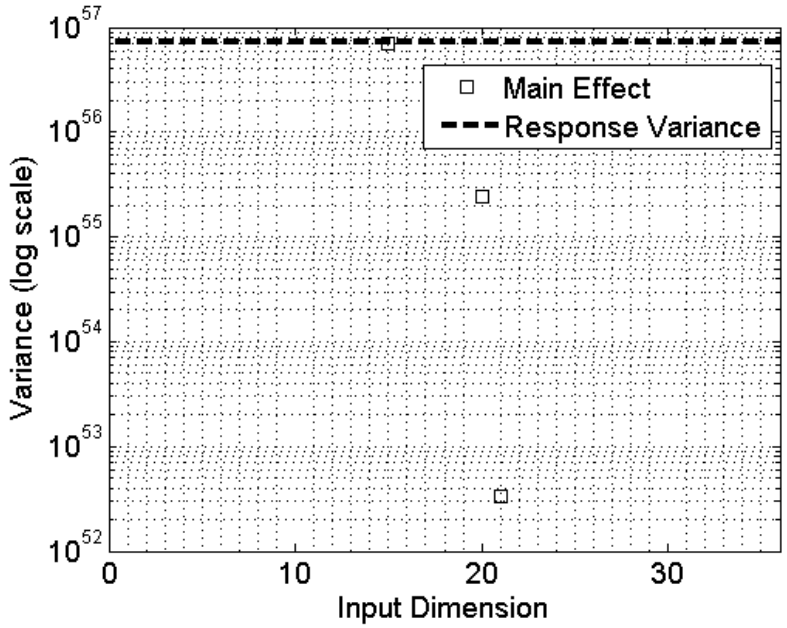


**Figure 125. QOI 4 Main Effects for 1-D Radial Oscillator Strength Problem with 32,000 Sample LHD.**

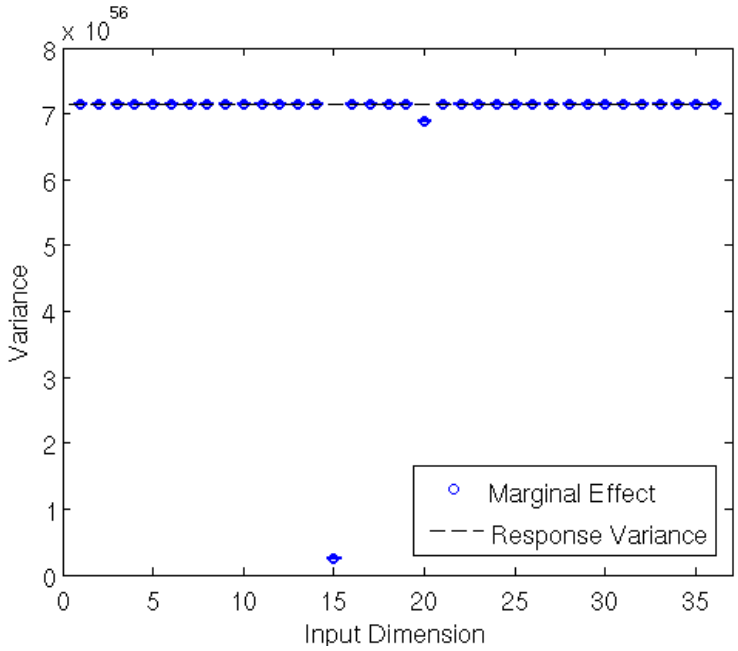


**Figure 126. QOI 4 Marginal Effects for 1-D Radial Oscillator Strength Problem with 32,000 Sample LHD.**

### 5.2.3.3 Important Parameters for the 1-D Radial Oscillator Strength Case

We present a list of the important parameters in Table 18.

**Table 18. Important Parameters for 1-D Radial Oscillator Strength Case.**

| LHD | QOI | $10^{-4}$ Screening | $10^{-3}$ Screening |
|---|---|---|---|
| 1000 | 1 | 15, 20 | 15, 20 |
| | 2 | 15, 20 | 15, 20 |
| | 3 | 15, 20 | 15, 20 |
| | 4 | 15, 20 | 15, 20 |
| 32000 | 1 | 15, 20, 21 | 15, 20 |
| | 2 | 15, 20, 21 | 15, 20 |
| | 3 | 15, 20, 21 | 15, 20 |
| | 4 | 15, 20, 21 | 15, 20 |

These oscillator strengths are important because they are the strong oscillator strengths with populated orbitals. The oscillator strengths that were either very small or had no or very low electron populations have been removed by this screening method. The sets of kept parameters for each of the QOIs are almost identical. These results for the 1,000 and 32,000 cases for the oscillator strengths have almost no variance in the PDFs, which means that the bound-bound interactions are not important. This is occurs because the opacities generated with the CRASH opacity code do not treat bound-bound interactions correctly, and this has led us to pursue the LANL adjusted opacities.

### 5.2.4 Results Using Oscillator Strengths with Adjusted Xenon Opacity

We perform the same uncertainty analysis as is done in the previous section; however, we use the LANL adjusted xenon opacity. We present the PDF, main effect, and marginal effect plots for the 1,000 sample LHD in Figure 127 through Figure 138 and for the 32,000 sample LHD in Figure 139 through Figure 150.

#### 5.2.4.1 Results with the 1,000 Sample Latin Hypercube Design

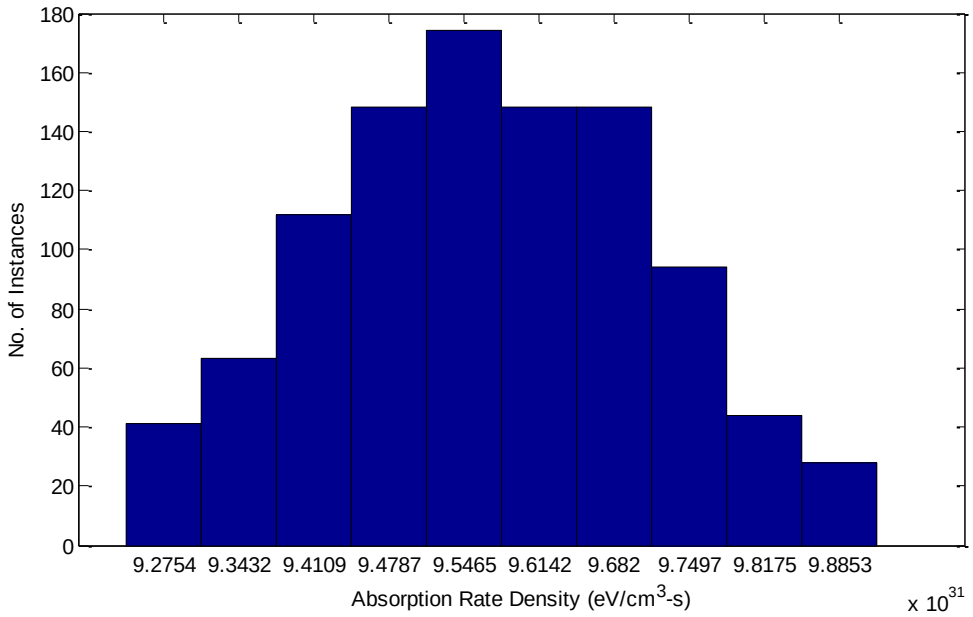


**Figure 127. QOI 1 for the Adjusted Xenon 1-D Radial Oscillator Strength Problem with 1,000 Sample LHD.**

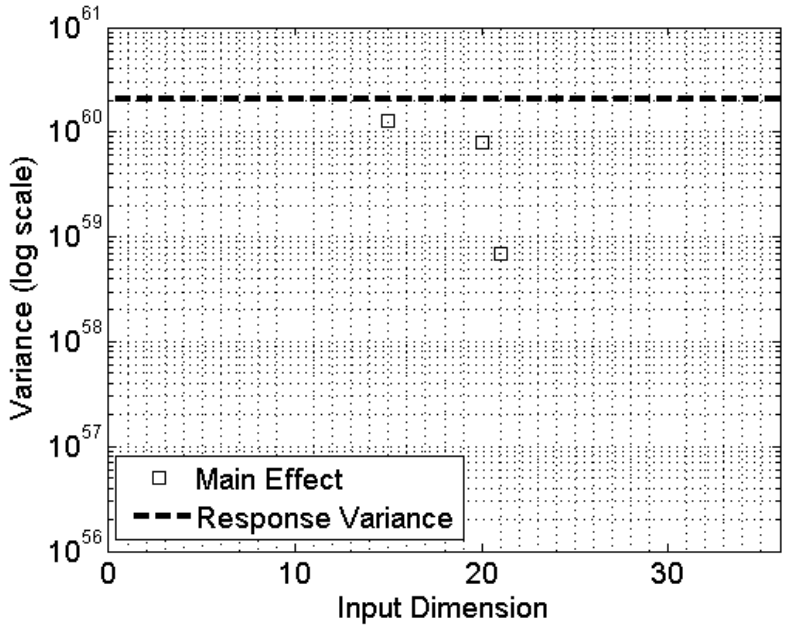


**Figure 128. Main Effects for Adjusted Xenon 1-D Radial Oscillator Strength Problem with 1,000 Sample LHD.**

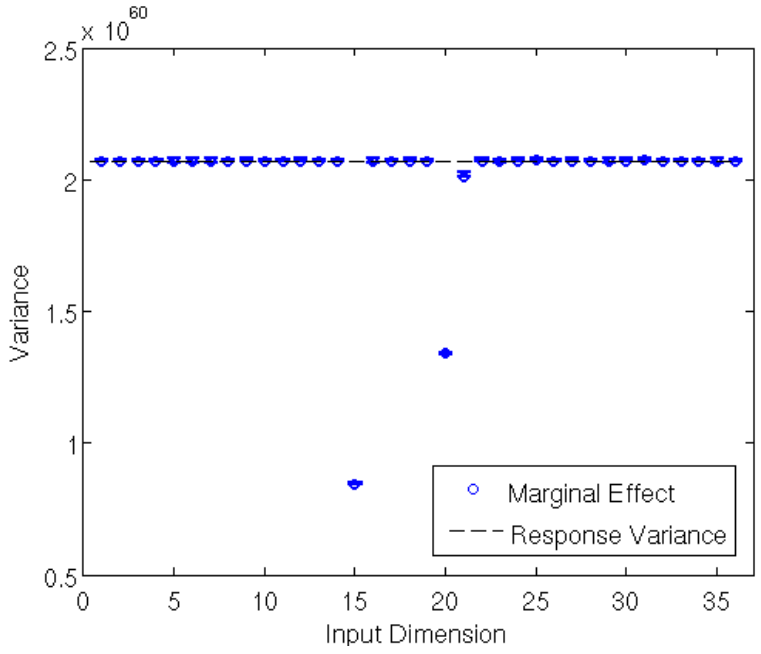


**Figure 129. QOI 1 Marginal Effects for Adjusted Xenon 1-D Radial Oscillator Strength Problem with 1,000 Sample LHD.**

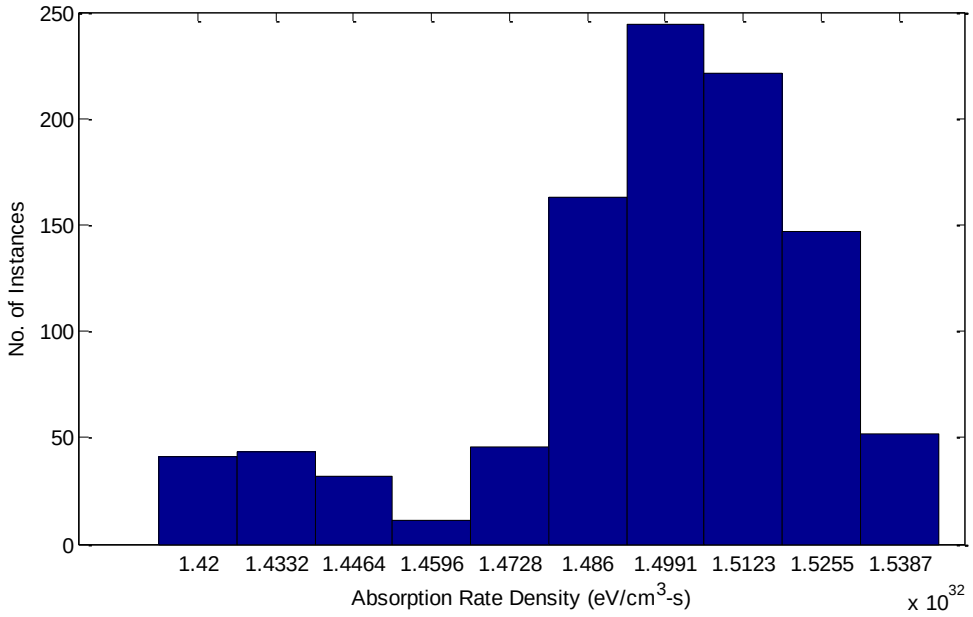


**Figure 130. QOI 2 for the Adjusted Xenon 1-D Radial Oscillator Strength Problem with 1,000 Sample LHD.**

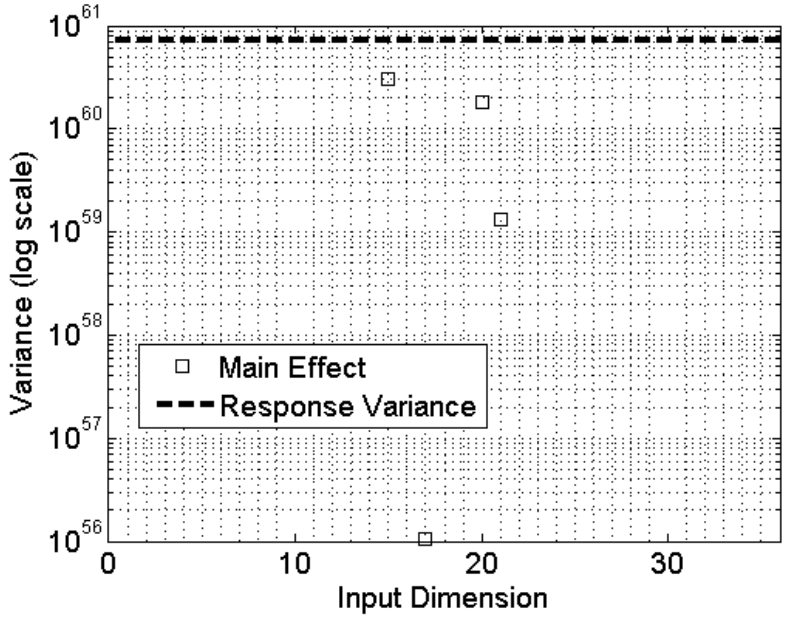


**Figure 131. QOI 2 Main Effects for Adjusted Xenon 1-D Radial Oscillator Strength Problem with 1,000 Sample LHD.**

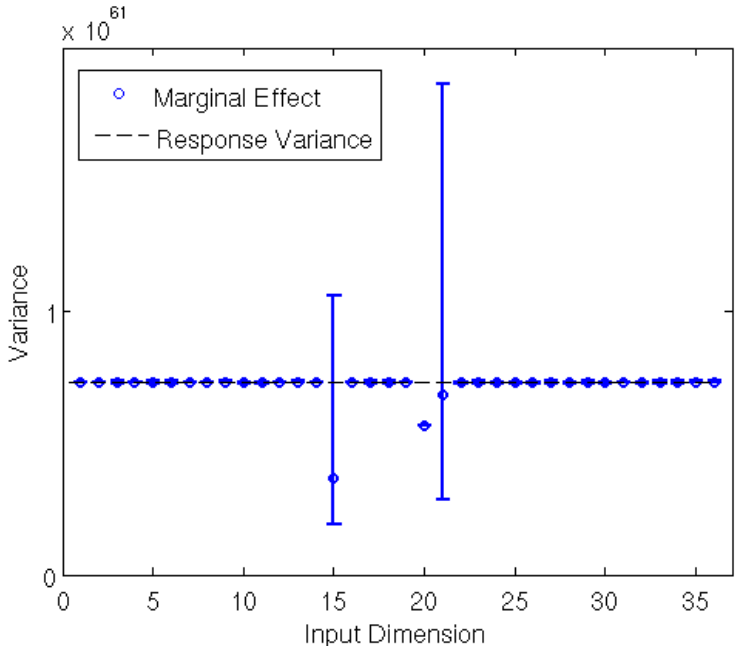


**Figure 132. QOI 2 Marginal Effects for Adjusted Xenon 1-D Radial Oscillator Strength Problem with 1,000 Sample LHD.**

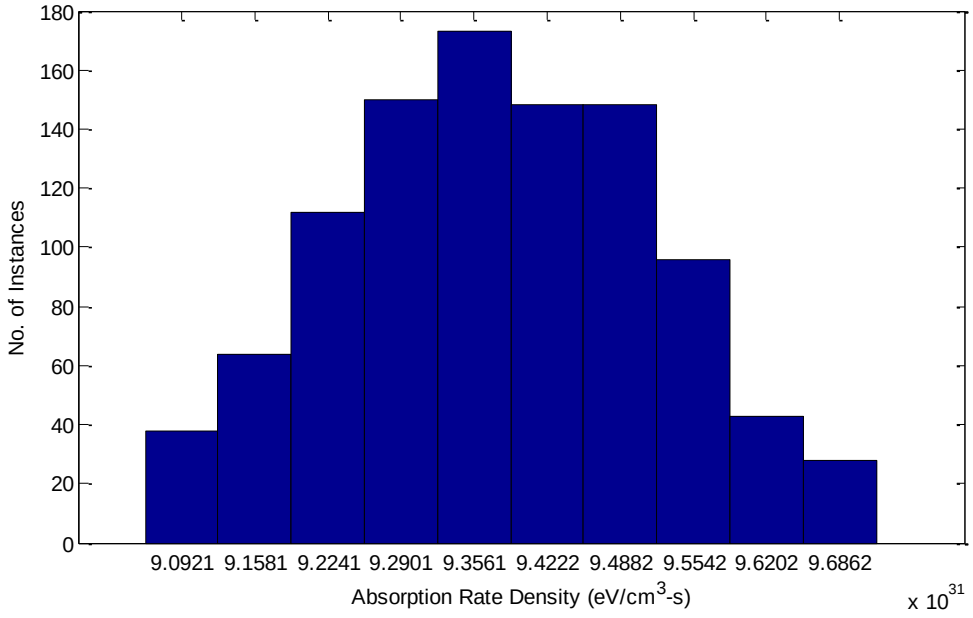


**Figure 133. QOI 3 for the Adjusted Xenon 1-D Radial Oscillator Strength Problem with 1,000 Sample LHD.**

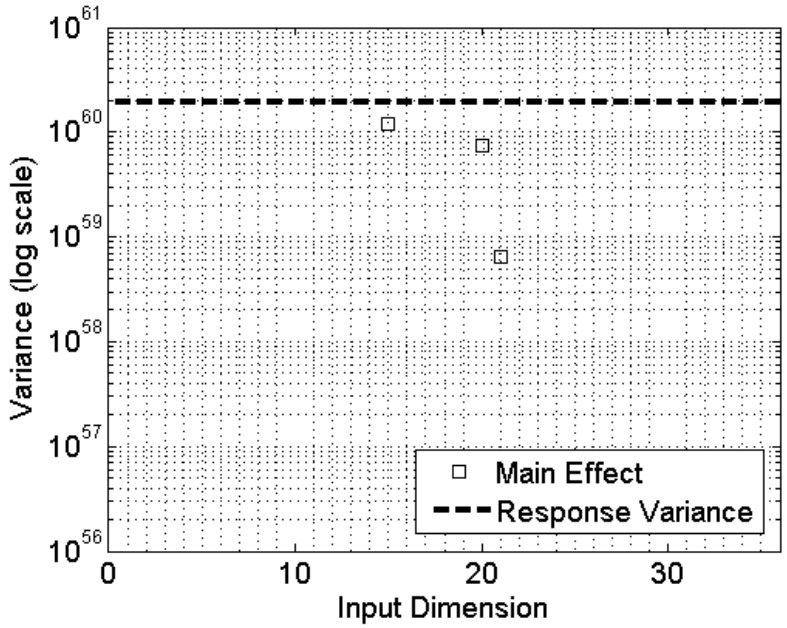


**Figure 134. QOI 3 Main Effects for Adjusted Xenon 1-D Radial Oscillator Strength Problem with 1,000 Sample LHD.**

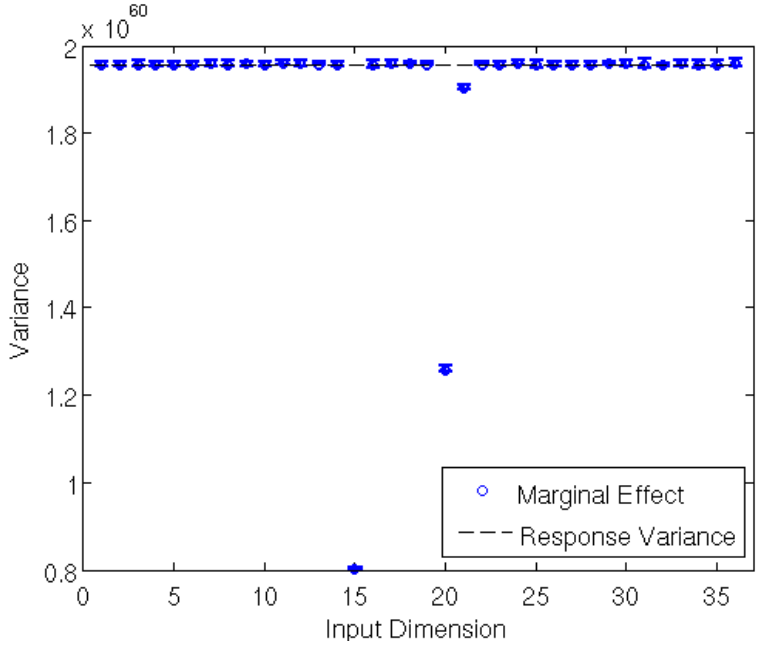


**Figure 135. QOI 3 Marginal Effects for Adjusted Xenon 1-D Radial Oscillator Strength Problem with 1,000 Sample LHD.**

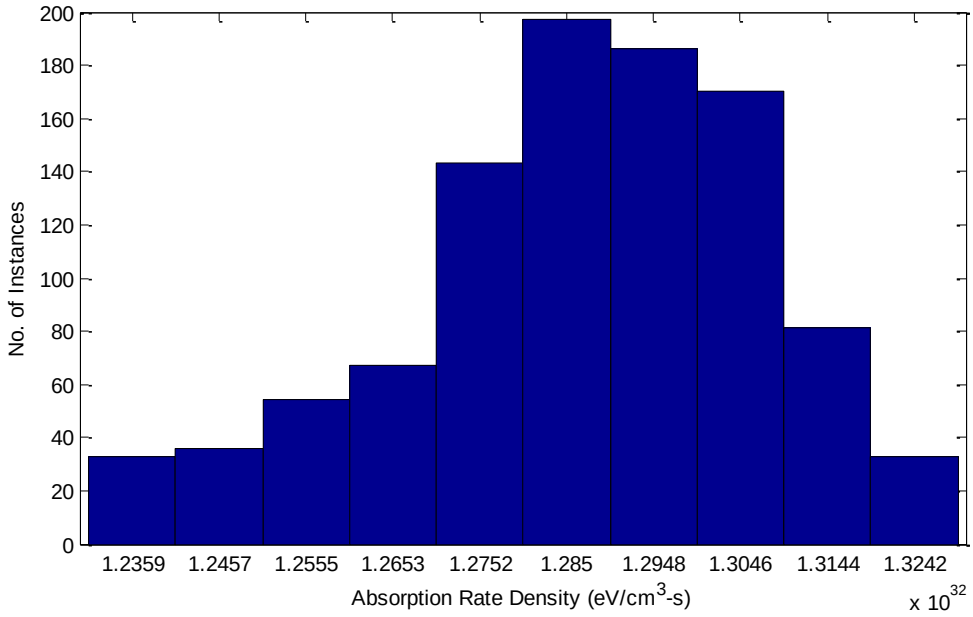


**Figure 136. QOI 4 for the Adjusted Xenon 1-D Radial Oscillator Strength Problem with 1,000 Sample LHD.**

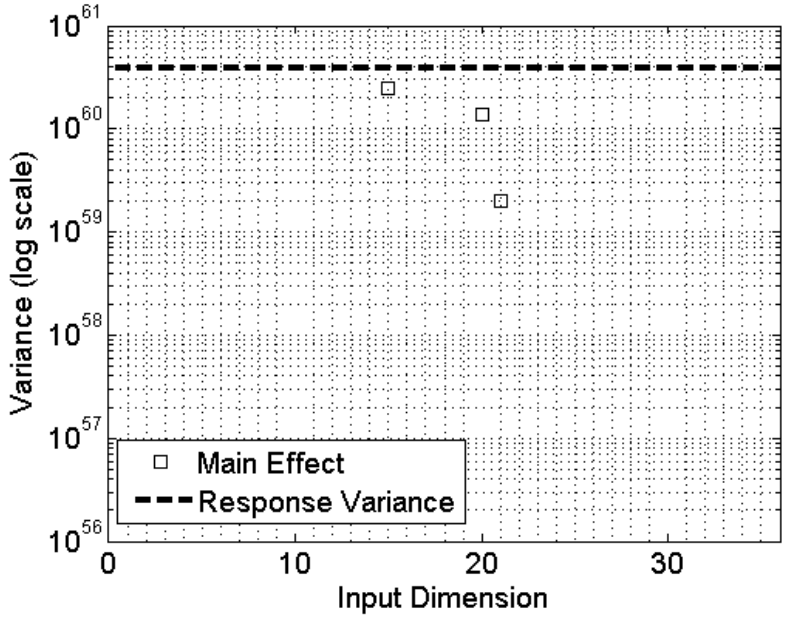


**Figure 137. QOI 4 Main Effects for Adjusted Xenon 1-D Radial Oscillator Strength Problem with 1,000 Sample LHD.**

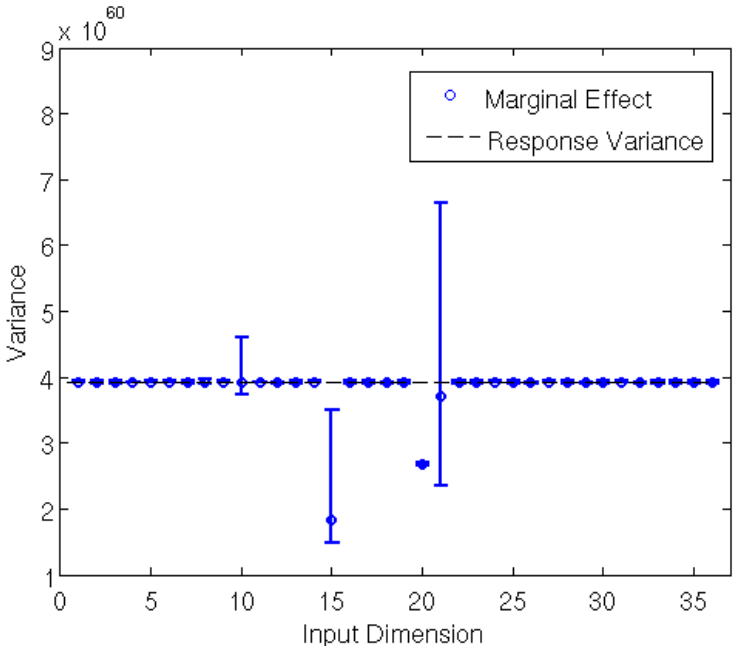


**Figure 138. QOI 4 Marginal Effects for Adjusted Xenon 1-D Radial Oscillator Strength Problem with 1,000 Sample LHD.**

### 5.2.4.2 Results with the 32,000 Sample Latin Hypercube Design

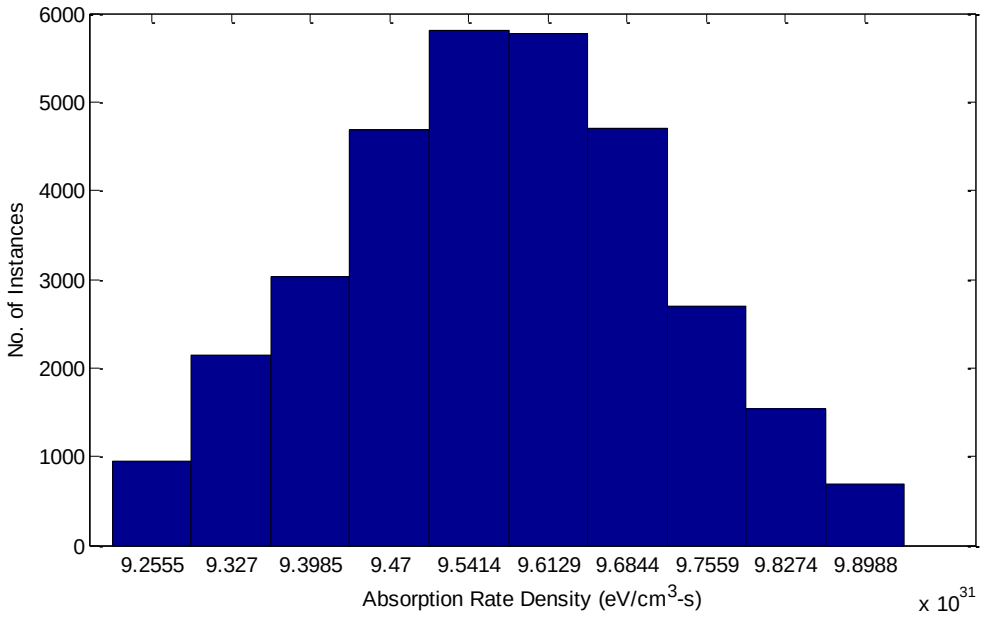


**Figure 139. QOI 1 for the Adjusted Xenon 1-D Radial Oscillator Strength Problem with 32,000 Sample LHD.**

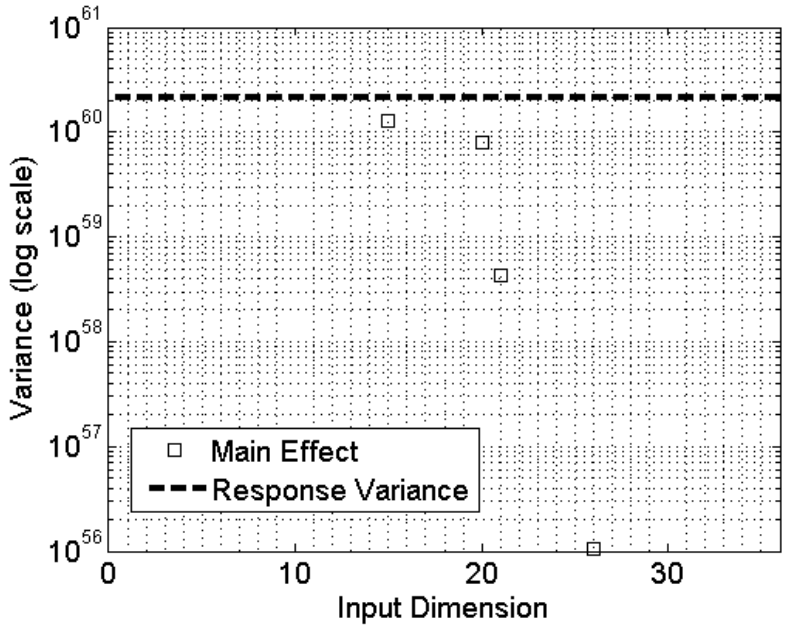


**Figure 140. QOI 1 Main Effects for Adjusted Xenon 1-D Radial Oscillator Strength Problem with 32,000 Sample LHD.**

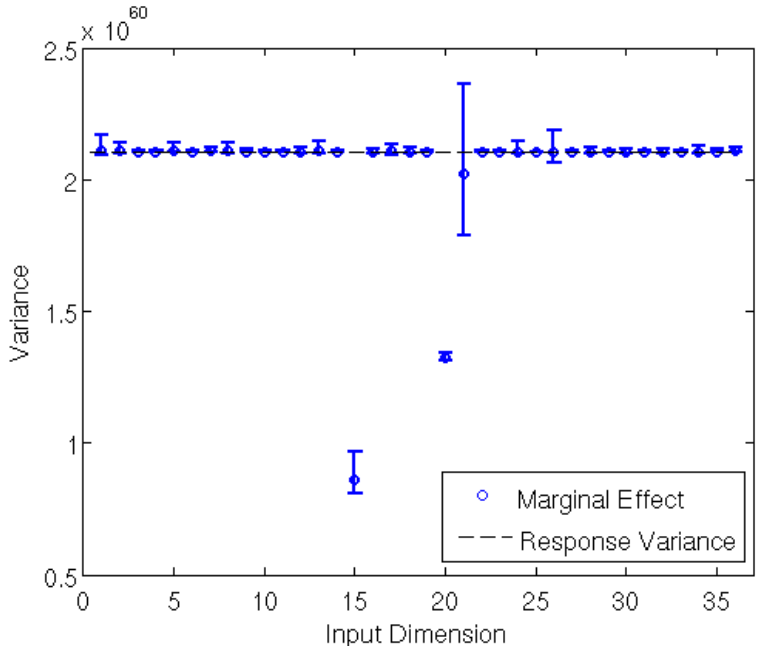


**Figure 141. QOI 1 Marginal Effects for Adjusted Xenon 1-D Radial Oscillator Strength Problem with 32,000 Sample LHD.**

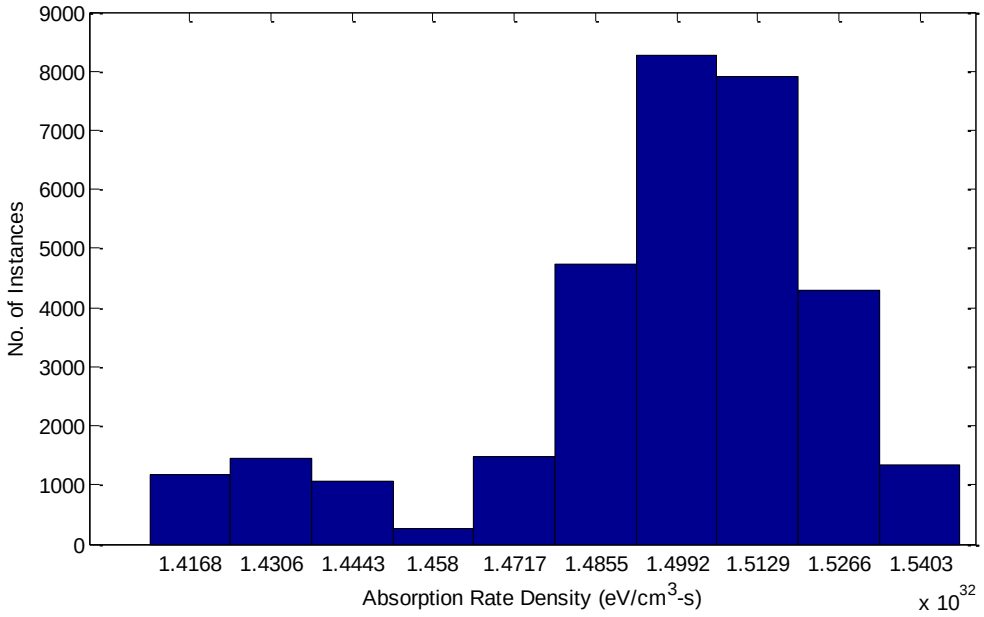


**Figure 142. QOI 2 for the Adjusted Xenon 1-D Radial Oscillator Strength Problem with 32,000 Sample LHD.**

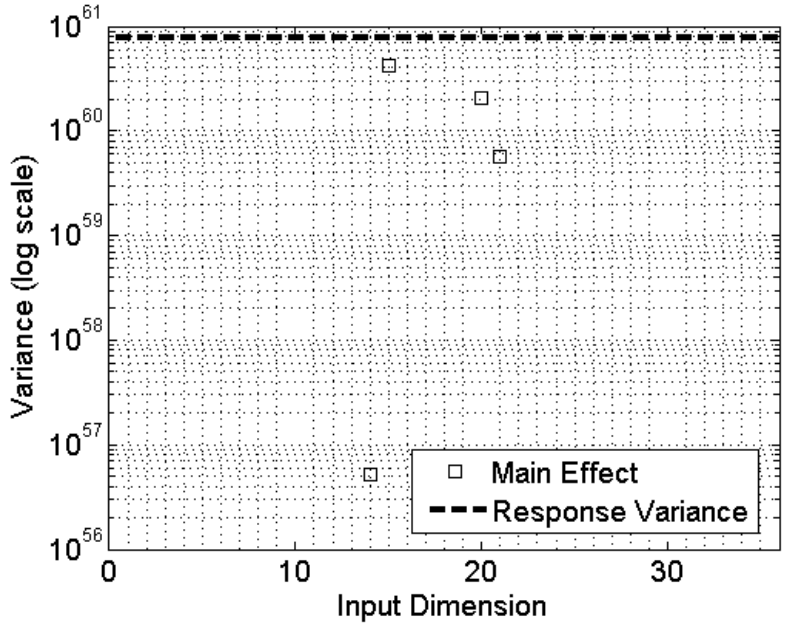


**Figure 143. QOI 2 Main Effects for Adjusted Xenon 1-D Radial Oscillator Strength Problem with 32,000 Sample LHD.**

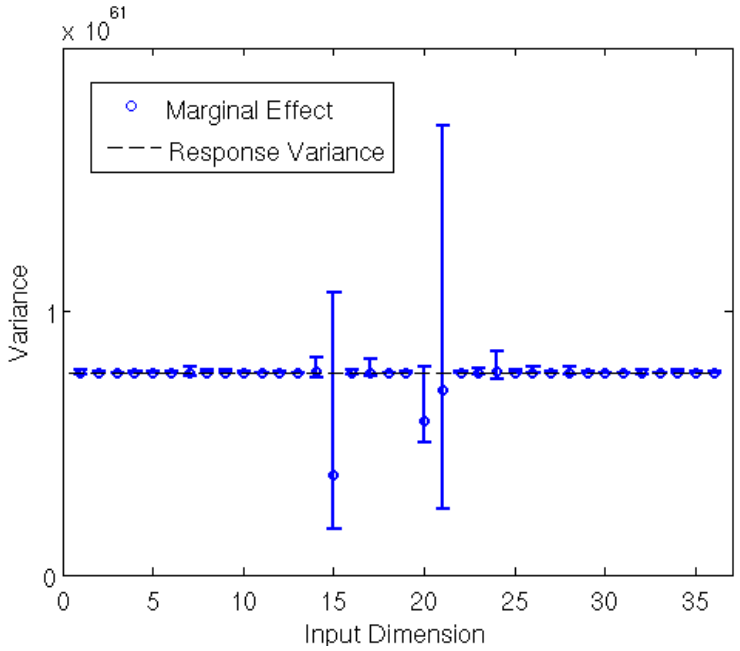


**Figure 144. QOI 2 Marginal Effects for Adjusted Xenon 1-D Radial Oscillator Strength Problem with 32,000 Sample LHD.**

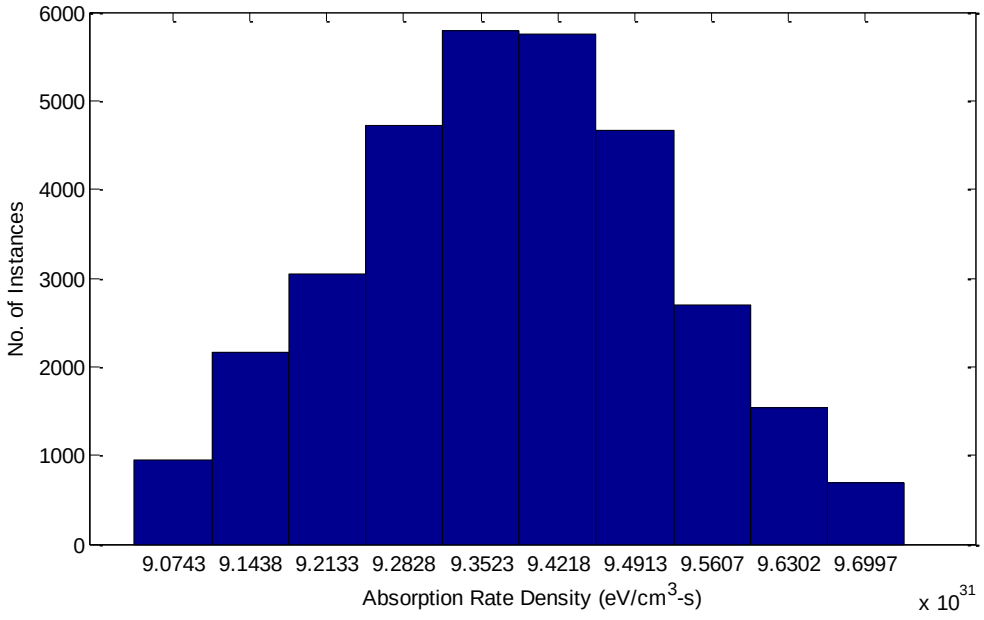


**Figure 145. QOI 3 for the Adjusted Xenon 1-D Radial Oscillator Strength Problem with 32,000 Sample LHD.**

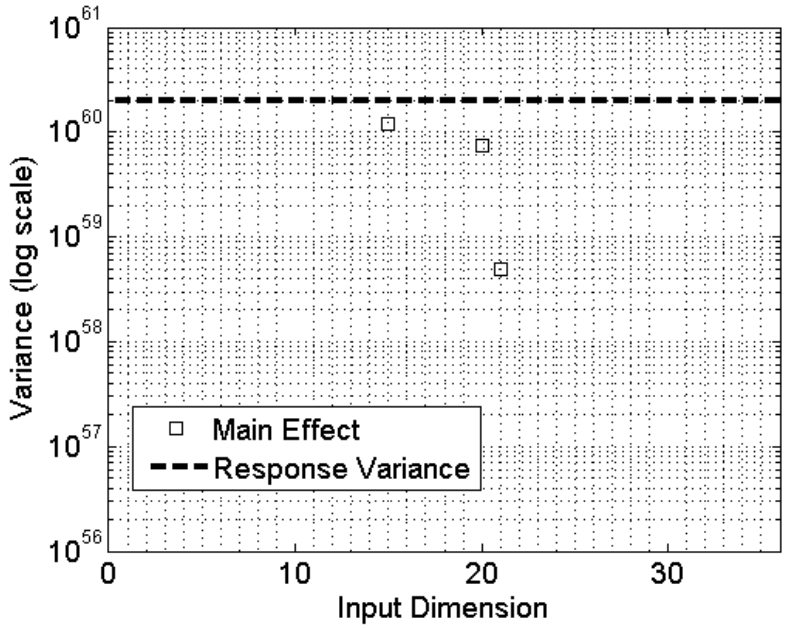


**Figure 146. QOI 3 Main Effects for Adjusted Xenon 1-D Radial Oscillator Strength Problem with 32,000 Sample LHD.**

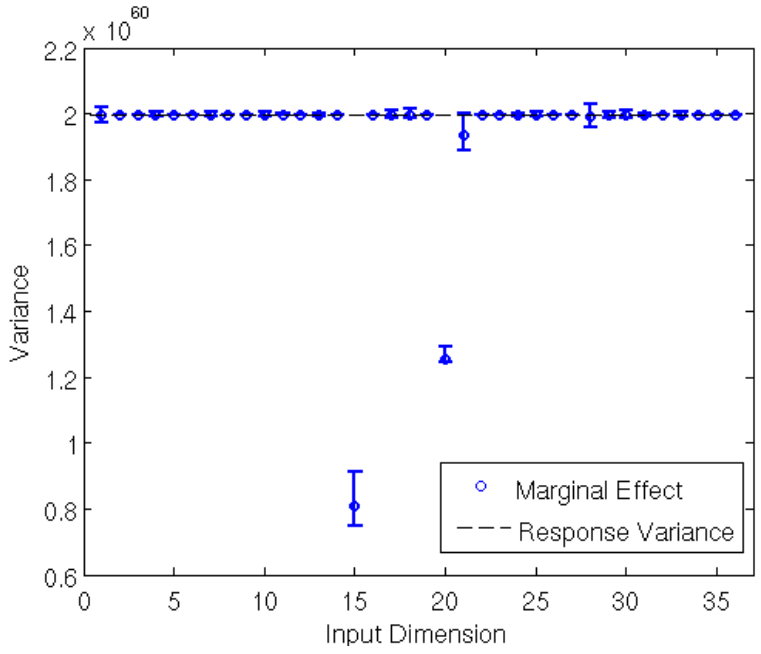


**Figure 147. QOI 3 Marginal Effects for Adjusted Xenon 1-D Radial Oscillator Strength Problem with 32,000 Sample LHD.**

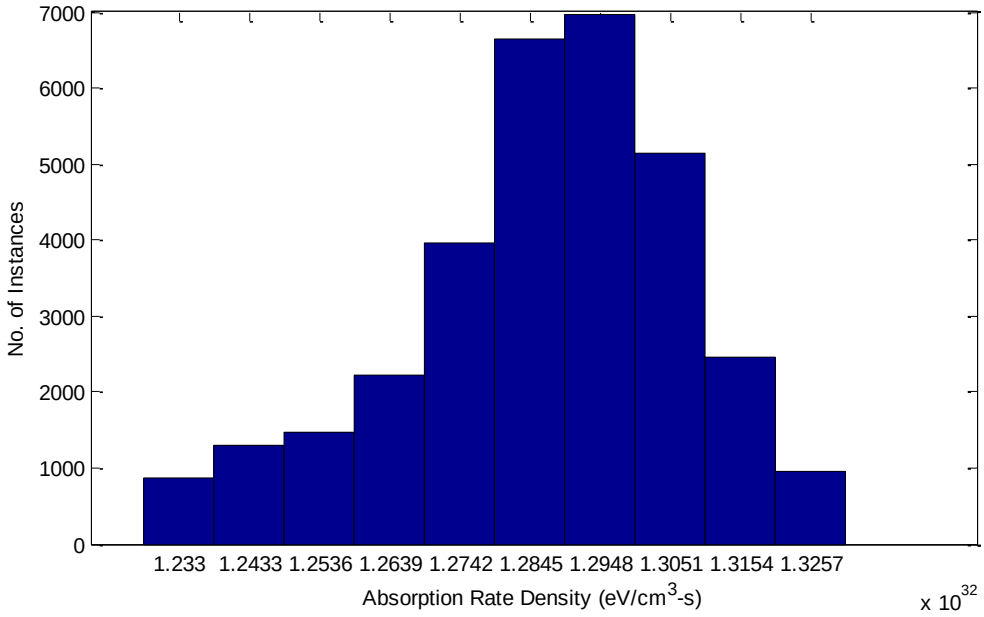


**Figure 148. QOI 4 for the Adjusted Xenon 1-D Radial Oscillator Strength Problem with 32,000 Sample LHD.**

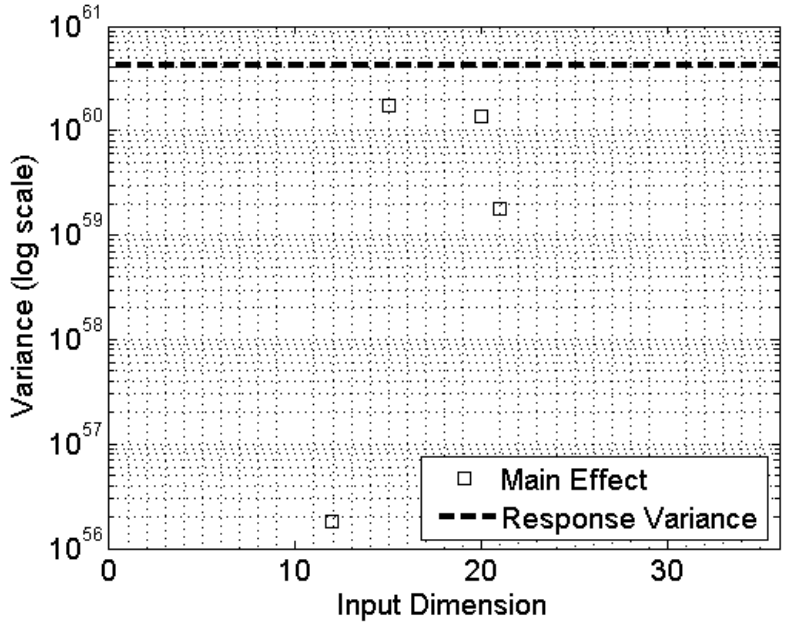


**Figure 149. QOI 4 Main Effects for Adjusted Xenon 1-D Radial Oscillator Strength Problem with 32,000 Sample LHD.**

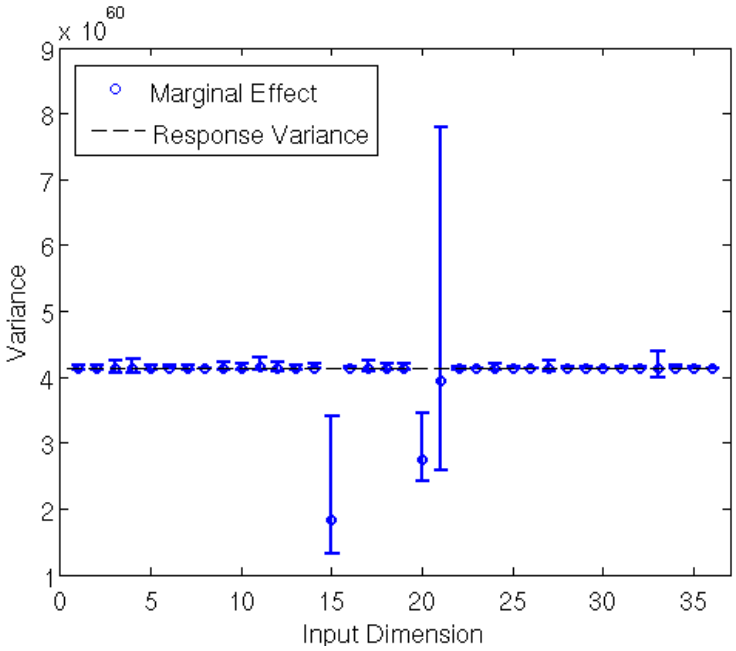


**Figure 150. QOI 4 Marginal Effects for Adjusted Xenon 1-D Radial Oscillator Strength Problem with 32,000 Sample LHD.**

### 5.2.4.3 Important Parameters for the 1-D Radial Oscillator Strength Case with Adjusted Xenon Opacities

We present the important parameters for these two LHDs in Table 19.

**Table 19. Important Parameters for the 1-D Radial Oscillator Strength Case with Adjusted Xenon Opacities**

| LHD | QOI | $10^{-4}$ Screening | $10^{-3}$ Screening |
|---|---|---|---|
| 1000 | 1 | 15, 20, 21 | 15, 20, 21 |
| | 2 | 15, 20, 21 | 15, 20, 21 |
| | 3 | 15, 20, 21 | 15, 20, 21 |
| | 4 | 15, 20, 21 | 15, 20, 21 |
| 32000 | 1 | 15, 20 ,21 | 15, 20 ,21 |
| | 2 | 15, 20, 21 | 15, 20, 21 |
| | 3 | 15, 20, 21 | 15, 20, 21 |
| | 4 | 15, 20, 21 | 15, 20, 21 |

These parameter sets agree well with the original xenon opacities, which implies that adjusting the xenon opacities has little effect on the importance of oscillator strengths in the 1-D radial problem. Comparing the main effects for the QOIS for the original and adjusted xenon cases, even the order of relative importance is consistent, where the main effects are from highest to lowest $15^{th}$, $20^{th}$, and $21^{st}$.

These sets of important parameters are compiled and used to compute QOIs for the 2-D CRASH-like problem.

## 5.3 Results for the 2-D CRASH-like Problem

We have performed the sensitivity analysis for the oscillator strengths and the ionization potentials in the two 1-D CRASH-like problems. We use these results to create two sets of uncertain parameters, which have been deemed important to study in the full 2-D problem. The results are presented below.

### 5.3.1 Summary Using Important Uncertain Parameters with Adjusted Opacities

By examining the main and marginal effects, it was determined that the main effects for the 1-D simulations provided a larger set of uncertain parameters; so, we use the main effects as our screening criteria. The two sets are chosen such that they include all parameters whose values are within $10^{-3}$ and $10^{-4}$ of the total variance for the main effects. These are presented in Table 20, and the numbering of the oscillator strengths is based on the numeric entry from the oscillator strength table when counting from left to right top to bottom.

**Table 20. Important Parameters Based on Screening Criteria.**

| | $10^{-4}$ | $10^{-3}$ |
|---|---|---|
| Oscillator Strengths | 6, 10, 14, 15, 19, 20, 21, 26, 27 | 6, 10, 14, 15, 19, 20, 21, 26, 27 |
| Xe Ionization Potentials | 4, 5, 6, 7, 8, 9, 16, 17, 18, 19, 21, 22, 23, 24, 25, 26, 27, 28 | 4, 5, 6, 7, 8, 19, 21, 22, 23, 24, 25, 26, 27, 28 |
| C Ionization Potentials | 1, 3 | 3 |
| N Ionization Potentials | 3 | - |

In the next two sections, results are presented using the two different parameter sets based on the screening criteria.

### 5.3.2 2-D CRASH-like Test Problem Results

Results and discussion for the three different QOIs are presented for the 2-D CRASH-like test problem. In the Figure 151, the PDF is presented for the first QOI. This PDF has been created by binning up the points into finely resolved bins and plotting using a line plot. There are six sets of data presented. These are the 1,000, 2,000, and 4,000 sample LHDs for the 33-parameter space represented on the legend as 1k, 2k, and 4k, and the 500, 1,000, and 2,000 sample LHDs for the 26-parameter space represented on the legend as 0.5kR, 1kR, and 2kR. Since, we want the QOIs from this problem to be as close to reality as possible, we use the LANL-adjusted xenon opacities.

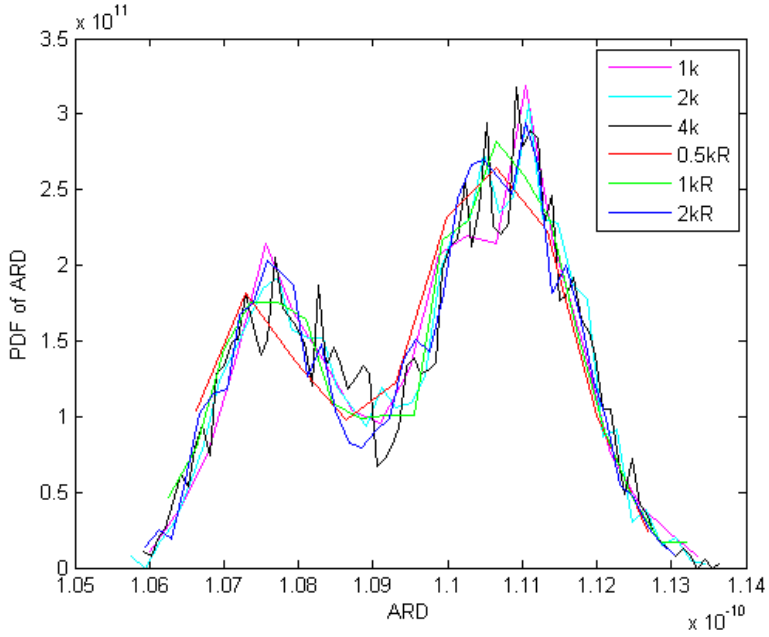


**Figure 151. PDF for QOI 1 for the 2-D CRASH-like Test Problem.**

There are two interesting features in this plot. First, it appears that the six distributions are highly correlated. This demonstrates that there are enough samples in the LHD to have a "converged" distribution. Second, the distribution is bimodal. If scatter plots of the parameter are examined, a non-physical anomaly appears in them. In the Figure 152, the non-physical anomaly is shown.

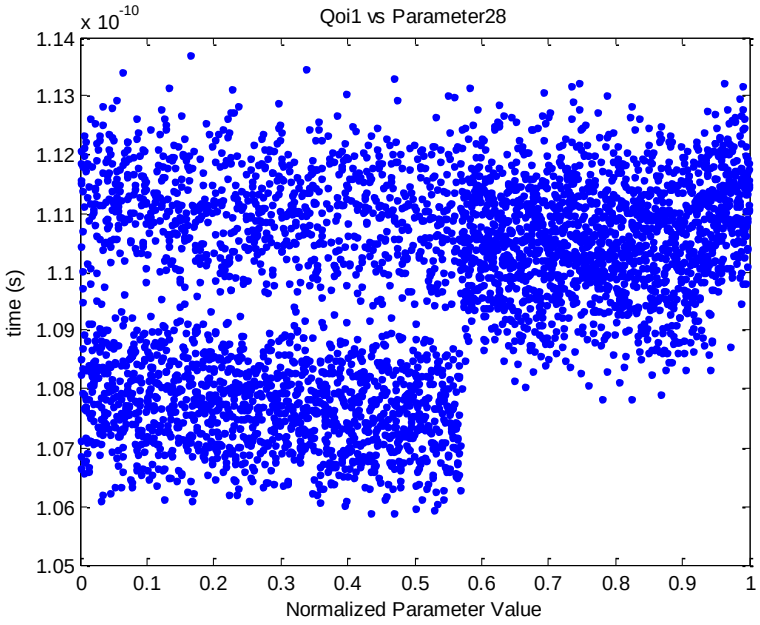


**Figure 152. 28th Xe Ionization Potential versus QOI 1.**

This appears to be non-physical because it is not expected that such an abrupt cutoff would occur at about 0.57 of the normalized ionization parameter. We believe some condition in the CRASH opacity code changes at this value leading to this discontinuous result. The CRASH opacity code should be examined to determine what causes this and determine if this is an acceptable result.

PDFs for the second and third QOIs are presented in Figure 153 and Figure 154.

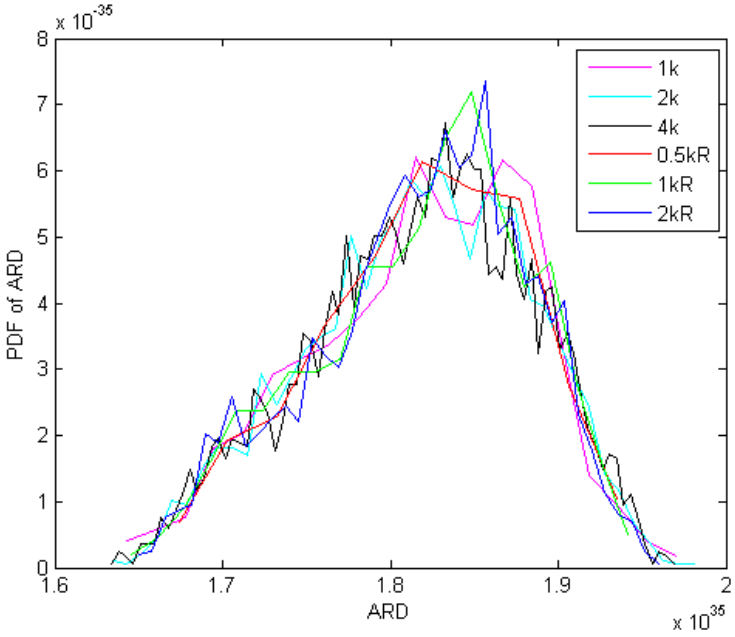


**Figure 153. PDF for QOI 2 for the 2-D CRASH-like Test Problem.**

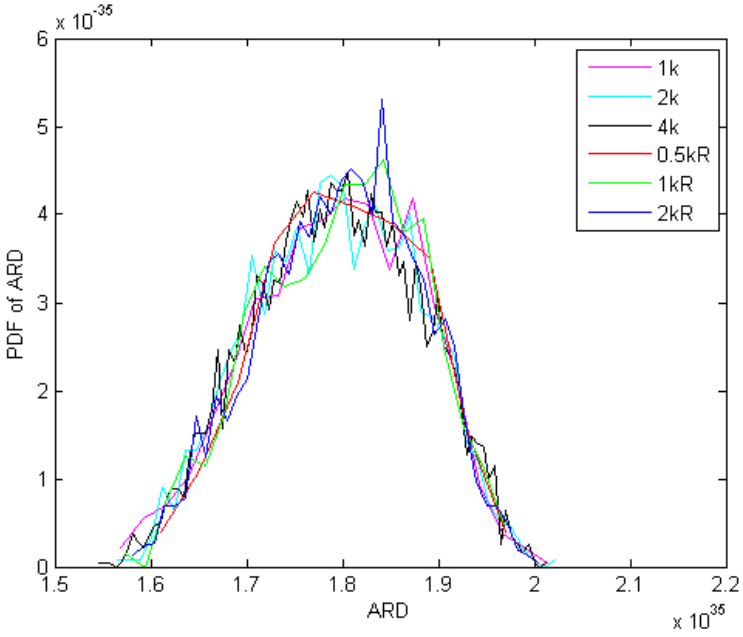


**Figure 154. PDF for QOI 3 for the 2-D CRASH-like Test Problem.**

From these results, the QOIs for the differing sizes of LHDs and parameter spaces appear to be converged. To further establish the amount of convergence, means and standard deviations have been computed for all three QOIs inTable 21, Table 22, and Table 23. Also, the Jensen-Shannon divergence (Ref. 23) has been computed to test the divergence of each LHD to the 4,000 sample LHD using 8 discrete bins.

**Table 21. Mean and Standard Deviation for QOI 1.**

| | Mean | Std. Dev. | Jensen-Shannon (.,4k) |
|---|---|---|---|
| **1k** | 1.097E-10 | 1.676E-12 | 0.0018 |
| **2k** | 1.097E-10 | 1.688E-12 | 0.0002 |
| **4k** | 1.097E-10 | 1.703E-12 | 0 |
| **05kR** | 1.096E-10 | 1.683E-12 | 0.0019 |
| **1kR** | 1.096E-10 | 1.711E-12 | 0.0008 |
| **2kR** | 1.097E-10 | 1.686E-12 | 0.0011 |

**Table 22. Mean and Standard Deviation for QOI 2.**

| | Mean | Std. Dev. | Jensen-Shannon (.,4k) |
|---|---|---|---|
| **1k** | 1.817E+35 | 6.660E+33 | 0.0040 |
| **2k** | 1.816E+35 | 6.557E+33 | 0.0004 |
| **4k** | 1.817E+35 | 6.594E+33 | 0 |
| **05kR** | 1.818E+35 | 6.205E+33 | 0.0061 |
| **1kR** | 1.817E+35 | 6.445E+33 | 0.0016 |
| **2kR** | 1.817E+35 | 6.365E+33 | 0.0018 |

**Table 23. Mean and Standard Deviation for QOI 3.**

| | Mean | Std. Dev. | Jensen-Shannon (.,4k) |
|---|---|---|---|
| **1k** | 1.793E+35 | 8.616E+33 | 0.0010 |
| **2k** | 1.793E+35 | 8.555E+33 | 0.0003 |

**Table 23. (continued)**

| | | | |
|---|---|---|---|
| **4k** | 1.793E+35 | 8.629E+33 | 0 |
| **05kR** | 1.799E+35 | 8.048E+33 | 0.0053 |
| **1kR** | 1.798E+35 | 8.324E+33 | 0.0026 |
| **2kR** | 1.798E+35 | 8.233E+33 | 0.0017 |

The ARD for the plastic downstream of the shocked xenon is an important area to understand because this is what drives the wall shock. From looking at these last two QOIs, we see that changes in the parameters underlying the calculation of opacities affect the ARD in the wall by approximately 10% of its mean value. This information could be used to study variations in wall shock that are induced by opacity uncertainties. For example, in the CRASH coupled radiation-hydrodynamics simulations, one could imagine applying a distribution to the ARD in the plastic wall the coupled simulations.

# 6 CONCLUSION

The problem that this research addresses is the curse of dimensionality associated with tabulated opacities, which are used in radiation transport calculations. We have devised physics-based dimension-reduction to attack this problem. Instead of examining the uncertainties in the tabular entries, we have modeled the uncertainty in the parameters that are inputs to the physics models used to compute the opacities. Also, computationally inexpensive simulations and sensitivity analysis on low-order emulators were used to perform further physics-based parameter-space reduction (screening). To help assess the veracity of the final analysis, two different reduced parameter sets and three different LHDs were used for simulation, and the results of the simulations were compared to see if they produced the same distribution of the QOIs.

We see that the final QOIs are well converged from the plots and the statistics. This gives us some confidence that the choice of simplified calculations and QOIs have been selected broadly enough to encapsulate the parameters that are important for the CRASH-like calculation, and that the LHDs employed in the 2-D study provided adequate sampling of the input space.

In many problems of interest in predictive science and engineering, simulations require some form of tabulated data, often of high dimension. This research has demonstrated that uncertainty quantification can be performed based on the parameters that are inputs to the models that generate the tabulated data. With this approach the dimensionality of the uncertain input space is radically reduced, and furthermore each realization of the table has the physical dependence and proper correlations inherent in

the data-generation model. In contrast, sampling the tabulated parameters presents several difficulties, including the high dimensionality, the specification of correlations, sampling while respecting those correlations, and maintaining proper physical relations among parameters so that each physics simulation is based on a possible realization of the input parameters. Future work should explore how broadly the techniques developed here might be applicable to UQ in other science and engineering problems that suffer from the curse of dimensionality.

There are many avenues for future work. This work used very simple LHDs; one could use more advanced schemes, such as using nested LHDs for those with varying sizes. The emulator used for this research is a very basic version of BMARS, and there are better ways to create the emulator such as using frequentist MARS to find the stationary point and then using BMARS and using a hierarchical BMARS. Also, there are many different divergence criteria to determine the amount that two PDFs agree that could be investigated.

REFERENCES


1. National Research Council, *Assessing the Reliability of Complex Models: Mathematical and Statistical Foundations of Verification, Validation, and Uncertainty Quantification*, Washington, D.C. 2012: The National Academies Press.

2. G. P. Box and N. R. Draper, *Empirical Model-Building and Response Surfaces*, Wiley, New York (1987).

3. R. P. Drake, et al., "Radiative Effects in Radiative Shocks in Shock Tubes," *High Energy Density Physics,* **7**, 130 (2011).

4. B. van der Holst, et al., "CRASH: A Block-adaptive Mesh Code for Radiative Shock Hydrodynamcis-Implementation and Verification," *The Astrophysical Journal Supplement Series,* **195**, *23*, 1 (2011).

5. W. D. Hawkins, et al., "Efficient Massively Parallel Transport Sweeps," *Trans. Amer. Nucl. Soc.,* **107**, 477, (2012).

6. S. Chandrasekhar, *Radiative Transfer*, Dover Publications, Inc, New York (1960).

7. D. Mihalas, *Stellar Atmospheres*, W. H. Freeman and Company, San Francisco (1970).

8. Y. B. Zel'dovich and Y. P. Raizer, *Physics of Shock Waves and High-Temperature Hydrodynamic Phenomena*, Dover Publications Inc., Mineola, New York (2002).

9. G. C. Pomraning, *The Equations of Radiation Hydrodynamics*, Dover Publications, Mineola, New York (1973).

10. R. Cowan, *The Theory of Atomic Structure and Spectra*, University of California Press, Berkeley, CA (1981).

11. H. B. Callen, *Thermodynamics and an Introduction to Thermostatistics*, John Wiley and Sons, New York (2005).

12. I. Sokalov, "Thermodynamics and Radiation Transport in Dense Plasmas," *Unpublished*.

13. J. J. Macfarlane, "IONMIX-A Code For Computing the Equation of State and Radiative Properties of LTE and Non-LTE Plasmas," *Computer Physics Communications,* **56**, 259 (1989).

14. S. Rosseland, "Note on the Absorption of Radiation within a Star," *Monthly Notices of the Royal Astronomical Society,* **84**, 525 (1925).

15. F. J. Rogers and C. A. Iglesias, "Radiative Atomic Rosseland Mean Opacity Tables," *The Astrophysical Journal Supplement Series,* **79**, 507 (1992).

16. M. J. Seaton, "Atomic Data for Opacity Calculations: I. General Description," *Journal of Physics B: Atomic, Molecular, and Optical Pysics,* **20**, 6363 (1987).

17. D. G. T. Denison, et al., "Bayesian MARS," *Statistics and Computing,* **8**, 337 (1998).

18. M. D. Morris and T. J. Mitchell, "Exploratory Designs for Computation Experiments," *Journal of Statistical Planning and Inference,* **43**, 381 (1995).

19. B. Tang, "Selecting Latin Hypercubes Uing Correlation Criteria," *Statistica Sinica,* **8**, 965 (1998).

20. A. B. Owen, "Controlling Correlations in Latin Hypercube Samples," *Journal of the American Statistical Associations,* **89**, *428*, 1517 (1994).

21. J. H. Friedman, "Multivariate Adaptive Regression Spines," *The Annals of Statistics,* **19**, *1*, 1 (1991).

22. A. Y. Faenov, et al., "Specr-W3 Online Database on Atomic Properties of Atoms and Ions," *AIP Conference Proceedings,* **636**, *1*, 253 (2002).

23. J. Lin, "Divergence Measures Based on Shannon Entropy," *IEEE Transactions on Information Theory*, **37**, *1*, 145 (1991).

# APPENDIX A

In this section, we describe the previous work performed by Hayes Stripling IV that shows that 10 energy groups are sufficient for the CRASH-like test problem. In Figure 155, line-outs have been plotted for different calculations of ARDs at 0.4 ns using the setting given in Table 24 for the 2-D CRASH-like test problem with more highly refined settings. Also, in Figure 156 line-outs have been plotted for different calculations of ARD at 0.4 ns 0.002 cm downstream of the shocked xenon. From these plots we observe that 10 group and 50 group line-outs are in good agreement.

**Table 24. Legend for ARD Line-outs.**

| **Energy Groups (denoted by line style)** | **Angular Quadrature (denoted by line color)** | |
|---|---|---|
| Solid: Grey (1 group) | Blue – S6 | Purple – LS 10 (15 angles/oct) |
| Dashed: 10 groups | Orange – S10 | Black – LS 16 (36 angles/oct) |
| Dotted: 50 groups | Green – S16 | |

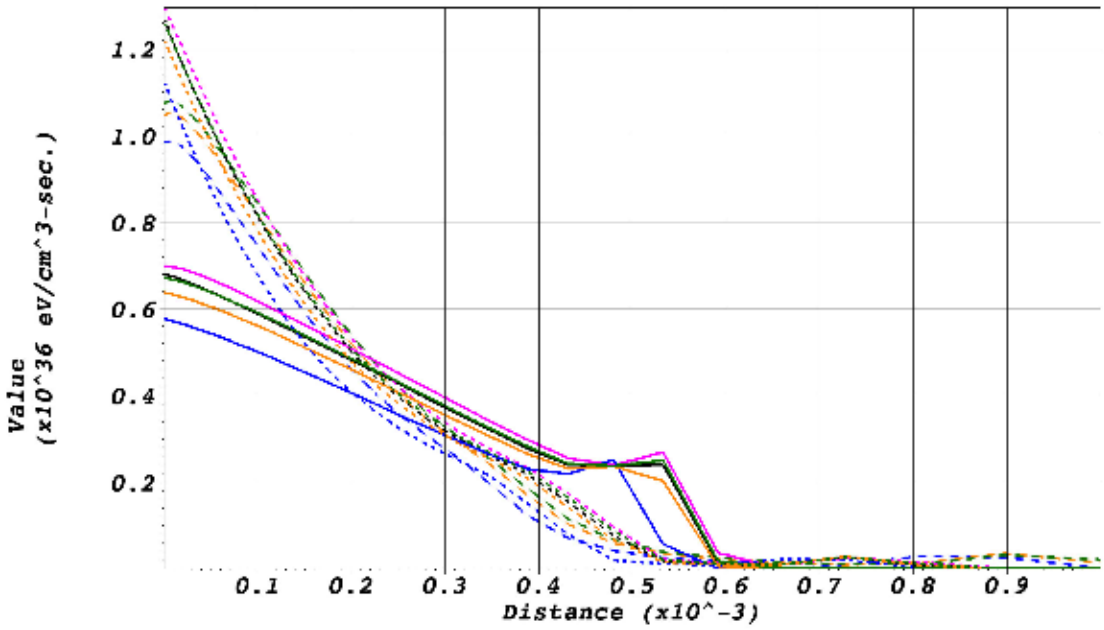


**Figure 155. Vertical Lineout Directly Above Center of Shocked Xenon.**

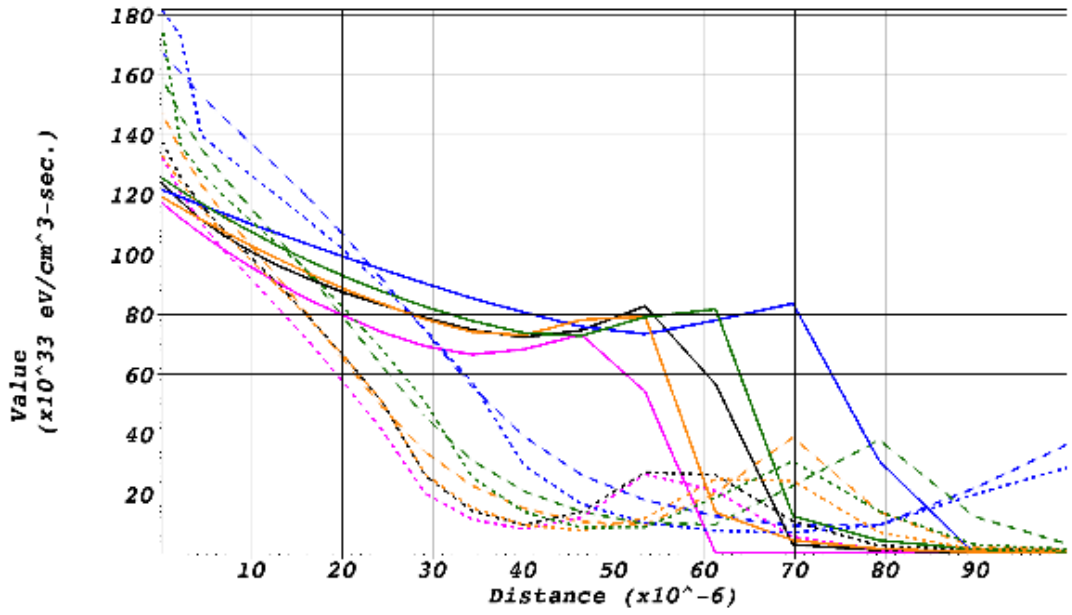


**Figure 156. Vertical Lineout 0.002 cm Downstream of Shocked Xenon.**

# APPENDIX B

The three PDT input decks for the 1-D axial, 1-D radial, and 2-D CRASH-like test problems are listed in this section.

Below is the input deck for the 1-D Axial CRASH-like test problem.

```
<prototype>
        <!-- Information Common to the problem -->
        <common>
    <problem_type>RADIATIVE_TRANSFER</problem_type>
                <td_info>
                        <method>SPECIFIED</method>
                        <diff_param.fp>1.0</diff_param.fp>
                       <ts_control.str>adaptive</ts_control.str>
      <t_start.fp>0.0</t_start.fp>
      <t_stop.fp>2.0E-9</t_stop.fp>
      <max_steps.int>20000000</max_steps.int>
      <dt_start.fp>1.0E-14</dt_start.fp>
      <dt_min.fp>1.0E-16</dt_min.fp>
      <dt_max.fp>1.0E-10</dt_max.fp>
      <dt_max_gain.fp>1.1</dt_max_gain.fp>
      <Te_max_change.fp>0.1</Te_max_change.fp>
      <Er_max_change.fp>0.1</Er_max_change.fp>
      <global_multiplier.fp>0.1</global_multiplier.fp>
      <material_properties.str>converged</material_properties.str>
                </td_info>

                <!-- Type of spatial_method used SDM_WDD, SDM_CBSTEP,   -->
                <spatial_method>SDM_PWLD</spatial_method>
                <fem_type>FEM_LUMP</fem_type>

                <!-- Type of geometry used XYZ, XY, RZ -->
                <geometry>XY</geometry>

                <!-- although some of this information is redundant -->
                <!-- it is used for check purposes -->
                <ngroups.int>10</ngroups.int>
                <energy_group_aggregation>single_set</energy_group_aggregation>
                <energy_info_source>
                     <data_file.str>XeLan1.cx</data_file.str>
                </energy_info_source>

                <dimensions.int>2</dimensions.int>
                <iscat.int>0</iscat.int>

                <ard_iterative_method.str>richardson</ard_iterative_method.str>
                <ard_residual_tolerance.fp>1.0E-7</ard_residual_tolerance.fp>
                <ard_residual_max_its.int>100</ard_residual_max_its.int>
                <ard_pointwise_tolerance.fp>1.0E-7</ard_pointwise_tolerance.fp>
                <ard_pointwise_max_its.int>1</ard_pointwise_max_its.int>
                <Te_pointwise_tolerance.fp>1.0E-7</Te_pointwise_tolerance.fp>
                <Te_pointwise_max_its.int>1000</Te_pointwise_max_its.int>
                <T_floor.fp>1.160450501E+05</T_floor.fp>

                <aggregation_type>PLANE_BASED</aggregation_type>
                <partition_type>OTHER</partition_type>
                <aggregation_factor_x>1</aggregation_factor_x>
                <aggregation_factor_y>1</aggregation_factor_y>
                <aggregation_factor_z>1</aggregation_factor_z>
```

```
                <partition_params>
                        <partition_x>1</partition_x>
                        <partition_y>1</partition_y>
                        <partition_z>1</partition_z>
                </partition_params>
        </common>
        <edits>
                <print_grid>on</print_grid>
        </edits>

        <!-- Group sets -->
        <!-- this section contains information about how energy groups get -->
        <!-- grouped into group sets-->

        <groupsets>
                <energy_set>
                        <!-- IDs must be unique. it is not necessary for -->
                        <!-- them to be in order, but you can't leave holes-->
                        <!-- ex. if you include 1 and 3, you must include 2-->

                        <ID>0</ID>
                        <!-- a block implies that you include all numbers between -->
                        <!-- begin and end, including begin and end. -->

                        <set_include>0</set_include>

                        <!-- Quadrature information for the Group Set-->
                        <quad_info>
                                <quad_plevel.int>8</quad_plevel.int>
                                <quad_norm.fp>12.566370614359173</quad_norm.fp>
                                <quad_type.st>LevelSym</quad_type.st>
                        </quad_info>

                        <!--Group angles into angle sets by octant-->
                        <angle_set_aggregation>quadrant</angle_set_aggregation>
                </energy_set>
        </groupsets>


<!-- Spatial Input Section -->

        <dimension>
                <dimension.id>0</dimension.id>
                <dim.division>
                        <dim.division.cells.int>25</dim.division.cells.int>
                        <dim.division.start.fp>0.0</dim.division.start.fp>
                        <dim.division.end.fp>0.1</dim.division.end.fp>
                        <dim.division.id>0.0</dim.division.id>
                </dim.division>

                <dim.division>
                        <dim.division.cells.int>20</dim.division.cells.int>
                        <dim.division.start.fp>0.1</dim.division.start.fp>
                        <dim.division.end.fp>0.18</dim.division.end.fp>
                        <dim.division.id>0.1</dim.division.id>
          </dim.division>

                <dim.division>
                        <dim.division.cells.int>5</dim.division.cells.int>
                        <dim.division.start.fp>0.18</dim.division.start.fp>
                        <dim.division.end.fp>0.2</dim.division.end.fp>
                        <dim.division.id>0.2</dim.division.id>
                </dim.division>

                <dim.division>
```

```
                        <dim.division.cells.int>50</dim.division.cells.int>
                        <dim.division.start.fp>0.2</dim.division.start.fp>
                        <dim.division.end.fp>0.4</dim.division.end.fp>
                        <dim.division.id>0.3</dim.division.id>
                </dim.division>
        </dimension>

        <dimension>
                <dimension.id>1</dimension.id>
                <dim.division>
                        <dim.division.cells.int>1</dim.division.cells.int>
                        <dim.division.start.fp>0.0</dim.division.start.fp>
                        <dim.division.end.fp>1.0E+7</dim.division.end.fp>
                        <dim.division.id>1.0</dim.division.id>
                </dim.division>
        </dimension>

<!-- Materials Section -->
<!-- Component Definitions-->
        <component_def>
  <id.str>Be</id.str>
    <Cv_constants>
      <Cv_constant_A.fp>1.1360e+19</Cv_constant_A.fp>
      <Cv_constant_B.fp>0.0</Cv_constant_B.fp>
      <Cv_constant_C.fp>0.0</Cv_constant_C.fp>
    </Cv_constants>
    <opac_type.str>OT_mg_planck</opac_type.str>
    <data_file.str>BeFixed.cx</data_file.str>
  </component_def>

  <component_def>
                <id.str>Xe</id.str>
    <Cv_constants>
      <Cv_constant_A.fp>9.8616e+17</Cv_constant_A.fp>
      <Cv_constant_B.fp>0.0</Cv_constant_B.fp>
      <Cv_constant_C.fp>0.0</Cv_constant_C.fp>
    </Cv_constants>
    <opac_type.str>OT_mg_planck</opac_type.str>
    <data_file.str>XeLanl.cx</data_file.str>
  </component_def>

<!--Materials Definitions-->
        <material_def>
                <material_def.name>Be</material_def.name>
                <material_def.component>
                        <material_def.component.id.str>Be</material_def.component.id.str>

        <material_def.component.density.fp>0.008</material_def.component.density.fp>
                </material_def.component>
        </material_def>

        <material_def>
                <material_def.name>post-shock-Xe</material_def.name>
                <material_def.component>
                        <material_def.component.id.str>Xe</material_def.component.id.str>

        <material_def.component.density.fp>0.018</material_def.component.density.fp>
                </material_def.component>
        </material_def>

        <material_def>
                <material_def.name>shocked-Xe</material_def.name>
                <material_def.component>
                        <material_def.component.id.str>Xe</material_def.component.id.str>
```

```
        <material_def.component.density.fp>0.1</material_def.component.density.fp>
                </material_def.component>
        </material_def>

        <material_def>
                <material_def.name>pre-shock-Xe</material_def.name>
                <material_def.component>
                        <material_def.component.id.str>Xe</material_def.component.id.str>

        <material_def.component.density.fp>0.00589</material_def.component.density.fp>
                </material_def.component>
        </material_def>

<!--Material Regions -->
        <regions>
          <regions-material_region>
                <material_reg.material.str>Be</material_reg.material.str>
                <material_reg.speed.fp>29979245800.0</material_reg.speed.fp>
      <material_reg.Te.fp>1.160450501E+05</material_reg.Te.fp>
      <material_reg.Tr.fp>1.160450501E+05</material_reg.Tr.fp>
                <material_reg.dim_bounds>
                        <material_reg.dim_bounds.dim.int>0</material_reg.dim_bounds.dim.int>

        <material_reg.dim_bounds.div_start.int>0</material_reg.dim_bounds.div_start.int>

        <material_reg.dim_bounds.div_end.int>0</material_reg.dim_bounds.div_end.int>
                </material_reg.dim_bounds>
                <material_reg.dim_bounds>
                        <material_reg.dim_bounds.dim.int>1</material_reg.dim_bounds.dim.int>

        <material_reg.dim_bounds.div_start.int>0</material_reg.dim_bounds.div_start.int>

        <material_reg.dim_bounds.div_end.int>0</material_reg.dim_bounds.div_end.int>
                </material_reg.dim_bounds>
          </regions-material_region>

          <regions-material_region>
                <material_reg.material.str>post-shock-Xe</material_reg.material.str>
                <material_reg.speed.fp>29979245800.0</material_reg.speed.fp>
      <material_reg.Te.fp>1.160450501E+05</material_reg.Te.fp>
      <material_reg.Tr.fp>1.160450501E+05</material_reg.Tr.fp>
                <material_reg.dim_bounds>
                        <material_reg.dim_bounds.dim.int>0</material_reg.dim_bounds.dim.int>

        <material_reg.dim_bounds.div_start.int>1</material_reg.dim_bounds.div_start.int>

        <material_reg.dim_bounds.div_end.int>1</material_reg.dim_bounds.div_end.int>
                </material_reg.dim_bounds>
                <material_reg.dim_bounds>
                        <material_reg.dim_bounds.dim.int>1</material_reg.dim_bounds.dim.int>

        <material_reg.dim_bounds.div_start.int>0</material_reg.dim_bounds.div_start.int>

        <material_reg.dim_bounds.div_end.int>0</material_reg.dim_bounds.div_end.int>
                </material_reg.dim_bounds>
          </regions-material_region>

          <regions-material_region>
                <material_reg.material.str>shocked-Xe</material_reg.material.str>
                <material_reg.speed.fp>29979245800.0</material_reg.speed.fp>
      <material_reg.Te.fp>1.160450501E+05</material_reg.Te.fp>
      <material_reg.Tr.fp>1.160450501E+05</material_reg.Tr.fp>
                <material_reg.dim_bounds>
                        <material_reg.dim_bounds.dim.int>0</material_reg.dim_bounds.dim.int>
```

```
      <material_reg.dim_bounds.div_start.int>2</material_reg.dim_bounds.div_start.int>

      <material_reg.dim_bounds.div_end.int>2</material_reg.dim_bounds.div_end.int>
              </material_reg.dim_bounds>
              <material_reg.dim_bounds>
                      <material_reg.dim_bounds.dim.int>1</material_reg.dim_bounds.dim.int>

      <material_reg.dim_bounds.div_start.int>0</material_reg.dim_bounds.div_start.int>

      <material_reg.dim_bounds.div_end.int>0</material_reg.dim_bounds.div_end.int>
              </material_reg.dim_bounds>
        </regions-material_region>

        <regions-material_region>
              <material_reg.material.str>pre-shock-Xe</material_reg.material.str>
              <material_reg.speed.fp>29979245800.0</material_reg.speed.fp>
    <material_reg.Te.fp>1.160450501E+05</material_reg.Te.fp>
    <material_reg.Tr.fp>1.160450501E+05</material_reg.Tr.fp>
              <material_reg.dim_bounds>
                      <material_reg.dim_bounds.dim.int>0</material_reg.dim_bounds.dim.int>

      <material_reg.dim_bounds.div_start.int>3</material_reg.dim_bounds.div_start.int>

      <material_reg.dim_bounds.div_end.int>3</material_reg.dim_bounds.div_end.int>
              </material_reg.dim_bounds>
              <material_reg.dim_bounds>
                      <material_reg.dim_bounds.dim.int>1</material_reg.dim_bounds.dim.int>

      <material_reg.dim_bounds.div_start.int>0</material_reg.dim_bounds.div_start.int>

      <material_reg.dim_bounds.div_end.int>0</material_reg.dim_bounds.div_end.int>
              </material_reg.dim_bounds>
        </regions-material_region>
      </regions>

      <boundary_info>
      <left_bound>
              <bound_type>PLANCK_ISOTROPIC</bound_type>
  <planck_temperature.dbl>1.160450501E+05</planck_temperature.dbl>
  <planck_multiplier.dbl>1.0</planck_multiplier.dbl>
      </left_bound>
      <right_bound>
              <bound_type>VACUUM</bound_type>
  <planck_temperature.dbl>1.16045050081E+5</planck_temperature.dbl>
  <planck_multiplier.dbl>1.0</planck_multiplier.dbl>
      </right_bound>
      <top_bound>
              <bound_type>VACUUM</bound_type>
  <planck_temperature.dbl>1.16045050081E+5</planck_temperature.dbl>
  <planck_multiplier.dbl>1.0</planck_multiplier.dbl>
      </top_bound>
      <bottom_bound>
              <bound_type>VACUUM</bound_type>
  <planck_temperature.dbl>1.16045050081E+5</planck_temperature.dbl>
  <planck_multiplier.dbl>1.0</planck_multiplier.dbl>
      </bottom_bound>
      </boundary_info>

<named_sources>
  <source_def>
    <source_type>electron</source_type>
    <source_def_name>shock</source_def_name>
    <intensity>4.25e+33</intensity>
  </source_def>
```

```
  </named_sources>

  <source_geometry>
    <source_region>
      <source_name>shock</source_name>
      <source_dim_bounds>
        <source_dim_bounds_dim>0</source_dim_bounds_dim>
        <source_dim_start>2</source_dim_start>
        <source_dim_end>2</source_dim_end>
      </source_dim_bounds>
      <source_dim_bounds>
        <source_dim_bounds_dim>1</source_dim_bounds_dim>
        <source_dim_start>0</source_dim_start>
        <source_dim_end>0</source_dim_end>
      </source_dim_bounds>
    </source_region>
  </source_geometry>
</prototype>
```

Below is the input deck for the 1-D Radial CRASH-like test problem.

```
<prototype>
  <!-- Information Common to the problem -->
  <common>
    <problem_type>RADIATIVE_TRANSFER</problem_type>
    <td_info>
      <method>SPECIFIED</method>
      <diff_param.fp>1.0</diff_param.fp>
      <ts_control.str>adaptive</ts_control.str>
      <t_start.fp>0.0</t_start.fp>
      <t_stop.fp>3.0E-9</t_stop.fp>
      <max_steps.int>20000000</max_steps.int>
      <dt_start.fp>1.0E-14</dt_start.fp>
      <dt_min.fp>1.0E-16</dt_min.fp>
      <dt_max.fp>1.0E-10</dt_max.fp>
      <dt_max_gain.fp>1.1</dt_max_gain.fp>
      <Te_max_change.fp>0.1</Te_max_change.fp>
      <Er_max_change.fp>0.1</Er_max_change.fp>
      <global_multiplier.fp>0.1</global_multiplier.fp>
      <material_properties.str>converged</material_properties.str>
    </td_info>

    <!-- Type of spatial_method used SDM_WDD, SDM_CBSTEP,   -->
    <spatial_method>SDM_PWLD</spatial_method>
    <fem_type>FEM_LUMP</fem_type>

    <!-- Type of geometry used XYZ, XY, RZ -->
    <geometry>XY</geometry>

    <!-- although some of this information is redundant -->
    <!-- it is used for check purposes -->
    <ngroups.int>10</ngroups.int>
    <energy_group_aggregation>single_set</energy_group_aggregation>
    <energy_info_source>
      <data_file.str>XeLanl.cx</data_file.str>
    </energy_info_source>

    <dimensions.int>2</dimensions.int>
    <iscat.int>0</iscat.int>

    <ard_iterative_method.str>richardson</ard_iterative_method.str>
    <ard_residual_tolerance.fp>1.0E-7</ard_residual_tolerance.fp>
    <ard_residual_max_its.int>100</ard_residual_max_its.int>
```

```
  <ard_pointwise_tolerance.fp>1.0E-7</ard_pointwise_tolerance.fp>
  <ard_pointwise_max_its.int>1</ard_pointwise_max_its.int>
  <Te_pointwise_tolerance.fp>1.0E-2</Te_pointwise_tolerance.fp>
  <Te_pointwise_max_its.int>1000</Te_pointwise_max_its.int>
  <T_floor.fp>1.160450501E+05</T_floor.fp>

  <aggregation_type>PLANE_BASED</aggregation_type>
  <partition_type>OTHER</partition_type>
  <aggregation_factor_x>5</aggregation_factor_x>
  <aggregation_factor_y>1</aggregation_factor_y>
  <aggregation_factor_z>1</aggregation_factor_z>
  <partition_params>
    <partition_x>1</partition_x>
    <partition_y>1</partition_y>
    <partition_z>1</partition_z>
  </partition_params>
</common>
<edits>
  <print_grid>on</print_grid>
</edits>

<!-- Group sets -->
<!-- this section contains information about how energy groups get -->
<!-- grouped into group sets-->

<groupsets>
  <energy_set>
    <!-- IDs must be unique. it is not necessary for -->
    <!-- them to be in order, but you can't leave holes-->
    <!-- ex. if you include 1 and 3, you must include 2-->

    <ID>0</ID>
    <!-- a block implies that you include all numbers between -->
    <!-- begin and end, including begin and end. -->

    <set_include>0</set_include>

    <!-- Quadrature information for the Group Set-->
    <quad_info>
      <quad_plevel.int>16</quad_plevel.int>
      <quad_norm.fp>12.566370614359173</quad_norm.fp>
      <quad_type.st>LevelSym</quad_type.st>
    </quad_info>

    <!--Group angles into angle sets by octant-->
    <angle_set_aggregation>quadrant</angle_set_aggregation>
  </energy_set>
</groupsets>


<!-- Spatial Input Section -->

<dimension>
  <dimension.id>0</dimension.id>
  <dim.division>
    <dim.division.spacing.str>logarithmic</dim.division.spacing.str>
    <dim.division.log_factor.fp>0.95</dim.division.log_factor.fp>
    <dim.division.cells.int>160</dim.division.cells.int>
    <dim.division.start.fp>0.0</dim.division.start.fp>
    <dim.division.end.fp>0.06</dim.division.end.fp>
    <dim.division.id>0.0</dim.division.id>
  </dim.division>

  <dim.division>
    <dim.division.spacing.str>logarithmic</dim.division.spacing.str>
```

```
    <dim.division.log_factor.fp>1.07</dim.division.log_factor.fp>
    <dim.division.cells.int>160</dim.division.cells.int>
    <dim.division.start.fp>0.06</dim.division.start.fp>
    <dim.division.end.fp>0.0625</dim.division.end.fp>
    <dim.division.id>0.1</dim.division.id>
  </dim.division>
</dimension>


<dimension>
  <dimension.id>1</dimension.id>
  <dim.division>
    <dim.division.cells.int>1</dim.division.cells.int>
    <dim.division.start.fp>0.0</dim.division.start.fp>
    <dim.division.end.fp>1.0E+7</dim.division.end.fp>
    <dim.division.id>1.0</dim.division.id>
  </dim.division>
</dimension>

<!-- Materials Section -->
<!-- Component Definitions-->
<component_def>
  <id.str>Pl</id.str>
  <Cv_constants>
    <Cv_constant_A.fp>1.1360e+19</Cv_constant_A.fp>
    <Cv_constant_B.fp>0.0</Cv_constant_B.fp>
    <Cv_constant_C.fp>0.0</Cv_constant_C.fp>
  </Cv_constants>
  <opac_type.str>OT_mg_planck</opac_type.str>
  <data_file.str>PlFixed.cx</data_file.str>
</component_def>

<component_def>
  <id.str>Xe</id.str>
  <Cv_constants>
    <Cv_constant_A.fp>9.8616e+17</Cv_constant_A.fp>
    <Cv_constant_B.fp>0.0</Cv_constant_B.fp>
    <Cv_constant_C.fp>0.0</Cv_constant_C.fp>
  </Cv_constants>
  <opac_type.str>OT_mg_planck</opac_type.str>
  <data_file.str>XeLanl.cx</data_file.str>
</component_def>

<!--Materials Definitions-->
<material_def>
  <material_def.name>Pl</material_def.name>
  <material_def.component>
    <material_def.component.id.str>Pl</material_def.component.id.str>
    <material_def.component.density.fp>1.43</material_def.component.density.fp>
  </material_def.component>
</material_def>

<material_def>
  <material_def.name>Xe</material_def.name>
  <material_def.component>
    <material_def.component.id.str>Xe</material_def.component.id.str>
    <material_def.component.density.fp>0.1</material_def.component.density.fp>
  </material_def.component>
</material_def>

<!--Material Regions -->
<regions>
  <regions-material_region>
    <material_reg.material.str>Pl</material_reg.material.str>
    <material_reg.speed.fp>29979245800.0</material_reg.speed.fp>
```

```
    <material_reg.Te.fp>1.160450501E+05</material_reg.Te.fp>
    <material_reg.Tr.fp>1.160450501E+05</material_reg.Tr.fp>
    <material_reg.dim_bounds>
      <material_reg.dim_bounds.dim.int>0</material_reg.dim_bounds.dim.int>
      <material_reg.dim_bounds.div_start.int>0</material_reg.dim_bounds.div_start.int>
      <material_reg.dim_bounds.div_end.int>0</material_reg.dim_bounds.div_end.int>
    </material_reg.dim_bounds>
    <material_reg.dim_bounds>
      <material_reg.dim_bounds.dim.int>1</material_reg.dim_bounds.dim.int>
      <material_reg.dim_bounds.div_start.int>0</material_reg.dim_bounds.div_start.int>
      <material_reg.dim_bounds.div_end.int>0</material_reg.dim_bounds.div_end.int>
    </material_reg.dim_bounds>
  </regions-material_region>

  <regions-material_region>
    <material_reg.material.str>Xe</material_reg.material.str>
    <material_reg.speed.fp>29979245800.0</material_reg.speed.fp>
    <material_reg.Te.fp>1.160450501E+05</material_reg.Te.fp>
    <material_reg.Tr.fp>1.160450501E+05</material_reg.Tr.fp>
    <material_reg.dim_bounds>
      <material_reg.dim_bounds.dim.int>0</material_reg.dim_bounds.dim.int>
      <material_reg.dim_bounds.div_start.int>1</material_reg.dim_bounds.div_start.int>
      <material_reg.dim_bounds.div_end.int>1</material_reg.dim_bounds.div_end.int>
    </material_reg.dim_bounds>
    <material_reg.dim_bounds>
      <material_reg.dim_bounds.dim.int>1</material_reg.dim_bounds.dim.int>
      <material_reg.dim_bounds.div_start.int>0</material_reg.dim_bounds.div_start.int>
      <material_reg.dim_bounds.div_end.int>0</material_reg.dim_bounds.div_end.int>
    </material_reg.dim_bounds>
  </regions-material_region>

</regions>

<boundary_info>
  <left_bound>
    <bound_type>PLANCK_ISOTROPIC</bound_type>
    <planck_temperature.dbl>1.160450501E+05</planck_temperature.dbl>
    <planck_multiplier.dbl>1.0</planck_multiplier.dbl>
  </left_bound>
  <right_bound>
    <bound_type>PLANCK_ISOTROPIC</bound_type>
    <planck_temperature.dbl>1.16045050081E+4</planck_temperature.dbl>
    <planck_multiplier.dbl>1.0</planck_multiplier.dbl>
  </right_bound>
  <top_bound>
    <bound_type>PLANCK_ISOTROPIC</bound_type>
    <planck_temperature.dbl>1.16045050081E+4</planck_temperature.dbl>
    <planck_multiplier.dbl>1.0</planck_multiplier.dbl>
  </top_bound>
  <bottom_bound>
    <bound_type>PLANCK_ISOTROPIC</bound_type>
    <planck_temperature.dbl>1.16045050081E+4</planck_temperature.dbl>
    <planck_multiplier.dbl>1.0</planck_multiplier.dbl>
  </bottom_bound>
</boundary_info>

<named_sources>
  <source_def>
    <source_type>electron</source_type>
    <source_def_name>shock</source_def_name>
    <intensity>4.25e+33</intensity>
  </source_def>
</named_sources>

<source_geometry>
```

```
    <source_region>
      <source_name>shock</source_name>
      <source_dim_bounds>
        <source_dim_bounds_dim>0</source_dim_bounds_dim>
        <source_dim_start>0</source_dim_start>
        <source_dim_end>0</source_dim_end>
      </source_dim_bounds>
      <source_dim_bounds>
        <source_dim_bounds_dim>1</source_dim_bounds_dim>
        <source_dim_start>0</source_dim_start>
        <source_dim_end>0</source_dim_end>
      </source_dim_bounds>
    </source_region>
  </source_geometry>
</prototype>
```

Below is the input deck for the 2-D CRASH-like test problem.

```
<prototype>
  <common>
    <problem_type>RADIATIVE_TRANSFER</problem_type>

    <td_info>
      <simtime_per_dump.fp>0.2e-9</simtime_per_dump.fp>
      <steps_per_dump.int>1000000</steps_per_dump.int>
      <method>specified</method>
      <diff_param.fp>1.0</diff_param.fp>
      <ts_control.str>adaptive</ts_control.str>
      <t_start.fp>0.0</t_start.fp>
      <t_stop.fp>10.0E-9</t_stop.fp>
      <!-- Either    200000000 or 20 -->
      <max_steps.int>200000000</max_steps.int>
      <dt_start.fp>1.0E-15</dt_start.fp>
      <dt_min.fp>1.0E-16</dt_min.fp>
      <dt_max.fp>0.25E-10</dt_max.fp>
      <dt_max_gain.fp>1.1</dt_max_gain.fp>
      <Te_max_change.fp>0.1</Te_max_change.fp>
      <Er_max_change.fp>0.1</Er_max_change.fp>
      <global_multiplier.fp>0.1</global_multiplier.fp>
      <material_properties.str>converged</material_properties.str>
    </td_info>

    <spatial_method>SDM_PWLD</spatial_method>
    <fem_type>FEM_LUMP</fem_type>

    <geometry>XY</geometry>
    <dimensions.int>2</dimensions.int>
    <iscat.int>0</iscat.int>

    <ngroups.int>10</ngroups.int>
    <energy_group_aggregation>single_set</energy_group_aggregation>
    <eg_floor.fp>.044721</eg_floor.fp>
    <energy_info_source>
        <data_file.str>pl_crash_10g.cx</data_file.str>
    </energy_info_source>

    <ard_iterative_method.str>gmres</ard_iterative_method.str>
    <ard_gmres_restart_value.int>25</ard_gmres_restart_value.int>
    <ard_residual_tolerance.fp>1.0E-7</ard_residual_tolerance.fp>
    <ard_residual_max_its.int>30</ard_residual_max_its.int>
    <ard_pointwise_tolerance.fp>1.0E-2</ard_pointwise_tolerance.fp>
    <ard_pointwise_max_its.int>1</ard_pointwise_max_its.int>
    <Te_pointwise_tolerance.fp>1.0E-2</Te_pointwise_tolerance.fp>
```

```
  <Te_pointwise_max_its.int>10</Te_pointwise_max_its.int>
  <T_floor.fp>116045.050089082</T_floor.fp>

  <aggregation_type>PLANE_BASED</aggregation_type>
  <partition_type>OTHER</partition_type>
  <aggregation_factor_x>12</aggregation_factor_x>
  <aggregation_factor_y>20</aggregation_factor_y>
  <aggregation_factor_z>1</aggregation_factor_z>
  <partition_params>
    <partition_x>2</partition_x>
    <partition_y>2</partition_y>
    <partition_z>1</partition_z>
  </partition_params>
</common>

<groupsets>
  <energy_set>
    <ID>0</ID>
    <set_include>0</set_include>
    <quad_info>
      <quad_plevel.int>10</quad_plevel.int>
      <quad_norm.fp>12.566370614359173</quad_norm.fp>
      <quad_type.st>LevelSym</quad_type.st>
    </quad_info>
    <angle_set_aggregation>quadrant</angle_set_aggregation>
  </energy_set>
</groupsets>

<dimension>
  <dimension.id>0</dimension.id>
  <dim.division>
    <dim.division.cells.int>16</dim.division.cells.int>
    <dim.division.start.fp>0.18</dim.division.start.fp>
    <dim.division.end.fp>0.2</dim.division.end.fp>
    <dim.division.id>0</dim.division.id>
  </dim.division>
  <dim.division>
    <dim.division.spacing.str>logarithmic</dim.division.spacing.str>
    <dim.division.log_factor.fp>1.02065</dim.division.log_factor.fp>
    <dim.division.cells.int>32</dim.division.cells.int>
    <dim.division.start.fp>0.2</dim.division.start.fp>
    <dim.division.end.fp>0.24</dim.division.end.fp>
    <dim.division.id>1</dim.division.id>
  </dim.division>
</dimension>

<dimension>
  <dimension.id>1</dimension.id>
  <dim.division>
    <dim.division.cells.int>2</dim.division.cells.int>
    <dim.division.start.fp>0.0</dim.division.start.fp>
    <dim.division.end.fp>0.0025</dim.division.end.fp>
    <dim.division.id>0</dim.division.id>
  </dim.division>
  <dim.division>
    <dim.division.cells.int>6</dim.division.cells.int>
    <dim.division.start.fp>0.0025</dim.division.start.fp>
    <dim.division.end.fp>0.045625</dim.division.end.fp>
    <dim.division.id>1</dim.division.id>
  </dim.division>
  <dim.division>
    <dim.division.cells.int>16</dim.division.cells.int>
    <dim.division.start.fp>0.045625</dim.division.start.fp>
    <dim.division.end.fp>0.06</dim.division.end.fp>
    <dim.division.id>2</dim.division.id>
```

```
  </dim.division>
  <dim.division>
    <dim.division.spacing.str>logarithmic</dim.division.spacing.str>
    <dim.division.log_factor.fp>1.1065</dim.division.log_factor.fp>
    <dim.division.cells.int>16</dim.division.cells.int>
    <dim.division.start.fp>0.06</dim.division.start.fp>
    <dim.division.end.fp>0.0625</dim.division.end.fp>
    <dim.division.id>3</dim.division.id>
  </dim.division>
</dimension>

<component_def>
  <id.str>Xe</id.str>
  <Cv_constants>
    <Cv_constant_A.fp>9.8616e+17</Cv_constant_A.fp>
    <Cv_constant_B.fp>0.0</Cv_constant_B.fp>
    <Cv_constant_C.fp>0.0</Cv_constant_C.fp>
  </Cv_constants>
  <opac_type.str>OT_mg_ross</opac_type.str>
  <data_file.str>xe_crash_10g.cx</data_file.str>
</component_def>

<component_def>
  <id.str>plastic</id.str>
  <Cv_constants>
    <Cv_constant_A.fp>1.1360e+19</Cv_constant_A.fp>
    <Cv_constant_B.fp>0.0</Cv_constant_B.fp>
    <Cv_constant_C.fp>0.0</Cv_constant_C.fp>
  </Cv_constants>
  <opac_type.str>OT_mg_ross</opac_type.str>
  <data_file.str>pl_crash_10g.cx</data_file.str>
</component_def>

<material_def>
  <material_def.name>Xe_shock</material_def.name>
  <material_def.component>
    <material_def.component.id.str>Xe</material_def.component.id.str>
    <material_def.component.density.fp>0.1</material_def.component.density.fp>
  </material_def.component>
</material_def>

<material_def>
  <material_def.name>Plastic</material_def.name>
  <material_def.component>
    <material_def.component.id.str>plastic</material_def.component.id.str>
    <material_def.component.density.fp>1.43</material_def.component.density.fp>
  </material_def.component>
</material_def>

<material_def>
  <material_def.name>Xe_ds</material_def.name>
  <material_def.component>
    <material_def.component.id.str>Xe</material_def.component.id.str>
    <material_def.component.density.fp>0.00589</material_def.component.density.fp>
  </material_def.component>
</material_def>


<regions>

  <regions-material_region>
    <material_reg.material.str>Plastic</material_reg.material.str>
    <material_reg.speed.fp>29979245800.0</material_reg.speed.fp>
    <material_reg.Te.fp>116045.050089082</material_reg.Te.fp>
    <material_reg.Tr.fp>116045.050089082</material_reg.Tr.fp>
```

```
    <material_reg.dim_bounds>
      <material_reg.dim_bounds.dim.int>0</material_reg.dim_bounds.dim.int>
      <material_reg.dim_bounds.div_start.int>0</material_reg.dim_bounds.div_start.int>
      <material_reg.dim_bounds.div_end.int>1</material_reg.dim_bounds.div_end.int>
    </material_reg.dim_bounds>
    <material_reg.dim_bounds>
      <material_reg.dim_bounds.dim.int>1</material_reg.dim_bounds.dim.int>
      <material_reg.dim_bounds.div_start.int>0</material_reg.dim_bounds.div_start.int>
      <material_reg.dim_bounds.div_end.int>0</material_reg.dim_bounds.div_end.int>
    </material_reg.dim_bounds>
  </regions-material_region>

  <regions-material_region>
    <material_reg.material.str>Plastic</material_reg.material.str>
    <material_reg.speed.fp>29979245800.0</material_reg.speed.fp>
    <material_reg.Te.fp>116045.050089082</material_reg.Te.fp>
    <material_reg.Tr.fp>116045.050089082</material_reg.Tr.fp>
    <material_reg.dim_bounds>
      <material_reg.dim_bounds.dim.int>0</material_reg.dim_bounds.dim.int>
      <material_reg.dim_bounds.div_start.int>0</material_reg.dim_bounds.div_start.int>
      <material_reg.dim_bounds.div_end.int>1</material_reg.dim_bounds.div_end.int>
    </material_reg.dim_bounds>
    <material_reg.dim_bounds>
      <material_reg.dim_bounds.dim.int>1</material_reg.dim_bounds.dim.int>
      <material_reg.dim_bounds.div_start.int>3</material_reg.dim_bounds.div_start.int>
      <material_reg.dim_bounds.div_end.int>3</material_reg.dim_bounds.div_end.int>
    </material_reg.dim_bounds>
  </regions-material_region>

  <regions-material_region>
    <material_reg.material.str>Xe_shock</material_reg.material.str>
    <material_reg.speed.fp>29979245800.0</material_reg.speed.fp>
    <material_reg.Te.fp>116045.050089082</material_reg.Te.fp>
    <material_reg.Tr.fp>116045.050089082</material_reg.Tr.fp>
    <material_reg.dim_bounds>
      <material_reg.dim_bounds.dim.int>0</material_reg.dim_bounds.dim.int>
      <material_reg.dim_bounds.div_start.int>0</material_reg.dim_bounds.div_start.int>
      <material_reg.dim_bounds.div_end.int>0</material_reg.dim_bounds.div_end.int>
    </material_reg.dim_bounds>
    <material_reg.dim_bounds>
      <material_reg.dim_bounds.dim.int>1</material_reg.dim_bounds.dim.int>
      <material_reg.dim_bounds.div_start.int>1</material_reg.dim_bounds.div_start.int>
      <material_reg.dim_bounds.div_end.int>2</material_reg.dim_bounds.div_end.int>
    </material_reg.dim_bounds>
  </regions-material_region>

  <regions-material_region>
    <material_reg.material.str>Xe_ds</material_reg.material.str>
    <material_reg.speed.fp>29979245800.0</material_reg.speed.fp>
    <material_reg.Te.fp>116045.050089082</material_reg.Te.fp>
    <material_reg.Tr.fp>116045.050089082</material_reg.Tr.fp>
    <material_reg.dim_bounds>
      <material_reg.dim_bounds.dim.int>0</material_reg.dim_bounds.dim.int>
      <material_reg.dim_bounds.div_start.int>1</material_reg.dim_bounds.div_start.int>
      <material_reg.dim_bounds.div_end.int>1</material_reg.dim_bounds.div_end.int>
    </material_reg.dim_bounds>
    <material_reg.dim_bounds>
      <material_reg.dim_bounds.dim.int>1</material_reg.dim_bounds.dim.int>
      <material_reg.dim_bounds.div_start.int>1</material_reg.dim_bounds.div_start.int>
      <material_reg.dim_bounds.div_end.int>2</material_reg.dim_bounds.div_end.int>
    </material_reg.dim_bounds>
  </regions-material_region>
</regions>
```

```
  <boundary_info>
    <front_bound>
      <bound_type>PLANCK_ISOTROPIC</bound_type>
      <planck_temperature.dbl>116045.050089082</planck_temperature.dbl>
      <planck_multiplier.dbl>1.0</planck_multiplier.dbl>
    </front_bound>

    <back_bound>
      <bound_type>PLANCK_ISOTROPIC</bound_type>
      <planck_temperature.dbl>116045.050089082</planck_temperature.dbl>
      <planck_multiplier.dbl>1.0</planck_multiplier.dbl>
    </back_bound>

    <left_bound>
      <bound_type>PLANCK_ISOTROPIC</bound_type>
      <planck_temperature.dbl>116045.050089082</planck_temperature.dbl>
      <planck_multiplier.dbl>1.0</planck_multiplier.dbl>
    </left_bound>

    <right_bound>
      <bound_type>PLANCK_ISOTROPIC</bound_type>
      <planck_temperature.dbl>116045.050089082</planck_temperature.dbl>
      <planck_multiplier.dbl>1.0</planck_multiplier.dbl>
    </right_bound>

    <top_bound>
      <bound_type>PLANCK_ISOTROPIC</bound_type>
      <planck_temperature.dbl>116045.050089082</planck_temperature.dbl>
      <planck_multiplier.dbl>1.0</planck_multiplier.dbl>
    </top_bound>

    <bottom_bound>
      <bound_type>PLANCK_ISOTROPIC</bound_type>
      <planck_temperature.dbl>116045.050089082</planck_temperature.dbl>
      <planck_multiplier.dbl>1.0</planck_multiplier.dbl>
    </bottom_bound>
  </boundary_info>

  <named_sources>
    <source_def>
      <source_type>electron</source_type>
      <source_def_name>shock</source_def_name>
      <intensity>4.2502273399795575e+33</intensity>
    </source_def>
  </named_sources>

  <source_geometry>
    <source_region>
      <source_name>shock</source_name>
      <source_dim_bounds>
        <source_dim_bounds_dim>0</source_dim_bounds_dim>
        <source_dim_start>0</source_dim_start>
        <source_dim_end>0</source_dim_end>
      </source_dim_bounds>
      <source_dim_bounds>
        <source_dim_bounds_dim>1</source_dim_bounds_dim>
        <source_dim_start>1</source_dim_start>
        <source_dim_end>2</source_dim_end>
      </source_dim_bounds>
    </source_region>
  </source_geometry>
</prototype>
```